SALT TECTONICS OF THE WESTERN SABLE SUB-BASIN: INSIGHTS FROM REGIONAL SEISMIC INTERPRETATION AND 4D SCALED PHYSICAL EXPERIMENTS

by

Cody MacDonald

Submitted in partial fulfillment of the requirements
for the degree of Master of Science

at

Dalhousie University
Halifax, Nova Scotia
October, 2009

DALHOUSIE UNIVERSITY

DEPARTMENT OF EARTH SCIENCES

The undersigned hereby certify that they have read and recommend to the Faculty of Graduate Studies for acceptance of a thesis entitled "**SALT TECTONICS OF THE WESTERN SABLE SUB-BASIN: INSIGHTS FROM REGIONAL SEISMIC INTERPRETATION AND 4D SCALED PHYSICAL EXPERIMENTS**" by Cody MacDonald in partial fulfillment of the requirements for the degree of Master of Science.

Dated: October 21, 2009

Supervisor:

Co-Supervisor:

External Examiner:

Department Reader:

Committee Chair:

DALHOUSIE UNIVERSITY

DATE: October 21, 2009

AUTHOR: Cody MacDonald

TITLE: **SALT TECTONICS OF THE WESTERN SABLE SUB-BASIN: INSIGHTS FROM REGIONAL SEISMIC INTERPRETATION AND 4D SCALED PHYSICAL EXPERIMENTS**

DEPARTMENT OR SCHOOL: Department of Earth Sciences

DEGREE: M.Sc. CONVOCATION: May YEAR: 2009

Table of Contents

LIST OF FIGURES

List of Tables

ABSTRACT

Salt tectonics strongly influenced the post-rift evolution of the western Sable sub-basin at the north-central Scotian margin. Understanding the interplay between structures and reservoir distribution is crucial for success in future exploration programs. Primary factors controlling salt tectonics in this area include: the rift basin geometry, salt thickness and varying sediment input and delta progradation during the Mid Jurassic to Late Cretaceous. Understanding the role of these primary factors on salt tectonics and regional depocenters is critical for unraveling the complex tectono-stratigraphic framework of the Scotian basin.

This study integrates interpretation of basin-scale 2D seismic reflection profiles of the Ion GX Technologies NovaSPAN data set, public domain seismic and well data with innovative 4D scaled physical experiments, to gain insight into the mechanics of thin-skinned salt tectonics and basin evolution of the western Sable sub-basin. Interpretation of seismic reflection data reveals that the original salt basin at the western Sable sub-basin was characterized by the small proximal Abenaki graben that is separated from the wide Sable sub-basin by the North Sable High. The Sable sub-basin floor is characterized by several asymmetric rift grabens that are infilled by syn-rift sediments. The basin floor of the Sable sub-basin climbs toward the transition to salt basin terminus via two distal ramp segments. Salt structures in the Abenaki sub-basin are shutdown reactive diapirs and basinward dipping growth faults. The Sable sub-basin is characterized by major salt with drawal basins and passive diapirs that appear to be positioned at changes in basin floor morphology. Key features of the Sable sub-basin are two allochthonous salt canopy systems that are present in the Sable sub-basin and developed during transgression events: 1) the Balvenie Roho System that is positioned beneath the modern-day slope and developed in the Early Cretaceous, and 2) an extensive allochthonous salt tongue canopy system that spread during the Late Cretaceous.

4D scaled physical experiments demonstrate that downdip variations in salt structures from shelf to deepwater can be grouped into three kinematic domains: (1) *Salt Weld and Reactive Diapir, (2) Expulsion Rollover/Passive Diapir and Early Cretaceous Canopy,* and *(3) Passive Diapir and Late Cretaceous Canopy* domains. Unlike the sequential seaward propagation of depocenters in the northern regions of the margin (e.g. the Laurentian sub-basin), all salt withdrawal basins developed at nearly the same time and the Early Cretaceous was the most active period for salt tectonics deformation in the western Sable sub-basin. Depocenter evolution was controlled by: 1) more regional deposition of deltaic and pro-deltaic sediments and 2) early post-rift, regional but low relief inflated salt complexes that did not hinder seaward transport of sediments. In a kinematic model of diapir and canopy evolution, early-inflated salt complexes in the downdip contractional domain focus at changes in the basin-floor and original salt thickness. These inflated salt complexes later evolved into passive diapirs and the extensive canopy systems during subsequent sediment progradation.

The derived kinematic concepts of salt tectonics and basin evolution for the first time explain the structural and related depocenter evolution in a regional framework, from the early post-rift stage to the modern margin. The evolution of early salt withdrawal basins and late canopy system evolution provide new ideas about reservoir distribution and trap formation in the slope and deepwater Sable basin.

ACKNOWLEDGEMENTS

This work would not have been possible without funding by PRAC/NSERC, AIF (ACOA) & CFI, and Pengrowth. A personal thanks also goes to Menno Dinkelmann, who permitted us to use of the NovaSPAN dataset by ION/GX Technology. The Canadian Nova Scotia Offshore Petroleum Board was instrumental in finding public seismic reflection datasets. Dr. Juergen Adam has played an integral role in my understanding of basin dynamics, salt tectonics, and physical modeling for numerous years at Dalhousie University, and has been as much a friend as he has a supervisor. Mladen Nedimovic has been very helpful with the organization and revision of this thesis, and for stepping in as a Co-Supervisor. Dr. Djordje Grujic originally introduced me to the study of structural geology, directed me to salt tectonics and physical modeling. I have had a keen interest in pursuing research related and applicable to the oil and gas industry, and have made numerous contacts through Dr. Grant Wach, all of which have been encouraging and enthusiastic about my studies throughout the years. The Dalhousie Geodynamics Group, particularly Sofie Gradmann, Steven Ings, and Christopher Beaumont, have been incredibly helpful for discussion relating to the evolution of passive margins and salt tectonics, and have pushed me to consider many factors of basin dynamics that I may have otherwise overlooked. Dr. Keith Louden was extremely generous for setting up and maintaining the Salt Dyanimcs Group seismic database, as well as for providing our entire group with important datasets, such as the SMART transects and sediment thickness maps. Finally, the department of Earth Sciences at Royal Holloway University of London was very accommodating during my stay in the UK, and deserves warm thanks.

1.0 Project Overview

1.1 Introduction

The Scotian Basin is located on the Atlantic continental margin, offshore Nova Scotia. Sedimentary basin formation was initiated during the Middle to Late Triassic when continental and shallow marine sediments, including salt, infilled rift valley systems. With the opening of the Atlantic Ocean starting in the late Triassic, the rift basin became a passive margin sedimentary basin with a thick sedimentary succession up to 16-18 km. Jurassic aggradation and Early Cretaceous progradation controlled by the Sable and Laurentian Deltas has mobilized a several kilometer thick evaporite succession within a structurally complex salt basin. Salt mobilization driven by passive downbuilding of sediments has resulted in the development of salt-withdrawal basins in the modern day shelf, and passive diapirs and extensive allochthonous salt-tongue/canopy systems in the slope and deep water.

This study blends structural and stratigraphic interpretation of available 2D seismic data with optically monitored 4D physical experiments to improve the understanding of the salt-tectonic system of the western Sable sub-basin. The 2D seismic data used for this project are long offset Ion GX Technology NovaSPAN 2003 profiles and other line in the public domain. Evolution of salt structures and first-order controls of related depositional systems (sedimentation patterns and rates, salt thickness, and basin geometry) are investigated. Regional, basin-scale concepts will decrease risk during exploration with improved understanding of the development and timing of salt structures. Specifically, understanding the relationship between structural style and sedimentation patterns and

rates will benefit exploration of deep-water targets such as turbidites, mass transport deposits, and deep-water channel systems.

Boundary conditions and parameters (salt basin geometry, initial salt thickness, and sedimentation rates) for scaled physical experiments are deduced from structural and stratigraphic interpretation of 2D regional seismic profiles. Scaled physical experiments simulate the interaction of salt-tectonic processes and sedimentation patterns/rates during the entire post-rift evolution of the margin. High-resolution 3D particle monitoring (Particle Imaging Velocimetry) combined with model cross-sections provide quantitative data for fault kinematics and salt-tectonic processes that are related to depositional patterns in lab-scaled experiments.

1.2 Problem Statement

The western Sable sub-basin, within salt province III, features complex salt-tectonic structures including: complex fault systems, shutdown and passive diapirs, primary, secondary and tertiary weld levels, and extensive salt canopy and tongue systems (Shimeld, 2004). These structures (see Appendix A) are believed to be the result of thin-skinned salt tectonics, in which sediment loading caused mobilization of salt. Primary factors controlling salt tectonics at the Scotian margin are thought to include pre-flexure salt-basin geometries, original salt thickness, and sediment deposition and progradation rates during the Mid - Jurassic to Late Cretaceous (Shimeld, 2004). What is not known is the individual contribution of these first-order factors to the evolution of salt structures through time. The original syn-rift salt basin architecture can be better understood and defined for physical modeling with recent 2D wide-angle refraction

seismic investigations of the present day crustal structure and rifting history (Wu et al., 2006; Funck et al., 2004).

Researchers of the Dalhousie Salt Dynamics Group have studied the controls of basin geometry, salt thickness, and varying post-rift sedimentation rates on salt tectonics (Krézsek et al., 2007; MacDonald, 2007; Campbell, 2007), and it is now possible to develop models for specific geological settings. To develop an improved understanding of the kinematic evolution of the western Sable sub-basin, scaled 4D analogue experiments that simulate conditions from the shelf to the deepwater extremity of the margin have been conducted. These experiments were capable of simulating the interaction of salt tectonics processes from early salt mobilization in the autochthonous salt basin and associated outboard salt inflation to the formation of allochthonous salt systems in the present slope and deepwater areas. Results from the models contribute to the understanding of: salt basin geometry, initial salt thickness, timing of salt-related structures, the interaction between salt tectonics and its control on paleo and modern shelf-slope depositional history, and the formation of allochthonous deepwater salt canopy and tongue systems in the modern shelf and at the basin-terminus.

1.3 Hypotheses

The two hypotheses tested for the western Sable sub-basin are:

1: Changes in salt thickness associated with variable original basin morphology have controlled early salt inflation and localization of diapirs; and

2: Salt-tectonic deformation was most vigorous during the Early Cretaceous when sedimentation rates were the highest.

1.4 Methodology

The Dalhousie Salt Dynamics Group uses scaled analogue experiments together with regional seismic interpretation to study sedimentary basin evolution and deformation during thin-skinned gravity spreading of passive margins with underlying salt (Adam et al., 2005, 2006; Krézsek et al., 2007; MacDonald, 2007). At the Analogue Deformation Laboratory at Dalhousie University scaled analogue models of brittle-ductile systems that simulate salt tectonics are monitored with Particle Imaging Velocimetry (PIV). Models consist of two-layer granular-viscous materials, silica sand and silicone polymer, which are appropriate for simulating evolution of sedimentary basins in a dynamic salt system.

PIV is an optical deformation monitoring technique adapted to analogue models (Adam et al., 2005) for the measurement of surface deformation. With the use of PIV, displacement and its many time-series derivatives may be calculated, including incremental and finite subsidence, strain, and overburden translation velocity. Structural models are built from final model cross-sections and time-series PIV data. By integrating structural interpretation with time-series data (strain, subsidence, etc.) reliable 3D fault/salt structure correlation and mechanical analysis is possible.

Experimental results are directly comparable to natural case studies and are helpful as a basis for the interpretation of structural, stratigraphic and sedimentological processes. Importantly, models are capable of investigating first-order controls on basin evolution and salt tectonics in the Scotian Basin as identified in regional studies (Shimeld, 2004).

1.5 Objectives

The main objectives of this study are to:

1. Identify migrating depocenters and sedimentation rates during the Late Jurassic to Late Cretaceous in the western Sable sub-basin and associated slope and deepwater regions;
2. Constrain the present day salt basin morphology and present empirical evidence for its syn-rift configuration and associated salt thickness;
3. Conduct 4D analogue model experiments with site-specific parameters (sedimentation rates, basin geometries, salt thickness) derived from seismic profiles to analyze salt mobilization and sediment interaction;
4. Analyze the mechanics, timing, and coupling of salt tectonic processes in the western Sable sub-basin based on concepts derived from physical models.
5. Construct and restore a structural cross-section of the Western Sable sub-basin based on concepts derived from analogue models and seismic interpretation.

2.0 Formation of Salt Basins and Mechanisms of Thin-Skinned Deformation

2.1 Formation of Salt Basins

Salt basins primarily form in rift basins at passive margins during continental rifting (Fig. 2-1). They may form during the early post-rift phase (U.S. Gulf Coast, West Africa, Brazil), pre-rift phases (North Sea, Germany, Persian Gulf), or during passive intervals between distinct episodes of rifting (Morocco, Scotian, Jean d'Arc) (Jackson and Vendeville, 1994).

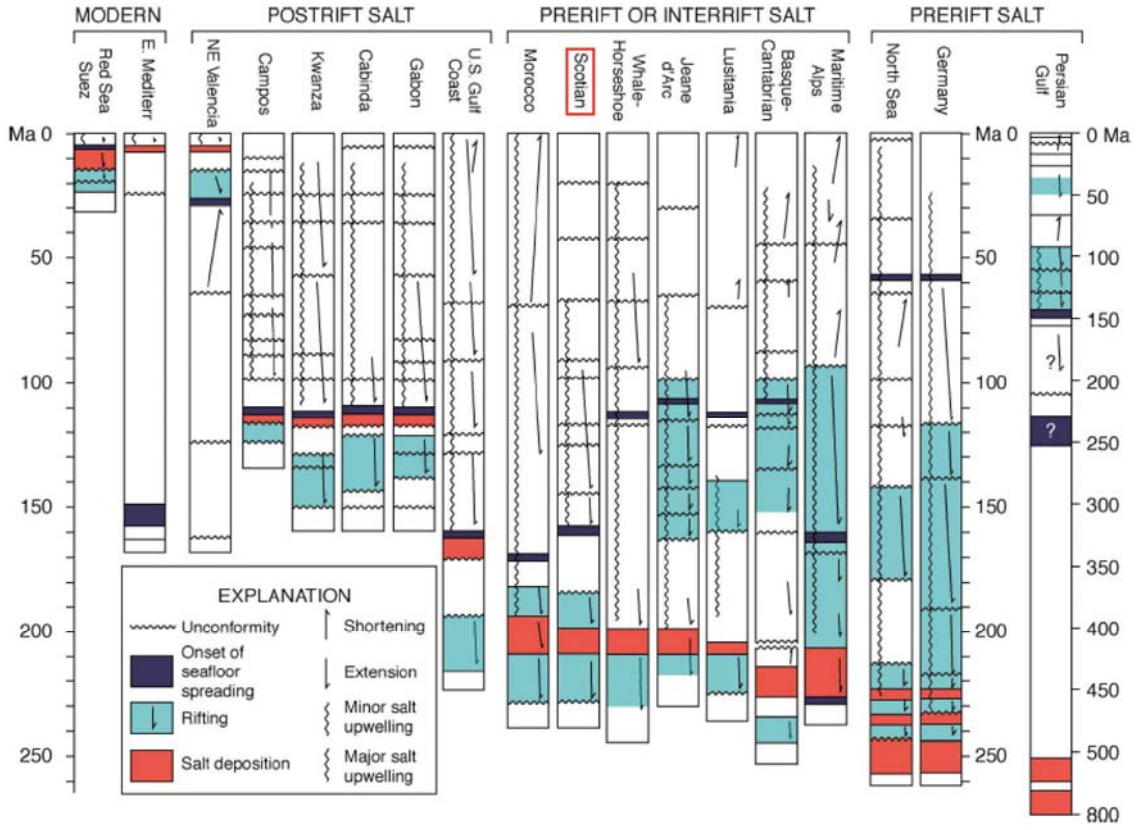

Figure 2-1: Timing of salt deposition relative to sea-floor spreading. Salt at the Scotian margin has been deposited during the syn-rift or "inter-rift" stage of its development. Modified from Jackson and Vendeville, 1994.

Salt basins typically form during extension of continental crust with the onset of rifting. Flanks of grabens that form during rifting (rift valleys) initially become sites of

widespread erosion due to regional uplift of rift margins during times of high heat flow. Subsidence of these grabens is created by offset along major fault systems, cooling, and sediment loading, leading to terrestrial deposition followed by marine incursion. During the transition from non-marine to marine conditions, evaporites form episodically and are often interbedded with different lithologies. However, the successions are usually dominated by halite. With further subsidence, true marine conditions follow and a post-rift succession, consisting of early shallow-water carbonates, deltaic sediments, and deepwater equivalents is deposited.

Rift-basins have distinct and unique basement architectures, which play an important role in the geometry of salt basins. This syn-rift fill is strongly controlled by rift-induced subsidence, accommodation space, and sediment supply. In cases such as the passive margin offshore of West Africa (Fig. 2-2), post-rift salt was deposited as a tabular layer because the accommodation space in rift-grabens was completely infilled by the time of its deposition, and there was likely no major fault system that was still active during salt deposition. At other passive margins (e.g. offshore Nova Scotia) variations in original salt thickness might be related to the incomplete infilling of rift grabens, or to continuous subsidence at major active fault/hinge zones during deposition. Variations in original salt thickness are a strong control on the mechanics of salt mobilization throughout the early, intermediate, and late stages of basin-scale salt tectonics (Ge et al., 1997; MacDonald, 2007; Campbell, 2007). Salt thickness has a strong control on the effective flow within a salt layer, and therefore on the early position of diapirs and expulsion rollovers.

At the Scotian margin, variations in original salt thickness down-dip and along strike are believed to be important to regional structural evolution and are associated with

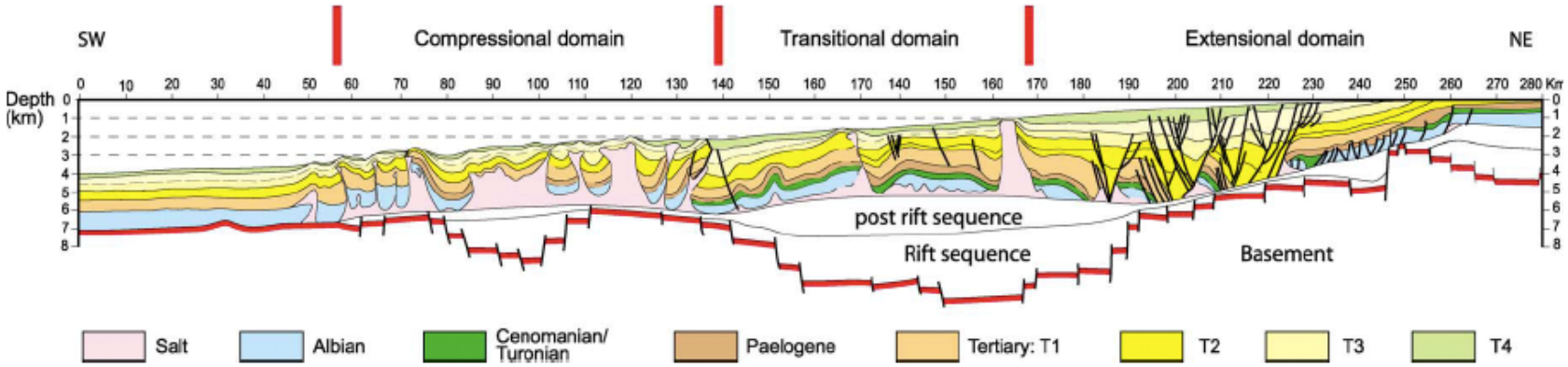

Figure 2-2: Cross-section of the West African margin showing domains of salt structures. Unlike at the border of offshore Angola/Congo, where salt was deposited in the post-rift, salt at the Scotian margin was been deposited during the syn-rift or "inter-rift" stage of its development. Modified from Calassou and Moretti, 2003.

local highs and syn-rift subsidence patterns. Much of the rift-grabens appear to be infilled almost completely, however, basement features appear to act as a strong control on regional salt tectonics. In later discussion, the role of highs and original salt thickness will be addressed with regard to decoupling of regional salt tectonics and their control on structural regimes.

2.2 Thin Skinned Deformation

2.2.1 Rheological Considerations

The mechanics of salt mobilization are controlled by its physical properties and how it differs from other sedimentary rock types. The two main factors that govern the physical behavior of salt are its low strength (Fig. 2-3) and density.

When affected by differential loading, the rheology of salt is similar to a Newtonian viscous fluid over geologic time-scales. Since natural rock salt contains traces of water, deformation may occur by solution-transfer creep under low strain rates and deviatoric stresses (Wawersik and Zeuch, 1986; Urai et al., 1986; Spiers et al., 1986; Weijermars, 1993; Heege et al., 2005). Under these conditions, salt has a low effective viscosity between 10^{16} and 10^{19} Pa•s (van Keken et al., 1993) that depends on temperature and grain size. Grain size is particularly important, as low grain sizes dramatically reduce viscosity (Vendeville and Jackson, 1992). The behavior of diffusion-controlled solution-transfer creep in salt containing traces of water is governed by the creep law (Weijermars, 1993):

$$(\sigma_{xx} - \sigma_{zz}) = (\dot{e}_{xx}/A)(Td^3)\exp(Q/RT)$$

Where; $(\sigma_{xx} - \sigma_{zz})$ is differential stress, $\dot{e}_{xx}$ is normal strain rate, A is the material constant

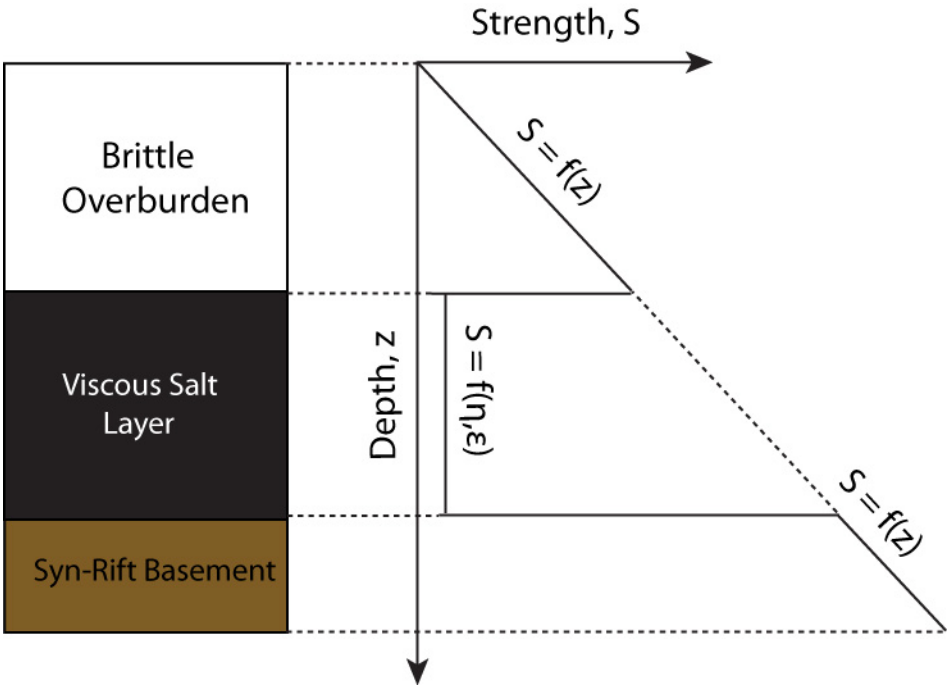

Figure 2-3: Simplified diagram of strength with depth for brittle overburden, salt, and syn-rift basement. After Vendeville and Jackson (1993). z is depth, S is strength, η is viscosity and ε is strain rate.

T is temperature in kelvin, d is average grain diameter, Q is the activation energy in $Jmol^{-1}$, and R is the gas constant R = 8.315 $JK^{-1}mol^{-1}$. Temperature is typically assumed to vary with depth (z), such that $T = T_0 + \xi z$; where T_0 is the surface temperature (K), and ξ is the geotherm (km^{-1}). As an important consideration, the viscosity of wet salt is temperature dependent, but virtually independent of stress and strain rate, the latter of which is a requirement for Newtonian rehology.

Other sedimentary rocks are mechanically different from halite, as they compact and become stronger with depth. These rocks display-frictional plastic behavior in which shear strength is controlled by depth-dependent confining pressure, but is independent of strain rate. Faulting in sedimentary rocks occurs when the effective deviatoric stress reaches yield strength. Yield stress levels for movement on normal faults are low in

comparison to those required for thrusting and strike-slip faults (about a quarter and a half respectively; Sibson, 1974). Most faults associated with salt tectonics are normal or reverse types, and the Mohr-Coulomb fracture criterion can be used to understand tensional and compressional failure. Expressed in terms of principal stresses (Weijermars, 1993) these are:

$$(\sigma_3 - \sigma_1) = (\sigma_{xx} - \sigma_{zz}) = [-2[c-\mu\sigma_{zz}(1 - \lambda)]/[(\mu^2 + 1)^{1/2} + \mu]]$$

for tension, and

$$(\sigma_1 - \sigma_3) = (\sigma_{xx} - \sigma_{zz}) = [2[c-\mu\sigma_{zz}(1 - \lambda)]/[(\mu^2 + 1)^{1/2} - \mu]]$$

for compression, where; principle total stresses are $\sigma_{xx} - \sigma_{zz}$ (horizontal and vertical stress respectively), c is cohesion, μ is internal friction, and λ is the Hubbert-Rubey coefficient of fluid pressure. Both expressions demonstrate that differential horizontal stress must be considerably large to initiate fault slip, and that this stress will become lower by increasing fluid pressure, λ. The stress required for activating frictional slip is largely insensitive to rock composition (Byerlee, 1968; 1975; 1978). If fractures already exist in the slip shallow rocks, they will preferentiall be areas of preferential slip, without the need for creating new fractures (Brace and Kohlshedt, 1980). The low strength of salt compared to other lithologies results in it being a décollement for faults in the overburden (Rowan, 2008).

The density of halite is ~2200 kg/m^3 and decreases slightly less with depth due to thermal expansion (Rowan, 2008). Clastic sediments are less dense than salt until ~1000–1500 m, after which compaction causes them to become more dense. This density inversion may be important when considering regional salt tectonics. However,

Vendeville and Jackson (1992) have shown that density contrast, and the effects of buoyant force, is only a second-order relative to the effects differential loading when viewing salt as a pressurized fluid.

There are multiple mechanical considerations for a pressurized fluid source layer underlying a brittle overburden. Fundamental concepts involving salt mobilization and diapir formation were proposed by Vendeville and Jackson (1992) for various scenarios:

1) An underlying diapir typically forms under an unimpeded overburden block independent of the density ratio, and its position either below or above a datum surface if it is less or more dense than the fluid.

2) Not all fluid ridges (reactive diapirs) can rise due to vertical restrictions imposed by friction or overburden shear strength. Similarly, not all thin overburden roofs over a fluid of constant thickness can be pierced, as the strength of the overburden must be overcome by the pressure of upwelling salt.

3) A thin roof of strong overburden above a fluid of constant thickness is inherently unstable, regardless of density ratio. If the strength of a locally thin/weak roof is overcome, the fluid and its overburden will inevitably rise. The forces from pressurized fluid under a trough are always larger than those in an open fluid column (passive diapir), such that P_2 is greater than P_1.

After inspecting the mechanics of salt as a pressurized fluid, it becomes clear that the major factor controlling salt mobilization is differential loading on both regional and local scales. Any force exerted on the salt causes it to adjust in such a way that it does not drive

extension or contraction in a system; rather it passively flows into existing space. For diapirism or salt withdrawal to occur, there must be a set of conditions:

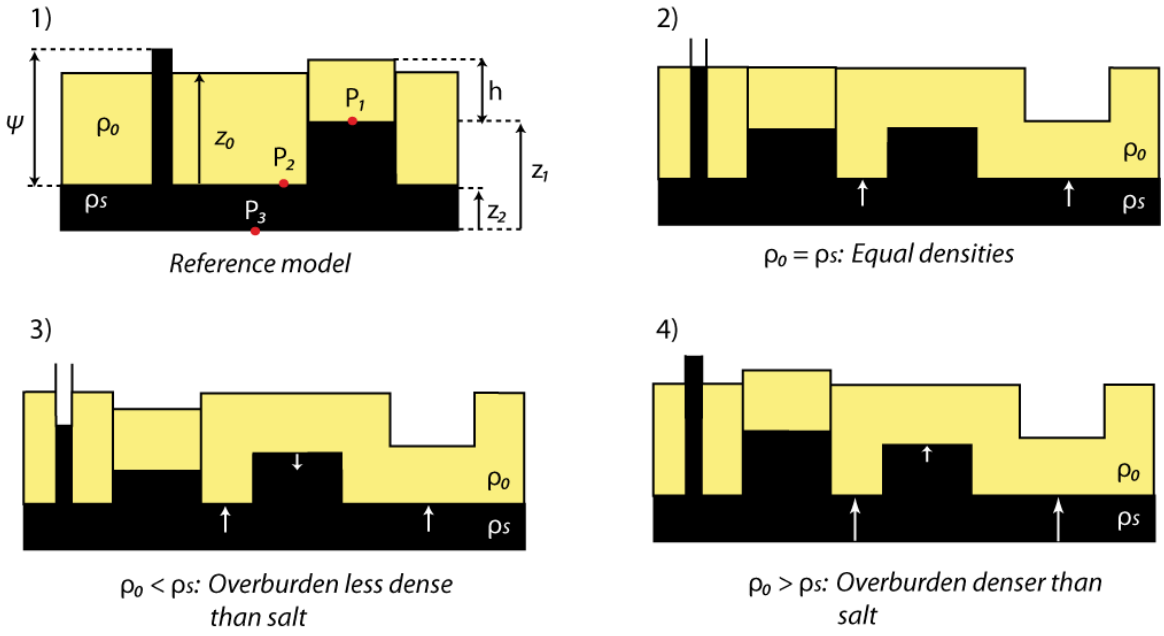

Figure 2-4: Conceptual model of salt as a pressurized fluid after Vendeville and Jackson (1992). Densities (ρ), thicknesses (h), pressures (P), pressure heads (Ψ), and elevations (z) are illustrated for all cases. The datum surface is the top of the left block and salt flows into an open conduit in all cases. The ratio of overburden and salt density is a secondary factor for diapir formation, as long as there is differential pressure and an opportunity for the salt to flow into areas with less pressure. Various density scenarios exist in the models, including: 1) The reference model; 2) Equal densities between sediment and salt; 3) An overburden that is less dense than salt; 4) An overburden that is more dense than salt.

1) There must be an open path to the surface close to a salt body;

2) Overlying sediments must be weak/faulted enough for differential fluid pressure in the salt to overcome overburden strength;

3) Some other processes must create space in the overburden (Rowan, 2008).

2.2.2 Mechanisms of Salt Flow at Passive Margins

During gravity spreading, salt generally flows by two mechanisms: Poiseuille flow and Couette flow (Fig. 2-5). Poiseuille flow results from differential overburden loading and is characterized by highest velocity vectors in the center of the fluid layer, and minimum to none at its boundaries. Couette flow results from overburden translation, and therefore the highest velocity vectors are at the salt/overburden interface and linearly decrease with depth. This flow type requires the overburden to exceed its yield strength and fail by landward extension and seaward contraction, which results in seaward overburden translation (Gemmer et al., 2005). Since Couette flow is the result of induced shear, forces at the salt-sediment interface oppose the motion of translating overburden resulting in viscous drag. In general, very unstable (failing and translating) overburden will yield Couette flow as the dominant flow mechanism, while mildly unstable overburden will induce mainly Poiseuille flow. In both physical experiments and natural cases, evidence of strong Couette flow and viscous drag forces can be seen in Roho systems: highly faulted and extended sedimentary wedge packages with little evidence for downbuilding (Appendix A).

2.2.3 Regional Force Balance of a Sedimentary Wedge Overlying Salt

Both Poisieulle and Coutte flow can be linked to regional deformation in the system at any continental margin with a sedimentary wedge overlying a salt layer (Fig. 2-5). F_1 and F_2 are horizontal forces resulting from landward tension and seaward compression that are related to failure in the overburden, as described in the ***2.2.1 rheological considerations* section**. The force associated with channel flow within the

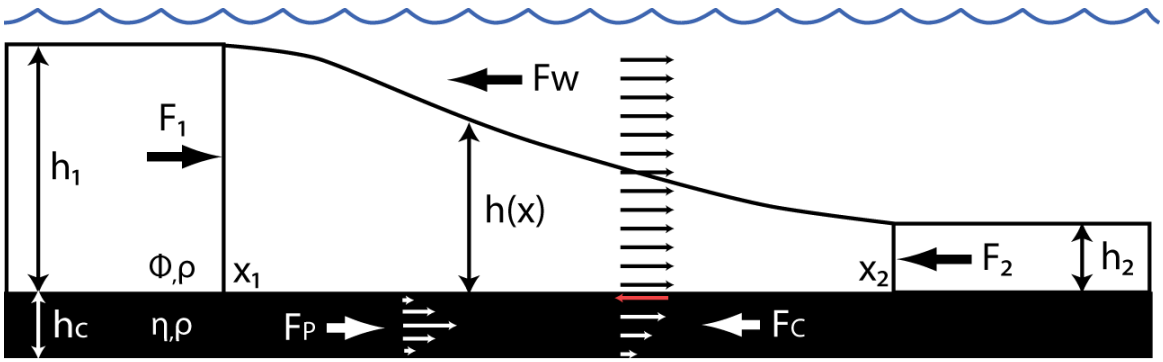

Figure 2-5: Force balance of a passive margin sedimentary wedge overlying a uniformly thick salt layer. Schematic flow vectors are shown to demonstrate the nature of both Poiseuille and Couette flow types. The red arrow is not indicative of flow direction within the salt layer; rather it demonstrates the force associated with overburden drag at the top of the layer. h_1 is the height of landward sediments, h_2 is the height of distal sediments, h_x is the height of sediments at an arbitrary distance, x, x_1 is the landward extremity of h_1, x_2 is the landward extremity of h_2, η is the viscosity of salt, ρ is the density of overburden sediments and salt, F_1 is the limiting tensile failure strength of the landward overburden at failure, F_2 is the compressive failure strength of the seaward overburden, F_P is the drag force exerted on the overburden due to Poiseuille flow in the salt layer, F_C is the basal traction associated with Couette flow, and opposes the landward translation of the overburden, F_W is the water loading force, which opposes the seaward translation of overburden. After Gemmer et al. (2005).

salt layer induced by differential loading, F_P, follows the thin sheet approximation of a viscous fluid (Lehner, 2000) and depends on salt thickness, overburden density, gravitational acceleration, and the height difference from points x_1 and x_2 ($h_1 - h_2$). The viscosity of the salt layer does not affect the force associated with Poiseuille flow, although it does affect the internal velocity distribution. F_C is the force involved with basal traction associated with Couette flow, which imposes a landward force on the translating overburden. F_C is dependent on the viscosity of the salt layer, overburden translation velocity, and salt thickness. F_W is the force associated with the water load, and opposes the seaward translation of the overburden at failure. If forces balance such that:

$$F_1+F_2+F_P+F_W+F_C = 0,$$

the system is stable and no deformation will occur. If the system is stable, there is no overburden translation and therefore no F_C component. F_1 and F_2 are independent of salt thickness, and between h_1 and h_2, the sedimentary wedge will fail by gravity in the difference is high enough to result in instability. Differential load between h_1 and h_2 will also induce Poiseuille flow, since it will induce differential pressure in the salt layer. The ratio between F_1 and F_2 determines the amount of horizontal translation that the overburden will experience in the basinward direction upon failure. The velocity of translating overburden governs the basinward directed Couette flow in the salt layer, which has an equal, but opposite force (F_C) to that resulting from overburden translation acting at the salt sediment interface. Therefore, with failure in the sedimentary wedge and both forms of salt flow, basinward directed deformation could be described as:

$F_1+F_P>F_2+F_C+F_W$.

Another important consideration is the effect of the load of the water column. From finite-element geodynamic models, it has been established that water load will generally cause the system to take twice as long to deform than without (Steven Ings of the Dalhousie Geodynamics Group, pers. comm.). Water load counteracts landward failure, causing the system to take longer to develop, through a number of mechanisms: 1) the water density acts as an extra load that increases the pressure and strength of seaward overburden, 2) the vertical component of the water load reduces the lateral density variation and differential load of the system at the slope of the sedimentary wedge, and therefore reduces the force associated with basal traction at the salt-sediment interface induced by Poiseuille flow (F_P), and 3) the water load acts as a pressure that is normal to

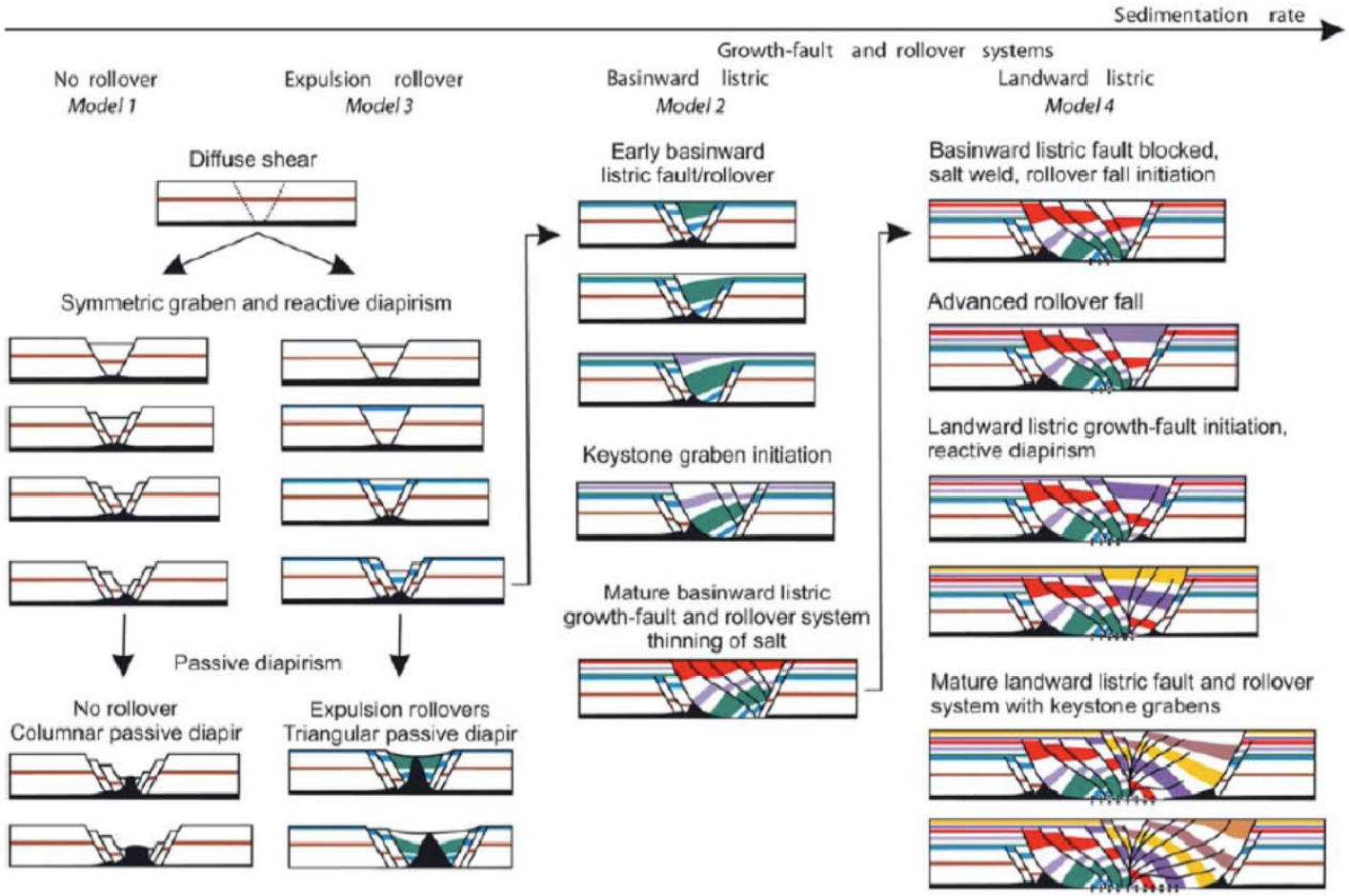

Figure 2-6: Structural evolution of passive diapirs and expulsion/fault rollover systems with increasing sedimentation rate. For a uniformly thick silicone layer, passive diapirs only form under low sedimentation regimes where sediment accumulation is too slow to counteract active diapiric rise. With increasing sedimentation rate, silicone is mobilized seaward, and the seaward flanks of early reactive diapirs become the site of a seaward dipping listric faults. After Krezek et al. (2007).

the sediment surface, which acts as a horizontal buttress to the sloping overburden (Gemmer et al., 2004). Further discussion about the implications of water column load is presented in Gemmer et al. (2004).

2.2.4 Effects of Sedimentation Patterns and Rates

Scaled physical experiments with layered brittle and ductile materials have shown that the development of salt structures, such as growth-fault and expulsion rollover systems are strongly affected by sedimentation patterns and rates (Krézsek, et al., 2007). Although differential loading was found to govern experimental margin-scale stress and extensional spreading, feedback between dynamic depositional systems, fault-controlled subsidence, and salt mobilization controlled the strain history of local structures. Symmetric grabens with reactive diapirs occurred during the early stage of extensional deformation in all experiments conducted by Krézsek et al. (2007). With low sedimentation rates, early graben evolution ceased and passive diapirs developed. In cases where silicone inflated sufficiently, expulsion rollovers developed as a result of long-lived downbuilding into their flanks. In experiments with high sedimentation rates, graben systems developed into basinward listric growth-fault and rollover systems. Observation of experiments with high sedimentation rates suggest that the increasing rate at which the transformation takes place is correlated with increasing sedimentation rate. With very high sedimentation rates it is possible to switch from basinward to landward listric growth-fault systems. This occurs when additional sediment loading increases salt withdrawal beneath the hanging wall of the basinward listric growth-fault and rollover, and increases basal coupling. This increased basal coupling results in a high degree of viscous drag, and consequently leads to the development of counter-regional faults. A

summary of experimental structures developed with varying sedimentation rates is shown in Fig. 2-6.

2.2.5 Effects of Basin Configuration

It has been proposed by Nelson (1991) that sediment progradation over a layer of salt with constant thickness is ineffective for diapir initiation. To test this idea, Ge et al. (1997) completed a series of physical experiments that had either a basin with a flat base, or a basin with basement steps representing landward-facing fault scarps (Fig. 2-7). Silica sand was used as an analogue for brittle overburden sediments, whereas either a silicone polymer or a dense Silbione gum simulated salt.

In experiments with a flat base, salt was expelled basinward of the prograding wedge and became evenly inflated, forming a distal, sediment-starved plateau. All brittle deformation in the overburden was concentrated in the distal region of the wedges and formed three seaward migrating domains. The first domain hosted an expulsion rollover, the second domain consisted of a rollover syncline, and the third domain included a progressively steepening landward-oriented limb of a salt-cored monocline. The migration of these zones also resulted in a seaward younging salt weld surface, upon the total evacuation of salt. Accordingly, no diapirs formed in the model testing a tabular pre-kinematic salt layer.

Experiments with basement steps each had a similar early evolution to those in the tabular salt models, but middle and late structural evolution was more complex. Continued seaward flow of salt was restricted at each basement step, resulting in broad inflation in the form of salt-cored anticlines. Anticlines were more likely to form when

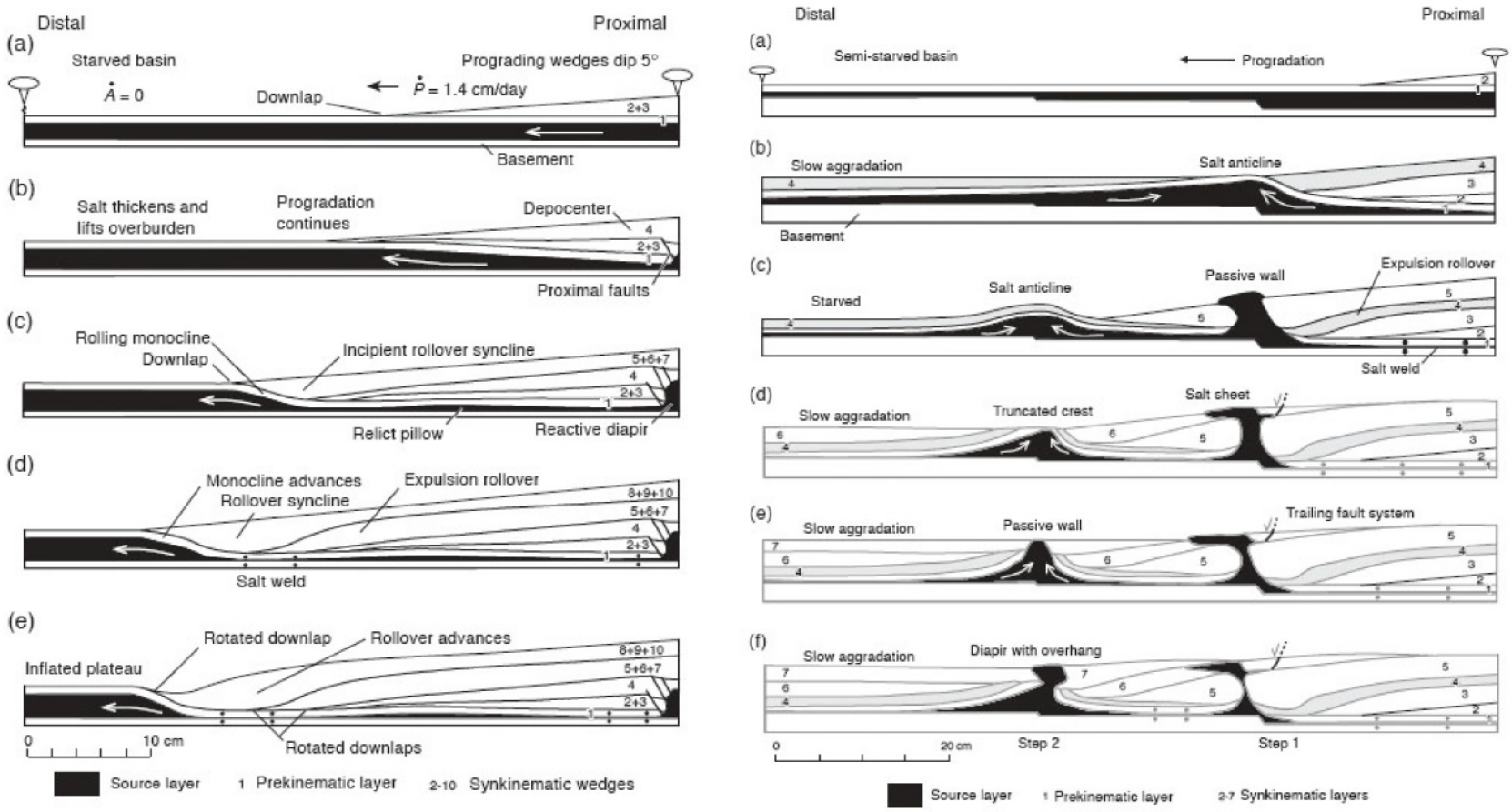

Figure 2-7: Comparison between model evolution with experiments testing a tabular basin (left) and a setup with landward dipping steps (right). In the case of the tabular basin, silicone is withdrawn from its autochthonous position with little to no restrictions. Sand progressively downbuilds into distally inflated silicone, resulting is a large monocline or expulsion rollover. When steps are present in the model basin, silicone inflation becomes localized at each change in silicone thickness, resulting in silicone-cored anticlines. These anticlines then evolve into passive diapirs, which may feed allochthonous silicone canopy systems. After Ge et al. (1997).

progradation overcame seaward salt movement. Aggrading distal sediments employed in these models pinned the position of salt-cored anticlines by hindering basinward propagation. The anticlines then became sites of active, and then passive diapirs, which fed allochthonous salt sheets and canopies. These long-fixed diapirs also formed expulsion rollovers on their flanks with continued downbuilding. To build on the concepts of Ge et al. (1997), MacDonald (2007) and Campbell (2007) tested a variety of basin geometries to further understand its effect on salt mobilization and diapir localization (Fig. 2-8). The experiment with a half-graben step closely resembled that of Ge et al. (1997), and yielded similar results. However, it was found that the buttress effect due to the geometry of fault steps or the basinward rift shoulder was less important than the self-limiting nature of salt thickness. As an example, salt withdrawal was more efficient at regions with abrupt changes in salt thickness than over a regionally tapering wedge of salt (Fig. 2-8). The conclusions of Ge et al. (1997) were then refined by MacDonald (2007) and Campbell (2007) to show that salt-cored anticlines and diapirs initiate at areas with changes in salt thickness. This finding can be understood by considering a 2D profile with an abrupt change from a thick layer to a thin fluid layer. Following that initial salt mobilization due to only differential loading should translate as Poiseuille flow; the flow vector conditions in both layers can be defined as (Gradmann et al., 2009):

$$F_P = (h_C/2)\rho g(h_1 - h_2)$$

Where h_c is the thickness of the ductile fluid, ρ is the density of the overburden, g is gravitational acceleration, and $(h_1 - h_2)$ is difference in thickness of the overburden.

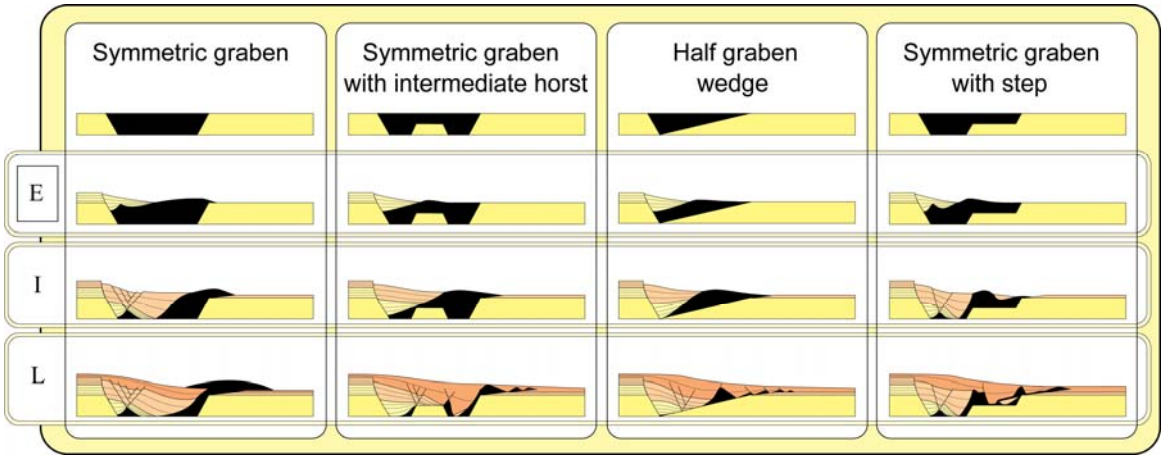

Figure 2-8: Comparison of early (E), intermediate (I), and late (L) stages of model evolution with varying basin architectures from MacDonald (2007) and Campbell (2007). Through these experiments it was found that the buttress effect of rift shoulders or intermediate steps was not as important for silicone inflation as the self-limiting characteristic of the silicone thickness itself.

Following this relationship, the region at the thicker layer will have a tendency to flow faster than the thin layer. When the large area of rapidly translating fluid encounters the thin and slow seaward flowing fluid, the result is the formation of an inflated complex that may evolve into a passive diapir with further progradation of the sedimentary wedge.

3.0 Geologic Framework of the Scotian Margin

3.1 Tectonic Evolution of the Scotian Margin

3.1.1 Rifting

The present-day Scotian margin (Fig. 3-1) extends from the Yarmouth Arch in the south to the Avalon Uplift of the Grand Banks in the north (Wade et al., 1995). The recent geologic history of the margin began with the break-up of Pangea during the Middle to Late Triassic (Fig. 3-2). The Scotian margin is located in a transitional area, being situated between volcanic margins in the south (southern Baltimore Canyon Trough) and non-volcanic margins to the north (Grand Banks and Newfoundland Basins) (Wu et al. 2006). In order to study rifting processes, Keen and Beaumont (1990) combined observations from seismic profiles with geodynamic models to understand differences in evolution between the southern (LaHave Platform) and northern regions (Sable sub-basin). Results demonstrated that the LaHave Platform and Scotian Basin had considerably different rifting histories, particularly for the relative timing and amount of crustal and sub-crustal thinning, and the width of the basinal transition zone. LaHave Platform models yielded a convex crustal thickness profile, with a narrow margin-perpendicular transition zone (~100 km). Early and landward sub-crustal thinning of the mantle lithosphere was noted to have produced significant uplift (2 km maximum), which limited crustal thinning was unable to counteract. Scotian Basin models yielded linear-concave crustal thickness profiles, with margin-normal transition zones of ~240 km. As the crust was thinned from the onset of rifting there was probably little to no initial uplift of the rift shoulder. The rapid and long-lived subsidence generated by this model helps to explain the formation of the deep Sable sub-basin and

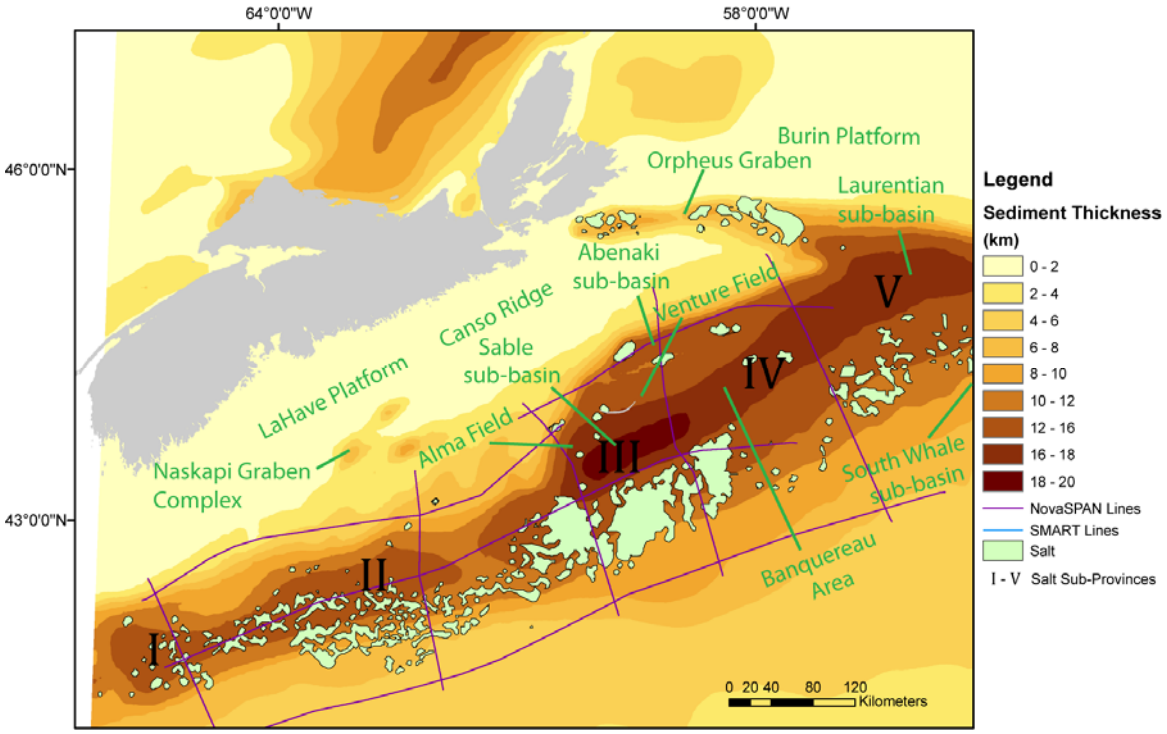

Figure 3-1: Sub-basins and Salt sub-provinces of the Scotian margin. The Sable sub-basin is the deepest region of the margin and hosts the thickest sediments as well as complex salt structures such as extensive tongue-canopy systems that define Salt Province III, as described by Shimeld, 2004.

the oblique trend of the hinge line. More recently, Funck et al. (2004) and Wu et al. (2006) have completed seismic refraction modeling of the SMART (Scotian MARgin Transects) wide-angle data in order to image and understand the nature of the crustal structure at the LaHave Platform and the northern Sable sub-basin. Results by both groups generally agree with thermo-mechanical modeling done by Keen and Beaumont (1990), with exception of having a predicted ~0.75 km uplift in the LaHave Platform rather than 2 km, due to more extensive crustal thinning in nature. Wu et al. (2006) also investigated the volcanic to non-volcanic transition along the margin strike and the character of the ECMA (East Coast Magnetic Anomaly). They discovered that rather than having magmatic intrusion and extrusion at the continent-ocean boundary, such as along the US East Coast, the Scotian margin is dominantly non-volcanic and the

continuation of the ECMA from the southwest documents regions of serpentinized mantle. The southern region of the Scotian margin was also found to have normal magma supply, whereas the northern region (including north-central Sable sub-basin) was found to be magma-starved.

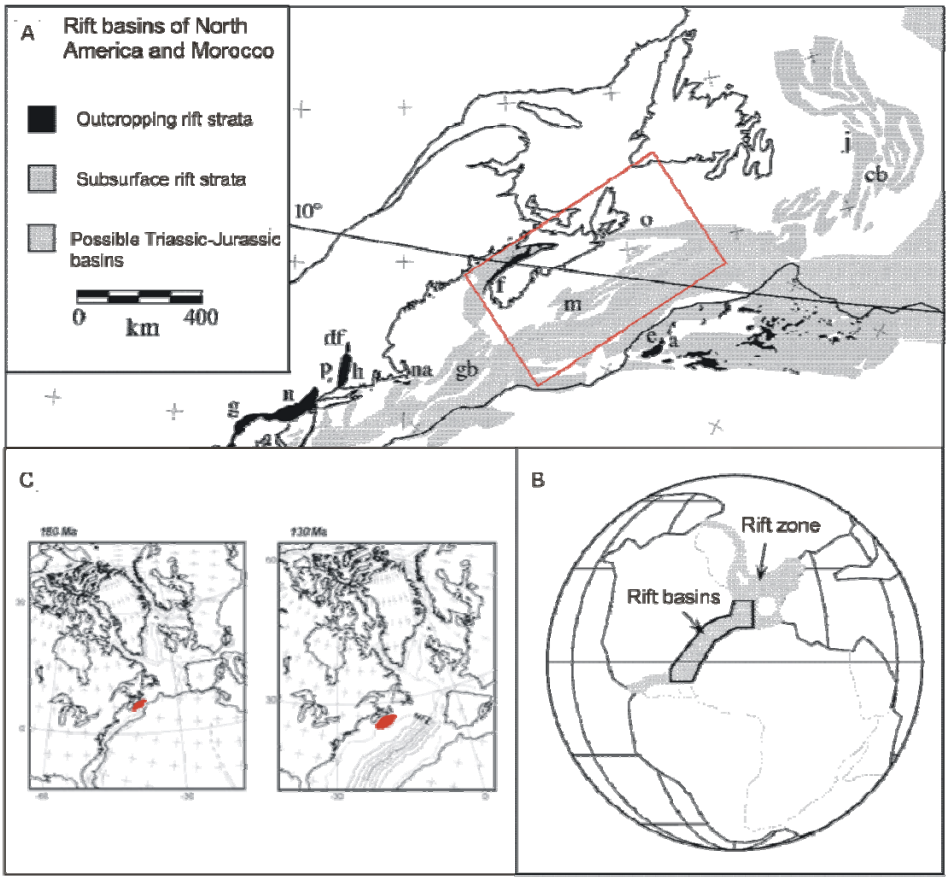

Figure 3-2: A) Rift basins of the Scotian margin (red box) basins: f, Fundy basin; m, Mohican basin; o, Orpheus basin. B) Paleogeographic reconstruction of Pangea during the Late Triassic (Carnian), showing the rift zone (grey) and the Scotian margin rift basins (outlined grey) that were shown in (A). Modified from Olsen, (1997). C) Plate reconstruction of North Atlantic rifting at 180 Ma, 130 Ma. Red indicates the approximate location of the Scotian margin at these times. The Scotian margin was formed during the separation of North America and Africa before chron M29 (160 Ma) (from Coffin *et al.*, 1992). Sources for map are Olsen et al (1989), Holser et al (1988), Tankard & Balkwill (1989), Heyman (1989), Hutchinson & Klitgord (1988a,b), Benson (1992), and Beauchamp (1988).

Representative crustal profile are based on nominal layer gravity models created by Zheng and Arkani-Hamed (2002) (Fig. 3-3 & 3-4) with the use of bathymetry data from ETOPO5 (NGDC) and depth to basement data (Oakey and Stark, 1995). Their

models were then compared to observed Bouger gravity anomalies that were acquired from Geostat data (National Gravity Data Base, Geomatics, Canada, and Sandwell and Smith, 1997). The nominal layer gravity models created by the authors agree with observed Bouger gravity anomalies (Zheng and Arkani-Hamed, 200), and reveal that the top crust surface along the Sable sub-basin is regular, but contains minor geometrical variations in its landward and distal regions. Although the profiles appear to represent a good regional fit in the basin trend, inspection of the recently acquired, 2003 ION/GXT NovaSPAN seismic reflection dataset demonstrates that the models are not high enough in resolution to represent local structural variations, such as the small horst block observed in NovaSPAN Line 1600.

3.2 Salt Sub-Provinces

A variety of salt structures have been documented at the Scotian margin. Shimeld (2004) attempted to describe these structures and put them into a geographical framework. Based on the interpretations of the dense, regional, time-domain TGS-Nopec seismic dataset, salt-related structures were categorized into five distinct sub-provinces, which vary laterally along strike at the margin (Fig. 3-1).

3.2.1 Salt Sub-Province I

Salt sub-province (SP) I is located in the southwest-most portion of the margin, in the Shelbourne region. Landward regions contain elongate diapir walls, which are arcuate in map-view and are 2 to 8 km wide. Marginal synclines between these walls document passive downbuilding and may be 8 to 10 km long. The diapirs appear to have

been depleted by the start of the Paleocene, as overlying seismic horizons are generally concordant.

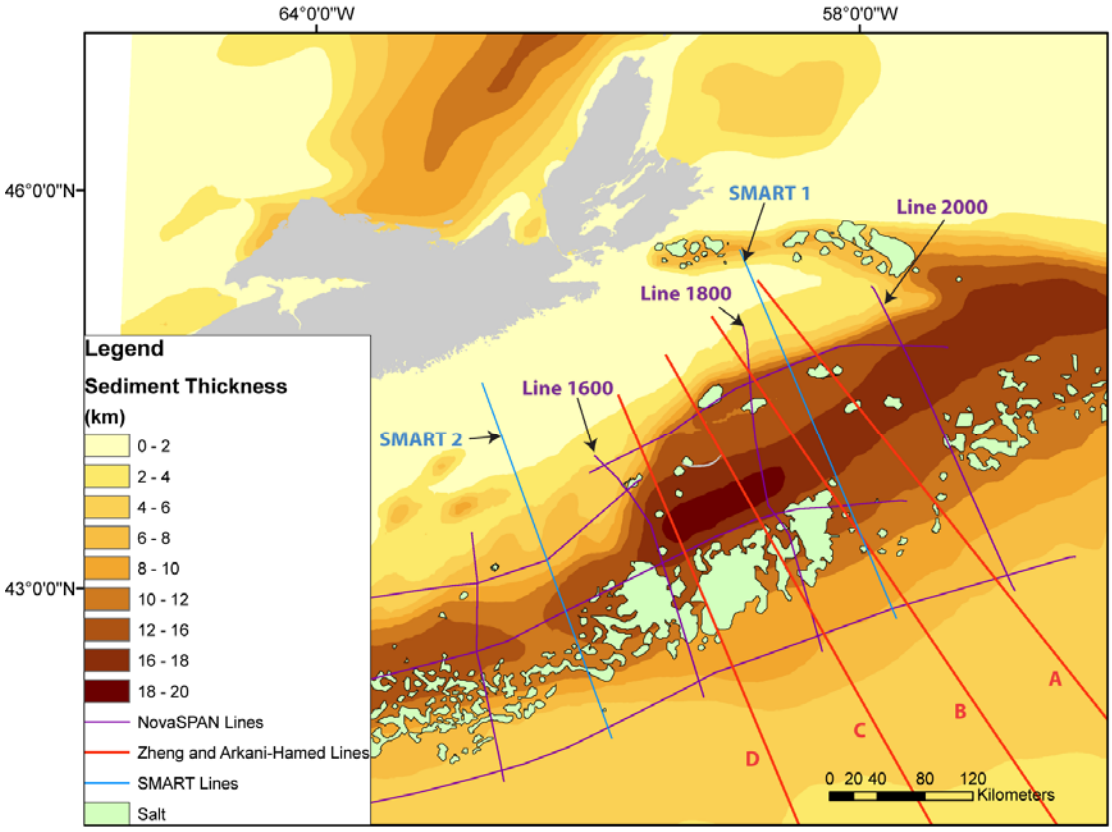

Figure 3-3: NovaSPAN, SMART and Zheng and Arkani-Hamed (2002) transects are overlain on sediment thickness to show the position of crustal profiles in figure 2. Transects by Zheng and Arkani-Hamed (2002) extend beyond the border of the map.

Diapirs in this region also have seaward overhangs; this is possibly due to a sea-floor gradient, reduction in sedimentation rate, and perhaps rejuvenation due to late-stage compression. The late-stage compression is marked by crestal grabens overlying diapirs, which potentially formed during the late Paleogene or early Neogene and ended by the Pliocene. Seaward, a salt tongue canopy-system is well imaged, with strong reflectors at its top and base. The tongues appear to extend 15-20 km seaward of their feeding stocks

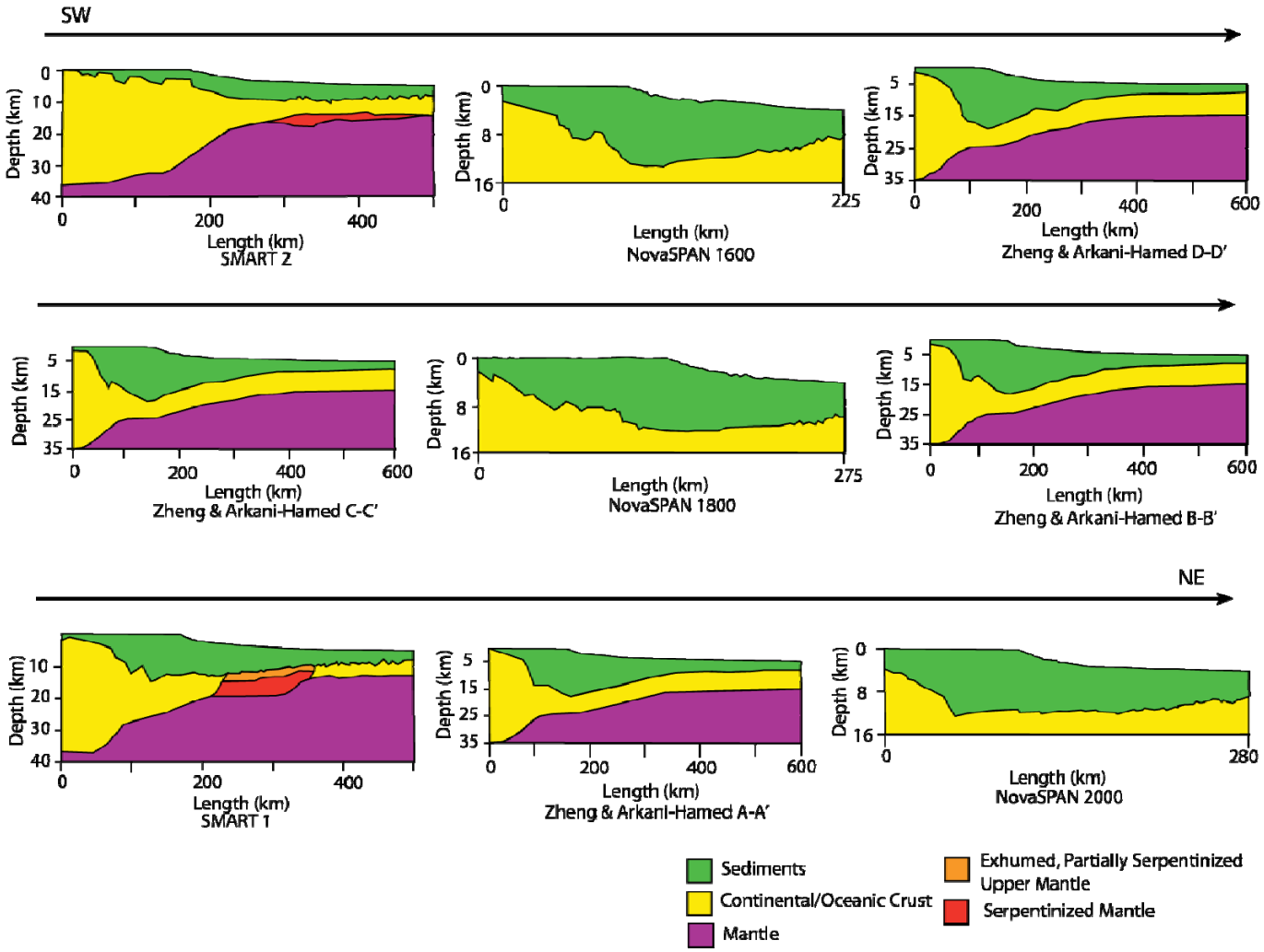

Figure 3-4: Crustal structure along the margin from southwest to northeast. Positions of each profile are shown in figure 1. For simplicity, both continental and oceanic crust (yellow) and sediments/salt (green) are grouped together.

and climb to a maximum interpreted stratigraphic level of Callovian to early Oxfordian, Upper Jurassic.

3.2.2 Salt Sub-Province II

SP I gradually transitions into SP II eastwards along-strike. Here, linear salt walls are generally parallel to the Jurassic carbonate bank (NE – SW), which is known as the Abenaki formation. Seaward, isolated cylindrical diapirs occur beneath the regions of the upper-slope. Marginal synclines between diapirs are generally broader than in SP I, ranging from 8 to 20 km. Tongue canopies are generally absent in this region, except at the western transition.

Vertical diapirs are common in the western portion of SP II; however, further east they become mushroom-shaped and have seaward-verging overhangs. This progressive change is interpreted to be the result of varying basin-floor morphology along-strike. It may be interpreted that during the passive stage of the mushroom-shaped diapirs, the seafloor was broad with very little slope. Diapirs further east with seaward-verging overhangs are interpreted to document a more pronounced seaward gradient of the seafloor. Diapirs in the easternmost region of SP II are highly squeezed, potentially detached, and have overlying crestal grabens. All of these features are interpreted as being related to compressional forces acting on pre-existing diapirs and considerable uplift of diapir crests (Shimeld, 2004).

3.2.3 Salt Sub-Province III

SP III is generally representative of the Sable and Abenaki sub-basins. The most significant features that are used to define this sub-province are extensive deepwater tongue canopies (Fig. 3-5), which overlie Cretaceous and potentially older units.

Youngest sediments overlying these canopy systems are believed to be latest Cretaceous, and appear to be mainly extensionally deformed into a variety of structures including turtles (Appendix A1) and mini-basins. Seismic imaging is generally poor below the canopies; however, it is believed that they are fed from multiple feeders rather than an elongate salt wall.

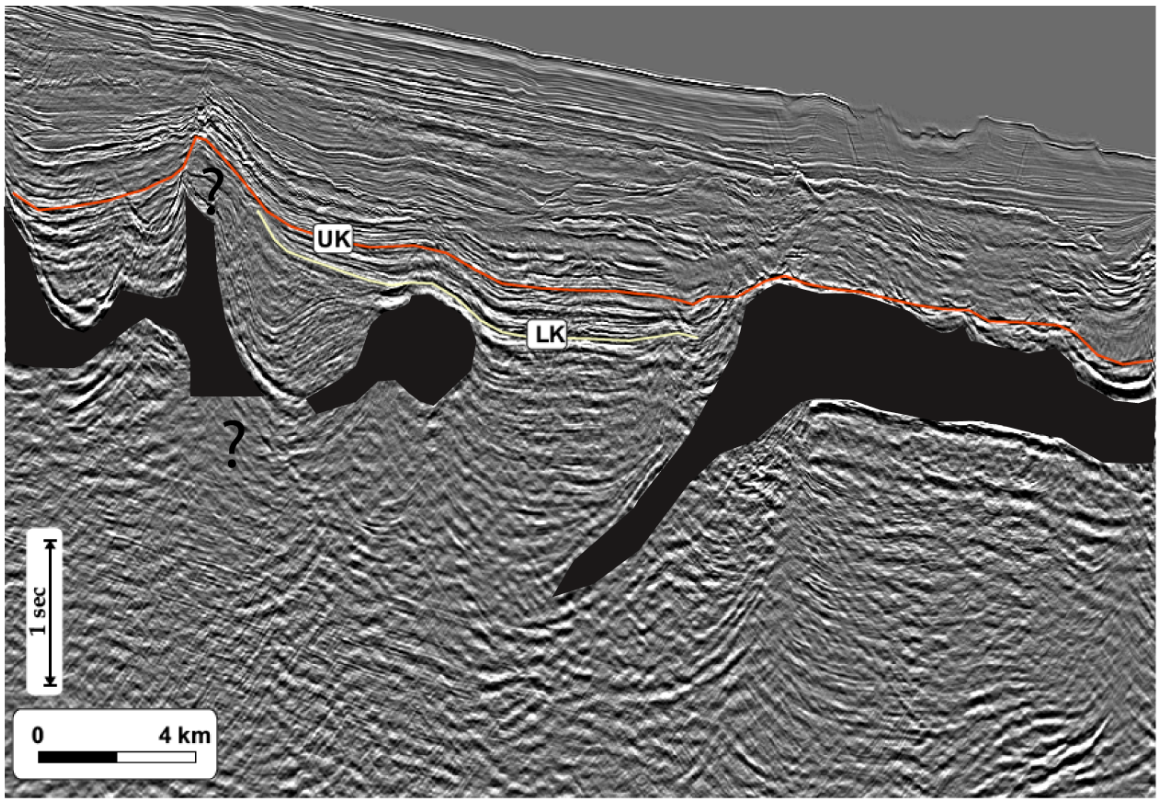

Figure 3-5: Salt diapir and tongue-canopy system in Salt Province III. Salt structures are interpreted as being covered by a thin portion of upper Cretaceous strata. Spreading of the allochthonous salt has occurred at the top of the lower Cretaceous horizon. Modified from Shimeld, 2004.

Eastern regions of SP III generally yield better seismic imaging under tongue canopy systems. In these regions, Lower Cretaceous reflectors underlying canopy systems appear to be undeformed and no feeders are present. This implies that the allochthonous salt canopies traveled 80 to 100 km seaward. The sub-horizontal nature of

the canopies also suggests a period of relatively rapid salt movement, and/or low sedimentation rate. These lobate canopies generally extend 150 km along strike.

3.2.4 Salt Sub-Province IV

Two major features define SP IV: the lack of diapirism and the Banquereau syn-kinematic wedge (BSW). The BSW is defined as a seaward thinning, ~3.5 km thick package of highly faulted landward, dipping reflectors between a regional salt detachment and the upper-most Jurassic. In the seaward direction the BSW is well above basement and climbing stratigraphically at discrete steps. This syn-depositional relationship suggests that the BSW was formed over a salt nappe as it climbed higher and further basinward in the stratigraphic section. The detachment level climbs higher at its eastern and western limits, giving it a concave-upward geometry. As there is little growth and high amounts of extension over the detachment, it is likely that it was an open-toe allochthonous salt body. Such a system would have an unstable overburden, which would result brittle failure, and therefore viscous drag at the salt/sediment interface with Couette flow in the salt layer. This viscous drag force would be a viable mechanism for the extensive faulting, and landward rotation of overlying sediments that characterize the BSW (Ings and Shimeld, 2006).

In the present-day middle and lower slope, isolated diapirs are sourced from the nappe salt level. These diapirs lie along an arcuate trend and are associated with rim synclines, which appear to have been affected by later compression.

3.2.5 Salt Sub-Province V

The BSW extends into the western portion of SP V, although it is often obscured by shallow salt tongue canopies. Over Jurassic salt detachments, extensional structures such as rafted mini-basins and turtle structures are observed within the Cretaceous section. Contraction affects the late Cretaceous to Neogene strata and emplaced salt structures, such as basinward-leaning diapirs that appear to be rejuvenated. Diapirs that exist in the slope climb highest through the stratigraphy, and extend to ~100 m below the sea floor.

3.3 Stratigraphy

The stratigraphy of the Scotian margin (Fig. 3-6) is defined on the basis of publicly available seismic reflection and well data in the shelf (Jansa and Wade, 1975; Wade and MacLean, 1990; Piper et al., 2004; Cummings et al., 2006). With new publicly available well data and seismic reflection datasets in the slope and deepwater, this study attempts to extend the chrono-stratigraphy into sparsely documented portions of the margin.

3.3.1 Break-up Unconformity

The break-up unconformity is indicative of the change from sub-aerial conditions with marine incursion, to a true marine setting. Sub-aerial conditions during continental break-up are the result of thermally induced uplift of the rift shoulder. Because of later cooling and thermal subsidence, the rift valleys then become submerged and are sites of early post-rift shallow marine deposits. In shelf regions, the break-up unconformity occurs as a regional seismic marker that separates the spatially restricted and deformed

Upper Triassic to Lower Jurassic strata from undeformed Lower Jurassic and younger strata. In the rift basins, the unconformity is unrecognizable as sediments are deformed by salt mobilization.

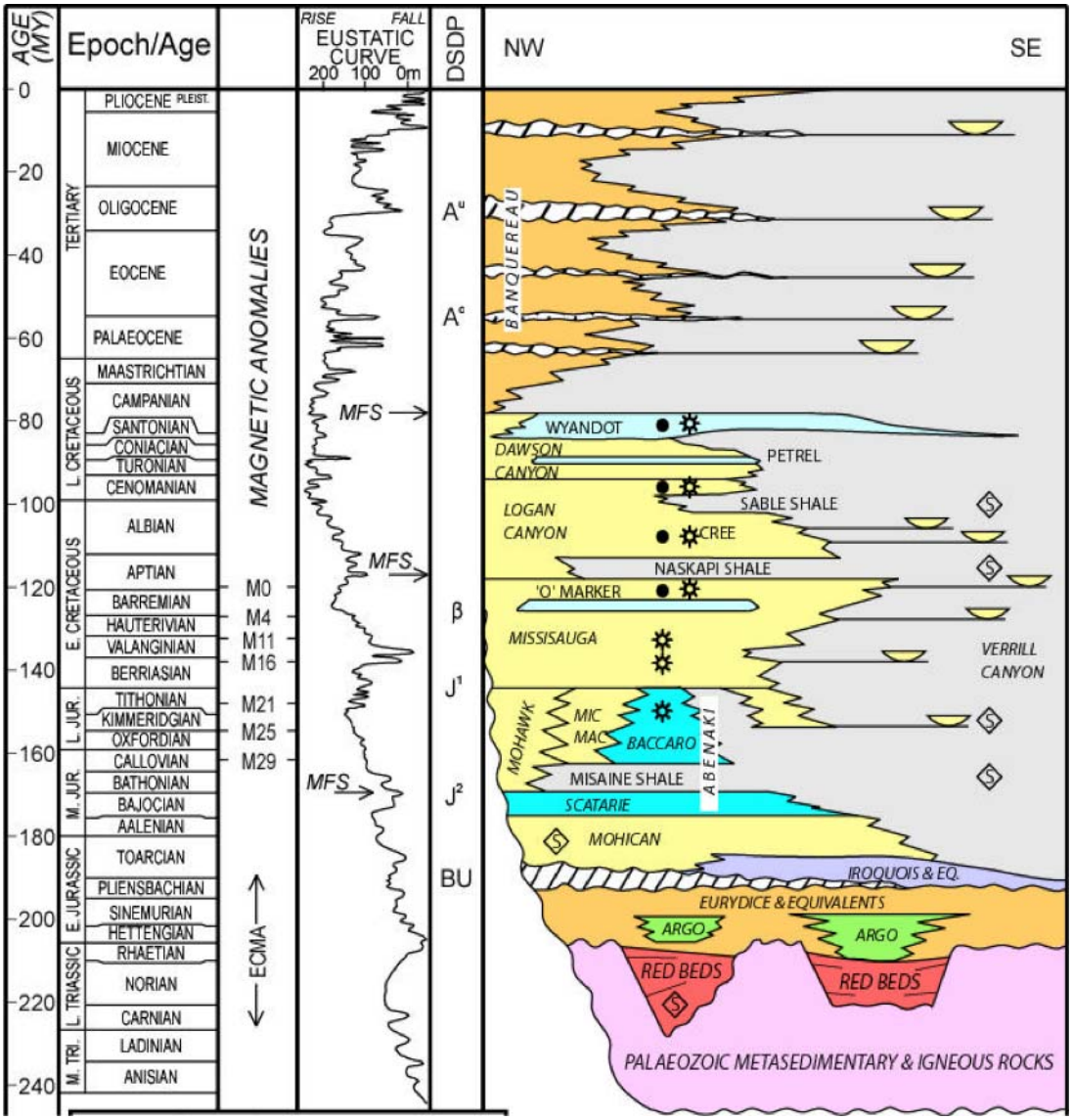

Figure 3-6: Stratigraphy of the Scotian margin with the global eustatic curve (Kidston et al., 2007). Stratigraphy modified from Wade (1993, 1995). Eustatic curve from Haq et al (1987). Time scale from Palmer and Geismann (1999).

3.3.2 Eurydice and Argo Formations

The oldest Mesozoic sequences in the Scotian Basin are the coeval Eurydice and Argo formations. The syn-rift sediments of the Eurydice formation are known from numerous wells to consist of red-brown silty shale, thin red sandstone and siltstone beds, and minor amounts of limestone and evaporites. The total thickness of the formation is interpreted to be greater than 3 km as evidenced by seismic data, reaching several kilometers in rotated fault blocks at the hinge zone of the LaHave Platform.

The Argo formation overlies and interfingers with the Eurydice formation in deep rift grabens. It consists of a series of massive colorless to pale-orange salt beds that is coarsely crystalline. The salt beds are separated by zones of red shale, suggesting that salt cumulates were deposited in brief periods of marine incursion that were followed by extended periods of little to no deposition. The Argo formation is anomalous in that it is anhydrite deficient. Typically, normal evaporation of seawater produces considerable amounts of early calcium carbonate and calcium sulphate. The absence of carbonate and sulphate minerals in the succession suggests that that salt precipitated from a previously depleted brine (Jansa et al., 1980).

The original thickness of the undeformed salt is not known, because of its present depth and extensive mobilization into distal parts of the basin. Regions affected by significant salt withdrawal are characterized by thick growth packages or by large, deeply soled listric faults. Recent regional seismic profiles provide evidence for a thick (>2 km) initial salt layer. Since the Argo formation was deposited during syn-rift crustal thinning, extension, and subsidence, salt thickness along the margin should vary along the margin (Fig. 3-7).

3.3.3 Iroquois and Mohican Formations

The post-rift succession begins with the deposition of the Mohican formation continental-clastic deposits and locally restricted carbonates of the Iroquois formation. The Iroquois formation is approximately late Sinemurian to early Pleinsbachian in age and is up to 1.6 km thick, as seen in wells at the southwestern Scotian

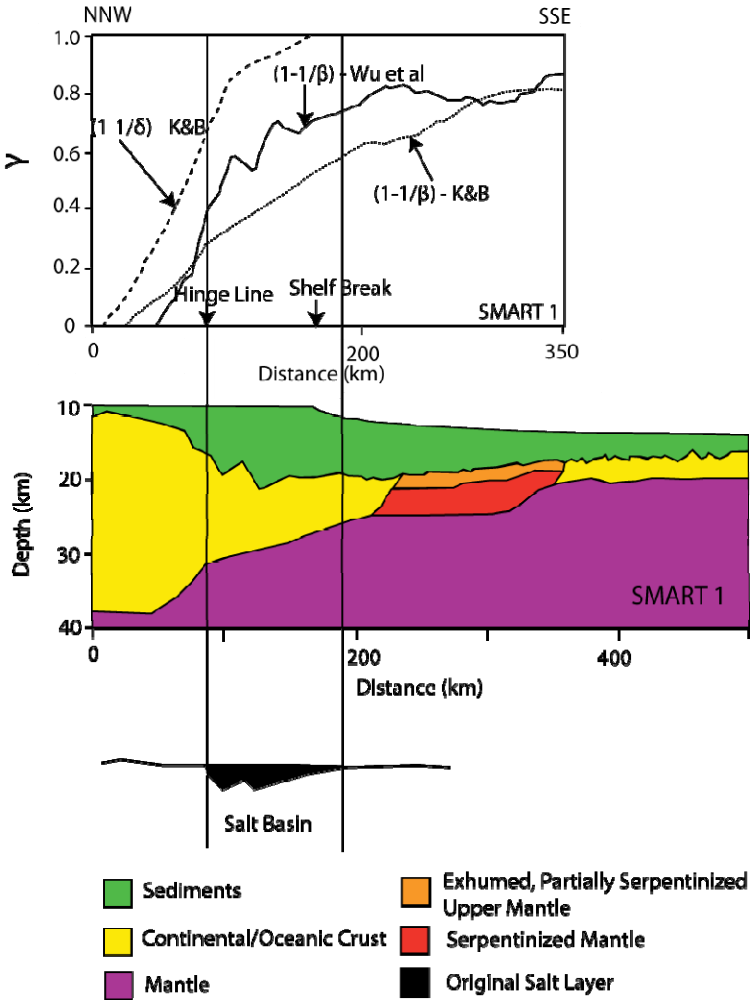

Figure 3-7: Relationship between syn-rift thinning of the mantle lithosphere (δ) and continental crust (β), and original salt thickness in the SMART 1 transect. γ refers to the amount of extension for either measurement of fractional thinning (1-1/ δ) or (1-1/β). Note that at the most abrupt crustal thinning (1-1/ β) there is thickest salt. K&B are model trends taken from Keen and Beaumont (1990). Thick salt in this region is based on growth relationships between seismic reflectors in the seismic profile, which is not shown in this report. Modified from Wu et al. (2006).

Shelf. It is typically dolomitic, and directly overlies salt diapir structures, leading to its interpreted as a caprock facies (Jansa and Wade, 1975). The Iroquois formation is coeval with the lower part of the Mohican formation and is best developed along the outer-edge of the LaHave Platform, where carbonate deposition was favored. Carbonate deposition was favored at the LaHave platform, because at this time water depth was relatively shallow in comparison to the northeast portion of the margin, where earlier and higher crustal extension resulted in increased subsidence.

The Mohican formation is a clastic unit with few sedimentary structures, which is stratigraphically positioned between the Iroquois dolostone and Abenaki formation limestone. The formation consists of dolomitic siltstones and fine-grained sandstones that are interbedded with shales. The age of the Mohican formation is approximately Aalenian to early Bajocian based on palynological studies (Davies, 1986) Post-breakup surfaces along the margin are completely in-filled by the Mohican formation, erasing extensional features in the shelf. This results in irregular thickness variations of syn- and post-rift graben fill. The top of the Mohican is generally picked below the Scatarie Member of the Abenaki formation, which is a thin regional carbonate layer. Thick carbonates within the Mic Mac formation are not part of the Abenaki formation. Instead, they are localized limestone facies that cap prograding clastic wedges.

3.3.4 Abenaki Formation

The Abenaki formation is predominantly a limestone unit and is broken into 4 members: the Artimon, Bacarro, Misaine and Scatarie (Eliuk, 1978). The formation is limited in areal extent, and is best developed at the hinge between the LaHave Platform and the Sable Sub-basin. To the southwest, the formation follows the hinge zone to the

southern termination of the Sable Basin. Beyond the platform to the northeast, the formation interfingers with the clastic and carbonate facies of the Mic Mac formation. The age of the Abenaki formation has been estimated as Callovian to Berriasian or Valanginian (Barss et al., 1979) or Callovian to Tithonian (Ascoli, 1976).

The lowermost member of the Abenaki formation (Scatarie Mbr) is the most extensive unit and is used to pick the top of the Mohican formation. The Scatarie Member is present over much of shelf from the Canso Ridge and the LaHave Platform. Since it is a relatively thin package of oolitic limestones, it provides good acoustic impedance contrast between Jurassic clastic sequences and is easily interpretable in seismic profile. In cross-section the member is a seaward thickening wedge. The Scatarie Member extends further seaward at the LaHave Platform than at the Canso Rdige. The age determined for the member is Bajocian to early Callovian (Ascoli, 1976; Barss et al., 1979).

3.3.5 Mohawk and Mic Mac Formations

The Mic Mac formation is the up-dip facies equivalent of the Bacarro Member of the Abenaki formation. The formation consists of shale and siltstone, sandstone, and carbonates, which are thought to be shallow marine back-bank deposits. Based on Formanifera and Ostracoda, the age of the Mic Mac formation is Bathonian-Callovian to Tithonian (Ascoli, 1976). Therefore, the top of the formation is slightly below the Cretaceous-Jurassic boundary.

The Mohawk formation is predominantly sandstone, representing a more continental/proximal facies than the Mic Mac formation, beneath the western Scotian

Shelf. In Mohawk B-93, the lithology is fine to coarse-grained feldspathic sandstone and siltstone, with interbeds of green, red, and grey shale, and light brown micritic to oolitic limestone. Its age is Berriasian-Valanginian (Barss et al., 1979) or Bathonian to Late Kimmeridgian or Tithonian (P. Ascoli *in* Wade and MacLean, 1990).

In the Sable Sub-basin, the Mic Mac formation is characterized by a series of thick, seaward and upward building sequences. These are interpreted to consist of a limestone-sandstone topset, a sandstone-shale foreset, and a shale-sandstone bottomset. As the sequences prograded seaward, the topset limestone beds become progressively younger. In the Venture area, the Mic Mac formation has been encountered at approximately 5100 m, and is present as predominantly dark grey shale with interbeds of siltstone and sandstone and occasional thin limestone beds. The depositional environment in this area was outer neritic.

East of the Abenaki carbonate bank is a thick alluvial plain that fed deltaic or paralic sequences into the rapidly subsiding sub-basins. Distally, all these units pass into Verrill Canyon formation shale.

3.3.6 Avalon Unconformity

At the end of the Jurassic, the eastern margin of Canada was affected by the breakup of the Iberian and North American plates. The Grand Banks south of Newfoundland were affected most strongly, with uplift, deformation, and extensive erosion of Jurassic sediments. In the Scotian Basin, the Avalon Unconformity is present across the inner part of the Canso Ridge, the Orpheus Graben, Burin Platform, the

western flank of the Laurentian Sub-basin and the eastern flank of the South Whale Sub-basin.

3.3.7 Missisauga Formation

The Missisauga formation conformably overlies the Mic Mac formation except in proximal areas of the LaHave Platform where erosion, associated with Early Cretaceous regession, cut into upper Jurassic sediments. There are two type sections that were originally used to describe the Missisauga formation as defined by McIver (1972). The updip facies observed in well Missisagua H-54 is a thick, dominantly sandstone sequence that is interpreted as being deposited in an alluvial plain environment. The downdip type section, which was defined in Cree E-35, has a much lower sand-shale ratio and yields less massive and thinner sandstone beds than the updip section. The depositional environment of the downdip section is interpreted as lower delta plain to inner neritic. In the Banquereau area (known from Banquereau F-34), coarse clastic content is reduced and there is increased shale content. The Banqeureau area was likely a marine shelf environment at this time.

As a result of its fluvial nature, the Missisauga formation is variable in thickness, and ranges from east to west as being absent in the Avalon Uplift, to 2 km in the Venture area, to less than 500 m on the LaHave Platform. The age of the formation is approximately Berriasian to Barremian (Williams et al., 1990). Jansa and Wade (1975) have further subdivided the Missisauga formation into three members: lower, middle, and upper. The middle and upper members are included within the updip facies by McIver (1972), whereas the base of the downdip facies is the top of the lower member and is not covered by McIver's descriptions. The lower member consists of fine-grained pebbly,

coarsening upward sandstone beds with minor limestone beds within grey marine shale. The base of the member is picked above a distinctive limestone bed that is dated at the Kimmeridgian, and the top of the Member is picked at the top of a prominently shale sequence dated at the Berriasian-Valanginian. From wells at the Venture Field, the depositional environment for the lower Member is interpreted as being at the Sable Delta front.

In seismic section, continuous parallel reflectors, with occasional localized depositional details, characterize the Missisauga formation. Generally, reflectivity of horizons strengthens from west to east as a function of carbonate content. Particularly, reflectivity is strongest on the LaHave Platform, where the carbonate content is highest, and the formation thins. The strongest reflector within the Missisauga formation is the "O" Marker, which is a transgressive unit that covers most of the shelf. The "O" Marker consists of a series of thin oolitic to skeletal and sandy limestone beds of Hauterverivian to Barremian age that occur at the top of the formation. As a result of its spatial extent, the "O" Marker is useful as a mappable horizon that is chosen as the top of the formation. Beyond the basement hinge zone the horizon becomes much more irregular, reflecting the effects of salt withdrawal on deposition.

Although the "O" Marker is representative of a minor transgression within a regionally regressive period, it is useful for understanding paleogeography. Over much of the Scotian Shelf, it covered a broad and flat delta plain. At the LaHave Platform it oversteps Jurassic sediments and onlaps onto basement. Distally it forms a clinoformal geometry that indicates a change in water depth. Further seaward it disappears with the facies change to deep-water shale of the Verrill Canyon formation. At portions of the

LaHave Platform there are downlapping geometries of the "O" Marker, suggesting that there may have been sediment starvation at this area at the time. In the vicinity of the Alma Field, Alma K-85 and F-67, and Wenonah J-75 wells reveal that deposition was relatively continuous. As a result of continuous deposition, the "O" Marker equivalent strata are present as a sigmoidal lens. Basinward of Sable Island, the degree of downlapping is less significant and the section between the top Jurassic and the "O" Marker is present as a thickening wedge.

3.3.8 Verrill Canyon Formation

The Verrill Canyon formation is the basinal facies equivalent to the Mic Mac, Abenaki, and Missisauga formations. As seen in the Oneida O-25 well, the Verrill Canyon formation is shale in type section. At this location it is underlain by the Abenaki formation, and is overlain by the Missisauga formation. In Glenelg J-48, 900 m of basinal shale equivalent of the lower part of the Missisauga formation were penetrated and interpreted as the Verrill Canyon formation. The shale is dark grey to olive grey, carbonaceous, and contains very fine-grained argillaceous sandstone and siltstone interbeds. At depth (4120 m), a zone containing abundant planktonic foraminifera suggests a deep-water depositional environment but the overall environment for the well is neritic (Wade and MacLean, 1990). The Jurassic portion of the Verrill Canyon formation has never been encountered by drilling in the Sable Sub-basin due to the great depths at which it is interpreted.

There is no distinctive seismic facies that is associated with the top of the Verrill Canyon formation. Its occurrence is interpreted where there is basinward weakening of semi-parallel reflectors that grade into a zone with little to no structure.

3.3.9 Logan Canyon Formation

The Logan Canyon formation is sub-divided into four Members: Naskapi, Cree, Sable, and Marmora. The Naskapi and Sable Members are present as shale tongues in the shelf, with the Naskapi marking the base of the Logan Canyon formation. The rest of the formation consists of an alternation of shale and sandstone-shale units, which were deposited during times of greater or lesser quartz rich clastic input. The dominant depositional environment at the modern day shelf during this section of the Early Cretaceous is believed to be a broad coastal plain or shallow shelf. In seismic profiles, sub-parallel, continuous reflectors that diminish in strength and continuity seaward and over the LaHave Platform characterize the Logan Canyon formation. In the numerous sub-basins the seismic character of the Naskapi and Sable Members is generally too poor for use as seismo-stratigraphic units. The reason for poor image quality of these members is that the Logan Canyon formation passes transitionally into a distal shale facies, reducing acoustic impedance between layers. This distal shale is separated from the underlying Verrill Canyon formation, and is termed as the Shortland Shale. All members of the Logan Canyon formation thicken and increase in shale content seaward into the Abenaki and Sable Sub-basins. Westward, in the direction of the LaHave Platform, the Logan Canyon formation thins and changes to a predominantly shale facies with minor sandstone and siltstone beds.

The Naskapi Member marks a particularly important transgressive episode during the early stage of the Logan Canyon formation, and is present beneath the Scotian Shelf as a thick shale tongue between Missisauga formation and Logan Canyon formation

sandstones. Based on interpretation of microfossils and well samples, its depositional environment was likely a tidal flat to marginal marine setting.

3.3.10 Dawson Canyon Formation

The Dawson Canyon type section consists of grey marine shale and mudstone, with thin beds of siltstone, sandstone, and limestone. A persistent series of thin limestone beds, termed the Petrel Member, forms a regional seismic marker and is useful when determining the occurrence of the formation. The age of the Dawson Canyon formation is Cenomanian to Santonian (Barss et al., 1979 *in* Wade and MacLean, 1990), and the age of the Petrel Member is slightly younger, at Turonian. The total thickness of the formation varies, and may be up to 500 m thick on the LaHave Platform and only 100 m in the sediment starved regions of the Sable Sub-basin.

The top of the formation is strongly reflective, as observed in seismic section; however, the reflectivity appears to weaken in both northward and southward directions. The Petrel Member is also a strong reflector in seismic section, and can be traced over much of the Scotian Shelf. The seismic characteristics of this member often vary with sediment thickness, such that its reflectivity diminishes when it broadens. In general, the Petrel Member regionally thickens from southwest to northeast.

3.3.11 Wyandot Formation

The Wyandot formation includes the Wyandot chalk, adjacent marls, and chalky mudstones. Based on nannofossils, Doeven (1983) has interpreted the succession as being Santonian to Maastrichtian in age. The dominantly carbonate lithology of the formation produces up to several strong reflectors in the shelf and slope regions of the

Scotian Basin, which can be used for regional interpretation. Although the Wyandot formation is useful as a regional marker, its occurrence is sometimes complicated by a Tertiary unconformity at the modern day slope. At the shelf, the Wyandot formation appears to coincide with a very low sedimentation rate of ~0.9 cm/ka (Wade and McLean, 1990).

3.3.12 Banquereau Formation

The entire Cretaceous and Tertiary sedimentary succession that overlies the Wyandot formation has been grouped into the Banquereau formation. The lithology of the formation is predominantly mudstone that grades into sandstone and conglomerate deposits. Its seismic character consists of continuous reflectors that prograded seaward; however, the occurrence of channel cut and fill sequences occur more frequently than in older successions. Several subaqueous unconformities are present in outer shelf and upper slope environments that probably reflect sea-level fluctuations (Wade and McLean, 1990).

4.0 Seismic Interpretation

4.1 Workflow

The recently acquired long offset 2D GX Technology NovaSPAN seismic survey (Fig. 4-1), totaling 3400 km, was the basis for seismic interpretation of the basin architecture, salt structures and stratigraphy. This dataset contains much more information about subsurface structures than previously available with public domain data due to advanced data acquisition (i.e. 9 km long streamer) and processing (pre-stack depth migration) techniques, which allow for deep penetration and improved imaging. To investigate salt tectonics and basin architecture of the western Sable region, line 1600 (Fig. 4-1) of the NovaSPAN dataset was of particular interest. With a length of 225 km and ~20 km depth penetration, this line covers much of the shelf and the entirety of the autochthonous salt-basin, and reaches deep enough to image the top of the crust.

Publicly available litho stratigraphic picks and formation tops for wells: Panuke H-08, Cree E-35, Alma F-67, Wenonah J-75, and Merigomish C-52, made it possible to identify equivalent seismic marker horizons in the shelf on line 1600 that can be correlated into slope and deep-water regions. The SMART ocean bottom seismometer (OBS) data results were also used for regional interpretation as they provide 2D coverage on regional structures from the shelf to deep water in surrounding regions. Deepwater seismic-stratigraphic picks made by Ebinger and Tucholke (1988) based on horizon pinch-outs on seamounts and oceanic crust of known age provided improved confidence when extending timelines beyond the sub-basin, where no well data is available.

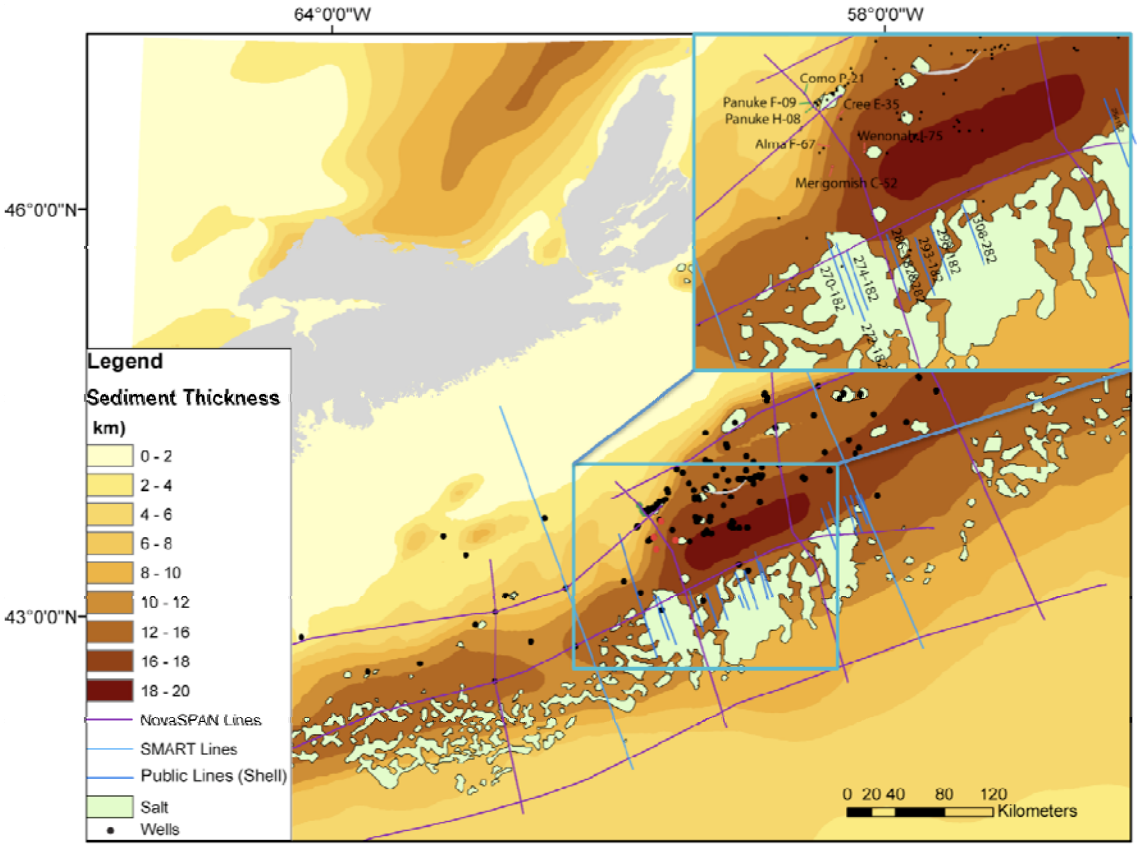

Figure 4-1: Location map of the NovaSPAN, SMART, and publicly available seismic transects. Line 1600 of the NovaSPAN survey is positioned at the western most portion of the Sable sub-basin and is used to constrain parameters for physical models conducted in this study. Offshore exploratory wells (see inset) highlighted in green are positioned at the shelf and carbonate platform, whereas those in red are positioned beyond the hinge zone. In general, wells at the shelf are much closer to line 1600 than those beyond the hinge zone. Although the NovaSPAN and SMART transect data are processed depth, the public lines are in time and are of poor image quality limiting their interpretation to only comparison between structures.

Public domain industry seismic reflection profiles are often too short to use in a regional context; however, they were inspected to improve the understanding of the lateral variability and extent of salt systems identified in the GXT line beneath the modern-day slope. The survey that has been selected for use in this study is: 8624-S006-032E, by Shell Canada (Fig. 4-1). To better understand present-day basin architecture, crustal velocity profiles obtained by analysis of SMART wide-angle OBS data (Wu et al. 2006) and nominal layer gravity models (Zheng and Arkani-Hamed 2002) were used for

qualitative comparison to the interpretation of seismic reflection profiles (Fig. 3-3 and Fig. 3-4).

From seismic interpretation of the regional Ion-GXT seismic reflection line 1600, the following first-order factors governing basin evolution at the western Sable sub-basin were established:

1. Timing and location of depocenters;
2. Sedimentation patterns and rates;
3. Salt thickness;
4. Basin floor geometry and rift architecture.

4.2 Datasets

Regional interpretation was based on numerous aspects of the geology of the Scotian margin, as basin evolution involves a variety of factors including: sea level change, delta migration, and salt tectonics. To handle the range of influences on basin evolution at the Scotian margin, two main databases were used: the Salt Dynamics Group GIS project, and the Salt Dynamics Group seismic interpretation project.

4.2.1 Scotian Basin GIS Database and Seismic Project

The Scotian Basin GIS database encompasses a variety of offshore datasets. These include: satellite Bouger and free-air gravity anomalies, satellite magnetic anomalies, sediment thickness, well positions, seismic transect positions, and present-day salt configurations (GSC MIRAGE database; GSC BASIN database; Louden et al., 2004). Depositional maps available on the GSC MIRAGE database and salt province maps by Shimeld (2004) were geo-referenced into the GIS database and allowed for visual

correlation of paleo-depositional systems and their relation to modern-day salt configuration.

The Scotian Basin seismic interpretation project was compiled within a Kingdom Suite (SMT®) author profile and contains all seismic reflection profiles and velocity models for the NovaSpan survey, as well as both seismic reflection profiles for the SMART survey. Vector objects such as present-day salt configuration from the GIS database were imported into Kingdom Suite to provide spatial correlation of salt features to interpretation.

4.3 Seismic Interpretation

In the seismic interpretation section of this chapter, basin architecture, stratigraphic framework (Fig. 4-2), and salt-tectonics structures of NovaSPAN line 1600 (Fig. 4-3) are discussed. Depocenter migration and sedimentation rates will be derived from interpretation of the stratigraphic framework. All interpretations are presented as segments of the basin, such that details can be observed easily with the use of annotated figures. Constraints from all of these factors are necessary for experiment setups for analogue models, which will provide insight into the salt tectonic evolution at the Scotian margin.

4.3.1 Basin Architecture

4.3.1.1 Rift Shoulder (Shelf)

Beneath the modern-day shelf (Fig. 4-4), the basin floor is evidenced by the sub-aerial break-up unconformity. In this portion of the margin, rotated faults blocks are

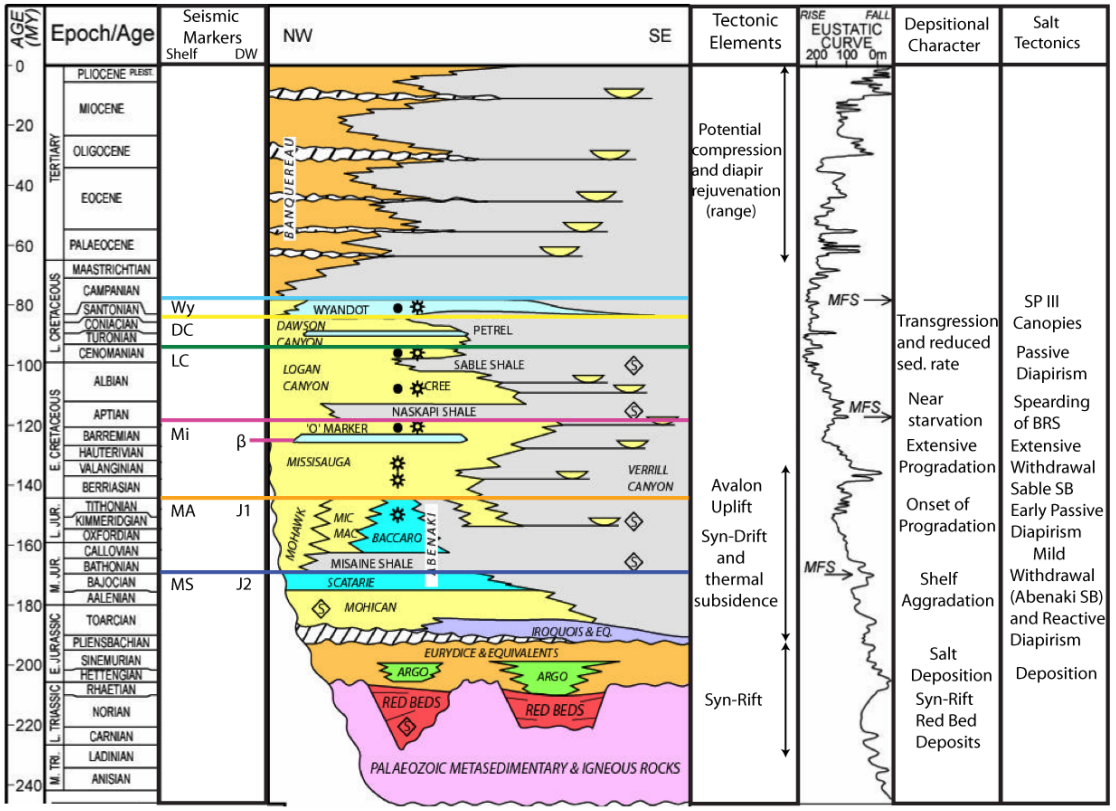

MS - Mohican and Scatarie Formations
J2 - Deepwater M. Jurassic Pick by Ebinger and Tucholke (1988)
MA - Mic Mac and Abenaki Formations
J1 - Deepwater L. Jurassic Pick by Ebinger and Tucholke (1988)
β - Deepwater "O" Marker Equivalent Pick by Ebinger and Tucholke (1988)
LC - Logan Canyon Formation
DC - Dawson Canyon Formation
Wy - Wyandot Formation

Figure 4-2: Stratigraphy of Offshore Nova Scotia including tectonic elements, eustatic sea level, depositional character, and salt tectonics. Modified from Kidston et al., 2007.

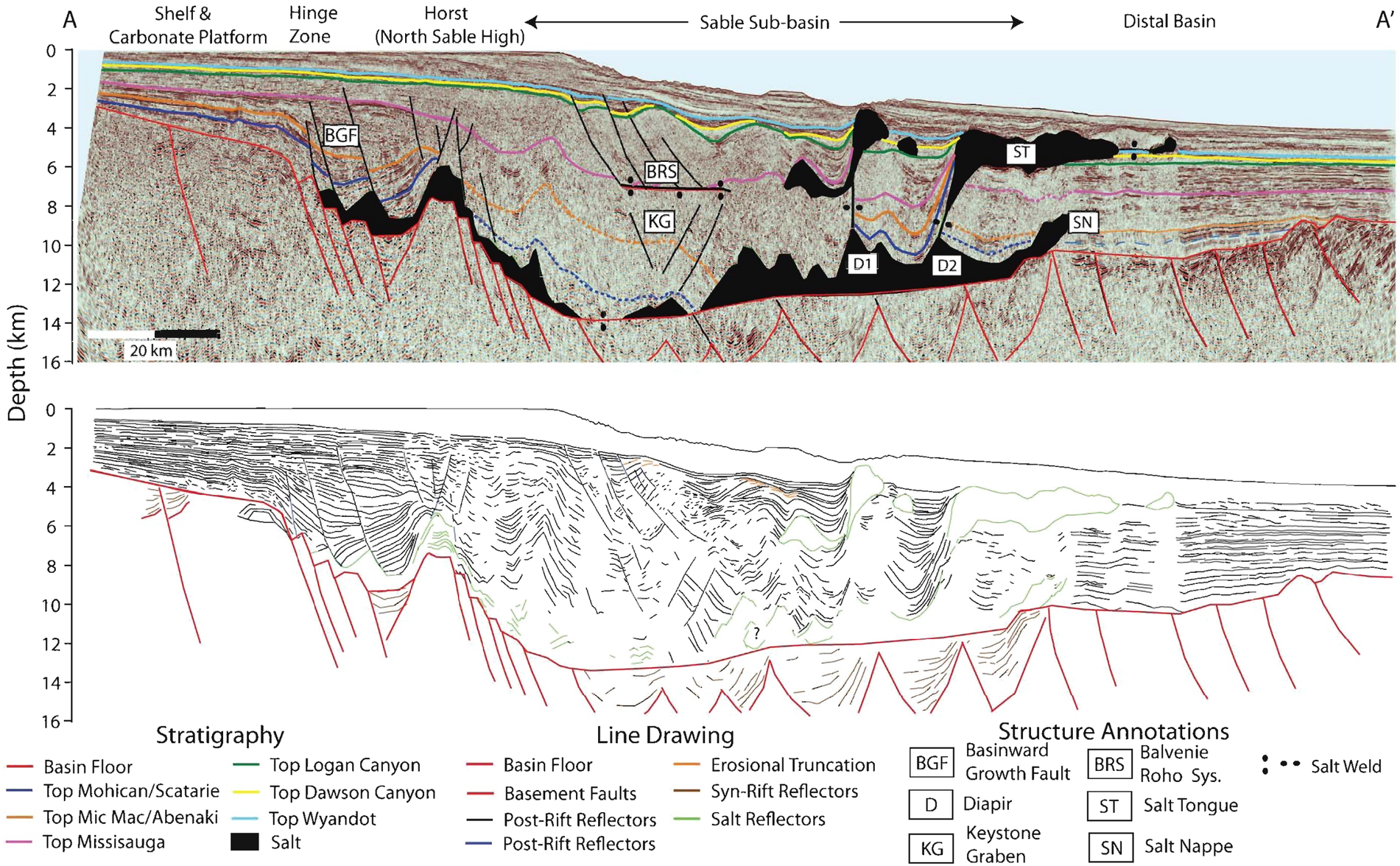

Figure 4-3: Seismic interpretation and line drawing for NovaSPAN line 1600. Major salt features are annotated. Formation tops are based on wells: Panuke H-08, Cree E-35, Alma F-67, Wenonah J-75, and Merigomish C-52, and are correlated into the modern day slope and deepwater as seismic horizons tied to deepwater markers tJ and β from Ebinger and Tucholke (1988) .

observed to contain thick (~1.5+ km) accumulations of syn-rift sediments, which were probably derived from river and lacustrine systems. When continental break-up occurred in the Mid – Late Triassic, an increase in thermal gradient related to thinning of the lithospheric-mantle resulted in uplift of rift valleys and shoulders, and widespread erosion, which characterizes the break-up unconformity. Uplift of the LaHave Platform, just west of the study area, is estimated to be ~0.75 km (Wu et al., 2006), so it may be that the break-up unconformity at the western Sable sub-basin may be more prominent than northeastern portions of the margin, although this is speculative. Basement faults planes dominantly dip seaward, and the faulted blocks and overlying syn-rift reflectors steeply dip landward. The unconformity can be observed where steeply landward dipping, high amplitude, and fan-like reflectors are truncated by overlying parallel-laminar horizons (Fig. 4-3). At the hinge zone, there is notable offset of strong basement and syn-rift reflectors, where prominent faults have formed. As a consequence, early post-rift reflectors take on seaward dips and downlap onto basement blocks.

4.3.1.2 Rift Margin (Hinge Zone)

At the hinge zone (Fig. 4-3 and Fig 4-5) there is a vertical displacement of about 4 km of the basement from the shelf to the proximal rift basin, where the basin floor is stepping down along numerous basinward dipping normal faults. However, at approximately 26 km basinward of the hinge zone is a ~5 km wide horst that acts as a prominent basement high in the proximal rift basin. Since the hinge zone contains numerous deep-seated normal faults, it is difficult to differentiate between the syn-rift sediments and the basement. Fault-controlled subsidence between the hinge zone and basement horst during syn-rift

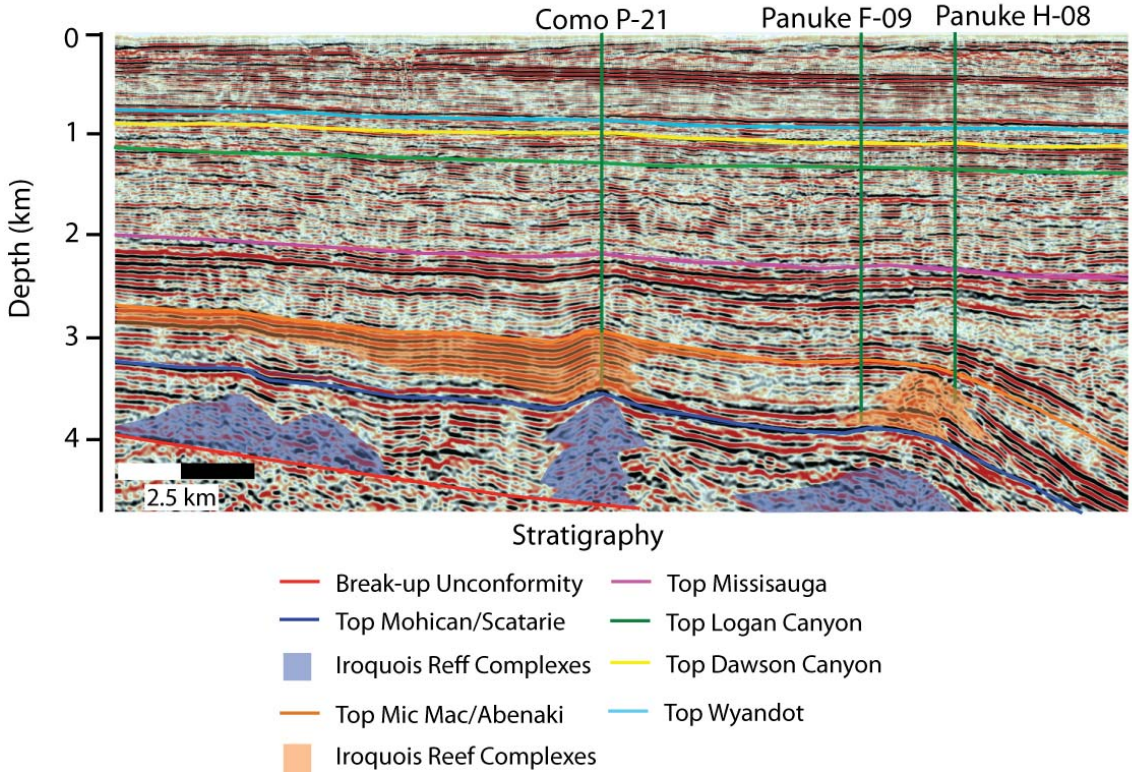

Figure 4-4: Seismic character and wells used for interpretation at the shelf and carbonate platform in NovaSPAN line 1600. Wells color-coded green are close to the transect, and the locations of the formation tops in the seismic section are believed to be accurately extrapolated from the wells.

evolution of the margin has formed a small, restricted salt basin. With later salt withdrawal, this became the locality of prolonged subsidence and accumulated significant sands, based on mapping done by Wade and MacLean (1990).

4.3.1.3 Sable Sub-basin

Seaward of the aforementioned horst, the basement steps down approximately 4.5 km via a series of normal faults. The deepest part of the Sable sub-basin floor (Fig. 4-6) in this region is interpreted to be located at ~14 km below sea level, and is poorly imaged due to complex seafloor geometries in the slope, overlying horizontal salt sheets, and the

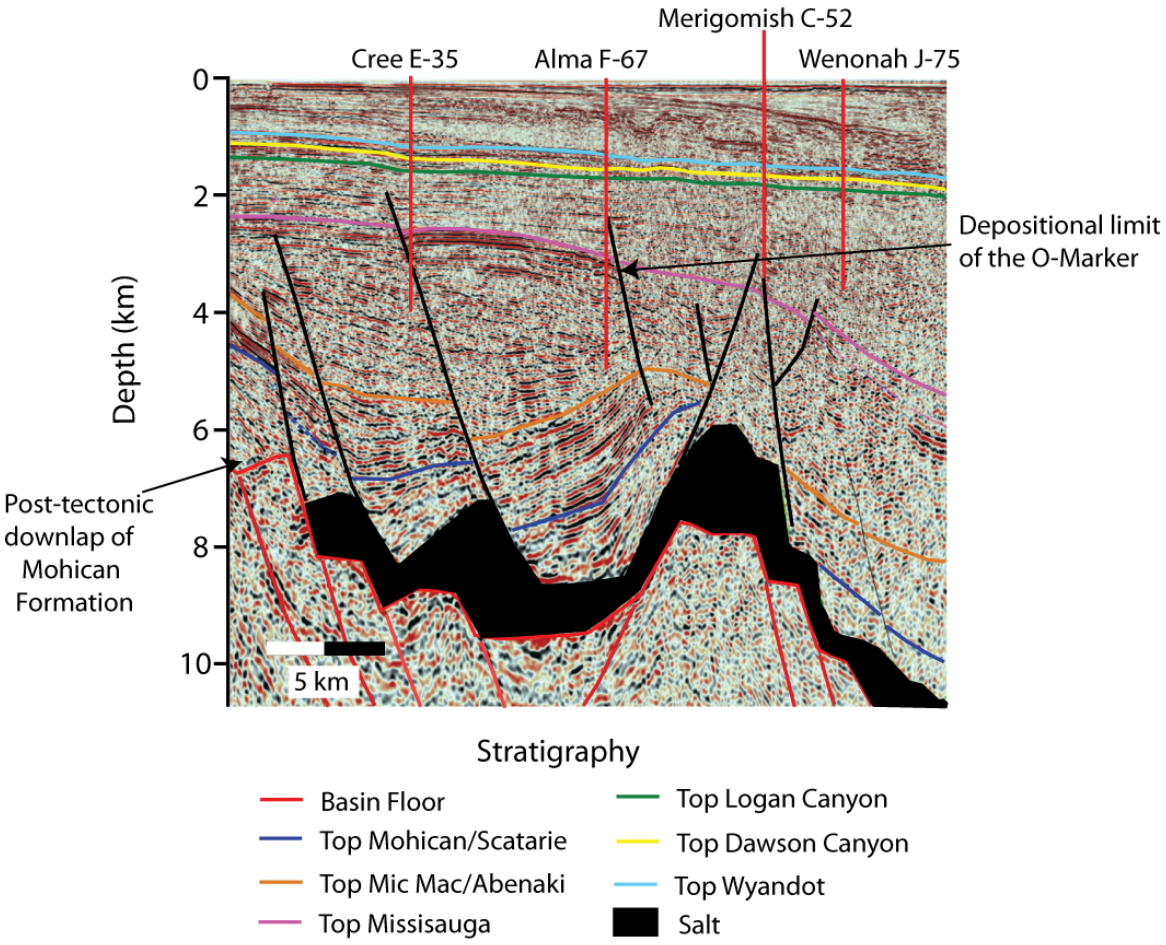

Figure 4-5: Seismic character and wells used for interpretation at the shelf and carbonate platform in NovaSPAN line 1600. Wells color-coded in red are relatively distant (~7.5 km on average) from the seismic transect and the locations of the extrapolated formation tops may be less accurate than in Fig. 4-4.

great depth at which it is positioned. Subtle onlaps of weak Jurassic horizons on seemingly sub-horizontal reflectors, and sparse fanning syn-rift reflectors are the only controls on the position of the basin floor at this locality, and have been used for a general interpretation. It appears that the basin floor is level for ~30 km, after which it begins to climb seaward with an incline at the distal portion of the salt basin. Fanning syn-rift reflectors become more clearly imaged and defined in the distal basin. The distal basin floor has a ramp-flat geometry, which remains level for ~20 km and then climbs further

for another ~25 km, at which point the salt basin terminates. Fault blocks separate fanning syn-rift packages and rotated basement blocks throughout the Sable sub-basin, and have a moderately regular spacing of ~17 km.

4.3.1.4 Ocean-Continent Transition Zone

The basement is faulted to a higher degree beyond the salt basin (Fig. 4-7), probably indicating considerable thinning of the crust and large amounts of extension. The most distal portion of the section is characterized by a series of highly rotated blocks that are considerably shallower (~2 km) than those proximal to the salt basin. The dips of these faults shallow toward the seaward limit of NovaSPAN line 1600, probably corresponding to progressive thinning of the crust (such as that seen in Wu et al., 2006). No oceanic crust is interpreted within the section, in agreement with interpretation by Wu et al. (2006) and Funk et al. (2004).

4.3.2 Pre- and Syn-Rift Seismic Stratigraphy

4.3.2.1 Basement

Basement reflections of the continental crust generally have discontinuous to chaotic geometries with low to moderate amplitudes. Rotated fault blocks are interpreted where overlying, strong, landward dipping reflections indicating syn-rift red beds occur. These rotated blocks are bounded by seaward-dipping, deep-seated faults. Occasionally there are complicated internal geometries of reflectors within the basement; however, the seismic character is too transparent to make accurate interpretations. The character of basement horizons changes dramatically at the continental transitional crust (Fig. 4-7).

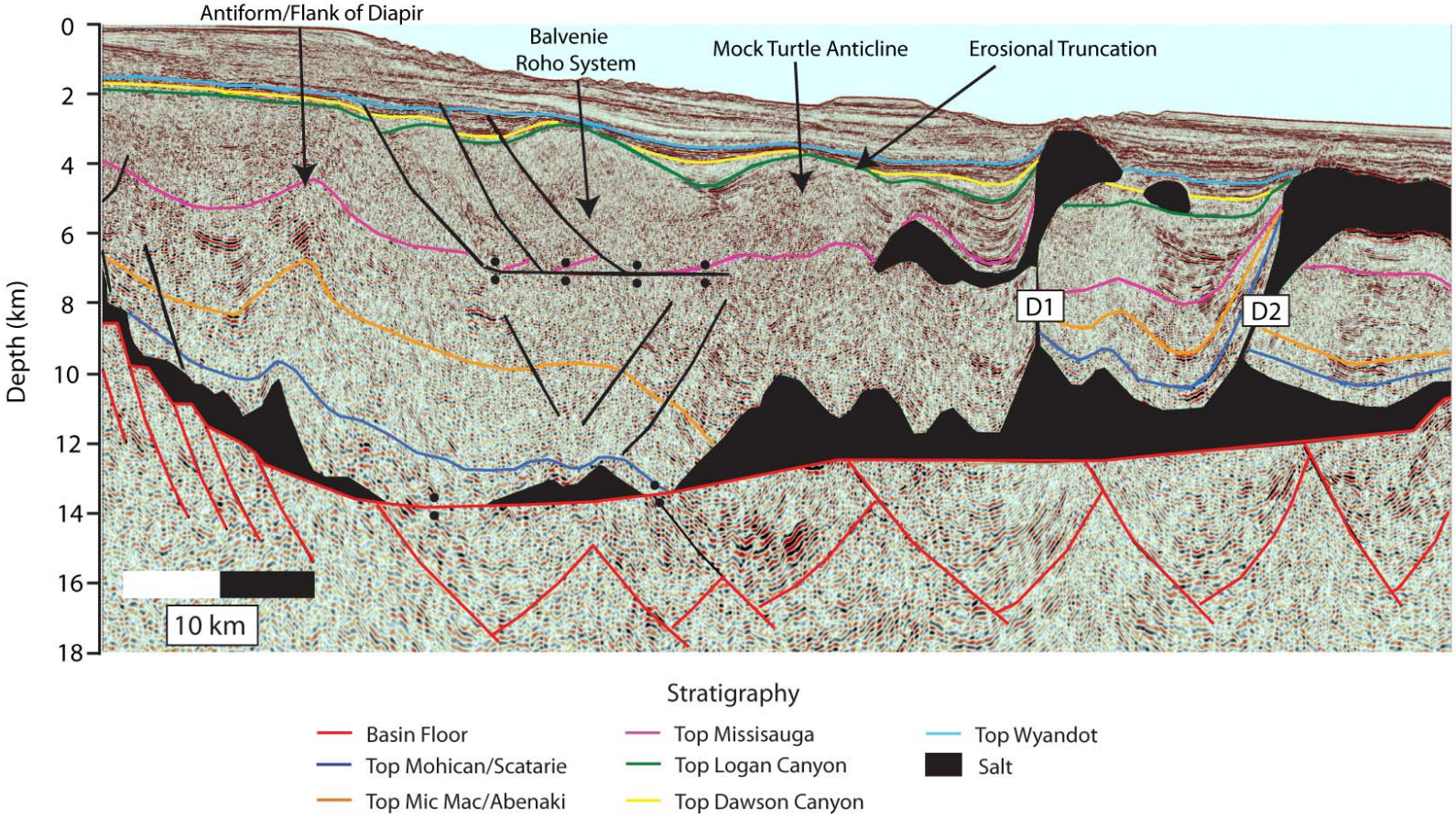

Figure 4-6: Interpretation of modern day slope in NovaSPAN line 1600. D1 and D2 are the only observable diapirs in the seismic section.

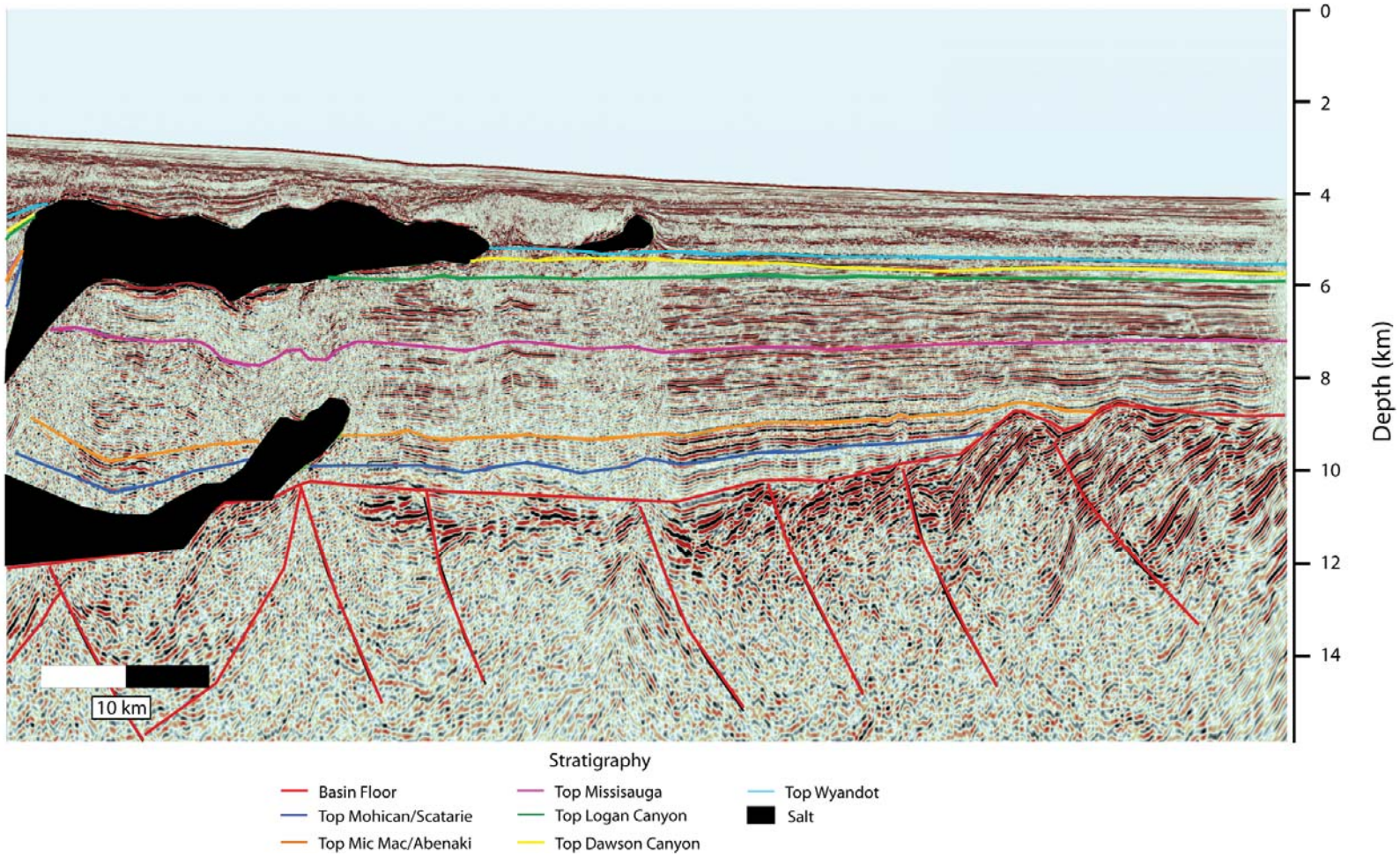

Figure 4-7: Interpretation of the deepwater salt structures and stratigraphy in NovaSPAN line 1600.

In this region, seismic reflections show maximum amplitudes at the sediment-basement boundary, losing strength with increasing depth. The high amplitude packages of reflectors tend to be ~1.5–2 km thick on average, with planar-discontinuous internal geometries. Below these high amplitude reflections, the seismic character abruptly loses strength and becomes chaotic. The high amplitude reflectors are generally landward dipping, and notable offset suggests that they make up a series of faulted blocks. The topography of the continental transitional crust, offset along faults, and thickness of high amplitude reflections all increase at the maximum seaward extremity of NovaSPAN Line 1600.

4.3.2.2 Eurydice Formation Syn-Rift Red Beds

Syn-rift red beds of the Eurydice formation (Fig. 4-2) occur as landward-dipping, fanning, parallel reflectors with moderate to high amplitudes. These reflectors strongly contrast with the underlying basement, and are useful for identifying rotated fault blocks. In all cases, the syn-rift fill appears to completely fill in the offset created by the rotated basement fault blocks.

4.3.2.3 Argo Formation

The Argo formation halite rock salt (Fig. 4-2) is typically chaotic in seismic expression, suggesting a homogenous lithology. However, in some cases (Fig. 4-5), salt is seen to have planar parallel internal reflectors, suggesting lithological heterogeneity, such as red bed sands and shales. In the extensive salt tongue (Fig. 4-7), the boundary of top salt is most obvious as a set of very strong, continuous reflections. Reflections that appear to originate at the base of salt are also strong; however, the polarity of amplitudes

is reversed, suggesting the interface between less dense salt underlying more dense overburden.

4.3.2.4 Break-up Unconformity

The break-up unconformity is only observable at the shelf and is identified on the basis of unconformable contacts between of post-rift strata on basement and syn-rift reflections. The unconformity is most readily identifiable when it truncates steeply landward dipping reflectors of rotated basement blocks and fanning syn-rift reflectors. The break-up unconformity is not traceable into the salt basin. It would overly the Argo formation salt, which has been strongly deformed.

4.3.3 Post-Rift Seismic Stratigraphy (Shelf and Hinge Zone)

4.3.3.1 Mohican and Iroquois Formations (Early – Mid Jurassic)

Beneath the shelf, the Mohican formation is characterized by parallel to sub-parallel, planar reflectors (Fig. 4-4), interpreted as broad continental clastic deposits. In the lower portion of the formation near the contact with the break-up unconformity, the reflectors are variably chaotic but exhibit planar relationships on either side of transparent zones. Between carbonate mounds of the Iroquois formation, reflectors are often discontinuous but retain a sub-parallel geometry. When mapping the formation beyond the shelf edge, reflectors plunge steeply over the hinge zone. Lowermost reflectors of the Mohican formation downlap onto offset basement reflectors, suggesting post-tectonic deposition (Fig. 4-5). At the hinge zone, the Mohican formation is displaced due to a combination of normal faulting and significant salt withdrawal. In this region (Fig. 4-5), reflectors gradually take on a landward dipping geometry, through rotation along a

number of faults. Reflectors appear to indicate reverse motion over the narrow horst and an overlying salt remnant. In a 2D framework, this may indicate that downdip contraction was localized proximally over the horst, where salt thinned. With rotation and seaward motion of strata along the main basinward-dipping growth fault, the package may have thrust over the underlying salt. In a 3D framework, this geometry may simply reflect along strike deposition, with more continuous sediment accumulation in the landward portion of the graben than over the horst.

The basal Iroquois formation occurs as local carbonate mounds that are chaotic in seismic section and are onlapped by the Mohican formation. The mounds are generally confined to the lower portion of the Mohican formation, but may extend almost to the Scatarie Member. The widest mound occurs at the shelf break, and is ~5.3 km wide in dip section (Fig. 4-4). Well Como P-21 targeted an antiform in the Baccaro formation, which is a direct consequence of differential sedimentation or compaction over an underlying Iroquois reef.

The top of the Mohican Formation is evidenced by the Scatarie marker, which is a strong, continuous reflector that spans the entire shelf. The Scatarie marker provides an excellent regional marker in the shelf, since it is a transgressive lag limestone that strongly contrasts with surrounding clastic sediments. However, this reflector is impossible to identify within the Sable sub-basin.

4.3.3.2 Mic Mac and Abenaki Formations (Mid – Late Jurassic)

The alluvial plain and neritic clastic sediments of the Mic Mac formation are characterized by sub-parallel, discontinuous to chaotic, low to moderate amplitude

reflections that pinch out basinward, near the hinge zone. Similar reflection patterns also occur between Baccaro Member carbonate reef mounds, which may represent clastic infill related to the Mic Mac formation. Contacts of reflections between the mounds tend to be gradational rather than onlapping, suggesting that infill occurred during reef growth (Fig. 4-4). Since there is a component of along-strike sediment transport on the LaHave Platform during the late Jurassic, clastics may not have been sourced solely from an updip locality. Highly reflective, parallel continuous seismic character dominated the Mic Mac formation at the Hinge Zone, suggesting clastic deposits. High amplitude, but discontinuous reflectors suggest the occurrence of the Abenaki carbonate bank, which appears to be restricted to the paleo shelf break. Here, the clastic section is offset and thickens significantly in the salt-withdrawal basin of the proximal Abenaki sub-basin. Reflectors are slightly more continuous than in the shelf, but still have low to moderate amplitudes.

The reef and platform carbonates of the Abenaki formation, particularly the Baccaro Member, dominate the Latest Jurassic section on the shelf. The Baccaro Member is imaged as a zone of parallel, continuous, high amplitude reflections that thickens toward the hinge zone (Fig. 4-4). Reef complexes are easily recognized as narrow (~1 km) antiformal structures and are commonly the position of control wells.

4.3.3.3 Missisauga Formation (Early Cretaceous)

On the shelf, the fluvial delta plain deposits of the Missisauga formation are characterized by parallel to sub-parallel reflections (Fig. 4-4), with local chaotic packages throughout. Differential compaction has resulted in antiforms over the Baccaro reef complexes; however, seismic character does not change preferentially, nor is there any

indication of growth of the clastic section. At the hinge zone, there is significant growth of the formation. This growth ceases by the top of the formation, and is not seen in overlying units. Reflections characterizing the growth package are dominantly sub-parallel to parallel, discontinuous, and low amplitude with minor high amplitude parcels (Fig. 4-5). The top of the formation is picked just above the O-Marker, which is a regional transgressive limestone imaged as a high-amplitude reflection with parallel, continuous seismic expression. The O-marker varies in thickness along the margin, but is generally thin in NovaSPAN line 1600 (~250 m). The O-marker blankets the entire shelf and hinge zone, but disappears seaward of the horst mid basement high suggesting that there is a facies change to the Verrill Canyon shale (Fig. 4-5).

4.3.3.4 Logan Canyon Formation (Early Cretaceous)

Both the thickness and seismic character of the Logan Canyon formation change very little from the shelf to hinge zone, suggesting that most salt was evacuated from the Abenaki sub-basin by the time of its deposition. Its seismic expression is uniformly sub-parallel or parallel discontinuous with low to moderate amplitudes, indicating increased shale content of the broad coastal plain and shelf clastics relative to the underlying Missisauga formation. Above the horst, the formation dips more steeply into the Sable sub-basin, and notable growth is observed (Fig. 4-5).

4.3.3.5 Dawson Canyon and Wyandot Formations (Late Cretaceous)

Since salt tectonics at the Sable sub-basin was generally shut down by the Late Cretaceous, the Dawson Canyon and Wyandot formations will be discussed briefly and together. The grey marine shale of the Dawson Canyon formation has a seismic

expression that is uniformly sub-parallel to parallel discontinuous with low to moderate amplitudes. The top of the formation is picked using the limestone rich condensed section, since it results in regional, high amplitude reflectors. No growth of the package occurs throughout the shelf or hinge zone. The Wyandot formation has a seismic character similar to the condensed limestone of the Dawson Canyon formation. The top of the formation is marked by a thin package of parallel, continuous, high-amplitude reflectors at its top, which represents a thin assemblage of chalks (Fig. 4-4).

4.3.4 Basin-scale Correlation of Seismic Horizons and Depocenters from Shelf into Sable sub-basin

4.3.4.1 Slope and Deepwater Equivalent Strata to the Mohican Formation (Early – Mid Jurassic)

There is very little evidence for the time-equivalent top of the Mohican formation in the Sable sub-basin (Fig. 4-6). The relative position of the transect in relation to the early Sable Delta suggests that only fine, pro-delta sediments were transported beyond the hinge zone. These homogenous, shale rich sediments provide little to no acoustic impedance contrast required for strong reflections. In addition, the deep burial of the Mohican equivalent in the Sable sub-basin would produce weaker reflectors. However, between the two major diapirs (Fig. 4-6), which are positioned at the seaward termination of the salt basin, there are unconformable growth packages that suggest its position. The lowermost unconformable growth package is interpreted to mark the top of its deep-water equivalent, and has been used for correlation. This package of sediments is thin in seismic section (~650 m), and is overlying trapped salt. The top of the sediments equivalent to the Mohican formation has been extrapolated across the hinge zone to the position seen between diapirs, but remains speculative.

4.3.4.2 Slope and Deepwater Equivalent Strata to the Mic Mac Formation (Mid – Late Jurassic)

There is little constraint on the deepwater correlation of the strata equivalent to the Mic Mac formation in the slope portion of NovaSPAN line 1600. However, weak seismic reflections are observed as dipping significantly from the horst to diapir 1 (Figs. 4-3 and 4-6), forming a regional expulsion rollover. Based on fault offset along the narrow horst structure, the top of Jurassic sediments is believed to be present at depths greater than 7 km. Further seaward, the top of equivalent strata is interpreted as terminating on salt rollers. Between the two major diapirs, an unconformable growth package indicates the top of the deepwater equivalent. Horizontal offset of the formation top suggests that the sedimentary package is a raft, marking horizontal translation during the development of diapirs and the regional rollover. The seaward portion of these sediments sheaths diapir D2, indicating that it had developed at the termination of the basin and that it had not been translated significantly during its evolution. From this evidence, the thick package of sediments between diapirs is interpreted to have formed as a salt-withdrawal basin that had continuously accumulated sediments and downbuilt passively into underlying salt.

4.3.4.3 Slope and Deepwater Equivalent Strata to the Missisauga Formation (Early Cretaceous)

Reflectivity within the deepwater strata equivalent to the Missisauga formation is generally weak and chaotic within the slope region of NovaSPAN Line 1600. However, sparse packages of strong reflections allow for the determination of general trends that make up the regional structure (Figs. 4-3 and 4-6). Strong, parallel continuous reflections reveal that strata dip considerably seaward beyond the horst structure as a result of

downbuilding over an originally thick salt layer. Proximal to these dipping strata, antiformal geometries are observed over a remnant salt body, which may have resulted from various mechanisms. One explanation for the antiform is that downdip contraction related to downbuilding and updip extension was localized in the Sable sub-basin. However, it is unusual for downdip contraction to become localized so close to extensional/translational regions. Another possibility is that the 2D profile cuts the flank of an out of section diapir that climbs higher up the stratigraphy. In this case, the antiformal geometry reflects the flanking of strata on the along-strike portion of a diapir, related to passive downbuilding rather than contraction. Basinward of the apparent antiform, the strata dip further as part of the regional expulsion rollover structure. The top of the Missisauga formation equivalent strata in the slope is based on the occurrence of an overlying salt sheet, which is known as the Balvenie Roho system (BRS) (Deptuck et al., 2009). This salt sheet has a sub-horizontal base, which necessarily required very low sedimentation to starvation conditions in the slope during the time of gravity spreading. This correlates with the minor transgressive event in the shelf that resulted in the Naskapi Member shale deposition. Since transgression is a gradual process, the base of salt is not necessarily the top for the deepwater equivalents, but it is close as a short period of pelagic sedimentation would have resulted in decreased deposition. Diapir D1 hosts a landward leaning overhang at the same stratigraphic interval supporting the notion that low sedimentation rates allowed for gravity spreading of salt at the sea floor during this event. Below the salt overhang, weakly imaged seismic reflections make interpretation of underlying strata difficult (BRS in Figs. 4-3 and 4-6). However, from patches of strong horizons it is clear that the strata have a complex geometry, which reflects the configuration of underlying salt remnants. Between the diapirs, another

unconformable growth package is chosen as the top of Missisauga formation equivalent strata, and is at a similar stratigraphic position as observed at the modern-day slope.

4.3.4.4 Slope and Deepwater Equivalent Strata to the Logan Canyon Formation (Early Cretaceous)

Reflectivity of the slope and deepwater equivalent strata to the Logan Canyon formation is generally weak and often transparent. Over the BRS, reflections are almost entirely chaotic, with only hints of true geometries. However, proximal to diapirs D1 & D2, stratigraphy is clearly imaged allowing the basinward extrapolation of the top of the formation equivalent strata. Reflections in this region are parallel and continuous, with moderate to high strength.

The slope and deepwater equivalent strata to the Logan Canyon formation immediately thicken as a growth package beyond the basement horst structure. The thickness of this growth package varies in position with respect to the aforementioned antiform; however, the top of the package remains at a relatively constant level indicating that the development of the antiform had been completed by the mid-late stage of the Logan Canyon formation deposition. Seaward of the antiform, the strata begins to dip basinward within the regional expulsion rollover structure. However, normal faults that sole out on the basal detachment of the BRS offset and rotate these reflections, giving them a landward dipping geometry. This is accomplished in a similar fashion as noted at the Banquereau syn-kinematic wedge (Ings and Shimeld, 2006) and is a result of basinward translation over the thin, open-ended salt sheet and landward rotation along fault planes. NovaSPAN strike line 5300 (Fig. 4-8) transects the basinward terminus of the BRS in this area parallel to the shelf and reveals a complex pattern of antiformal and

synformal geometries related to variable growth and extension over the salt detachment levels. At the intersection of lines 5300 and 1600, reflections take on synformal geometries as landward rotation along arcuate faults has resulted in vertical displacement relative to surrounding strata (Figs. 4-6 and 4-8). The salt sheet and deformed overlying strata appear to be narrow in the strike section; however, this is believed to reflect the profile's position at the terminus of the structure.

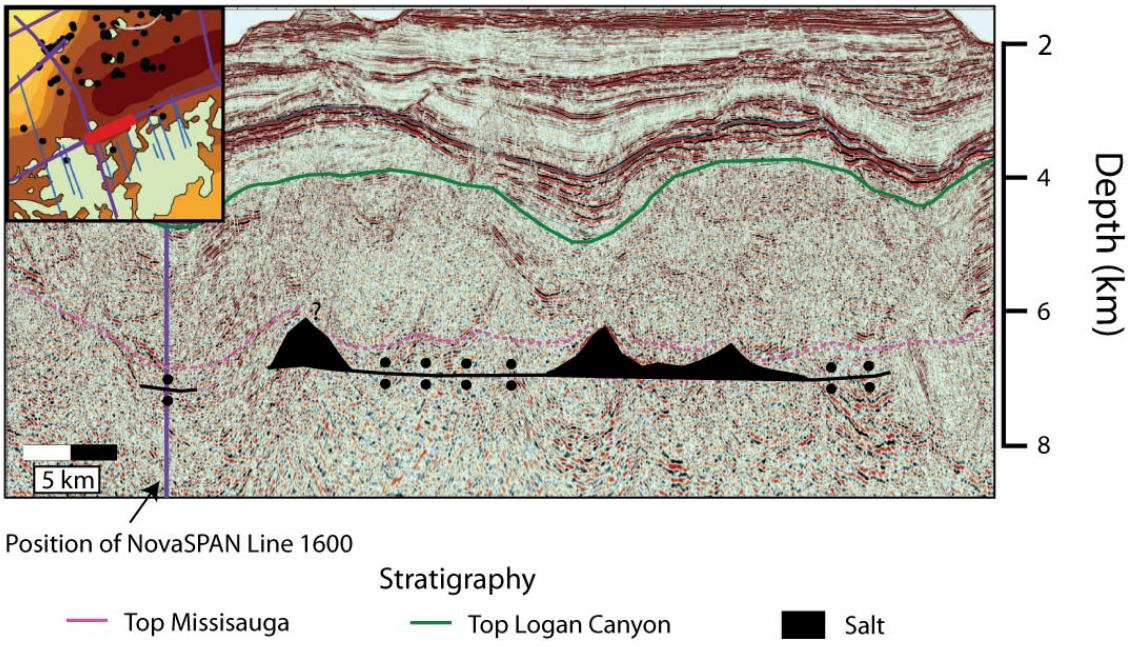

Figure 4-8: Along-strike profile of the Balvene Roho System in NovaSPAN line 5300. There are two main faulted packages, which are poorly imaged due to complex geometries. These two packages are separated by a mini-basin that appears to allow strata to plunge to slightly greater depths (i.e. Missisauga formation to ~6.5 km). Where Line 1600 intersects is close to the seaward terminus of its own semi-connected salt sheet. Here, the stratigraphy plunges to depth as well but as a result of rotation along a basinward-dipping fault plane.

Between the BRS and the landward leaning overhang from diapir D1, uppermost strata appear to take on an antiformal geometry. This feature is similar to a turtle anticline, which is typically the late stage result of salt-withdrawal basin formation during extension. For true turtle structures, salt is withdrawn from the center of the mini-basin

until welded, after which the basin flanks become the site of growth and local expulsion rollovers. For the feature seen in NovaSPAN Line 1600, there was never salt in the center of the structure, but withdrawal at the flanks has resulted in the development of a similar feature. For this reason, the structure has been labeled as a mock turtle anticline. The basinward portion of the mock turtle anticline has experienced considerable erosion, as evidenced by reflections that are abruptly truncated by overlying Wyandot or older sediments that are parallel laminated and sub-horizontal in geometry. Between diapirs D1 & D2 (Fig. 4-3), the top of deepwater equivalent strata is picked based on similarity of seismic character, as the overlying strata are easily distinguished as a homogenous, weak or transparent section representing pelagic shale. This package of sediments makes up the most significant accumulation between the two diapirs.

4.3.4.5 Slope and Deepwater Equivalent Strata to the Dawson Canyon and Wyandot Formations (Late Cretaceous)

At the modern day slope, the pelagic shale and condensed section limestone of the strata equivalent to the Dawson Canyon formation (Fig. 4-6) are easily recognized as a weakly reflective or transparent package as there is little impedance contrast within the homogenous shale condensed section. The package passively fills in minor accommodation space created by late-stage salt withdrawal, but does not generally drive deformation within the system. The low sedimentation rate during the deposition of the Dawson Canyon formation has apparently allowed for the spreading of extensive salt canopies that characterize Salt Province III (Fig. 4-7).

The top of the Wyandot formation is interpreted based on lithostratigraphic picks available in public wells at the slope (Annapolis G-24 And Crimson F-81). Generally, it

occurs as chalk and is correlated with strong, parallel continuous reflections that overlie the dominantly transparent Dawson Canyon formation equivalent package of pelagic shale (Fig. 4-6). The Wyandot formation also passively fills in minor accommodation space created by minor, late-stage salt withdrawal, and does not drive deformation within the system.

4.3.5 Basin-scale Correlation of Seismic Horizons and Depocenters (Ocean-Continent Transition)

4.3.5.1 Deepwater Equivalent Strata to the Mohican Formation (Early – Mid Jurassic)

The deepwater equivalent strata to the Mohican formation in the deepwater basin are constrained by the J_2 marker (Fig. 4-2) in Ebinger and Tucholke (1988). Similar to the package between the diapirs (Figs. 4-3 and 4-6), this package is relatively thin over the transitional crust (Fig. 4-7). A similar thickness as seen between the diapirs is therefore used in the interpretation of the top of this sediment package, which generally hosts weak amplitude reflections that have parallel-continuous geometries.

4.3.5.2 Deepwater Equivalent Strata to the Mic Mac Formation (Mid – Late Jurassic)

The Top Jurassic pick, which is time correletable with the slope and deepwater equivalent strata of the Mic Mac formation, is based on the J1 marker (Fig. 4-2) in Ebinger and Tucholke (1988). For interpolation into NovaSPAN Line 1600, the pick was observed in the Lithoprobe 89-1 time-domain profile (Ings and Shimeld, 2006) and then re-picked on the depth migrated section based on seismic character. The pick was then correlated along strike via NovaSPAN Line 5100 to Line 1600 and traced up-dip to the salt nappe and diapir D2 (Fig. 4-7). The stratigraphic position of the J1 marker is very similar to the package of strata equivalent to the Mic Mac formation between diapirs D1

and D2, suggesting that the aforementioned unconformable growth packages are valid picks for its top. The seismic character of the deepwater strata equivalent to the Mic Mac formation is marked by moderate to high amplitude parallel continuous reflections, and is interpreted to reflect hemi-pelagic sediments.

4.3.5.3 Deepwater Equivalent Strata to the Missisauga Formation (Early Cretaceous)

The top of the deepwater strata equivalent to the Missisauga formation in the distal basin is picked based on the β marker in Ebinger and Tucholke (1988). This marker is interpolated into NovaSPAN Line 1600 as was done with the J_1 marker. The β marker is time-equivalent to the "O" marker, and serves a reasonable proxy to the top deepwater equivalents of the Missisauga formation. This package of Missisauga formation equivalent strata has two major divisions in seismic character. The lower portion of the succession is dominated by weak sub-parallel to parallel continuous reflections, and is interpreted as hemi-pelagic sediments. The upper portion of the succession is dominated by moderate to high amplitude, sub-parallel, discontinuous reflections and possibly marks the influence of deepwater channel systems and turbidite flows. Based on this change in seismic character, it is believed that true deepwater depositional systems did not influence the distal basin overlying the transitional crust until approximately mid-Missisauga formation deposition.

4.3.5.4 Deepwater Equivalent Strata to the Logan Canyon Formation (Early Cretaceous)

The top pick of the deepwater strata equivalent to the Logan Canyon formation at the distal basin (Fig. 4-7) is based on the change in seismic character to the overlying Dawson Canyon formation. The seismic character of this entire package of sediments is

dominated by moderate to high amplitude, sub-parallel, discontinuous reflections and is interpreted to represent a series of deepwater channel and turbidite complexes. At the top of this package of strata, reflections lose strength and may correlate with the onset of more hemi-pelagic sedimentation, as a consequence of sea level rise.

4.3.5.5 Deepwater Equivalent Strata to the Dawson Canyon and Wyandot Formations (Early Cretaceous)

The deepwater seismic character of the Dawson Canyon and Wyandot formations (Fig. 4-7) are similar to what is observed at the modern day slope and these formations are interpreted to have a similar lithology, although the Wyandot formation probably has increased in shale content compared to the modern-day slope. The Dawson Canyon formation is mainly characterized by a weak reflectivity or transparent package, whereas the occurrence of the Wyandot formation is marked by the onset of strong, parallel-continuous reflections.

4.4 Salt and Fault Structures

All major salt structures in NovaSPAN line 1600 are illustrated in figure 4-3. These structures will be described throughout the following sub-sections based on their occurrence from the shelf to deepwater.

4.4.1 Rift Margin (Hinge Zone)

Most autochthonous salt has been withdrawn from the hinge zone, with the exception of two salt remnants and an inactive diapir. The salt remnants are situated at the landward limit of the salt basin, and are observable as transparent packages of highly discontinuous reflections that strongly contrast with overlying parallel-continuous

reflections. Basinward growth faults (BGF) sole out on the basinward flank of the salt rollers, leaving them trapped in the footwall of the growth packages. Strata have also been displaced and rotated along the basinward growth faults, resulting in landward dipping geometries.

There is a shut-down diapir situated above the basement horst structure that is interpreted based on its relationship with overlying strata. The outline of the shutdown diapir is marked by strong reflections that do not share geometries that are similar to surrounding overburden. Unlike typical salt structures observed in the profile (D1 and D2, Fig. 4-3), there are parallel continuous reflections throughout the lowermost portion of the salt body that may reflect internal heterogeneity (Fig. 4-5). The shutdown diapir is also flanked by complex faults structures. On the landward flank, a fault appears to display reverse sense within the Jurassic package. However, the fault did not necessarily develop during the Jurassic as the salt would act as an efficient detachment surface, negating the need for brittle faulting. Conversely, normal sense fault movement is present within the Early Cretaceous Missisauga and Logan Canyon formations, indicating minor downbuilding. Conjugate fault sets are also related to the major landward-dipping fault but appear to have little associated offset. On the basinward flank of the shut-down diapir there is a large normal fault, which appears to have developed as Jurassic and Early Cretaceous strata down-built into the deep Sable sub-basin. Conjugate faults associated with the prominent basinward growth fault display minor offset.

4.4.2 Sable Sub-basin

In the deep portion of the Sable Sub-basin (Fig. 4-6) a variety of salt structures including numerous salt remnants, a regional expulsion rollover, the Balvenie Roho System (BRS), and two vertically welded diapirs were observed.

The furthest landward salt remnant is poorly imaged at depth, but is interpreted based on strong anomalous reflections that outline a chaotic and discontinuous package. The salt pillow is situated below the crest of the antiform, and may have evolved via various mechanisms depending on interpretation. Since there is no constraint on its 3D geometry, the interpretation of the salt pillow is indeterminate. However, the two main interpretations are: (1) that it is remnant salt that infilled space created during folding; or (2) that it is part of a purely extensional diapir that climbs out of section. If the salt pillow is in fact part of a diapir, the antiform observed in the profile may reflect strata flanking the diapir, rather than folding that requires contraction.

Beyond the antiform, strata dip strongly seaward as part of a regional expulsion rollover structure, similar to the Cabo Frio structure, offshore Brazil (Ge et al., 1997). Although it is not actually a salt body, the expulsion rollover probably required basinward directed salt withdrawal from an originally inflated/thickened salt massif. With prolonged downbuilding into the salt massif during the Early Cretaceous, the strata have attained basinward dipping geometries that appear to become more significant toward the remnant salt bodies and diapirs D1 and D2. Where the strata changes most dramatically in dip, there are numerous faults that make up a set of keystone grabens (KG in Fig. 4-3). A poorly imaged package in the center of the complex may be caused by numerous

poorly imaged faults or may be related to acoustic shadowing below the Balvenie Roho System.

At NovaSPAN Line 1600, the Balvenie Roho System is a welded salt sheet/canopy that is interpreted to have spread during the minor Early Cretaceous transgression that led to the deposition of the Naskapi shale member in shelf regions. As this depositional event marks the transition from the Missisauga formation to the Logan Canyon formation, the BRS is used to approximately pick the top Missisauga formation equivalents in the slope. The BRS can be readily interpreted based on the occurrence of faults that sole out onto a common detachment surface in the modern-day slope. Strata have been translated seaward and rotated landward along these faults, as seen by landward dipping reflections. A high amount of extension in the overburden triggered by increased seaward flow within an open-ended salt sheet has led to extensive faulting, which has resulted in a poorly imaged package of the dip profile. Along strike (Fig. 4-8) the BRS appears to be extensive, and hosts complex fault systems that are bounded by small salt remnants. Further complicating the structural evolution of this feature are small mini-basins that flank strongly faulted packages of strata. The relationship between mini-basins and highly deformed strata suggest a complex interplay between overburden translation/extension and passive downbuilding.

Numerous salt remnants are interpreted to be present landward of diapir D1 (Fig. 4-6). Salt bodies are larger than those observed at the hinge zone and at the landward limit of the Sable sub-basin. Salt appears to contribute to the geometry of overlying strata, as dips of reflections are found to correlate with the geometry of their boundaries. Small remnants of autochthonous salt suggest that salt withdrawal in the region was

hampered, and that it was probably an area of inflated salt during the Late Jurassic/Early Cretaceous.

The trapped salt remnants are connected to the extensive diapir D1 structure, which is interpreted based on transparent zones and the relationship of overburden reflections and salt boundaries, such as steeply-dipping onlap occurrences (Fig. 4-6). The middle portion of D1 appears to be welded vertically, indicating that it was likely squeezed by late-stage contraction. Above the welded portion of the diapir, there is a landward overhang that has become the locality of mini-basin formation, as overlying strata appear to display growth patterns throughout the Early and Late Cretaceous. The landward overhang occurs at approximately the same stratigraphic interval as the BRS and is interpreted to have spread during the same transgression event. The diapir continues to climb through Early Cretaceous strata until it is finally shut-down in the Tertiary. The diapir has a small basinward overhang that spread during the Late Cretaceous; however, it did not form an extensive salt tongue or canopy system, as insufficient salt was supplied from lower levels.

There is a thick salt-withdrawal basin, containing deepwater equivalent strata of all formations, between diapirs D1 and D2 (Fig. 4-6). Early deposits (Mohican to Missisauga formations; Fig. 4-2) appear to display relatively little growth, suggesting only minor subsidence within a inflated salt massif. As a result of minor downbuilding during these times, older strata appear to sheath diapir D2 as a wide, shallow mini-basin. However, during the deposition of the Logan Canyon formation, basinward migration of depocenters appears to have provided enough sediment for downbuilding to accelerate, and significant growth is seen within the package. Growth patterns dramatically decrease

in the Dawson Canyon and Wyandot formations, coinciding with reduced sedimentation rate.

Diapir D2 appears to climb more prominently basinward than D1 and is welded at depth. Since the basinward flank of D2 climbs the stratigraphy with more of an incline than D1, it is interpreted that it had either a relatively high extrusion rate, climbed during a low sedimentation rate, or both. For this to occur, it is believed that subsidence in the salt withdrawal basin between D1 and D2 provided enough pressure within the massif to supply salt to D2 at a higher rate than seen at other diapirs at the margin. D2 feeds an extensive salt tongue (ST), which is part of an extensive canopy system within Salt Province III (Fig. 4-3). In NovaSPAN Line 1600, the salt tongue extends 40 km from its feeder, is ~1.4 km thick on average, and has spread during the deposition of the Dawson Canyon and Wyandot formations (Late Cretaceous; Fig. 4-3). Close to its seaward termination is a tertiary salt weld that is associated with extensive faulting in the overburden. Reflections within this faulted package have complex geometries, which are likely to be further complicated in 3D. The mechanism for this deformation is believed to be similar to what was described at the BRS, and it is believed that down-dip contraction was accommodated by the small, connected salt pillow. Although there is reflectivity within D2 and ST, the overall seismic expression is characteristically weak or transparent. Both diapirs D1 and D2 are situated over the portion of the Sable sub-basin where the basement climbs to shallower depths.

Below the salt tongue, there is a small salt nappe (SN) that appears to climb out of the autochthonous basin. The occurrence of SN is interpreted on the basis of strong reflections that do not conform to the horizontal geometry of pelagic sediments that are

present over the oceanic basement. Between these reflections, there is a weak to transparent area of reflectors that is similar in character to ST. There, the strong reflections define a salt geometry that climbs the stratigraphy relatively abruptly through the Jurassic section but ends in the Early Cretaceous. The overburden that overlies SN appears to follow its final geometry in a similar fashion as to what is seen at the salt remnants landward of D1.

4.5 Depocenter Evolution and Migration

Interpretation of 2D regional seismic data suggests that salt withdrawal has been a major factor controlling the development of depocenters throughout the evolution of the Sable sub-basin. In general, depocenters migrate seaward through time, but this trend is complicated by the proximal graben, as well as cessation of late-stage salt tectonics. Depocenters have been generalized for each formation (Fig. 4-9), as they relate to the salt tectonic development in NovaSPAN line 1600.

4.5.1 Mohican Formation (Early – Mid Jurassic)

The Early – Mid Jurassic Mohican formation is characterized by proximal, continental clastic deposition, as sediments made their way beyond the hinge zone. Early salt withdrawal was initiated in the proximal graben as sediments loaded underlying salt. Since the salt basin was not inflated at this time, sediments also made it seaward of the graben and horst (NSH) and settled out as far as the position of the modern-day slope. However, the more distal sediments were likely fine, pro-delta clays that were deposited over a mildly inflating complex of salt. Although sediments were accumulating in this

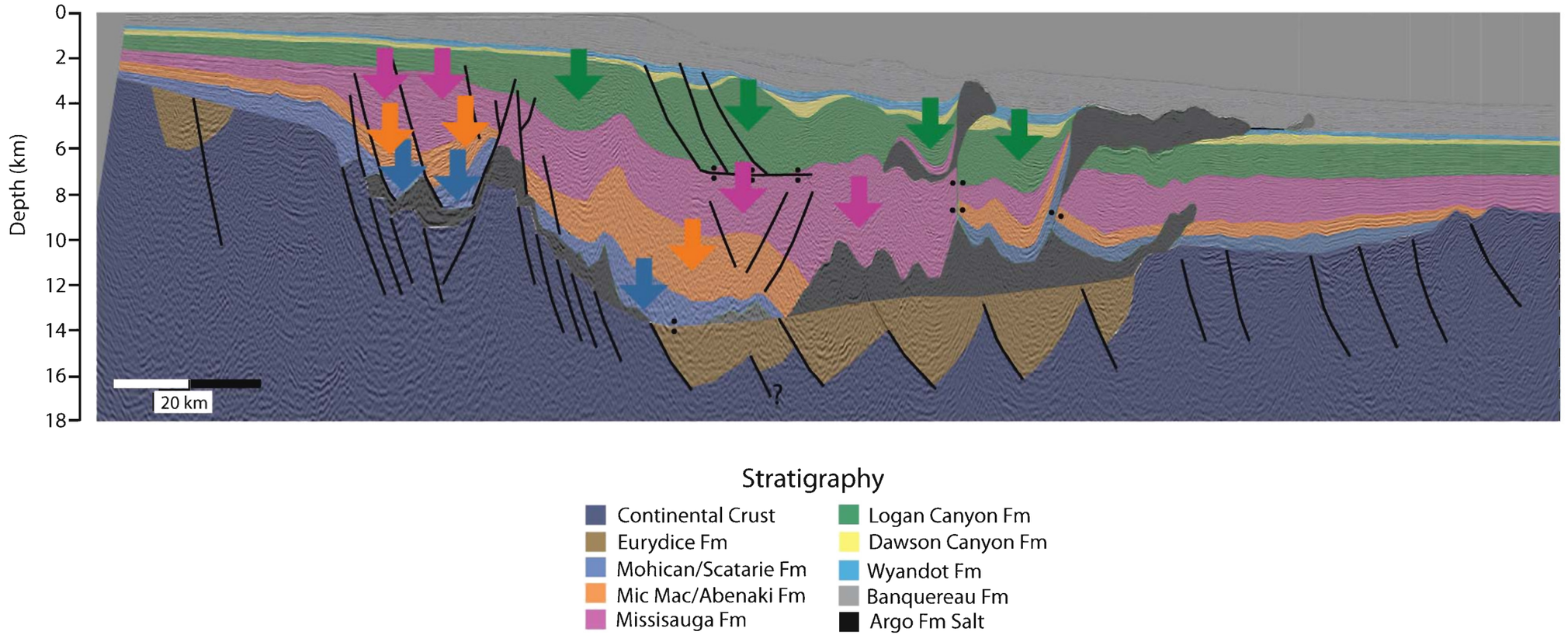

Figure 4-9: Major depocenters of NovaSPAN line 1600 indicated by colored arrows that correspond to their respective formations. Key stratigraphic packages are filled in to emphasize areas of thickest fill. Unlike northern regions of the margin, i.e. at NovaSPAN line 2000, the depocenter migration over time is complicated as a result of widespread deposition.

region, it is not likely that they initiated much, if any downbuilding. Therefore, the major depocenter for the Early – Mid Jurassic was within the proximal graben.

4.5.2 Mic Mac Formation (Mid – Late Jurassic)

The Mid – Late Jurassic Mic Mac formation shows a complex depocenter evolution, as it is interpreted to have considerable accumulations in both the proximal graben and within the main Sable sub-basin trend (Fig. 4-9). Although downbuilding in both regions was likely coeval, it is probable that early development was strongest in the proximal graben. As increased accumulation of pelagic sediments resulted in subsidence in the main Sable sub-basin trend, more accommodation space could be available for further deposition. Based on the thickness of sedimentary packages, it is interpreted that deposition and downbuilding was broad and relatively uniform. It is likely that this downbuilding and salt mobilization inflated salt in the distal region, just beyond the modern day slope. Therefore, it is not likely that the aforementioned region was the site of significant accumulation.

4.5.3 Missisauga Formation (Early Cretaceous)

The deposition of the Early Cretaceous Missisauga formation and equivalent strata was widespread and provides insight into depocenter evolution (4-9). Substantial growth is observed in the proximal graben and is probably the result of increased sedimentation rate/influx and salt withdrawal. However, only ~2 km of this thickened package probably documents true growth, as reflections tend to become sub-horizontal just over halfway up the package (Fig. 4-5). Where these reflections become sub-horizontal correlates with the drastic thinning of Missisauga formation sediments over the horst and the proximal region

of the Sable basin beneath the modern slope. This suggests that during the Early Cretaceous, this region quickly became an area of sediment bypass toward the main Sable sub-basin. The formation in Sable sub-basin thickens and rotates asymmetrically into diapir D1, where there was an inflated salt complex. This region was the dominant depocenter during deposition of the Early Cretaceous as indicated by seaward thickening of the package. Increased downbuilding into the inflated salt complex where the basin-floor becomes a ramp has resulted in the regional expulsion rollover structure which gives strong basinward dips of older reflections. The Missisauga formation is thin between diapirs D1 and D2 and overlies older Jurassic formations. This sediment package originated as a mini-basin, but was considerably translated seaward as a result of strong, asymmetric expulsion rollover landward of the passive diapir D1. Beyond the autochthonous salt basin there is a significant accumulation of sediments that are probably dominated by pelagic deposits. However, it is possible that deepwater turbidites had reached this position before D1 and D2 became prominent bathymetric ridges.

4.5.4 Logan Canyon Formation (Early Cretaceous)

The deposition of the Early Cretaceous Logan Canyon formation is even more widespread than the Missisauga formation; however, the modern-day slope appears to be the site of thickest accumulations and therefore the main depocenter (Fig. 4-9). This region not only hosts salt withdrawal from the original salt source layer, but also from allochthonous salt sheets that are at the uppermost portions of the Missisauga formation, complicating this period of margin evolution. Loading of the Balvenie Roho System has also resulted in extensional failure of sediments as they were deposited, and growth patterns are thickest at faults that are positioned at the landward portions of the structure.

This complex interplay of structural evolution highlights how the regional depocenters can be internally complicated by supra-salt deformation. Between diapirs D1 and D2, there is significant growth, suggesting that the region at this time became a true salt-withdrawal basin and depocenter. Beyond the salt basin, there is a considerable accumulation of equivalent strata, but these are not as thick as the main depocenter. These deposits are likely fine pelagic sediments and turbidites transported beyond the actively deforming system.

4.5.5 Dawson Canyon and Wyandot Formations (Late Cretaceous)

Compared to previous times, there are no true depocenters throughout the deposition of the Dawson Canyon and Wyandot formations. In areas where there was still active deformation over allochthonous salt sheets (e.g. BRS) and within the mini-basin bounded by D1 and D2, there is minor thickening of packages. However, this period generally tends to be characterized by little deposition and cessation of salt tectonics.

4.6 3D Variations in Basin Morphology and Salt Structures

4.6.1 Basin Morphology and Locations of Diapirs

Public seismic reflection profiles have been used to understand along-strike variations of basin morphology and salt structures (Appendices B1 and B2). The Western portion of the Sable sub-basin is geologically complex along strike, as variable rifting processes have led to a distinct basin evolution at the LaHave Platform (Appendix B-3). Since there was less syn-rift crustal extension at this region, reduced subsidence led to only minor salt accumulation. The present-day basin floor climbs ~4 km from the Sable

sub-basin to the LaHave Platform at the modern day slope (Appendix B-4), which is the deepest portion of the margin at Salt Province II. Similar to observations in NovaSPAN Line 1600, diapirs are situated at regions where the basin floor climbs to shallower depths. These diapirs feed extensive canopies that appear to have spread during the relatively slow deposition of the Dawson Canyon and Wyandot formations. The interpretation results clearly indicate a relationship between the position of diapirs and basin morphology, particularly where the basin floor shallows.

West of NovaSPAN Line 1600, diapirs that likely feed shallow canopies are situated further landward than at the Sable sub-basin (Appendix B-1: following the canopy trend). These diapirs probably coincide with shallowing of the basement and canopies occur chiefly at stratigraphic levels of the Late Cretaceous Dawson Canyon and Wyandot formations. Unfortunately, no obvious feeder diapirs have been found in the public seismic lines due to the limited number of profiles and their poor image quality at later two-way travel time (deeper than 6 s TWTT). The only diapirs west of NovaSPAN line 1600 in the Sable Sub-basin are observed in NovaSPAN 5300 (Appendix B4), and are positioned where the basin-floor shallows toward the LaHave Platform.

East of NovaSPAN Line 1600, the diapir trend continues through the deepest portion of the Sable sub-basin, where the basin floor begins to shallow. In line 293-182 (Appendix B-5) there is a diapir with a similar position and geometry to D1 in NovaSPAN line 1600 (Fig. 4-6). It is interpreted that this diapir is also welded at depth, due to late-stage contraction. Further east, in line 298-182 (Appendix B-6), there appears to be a series of relatively small, bulbous diapirs that tend to have slight seaward-leaning overhangs at the shallow, Early Cretaceous canopy level. The quality of the seismic data

is too poor to ascertain whether or not these diapirs are fed from thin/welded stocks within the section, but it is likely that at least two are. Although there are no prominent mini-basins developed between the shallow areas above the diapirs, there may be thin welded salt sheets connecting them. These diapirs, like most others observed, follow a shallowing basin-floor trend at the seaward exremity of the basin.

4.6.2 3D Extent of Canopies and Salt Withdrawal Basins

West of NovaSPAN line 1600, the dominant stratigraphic levels at which allochthonous salt canopies have spread are with the Late Cretaceous Dawson Canyon and Wyandot formations. However, within certain profiles there are salt structures that suggest that minor gravity spreading during the Early Cretaceous transgression event that was responsible for the spreading of the BRS (Appendices B-2, B-4, B-7 and B-8). Although lower accommodation space led to minor accumulation and shallow stratigraphic depth compared to what is observed in the deeper portions of the Sable sub-basin, the chronological tie is consistent with the relative starvation event, such that it allowed for the spreading of a small overhang of the most basinward diapir in Lithoprobe transect 88-1a (Appendix B-1 and B-3). In lines 270-182 and 272-182 (Appendices B-7 and B-8), there are small salt withdrawal basins that developed over what is believed to be a salt sheet equialent to the top of the Missisauga formation. The salt sheet is welded at this position (~6.6 s TWTT), but climbs to and connects with the main canopy level. The climbing geometry of this salt body reflects the overall transgressive nature of the Early Cretaceous Logan Canyon formation.

East of NovaSPAN line 1600, along lines 286-182 and 282 (Appendix B-9, ~7 s TWTT), there is a salt canopy system that is sub-horizontal with small salt pillows. This canopy coincides with the occurrences of the BRS and the landward-leaning overhang from D1. There is no obvious feeder in the seismic profile, so it is assumed that all salt has spread into the section from lateral flow. Sediment downbuilding has led to mini-basins that were initiated during the time of Early Cretaceous Logan Canyon formation deposition; however, growth of these packages ceased by the Tertiary. In line 293-182 (Appendix B-5), the BRS is likely present, although not obvious, as there are landward-dipping reflections that are truncated by a Tertiary unconformity. By line 298-182 (Appendix B-6), the BRS is no longer evident. Landward of this line however, the BRS is present as evidenced in the along-strike NovaSPAN 5300 profile. This suggests that there is a correlation between basin architecture and its position, as its occurrence generally follows the slightly more landward, deepening trend of the basin in this region. At line 308-282 (Appendix B-10) there is generally thick salt at the shallow canopy level. The occurrence of thick allochthonous salt further landward than previously observed also follows the along-strike shallowing trend of the basin as evidenced by sediment thickness (Fig. 1; Appendices B-1 and B-2), and is likely fed by diapirs that follow the trend. Over the salt canopy there are multiple mini-basins that have formed from passive downbuilding of sediments throughout the Tertiary.

4.7 Derived Physical Experiment Constraints

The interpretation of NovSPAN line 1600 is the basis for salt basin morphologies and sedimentation rates used in physical experiments. By using a regional seismic profile for the determination of these parameters, experiments should have more meaningful

results that are directly comparable to the natural case. If experiments result in overburden and salt structures that are similar to those seen at the western Sable sub-basin, their evolution should provide insight into how the real structures formed, providing further confidence and understanding of the interpretation.

Two end-member-interpretations of NovaSPAN line 1600 were used to constrain experimental setup and parameters, e.g. salt basin architecture (Fig. 4-10) and sedimentation rates for the analogue models (Fig. 4-11). The main differences between models were the amount of Jurassic strata, as they are unconstrained at depth where there is no well constraint available, syn-rift basin geometry, and original salt thickness. Interpretation 1 depicts a scenario in which there are more Jurassic strata at depth in the Sable sub-basin. This interpretation assumes that a considerable amount of Jurassic sediment prograded into the Sable sub-basin, which could have occurred when the Sable Delta lobe was migrating southwest and sea level was dropping. The basin morphology is simplified as two half-graben wedges that taper to their basinward limits. The NSH is less pronounced than is seen seismic interpretation but is simplified to show how salt mobilization would occur if the Abenaki basin had at least some taper in its geometry.

Interpretation 2 has less Jurassic sediments and assumes that most of the stratigraphy in the Sable sub-basin is Early Cretaceous and was delivered after the southwest migration of the Sable Delta lobe. In this interpretation, the salt tectonics system decouples between the proximal graben and deep salt basins. The basin morphology is more complex than in interpretation 1 and is meant to test the effect of subtle changes in salt-thickness and basin-floor geometry. The Abenaki sub-basin is

interpreted as being a symmetric graben with no seaward taper to test the effects of early salt mobilization.

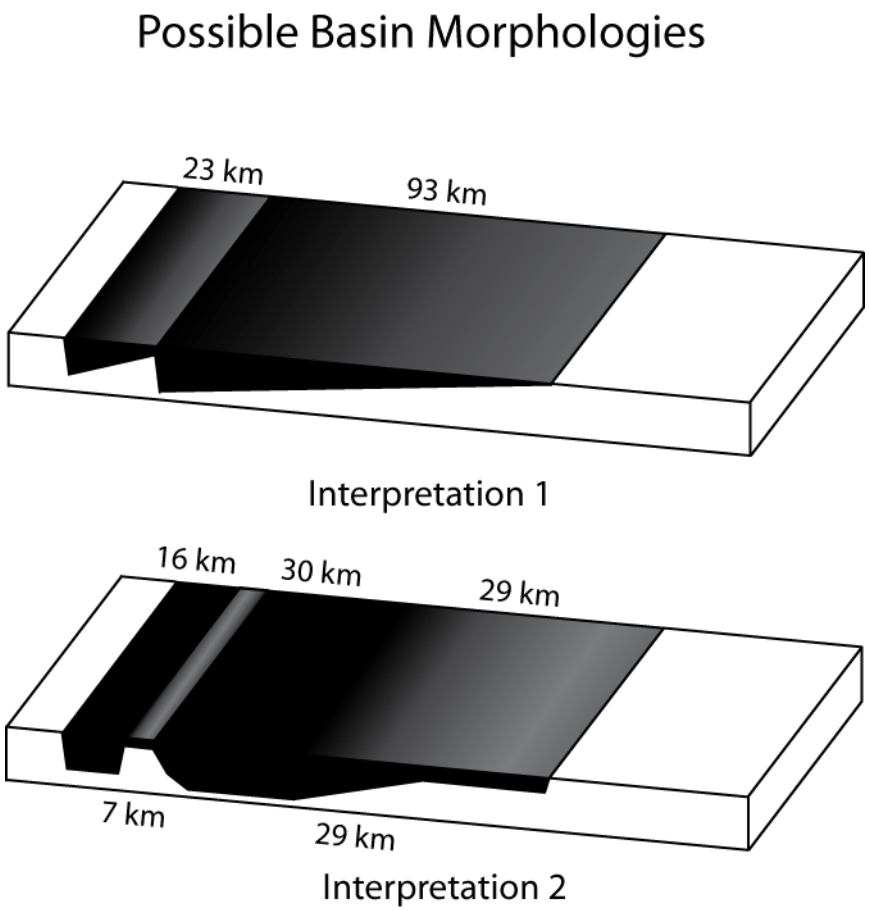

Figure 4-10: Basin morphologies for interpretations 1 and 2 of the western Sable sub-basin. Interpretation 1 comprises of two half-graben wedges. The small, landward wedge is 20 cm long and 0.5 – 2.5 cm thick; the second, large wedge is 60 cm long and 0 – 3 cm thick. Interpretation 2 has a complex basin morphology consisting of a symmetric graben, and a large basin with a ramp and flat at its seaward terminus. The symmetric graben is 10 cm long and 2.5 cm thick, and is bounded on its seaward limit by a horst that is 5 cm long with 0.5 cm silicone cover. The deep basin has a constant silicone infill of 3 cm for 25 cm, after which the basin floor ramps up to a thickness of only 1 cm silicone cover over a distance of 20 cm. The ramp extends for another 20 cm to the seaward terminus of the silicone basin, and has a constant, tabular silicone thickness of 1 cm.

Although the experiments were based on earlier versions of the interpretation presented here, the variations are not different enough to invalidate their applicability to

the study. In certain instances, model results influenced the development of the interpretation described in detail throughout this chapter.

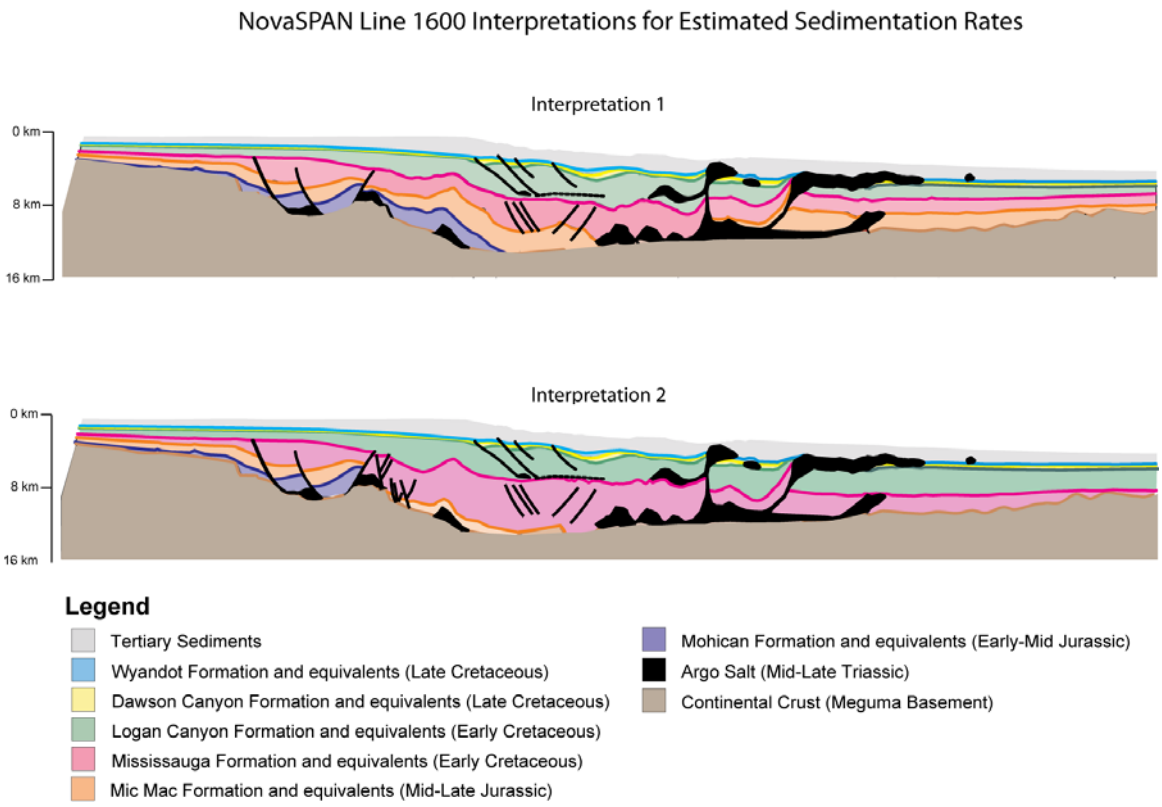

Figure 4-11: End-member interpretations used for sedimentation rate calculations in physical models. Interpretation 1 has much more Jurassic strata, as it is uncertain how much is present at depth. Model 2 has a low amount of Jurassic strata, and stresses the onset of progradation from the Sable Delta during the Early Cretaceous. In interpretation 2, the top Missisauga formation is picked at the base of the Balvenie Roho System, based on a known transgressive event that deposited an overlying shale tongue in the shelf. During this time, the model undergoes a sediment starvation for approximately 12 hours (3.6 Ma) to simulate the transgression, and allow for the spreading of silicone sheets.

4.7.1 Basin Morphology

As a consequence of having alternative possible geometries for the basin-floor due to generally poor imaging at depth, two end member configurations were used for the experiment setup (Fig. 4-11). The setups are generalized to represent the fundamental basin characteristics, for example, silicone thickness and geometry of the salt basin.

Since the experiment base is limited by the field of view of the cameras, the experiment basin width is scaled down to ~70% of its natural dimensions to meet the constraints of the model base table. The experimental salt basins are not exactly proportional to nature; however, the aim of the experiments is not to recreate the prototype, but to test similar first order conditions in order to understand fundamental processes. These experimental salt basins still test the effects of basin morphology, and initial syn-rift salt thickness on regional-scale salt tectonic processes, and results can still be understand aspects of the natural system. The experimental setup will be further explained in chapter 5 of this thesis under (*section 5.5: Applied Experimental Procedures*).

4.7.2 Sedimentation rates

Overall sedimentation rates for each formation (m/My) are calculated from average sediment thicknesses, their depth/stratigraphic level, general compaction trends, and the duration of deposition (Table 4-1). Areas of maximum sediment thickness within seismic packages are interpreted as locations of depocenters in different time intervals of the sub-basin history.

While the physical experiments were conducted, sands were deposited by sieving into individual layers. This was important as it generated homogeneous mechanical properties in the experiment, which is the main requirement for the consistent scaling of models to nature. Sifted sand already experiences maximum compaction (Lohrmann et al., 2003) and will not be affected by dynamic compaction during the experiment; so only a minor decompaction correction was applied to avoid a significant underestimation of model sedimentation rates. Therefore, the experiment sedimentation procedure does not

attempt to exactly re-produce the dynamics of a natural depositional system; instead, the goal is to realistically represent first-order regional variations in sedimentation rates in time.

Geologic Period	Formation	Experiment 1 Sed. Rate (m/My)	Experiment 1 Sed. Input/km of margin (km^3/My)	Experiment 2 Sed. Rate (m/My)	Experiment 2 Sed. Input/km of margin (km^3/My)
Early - Mid Jurassic	Mohican Fm	70	3.1	40	1.8
Mid - Late Jurassic	Mic Mac Fm	85	6.2	50	3.7
Early Cretaceous	Missisauga Fm	110	14.2	160	20.7
Early Cretaceous	Logan Canyon Fm	90	12.5	120	16.7
Late Cretaceous	Dawson Canyon Fm	55	6.7	30	3.6
Late Cretaceous	Wyandot Fm	45	6.8	30	4.5
Tertiary	Banquereau Fm	NC	NC	NC	NC

NC - Not Calculated

Table 4-1: Sedimentation rates derived from end-member seismic interpretations used for scaled physical experiments.

4.7.3 Salt Basin Setup 1: Two Asymmetric Half-Graben Wedges

4.7.3.1 Basin Morphology

For experiment 1 (Fig. 4-10), the basin morphology is simplified as two asymmetric half-graben wedges. The first wedge represents a smaller salt basin (Abenaki sub-basin) that formed as a local graben in the rift shoulder landward of the hinge. In seismic profile, the first small basin is interpreted as being approximately 23 km in length. The original salt thickness in the landward portion of the half-graben is ~2.5 km, and uniformly tapers to ~0.5 km at its basinward terminus.

The second wedge represents the deeper portion of the Sable Sub-basin trend, which makes up the main extent of the salt basin. The thickest portion of the salt basin close to the basement high is 3 km, but it uniformly tapers to 0 km at its seaward extent. This second, larger, basin extends ~93 km downdip from the horst structure in

NovaSPAN line 1600. Original syn-rift salt thickness of 3 km is approximated from basin fill in salt-withdrawal basins.

4.7.3.2 Sedimentation Rates

For setup 1 (Fig. 4-11; Table 4-1), the Mid Jurassic has a moderate sedimentation rate of 70 m/My (including 20% decompaction) that corresponds to aggradational deposition with relatively little progradation. During the Late Jurassic, the sedimentation rate increases slightly to 85 m/My (15% decompaction), corresponding to the onset of progradation. At the beginning of the Early Cretaceous, the Sable Delta becomes the main source of sediment input at the central Scotian margin. Consequently, the Missisauga formation is characterized by a sedimentation rate of 110 m/My (10% decompaction), making it the period of most rapid deposition. Throughout the remainder of the Early Cretaceous, eustatic sea level rise resulted in reduced sediment influx. The sedimentation rate of the Logan Canyon formation decreases to an average of 90 m/My (7% decompaction). During the Late Cretaceous, when extensive shallow salt sheets began to spread at distal regions of the margin, the Scotian basin was relatively sediment starved. The sedimentation rates for the Dawson Canyon and Wyandot formations are 55 m/My (5% decompaction) and 45 m/My (5% decompaction) respectively. The Banquereau formation sedimentation was not calculated, since most salt movement had ceased by the Tertiary.

4.7.4 Salt Basin Setup 2: Proximal Graben and Ramp-Flat Basin

4.7.4.1 Basin Morphology

The basin morphology of setup 2 (Fig. 4-10) is more elaborate than interpretation 1, and is meant to investigate subtle changes in basin geometry and silicone thickness. The proximal salt basin formed in a small but deep symmetric rift graben and is characterized by tabular salt with a thickness of 2.5 km. The width of the graben is ~16 km in dip-direction and it is separated from the main portion of the Sable Sub-basin by the intra-basin horst structure (NSH). From seismic observation the horst is approximately ~7 km wide. It is uncertain if any syn-rift sediments covered the horst before salt, but it is possible that it had a thin cover. An extensive fault system steps into the main trend Sable sub-basin from the horst structure of the North Sable High. Based on seismic interpretation, the width of the Sable sub-basin sums up to a total of ~93 km and its basin floor has a flat-ramp-flat geometry rather than of a simple half-graben wedge. The geometry of the main extent of the sub-basin can be summarized as a deep (35 km long; 3 km thick) tabular salt basin, followed by a ramp in the basin floor (29 km long) that climbs to a shallow flat that has a decreased salt thickness (29 km long; 1 km thick). It is uncertain whether the "flat" segment at the end of the basin was truly sub-horizontal or if it had a slight gradient that tapered to the seaward termination.

4.7.4.2 Sedimentation Rates

The sedimentation rates for setup 2 (Fig. 4-11; table 4-1) depict a depositional scenario with dominant Early Cretaceous (Missisauga formation) sediment input. Minor sediment input during the Jurassic is simulated to study the effects of minor pre-Sable

sedimentation on basin evolution. Unlike interpretation 1, the top Missisauga formation is picked in the modern slope region at the base of the BRS. The setup also simulates a short sediment starvation event following a basin-scale transgression that would allow silicone canopies to spread in a similar fashion as the BRS in nature.

In setup 2, the Mid Jurassic is represented by a very low sedimentation rate of 40 m/My (20% decompaction) corresponding to only continental clastic deposition in the shelf that allowed for the development of the Abenaki carbonate reef complex. Through the Late Jurassic, minor deposition from the Sable Delta had a sedimentation rate of 50 m/My (15% decompaction) that was mainly focused in the shelf and proximal, small salt basin. The Sable Delta becomes the major sediment source in the Early Cretaceous as much of the accommodation space in the north-eastern portion of the margin has been filled during the Early – Mid Jurassic. The drastically increased sediment influx is documented by a very high sedimentation rate of 160 m/My (10% decompaction) and was the main driver of the salt tectonics in the deep portion of the Sable sub-basin. A sedimentation break of about for ~3.6 ma was caused by the minor transgression that allowed for the spreading of allochthonous salt sheets.

Through the remainder of the Early Cretaceous, rising sea level led to reduced sedimentation rates. Subsequently the Logan Canyon formation had an average sedimentation rate of 120 m/My (7% decompaction), that drove the remainder of the deepwater salt tectonics. In setup 2, the Late Cretaceous Dawson Canyon and Wyandot formations are sediment starved, with rates of 25 m/My (5% decompaction) and 30 m/My (5% decompaction) respectively.

4.8 Problems with Seismic Interpretation and Objectives of 4D Physical Models

There are limitations to what information can be extracted by seismic interpretation at the western Sable Sub-basin, including:

1. The timing of emplacement and style of salt structures;
2. Effects of basin morphology and salt thickness on salt mobilization and diapir localization;
3. Subsidence patterns and depocenter migration during salt mobilization;
4. Insight into late stage salt tectonics process, when passive diapirs have already developed;
5. The interplay between loading subsidence and allochthonous sheet emplacement;
6. The spreading of allochthonous salt during starvation events;
7. Targeted structural closure problems.

Analogue modeling constrained by seismic data has the potential to provide insight into this missing information.

The timing of emplacement and style of salt structures are relatively unconstrained due to poor seismic reflectivity under the modern-day slope and at depth. The positions and possibly the geometries of salt structures, particularly diapirs, have been described with respect to basin morphology and original salt thickness. Analogue modeling should demonstrate the relationships and mechanisms of diapir formation with respect to basin morphology and salt thickness, if any exist. Furthermore, model subsidence patterns should aid in the understanding of regional-scale depocenter evolution at the western Sable Sub-basin, which should aid future discovery of reservoir sands.

Since salt is weaker than other lithologies, passive diapirs may often take on all, or close to all strain in the system as it deforms. This typically hides late-stage tectonic processes that may be important in the understanding of the evolution of the margin.

Analogue modeling should demonstrate how up-dip extension is counteracted by down-dip contraction, with or without the presence of diapirs. Some examples of structures that may be better explained by models include the regional expulsion rollover, the Balvenie Roho System, the geometry of diapirs, and the geometry of the salt withdrawal basin that is positioned between those diapirs. The Balvenie Roho System is not apparently fed by underlying feeders in NovaSPAN line 1600, and public seismic profiles do not have the quality at depth required to allow for their interpretation. It is expected that model results should demonstrate whether or not diapirs are likely to form under the modern-day shelf that would feed the allochthonous sheet, or if the feature had to spread into section from up-dip or down-dip localities. Furthermore, the importance of starvation events, such as the mid Early Cretaceous and Late Cretaceous transgressions, and their role of allochthonous salt emplacement will be investigated.

5.0 4-D Physical Experiments of Salt Tectonics at the Western Sable Sub-basin

5.1 Physical Experiments of Salt Tectonics at Passive Margins

Scaled physical experiments that use silica sand to represent brittle overburden and silicone putty to represent salt have greatly contributed to the current understanding of thin-skinned salt tectonic processes at passive margins (Mauduit et al., 1997; Fort et al., 2004; Vendeville, 2005). The quantitative information that these experiments provide into coupled tectonic and sedimentary processes is extremely valuable, as is insight into the evolution of key structures, such as diapirs (Vendeville and Jackson, 1992), rollover anticlines (Mauduit and Brun, 1998; Vendeville and Jackson, 1992a; Ge et al., 1997), and salt rollers (Brun and Mauduit, 2009). However, physical experiments have rarely investigated the syn-sedimentary evolution of these structures in a regional context, extending from proximal updip extensional domains (Brun and Mauduit, 2008), to distal contractional domains (Fort et al., 2004). Even fewer experiments employ appropriate model time-scales and sedimentation concepts to simulate natural passive margin salt systems (Krézsek et al., 2007).

This study uses dynamically scaled 3D physical experiments to investigate basin-scale salt-tectonic processes at the Scotian passive margin, to further aid the understanding of basin evolution. These experiments are monitored by Digital Imaging Correlation (DIC) techniques (Adam et al., 2005; Krézsek et al., 2007) to allow for the quantification of model deformation. Their geological constraints (e.g., sedimentation patterns, salt thickness, salt basin floor geometry) have been derived from interpretation of the Ion GXT NovaSPAN seismic reflection surveys.

5.2 Objectives of Physical Experiments in this Study

The main objective of the physical experiments was to advance from generic thin-skinned salt tectonic experiments to specific basin-scale experiments that have conditions similar to those interpreted at the western Sable sub-basin. Specifically, the physical experiments were set up to test first-order control factors including:

1) Basin architecture (salt basin geometry/basement morphology)

2) Sediment input (volumes and sedimentation rates)

By testing these parameters, experiments have provided insights into the post-rift evolution of the western Sable sub-basin, and have aided in the development of mechanically constrained concepts and structural templates for:

1) Kinematic modeling and regional correlations of salt features in the western Sable sub-basin

2) Paleogeographic reconstructions of depositional systems and salt features, and a tectono-stratigraphic framework for the western portion of salt province III.

These concepts were used to improve the understanding and minimize uncertainty of the interpreted salt structures and stratigraphic framework at the western Sable sub-basin. Results should be useful for future petroleum exploration in the study area, but also potentially worldwide where complex salt-tectonic processes have affected passive margins in a similar way.

Experiments were specifically used to answer currently open questions that remain about the salt-basin evolution at the western Sable sub-basin including:

1) The controls on the position and emplacement of the Balvenie Roho-System;

2) The tectono-stratigraphic framework in the Sable sub-basin and the role of the North Sable High (NSH);

3) The specific position of diapirs and a rationale for their localization and style of development.

5.3 Materials and Scaling

Sifted silica sand (grain size: 0.02-0.45 mm; angle of internal friction: 34°; density: 1.6 g/cm^3, strain softening c. 10-20%) was used in analogue models to simulate non-linear frictional-plastic deformation behaviour of brittle sedimentary rocks (Krézsek et al., 2007; Lohrmann et al., 2003). Peppered silica sand was used to allow for pattern recognition with digital image correlation (DIC), and color silica sand was used for marker horizons in structural and stratigraphic interpretation of final deformed model sections. Silicone elastomer (PDMS: polydimethylsiloxane; Wacer Elastomer NA USA; viscosity: 6 x 10^4 Pa s; density, 0.99 g/cm^3) was used to simulate viscous flow of salt sediments under gravitational load. This elastomer is appropriate as an analogue to salt as it has linear viscous behavior under experimental strain rates (Weijermars, 1986; Weijermars and Schmeling, 1986).

Models are dynamically scaled such that their geometries, kinematics, and dynamics in the experiments can be quantitatively compared to natural prototypes (Ramberg 1981; Weijermars and Schmeling 1986; Weijermars et al., 1993; Costa and Vendeville, 2002). For various parameters, a scaling factor f^* is derived from the non-

dimensionalized ratio of f_m/f_p, where subscripts m and p are model and prototype respectively.

The geometric scaling factor l^* is 10^{-5} and is deduced from the density and cohesion of sand and gravitational acceleration $(C/\rho g)_m/(C/\rho g)_p$ (Lohrmann et al., 2003). Therefore, 1 cm in models is equivalent to 1 km in nature. The density ratio ρ^* is 0.70, and is derived from the ratio between model sand and typical natural sediments, which are 1.6 g/cm^3 and 2.3 g/cm^3 respectively. The stress ratio σ^* ($l^* \times \rho^* \times g^*$) is 6.9×10^{-5}, where gravity is the same in experiments as in nature, and therefore g^* is inherently 1. The viscosity ratio η^* between model silicone (6×10^4 Pa s) and natural halite-dominated salt ($c = 10^{18}$ Pa s) is 6×10^{-14}. The ratio of σ^*/η^* defines the strain rate ratio, ε^*, and is 1.15×10^9. The time ratio without consideration for water load is inversely proportional to ε^*, such that t^* is 8.73×10^{-10}. However, numerical models of passive margin sedimentary wedges spreading over a salt detachment have established that the water column generally causes the system to take twice as long to evolve Steven Ings of the Dalhousie Geodynamics Group, pers. comm.), and therefore a t^* of 4.37×10^{-10} is more appropriate. This time factor implies that 1 hour experiment time is equivalent to 300,000 years geologic time.

5.4 Optical Strain Monitoring

All experiments are monitored with PIV techniques, which is a non-intrusive optical strain monitoring technique adapted for use in measuring 2D/3D surface flow and deformation in analogue experiments (Adam et al., 2005). Two stereoscopically mounted high-resolution digital cameras (Fig. 5-1) take time-series images of the experiment

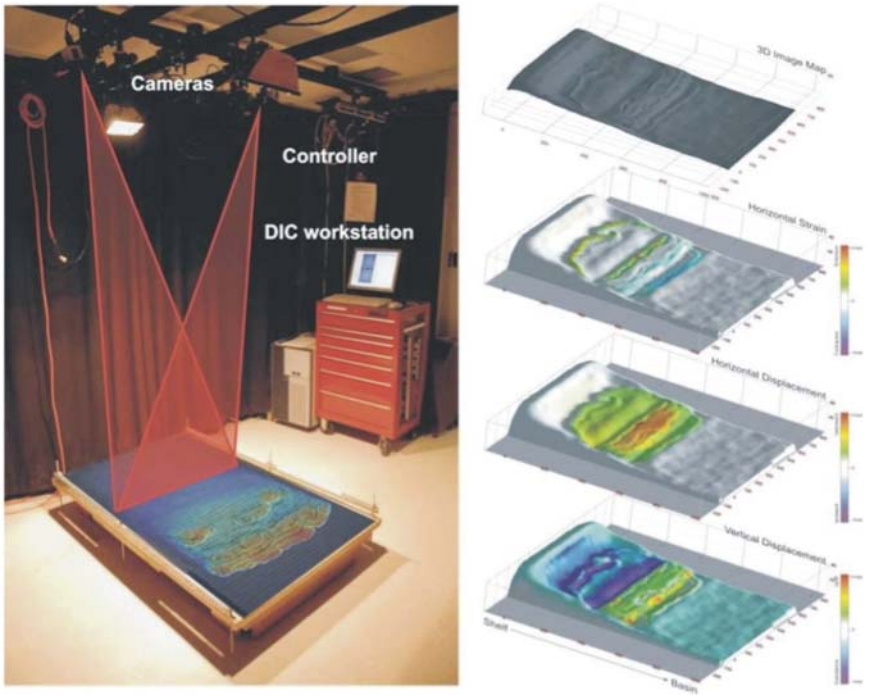

Figure 5-1: Physical modeling laboratory with schematic stereoscopic setup of high-resolution CCD cameras (left). Experiment surface shown with overlay of deformed vector grid showing horizontal displacement. Example 3D model data of an image mapped surface (top), horizontal strain (Exx; second from top), horizontal translation (Vx; second from bottom), and vertical displacement (Vz; bottom) (right).

surface. From stereo images, 3D surfaces are calculated with the use of LaVision's DaVis software package. From time-series images, 3D surfaces, 3D displacement data, displacement components, and strain derivatives can then be calculated with sub-millimeter (0.05-0.10 mm) accuracy including: incremental and finite subsidence, strain, and overburden translation. High-resolution 3D displacement (DIC) data provide accurate information about fault kinematics, silicone mobilization, and coupled depositional systems during basin evolution in the scaled experiments. Salt tectonics concepts and basin interactions derived from scaled experiments are used to further analyze the mechanics, timing, and coupling of salt-tectonic processes.

5.5 Applied Experimental Procedures

The western Sable sub-basin 4D physical experiments were performed on a horizontal rigid 140 cm x 90 cm base plate. Initial salt basin morphologies were based on seismic interpretation. The salt basin floor was built with silica sand and in-filled with silicone elastomer. Sediment volumes and sedimentation rates for various formations were generalized from seismic interpretation and then scaled for the experiments (Tables 4-1, 5-1, and 5-2). Sedimentation was simulated with incremental sieving procedures using predefined amounts of sand and sieving cups.

The sieving procedure provides homogenous mechanical conditions in the sand layer and allows for dynamic sedimentation patterns in response to the structural evolution of the model surface. Experiment sedimentation simulates early aggradation and subsequent progradation of a sedimentary wedge. Actively subsiding areas (e.g. grabens and silicone withdrawal basins) receive slightly higher sediment input. Similarly, topographic features control sediment transport and determine the location of thick sediment accumulations (e.g. at grabens and silicone withdrawal basins) or highs (e.g. diapir ridges, inflates silicone complexes, etc.) that are areas of bypass (Fig. 5-2 a). At the end of the aggradation phase, the major depocenters shift to the slope and deepwater (Fig. 5-2 b).

Two experiments focusing on the western Sable sub-basin were conducted for two weeks each, with sedimentation at eight and four-hour intervals. After the experiments were completed and silicone mobilization had ceased, experiments were covered with sand, wetted and cut in dip-oriented parallel sections. Digital photos were then taken of

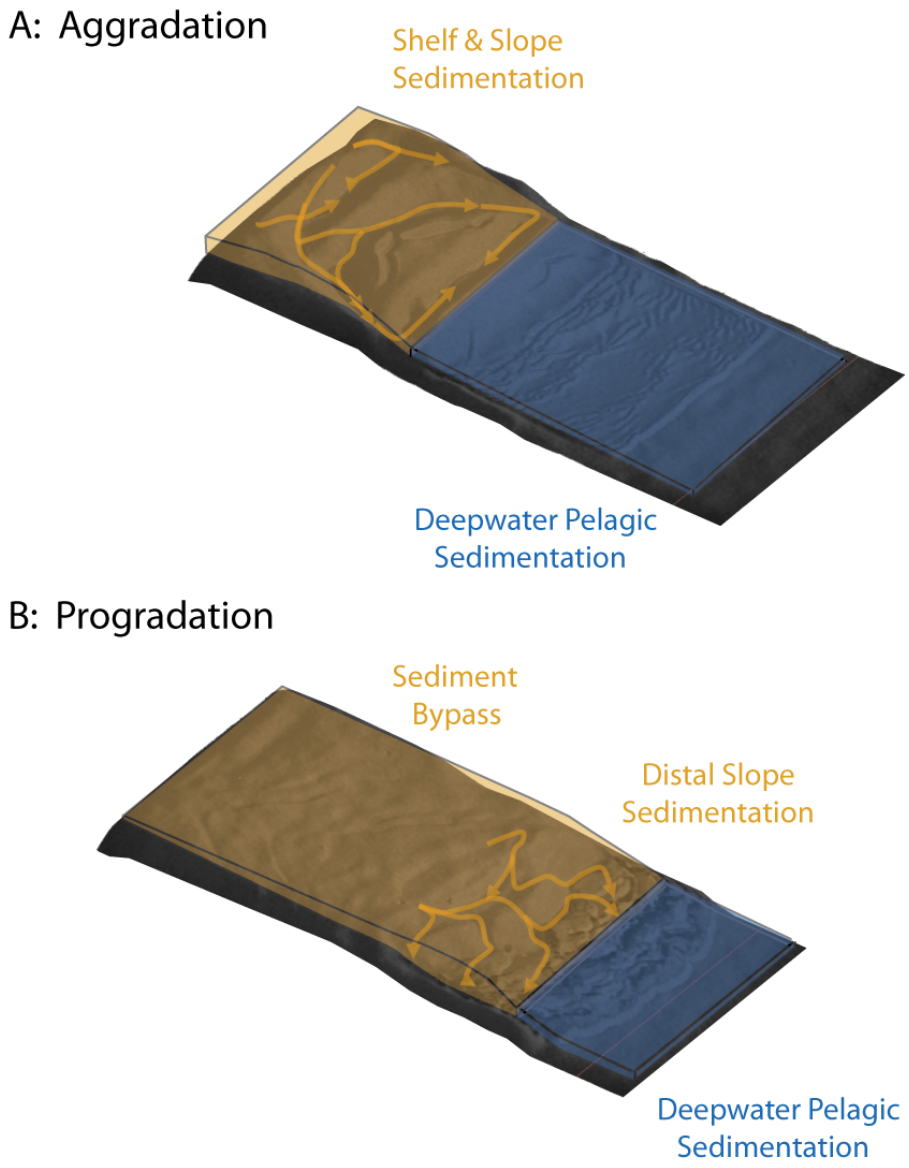

Figure 5-2: Experiment sedimentation procedure. A) Early stage aggradation: shelf and slope sedimentation. Grabens, silicone withdrawal basins are sites of increased deposition, topographic highs (e.g. diapir ridges) control sediment fairways. B) Late stage progradation: shelf characterized by sediment bypass, slope regions receive significant sediment.

each cross-section to document along-strike (lateral) variations of silicone structures, fault structures and depocenters in overburden sand layers.

5.6 Experiment Setups

Setups for experiments 1 and 2 are based on the two interpreted scenarios of NovaSPAN line 1600 that were presented and discussed in Chapter 4 (Fig. 4-10). These experiments test interpretation concepts with moderately differing sedimentation rates and salt basin geometries. Both scenarios have helped to resolve the effects of basin architecture and sediment input, leading to the development of concepts that can be used to improve the final interpretation of NovaSPAN line 1600. Particularly, experiments have provided insight into salt-sediment interaction from initial salt mobilization in the early Jurassic post-rift stage to the late allochthonous salt canopy emplacement in the Late Cretaceous.

5.6.1 Experiment 1 – Two Asymmetric Half-Grabens with Early Proximal Depocenters

The objectives of experiment 1 were to:

1) Test the effects of a basin geometry consisting of two half-graben wedges to assess the control of a broadly tapering basin

2) Test the effects of proximal deposition, with an abruptly tapering progradational sedimentary wedge.

5.6.1.1 Salt Basin Geometry

The salt basin geometry of experiment 1 (Fig. 5-3) is set up as two asymmetric half-graben wedges. Although the first half-graben presented in interpretation 1 is ~23 km wide in nature, it has been shortened to 20 cm in the model, which

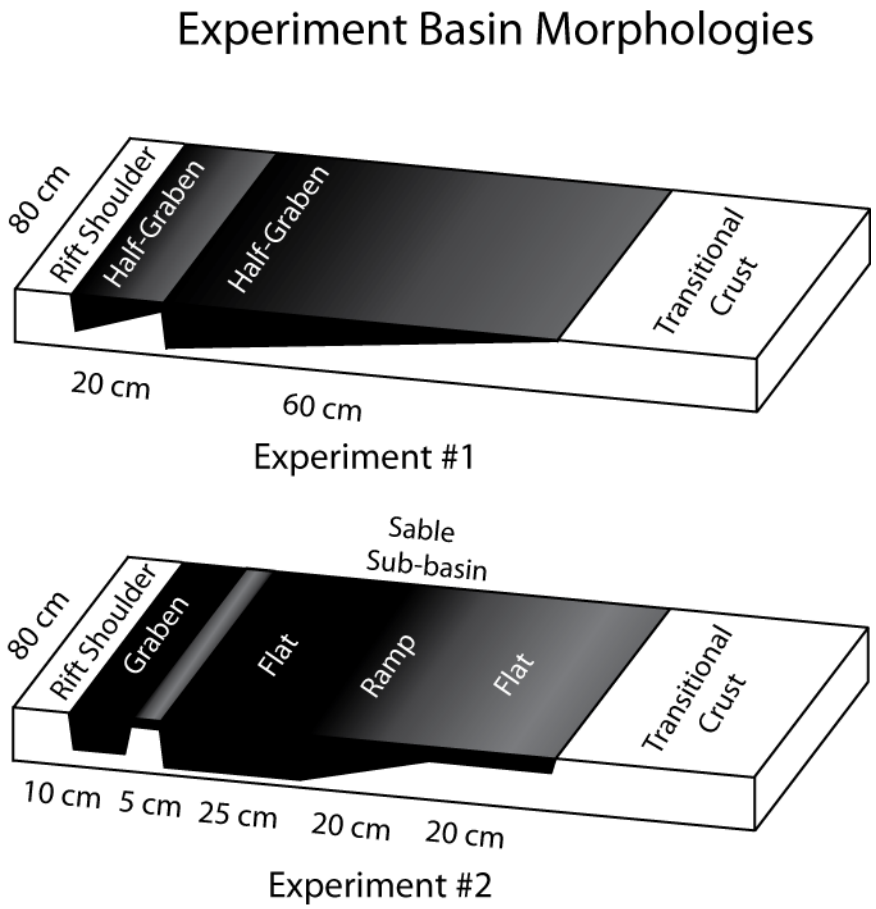

Figure 5-3: Silicone basin setups for experiments 1 and 2 of the western Sable sub-basin.

corresponds to 20 km in nature. In the experiments, the width and proportions of the salt basins are scaled with a length scaling factor of $l^*_{Salt\ Basin} = 0.7\text{x}10^5$ to fit within field of view of the DIC stereo camera system. The model sediment volume is accordingly scaled down to represent a comparable depositional input in relation to the salt basin volume. This moderate scaling of the salt basin dimension of 30% is still in the range of the overall geometric scaling factor of the experiments $l^* = 10^5$. Vertical dimensions are not affected and are scaled with l^* to assure proper dynamic scaling of force, stress & strain rates in the experiment. This is particularly important to enable direct comparison of gravity-driven deformation in model and nature. As mentioned in ***4.7.1 Basin Morphology***, the aim of the experiments is not to exactly recreate the prototype

structures, but to investigate first-order processes and parameters of the basin evolution. Experiment salt basins are setup similarly, but not exactly, as the interpreted prototype to test the general effects of basin morphology, and initial syn-rift salt thickness on regional-scale salt tectonic processes, so that concepts learned can be applied to the natural case.

The thickest portion of the model salt layer is 2.5 cm but it uniformly tapers to 0.5 cm seaward termination. The seaward half graben is deeper and is much wider (60 cm). The thickest portion of the seaward salt layer is 3 cm, but it uniformly tapers to 0 cm at the seaward termination of the autochthonous salt basin. This second, larger basin represents the main extent of the Sable sub-basin, which in nature extends ~93 km downdip from the horst structure (NSH) in NovaSPAN line 1600. Original syn-rift salt thickness is speculative but seismic interpretation of the GXT data constrain the lower limit to be at least 2 km. The experiment is set up with maximum thickness of 3 cm of salt, which corresponds to 3 km in nature; however, this is only at the deepest part and does not represent the average thickness.

5.6.1.2 Sedimentation Rates and Depositional Scenario

Sedimentation rates for experiment 1 (Table 5-2) are scaled to reflect interpretation 1 (Fig. 4-10), which was outlined in Chapter 4. This interpretation tests a more proximally deposited style in the early post-rift stage than interpretation 2. The Sable Delta was the source of the Early – Middle Jurassic Mohican formation sediment. Delta deposits were focused in the Abenaki sub-basin, and were delivered with some component of NE-SW (along-strike) direction and a derived sedimentation rate of ~70 m/My. The Mic Mac formation comprises the Middle and Late Jurassic and has an

Formation	Period	Epoch	Geo. time (Ma)	Mod. Geo. Time (My)	Duration (My)	Sed. Rate	Mod. Sed. Rate	Hours	Days
Missisauga	Early Cretaceous	Aptian	124	71	20	110 m/My	0.9 mm/4 h	244	11
			124	71				240	11
		Barremian	125	70				238	11
			127	68				232	11
			128	67				228	11
			129	66				224	10
		Hauterivian	130	65				220	10
			131	64				216	10
			133	62				212	10
		Valanginian	134	61				208	10
			135	60				204	10
			136	59				200	9
			137	58				196	9
			139	56				192	9
		Berriasian	140	55				188	9
			141	54				184	9
			142	53				180	9
			143	52				176	8
			145	50				172	8
Mic Mac	Late Jurassic	Tithonian	146	49	20	85 m/My	1.2 mm/8 h	168	8
			147	48				164	8
			148	47				160	8
			149	46				168	8
		Kimmeridgian	151	44				152	7
			152	43				144	7
			154	41				136	7
		Oxfordian	157	38				128	6
			159	36				120	6
	Middle Jurassic	Callovian	161	34				112	6
			164	31				104	5
		Bathonian	166	29				96	5
Mohican		Bajocian	169	26	26	70 m/My	1.1 mm/8 h	88	5
		Aalenian	171	24				80	4
			173	22				72	4
	Early Jurassic	Toarcian	176	19				64	4
			178	17				56	3
			181	14				48	3
		Pliensbachian	183	12				40	3
			185	10				32	2
		Sinemurian	188	7				24	2
			190	5				16	2
			193	2				8	1
			195	0				0	1
			195	0				0	1

Table 5-3: Relationships between geologic and model time and sedimentation rates for experiment 1. General durations of the formations used for this study are also presented within the table, each with their respective sedimentation rates. Sedimentation rates used for these scenarios are dependant on interpretation 1, which was presented in chapter 4.

interpreted sedimentation rate of 85 m/My. The Sable Delta was becoming the major source for deposition at the margin during this time and was prograding further seaward. Unlike the Early - Middle Jurassic deposition, sediment was not only focused in the small proximal graben, but was beginning to bypass the North Sable High into the main portion of the Sable sub-basin. By the Early Cretaceous Missisauga formation, the Sable Delta lobe had shifted southwest, and the sedimentation rate increased to 110 m/My. Early deposition during this time was slightly focused in the proximal graben. However,

complete salt withdrawal shortly afterwards resulted in bypass into the deep portion of the Sable sub-basin. During deposition of the Early Cretaceous Logan Canyon formation, the sedimentation rate in the basin decreased with rising sea level. The Sable Delta is no longer the dominant sediment source, but there are numerous smaller channels resulting in widespread deposition in the main trend of the Sable sub-basin. In interpretation 1, the sedimentation rate is estimated as 90 m/My in nature. The Late Cretaceous Dawson Canyon formation is a condensed section in the shelf that slightly thickens at the modern-day slope and deepwater, particularly were overlying allochthonous salt sheets where actively deforming during its deposition. The sedimentation rate slowed considerably to ~55 m/My. The Wyandot formation chalks also document a particular period of reduced sedimentation rate of ~45 m/My.

5.6.2 Experiment 2 – Proximal Graben and Ramp-Flat Basin with Widespread Deposition

The objectives of experiment 2 were to:

1) Test the effects of a basin geometry consisting of a small symmetric graben separated from a distal basin with ramp-flat geometries by a horst.

2) Test the effects of widespread, delta and pro-delta deposition with a broadly tapering progradational sedimentary wedge.

5.6.2.1 Salt Basin Geometry

The salt basin geometry for experiment 2 (Fig. 5-3, b) is more complex than for experiment 1 and tested subtle differences in initial basin geometry and original salt thickness. The small, proximal salt basin is symmetric, with constant model salt

thickness of 2.5 cm. The length of the experiment graben is 10 cm and it extends to the horst structure. The horst is 5 cm wide in the model and is covered by a thin layer of silicone (~0.5 cm), although it is not known if the natural horst was covered by salt. From observation of seismic profiles, the horst is approximately 6.8 km wide, and separates the two salt basins. Although the fault system that steps into the basin is extensive in nature, it has been simplified in the model, such that it is represented by a fault scarp that abruptly dips into the distal salt basin. This portion of the Sable sub-basin also has a more complex basin-floor geometry in this model than in the previous experiment. The basin floor is divided into three segments: a deep (25 cm long, 3 cm thick) flat salt basin; a ramp in the basin floor (20 cm long); this climbs to a shallow flat level that has a tabular silicone thickness (20 cm long, 1 cm thick). The entire length of the model basin is 65 cm and represents ~93 km in nature.

5.6.2.2 Sedimentation Rates and Depositional Scenario

Sedimentation rates for experiment 2 (Table 5-2) reflect interpretation 2 (Fig. 4-10), which was outlined in Chapter 4. Unlike experiment 1, this interpretation tests more regionally spread early post-rift deposition of a delta and pro-delta setting. In this scenario, early depositional systems are interpreted to have yielded lower sedimentation rates until the Early Cretaceous, when the southwest migration from the northeast of the Sable delta lobe resulted in higher sediment input.

The Mohican formation spans the Early – Mid Jurassic with a low interpreted sedimentation rate of ~40 m/My corresponding to minor pro-delta deposition from the Sable Delta to the northeast that was confined dominantly to the proximal graben. The

Mic Mac formation covers most of the Middle Jurassic and all of the Late Jurassic and has a sedimentation rate of 50 m/My that corresponds to mainly pro-delta deposition sourced from the Sable Delta, which was located to the northeast. By the Early Cretaceous Missisauga formation, the sedimentation rate increases to 160 m/My, which correlates to the southwest migration of the Sable Delta lobe. The Missisauga formation has a significantly higher sedimentation rate as the Sable Delta is now extending to the region of NovaSPAN line 1600. At the end of the Missisauga formation is a short (12 hours, ~3.6 Ma) experiment sedimentation break that emulates the effect of a minor transgression at the Scotian margin, which resulted in the deposition of the Naskapi shale in the shelf. During deposition of the Early Cretaceous Logan Canyon formation, the sedimentation rate in the basin decreased with overall transgression, and the shutting down of the Sable Delta. In interpretation 2, the sedimentation rate is estimated as 120 m/My in nature. The Late Cretaceous Dawson Canyon formation is a condensed section in the shelf that slightly thickens at the modern day slope and deep water, particularly when overlying allochthonous salt sheets were actively deforming during its deposition. Its sedimentation rate is approximately 30 m/My. The Wyandot formation is also a period of low sedimentation, with a rate of 30 m/My.

5.7 Experimental Results

5.7.1 Experiment 1 - Two Asymmetric Half-Grabens with Proximal Deposition

Experiment 1 was conducted over 11 days, for a total of 244 hours, and simulated approximately 73 m.y. of post-rift evolution comprising the early Jurassic (Sinemurian) to mid-early Cretaceous (Aptian) at the western Sable sub-basin (Table 5-1).

5.7.1.1 Structural Overview

Structural cross-sections were prepared from the final experiment by slicing it in 5 cm intervals in the shelf-slope direction. Each slice was photographed, digitally stitched, and interpreted (Appendix C-1). Although main structures are generally consistent along strike, their style and appearance may vary significantly. This reflects the lack of major strike-parallel variations in sediment input or basin structure. The variability in the individual structures is considered to be the result of local variations in timing of silicone flow, coupled subsidence, and deposition.

Figure 5-4 displays three representative cross-sections (15 cm, 30 cm, and 50 cm) of the final experiment. The landward margin of the silicone basin is indicated by a continuous, seaward-dipping, listric growth fault system (BGF1) in the overburden that was active throughout the early stage of basin evolution. At the center of the proximal half-graben, there is a small, buried diapir (~3.5 cm wide, extending to ~32 hours) with an overlying expulsion rollover. The base of the expulsion rollover and associated set of keystone grabens overlie the seaward flank of the small diapir. The expulsion rollover steeply dips into the landward flank of another diapir (D1) that is situated directly seaward of the small diapir. This diapir is larger (~5 cm wide, extending to ~112 hours) and is flanked by expulsion rollovers. These expulsion rollovers are welded to the basin floor, which prevented the further seaward translation of the large diapir, and also led to the formation of the bulk of salt withdrawal basins (SW1a and SW1b at stratigraphic intervals ~112 h).

Formation	Period	Epoch	Geo. time (Ma)	Mod. Geo. Time (My)	Duration (My)	Sed. Rate	Mod. Sed. Rate	Hours	Days
Dawson Canyon	Late Cretaceo	Turonian	92	103	3	30 m/My	0.5mm/4 h	356	16
			93	102				348	16
			94	101				340	15
		Cenomanian	95	100				336	15
Logan Canyon			96	99	23	120 m/My	0.8 mm/4 h	332	15
			97	98				328	15
			98	97				324	15
			99	96				320	14
	Early Cretaceous	Albian	100	95				316	14
			101	94				312	14
			103	92				308	14
			104	91				304	14
			105	90				300	14
			106	88				296	13
			107	88				292	13
			108	86				288	13
			110	85				284	13
			111	84				280	13
		Aptian	112	83				276	13
			113	82				272	12
			115	80				268	12
			116	79				264	12
			117	78	Sedimentation Break			260	12
			118	77				256	12
			119	76				252	12
Missisauga			121	74	24	160 m/My	1.0 mm/4 h	248	11
			122	73				244	11
			123	72				240	11
			124	71				236	11
		Barremian	125	70				232	11
			127	68				228	11
			128	67				224	10
			129	66				220	10
		Hauterivian	130	65				216	10
			131	64				212	10
			133	62				208	10
		Valonginian	134	61				204	10
			135	60				200	9
			136	59				196	9
			137	58				192	9
			139	56				188	9
		Berriasian	140	55				184	9
			141	54				180	9
			142	53				176	8
			143	52				172	8
			145	50				168	8
Mic Mac	Late Jurassic	Tithonian	146	49	23	50 m/My	0.8 mm/8 h	164	8
			147	48				160	8
			148	47				156	8
			149	46				152	7
		Kimmeridgian	151	44				148	7
			152	43				144	7
			153	42				140	7
			154	41				136	7
		Oxfordian	155	40				132	7
			157	38				128	6
			158	37				124	6
			159	36				120	6
			160	35				116	6
			161	34				112	6
	Middle Jurassic	Call/Bath.	163	32				108	6
			164	31				104	5
			165	30				100	5
			166	29				96	5
			167	28				92	5
			169	26				88	5
Mohican		Bajocian	170	25	25	40 m/My	0.7 mm/8 h	84	5
			171	24				80	4
		Aalenian	172	23				76	4
			175	20				68	4
	Early Jurassic	Toarc	177	18				60	4
			179	16				52	3
		Pliensbach	182	13				44	3
			184	11				36	3
			187	8				28	2
		Sinem.	189	6				20	2
			191	4				12	2
			194	1				4	1
			195	0				0	0
			195	0				0	0

Table 5-4: Relationships between geologic and model time and sedimentation rates for experiment 2. General durations of the formations used for this study are also presented within the table, each with their respective sedimentation rates. Sedimentation rates used for these scenarios are dependant on interpretation 2, which was presented in chapter 4.

The transition into the larger half-graben is also marked by a seaward dipping, listric growth fault system (BGF2) that persisted from ~72 to 120 hours. The major fault of this system is underlain by a small diapir that was trapped as overriding sediments downbuilt into the seaward silicone basin. This downbuilding of sediments on the seaward flank of the diapir has resulted in thick growth packages developing from ~72 to 116 hours, and demonstrates landward rotation along the fault. Further seaward (at ~50 cm) is another diapir (D2) that varies in size along strike (2–5 cm wide extending to a max stratigraphic interval of ~128 hours). There is also commonly a landward verging silicone overhang that spread on the experimental surface at ~72 hours from D2. Sand that was downbuilding asymmetrically into D2 resulted in the development of a minor fault keystone graben, with faults that sole out onto the landward overhang. However, where no overhang is present (section 50 cm), a seaward-dipping growth fault that was active from ~112 hours to ~152 hours flanks the seaward boundary of the diapir and extends to the basin floor. Basinward of D2 a major expulsion rollover developed during ~112 to 192 hours with extensive keystone grabens (ER/KG2). The expulsion rollover steeply dips into diapir D3 (~10 cm wide; max stratigraphic extent of 192 hours), which varies considerably in style along strike. This diapir is different in all profiles in Fig. 5-4, and has developed a seaward leaning diapir and late seaward extensive canopy at ~152 hours. When there is no true diapiric structure, but only remnant silicone, there is a counter-regional fault in some sections (i.e. section 30 cm) that indicates late diapir fall and depletion. The entire package of sediments contained between BGF2 and D3 comprises salt withdrawal basin SW2a. Beyond D3 at ~95 cm and at the seaward

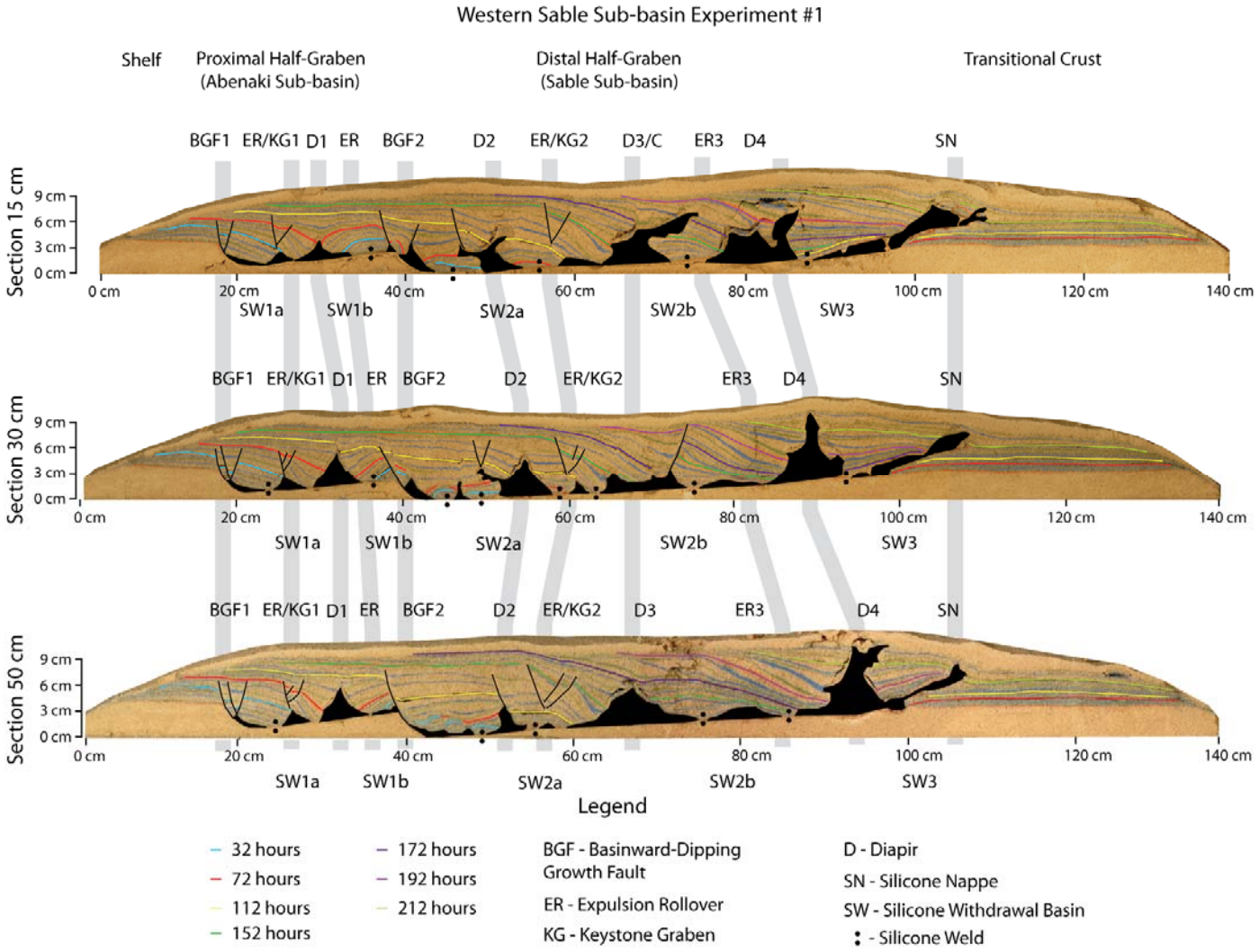

Figure 5-4: Three representative downdip final sections (15 cm, 30 cm, and 50 cm) of experiment 1.

terminus of the silicone basin, there is another rollover package that has no keystone grabens and terminates into that last diapir, D4. This diapir is ~5–10 cm wide, most commonly climbs through the extent of the model stratigraphy (152 to 244 hours), and has a small landward leaning overhang in some sections that spread at ~212 hours. The expulsion rollover landward of D4 is considered as being a separate silicone withdrawal basin (SW2b). On the seaward flank of D4, there is a package of rotated sediments that is considered to be the final silicone withdrawal basin (SW3), that developed from ~192 to 244 hours. This package of sand overlies a silicone nappe that has climbed much of the late stratigraphy (during 144 to 216 hours), and appears to have been translated seaward. This rafted package of sand is thrust over earlier basinal deposits using the silicone nappe as a detachment surface.

5.7.1.2 Experiment Evolution

The complex evolution of experiment 1 is illustrated in two time-space diagrams (Fig. 5-5 and 5-6) and time-series 3D experiment image and strain data (Fig. 5-7, 5-8 and 5-9). A representative section (35 cm) of the experiment has been sequentially restored in 24- and 48-hour intervals with the aid of time-series 3D surface elevation and strain data (e.g. vertical displacement and horizontal strain).

The time-space diagrams (Fig. 5-5 and 5-6) are a synoptic presentation of the spatial and temporal evolution of salt-tectonic structures and their associated depositional systems as deduced from time-series images and PIV analysis. The positions of structural and depositional elements (and strain data) are tracked on the shelf-basin transect at the 30 cm slice, which is plotted on the x-axis. The geographic variation of

these structural elements and deformation processes was determined for 24-hour intervals and plotted on the y-axis.

Figures 5-7, 5-8, and 5-9 depict the experiment evolution in 24-hour intervals with a set of 3D surfaces and image, displacement, and strain overlays. The lower panels display the original model surface on a 3D DEM. Active deformation processes are visualized by horizontal strain (E_{xx}; top) with extension shown in warm colors (diapirs, grabens, and faults) and contraction in cold colors (folds and thrusts). Margin normal translation and spreading of the prograding sedimentary wedge is visualized with horizontal displacement (V_x; middle) with seaward transport in warm colors and landward transport in cold colors (typically showing landward spreading canopies). The distribution and migration of depocenters is shown as vertical displacement (V_z) with uplift depicted with warm colors (silicone inflation, folds, diapiric rise) and subsidence with cold colors (grabens and withdrawal basins).

Although there are no abrupt transitions in the structural evolution of experiment 1, its evolution can be divided into characteristic early, intermediate, and late kinematic stages (Fig. 5-7 and 5-8).

- The *early stage (0 – 72 hours)* is characterized by silicone evacuation in the small, proximal, half-graben indicated by the development of a seaward-dipping, listric growth fault at the landward limit of the silicone basin. Other notable features include the development of a passive diapir at the mid-portion of the proximal graben, and inflation of silicone in the proximal part of the basinward half-graben. Complex patterns of contractional deformation, such as folds and silicone-cored

thrusts, between diapirs and inflated silicone massifs record the interplay between gravity driven extensional processes and early, downdip silicone inflation.

- The *intermediate stage (72 – 180 hours)* is characterized by the propagation of depocenters into the large half-graben that represents the main Sable sub-basin, the development of two diapirs at the mid-region of the basinward half-graben, and strong inflation and uplift in the distal region of the autochthonous silicone basin. This advancement of seaward propagation of depocenters coincides with silicone withdrawal and welding in the proximal half-graben and the onset of growth faulting in the second and larger half graben.

- The *late stage (180 – 244 hours)* is characterized by progradation of the sedimentary wedge beyond the autochthonous silicone basin, the development of the final diapir out of an inflated silicone complex, and the emplacement of an extensive silicone nappe. This stage is marked by late stage welding from 55 cm to 65 cm, the shut-down of D3, and the development of D4.

- *Early Stage (0 - 72 hours)*

The early stage (earliest post-rift) is characterized by seaward silicone evacuation in the small, proximal half-graben. The extensional domain at this stage is characterized by passive diapirism and normal faulting related to sediment downbuilding. An early basin-scale listric fault (BGF 1: Fig. 5-4) developed at the landward margin of the proximal half-graben, caused by differential subsidence in response to downbuilding of sand within the silicone basin. Coeval with BGF 1 is extension in the overburden in the mid-portion

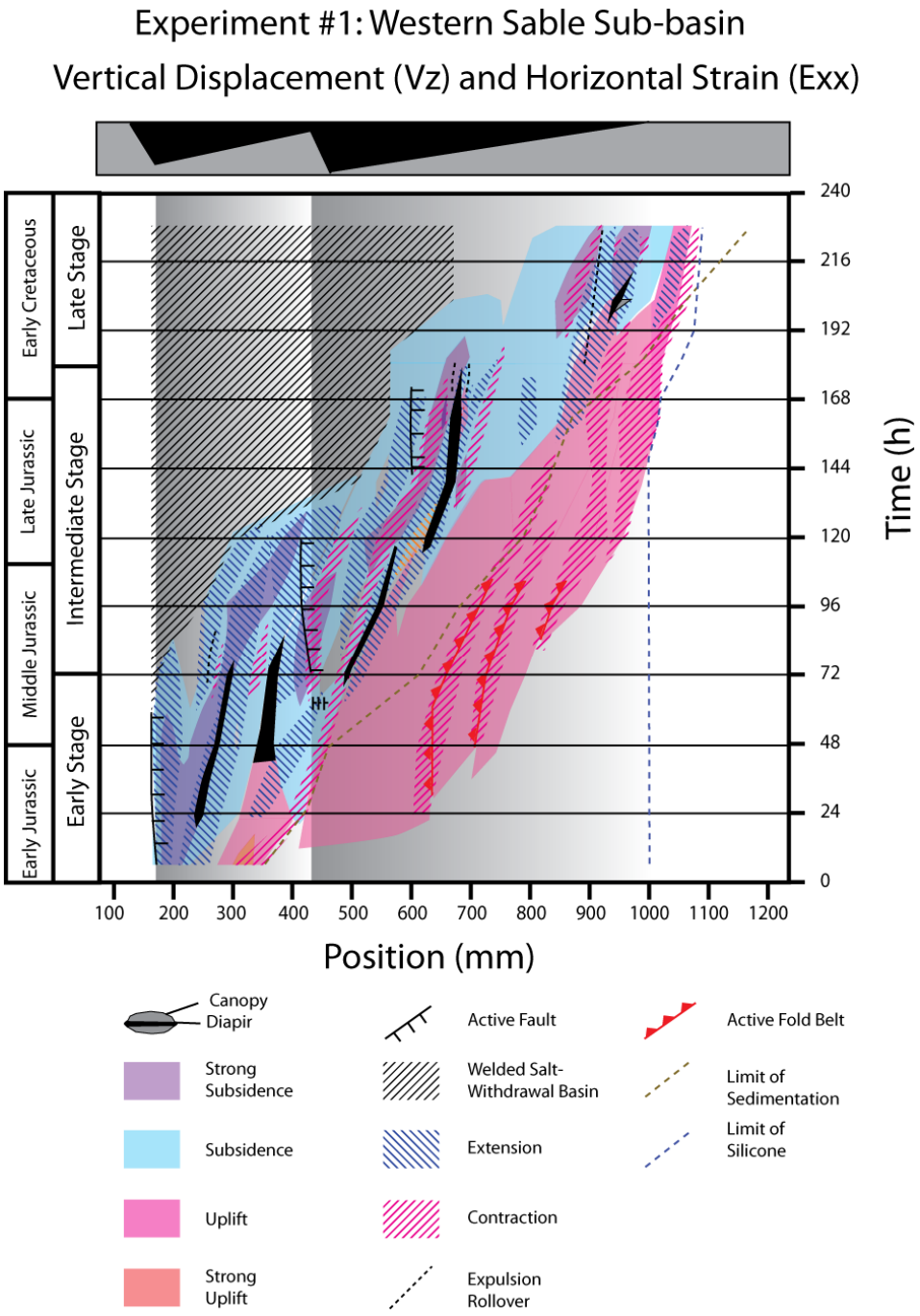

Figure 5-5: Time-space diagram of vertical displacement and horizontal strain, with respect to structures as they developed throughout the evolution of section 35 cm of experiment 1. Geologic time and salt tectonic stages are presented on the left border of the diagram, the downdip position in mm is on the bottom, and model time is on the right. A schematic illustration of the model basin setup is presented above, which correlates to dark (thick silicone) and light (thin silicone) shades of grey in the diagram.

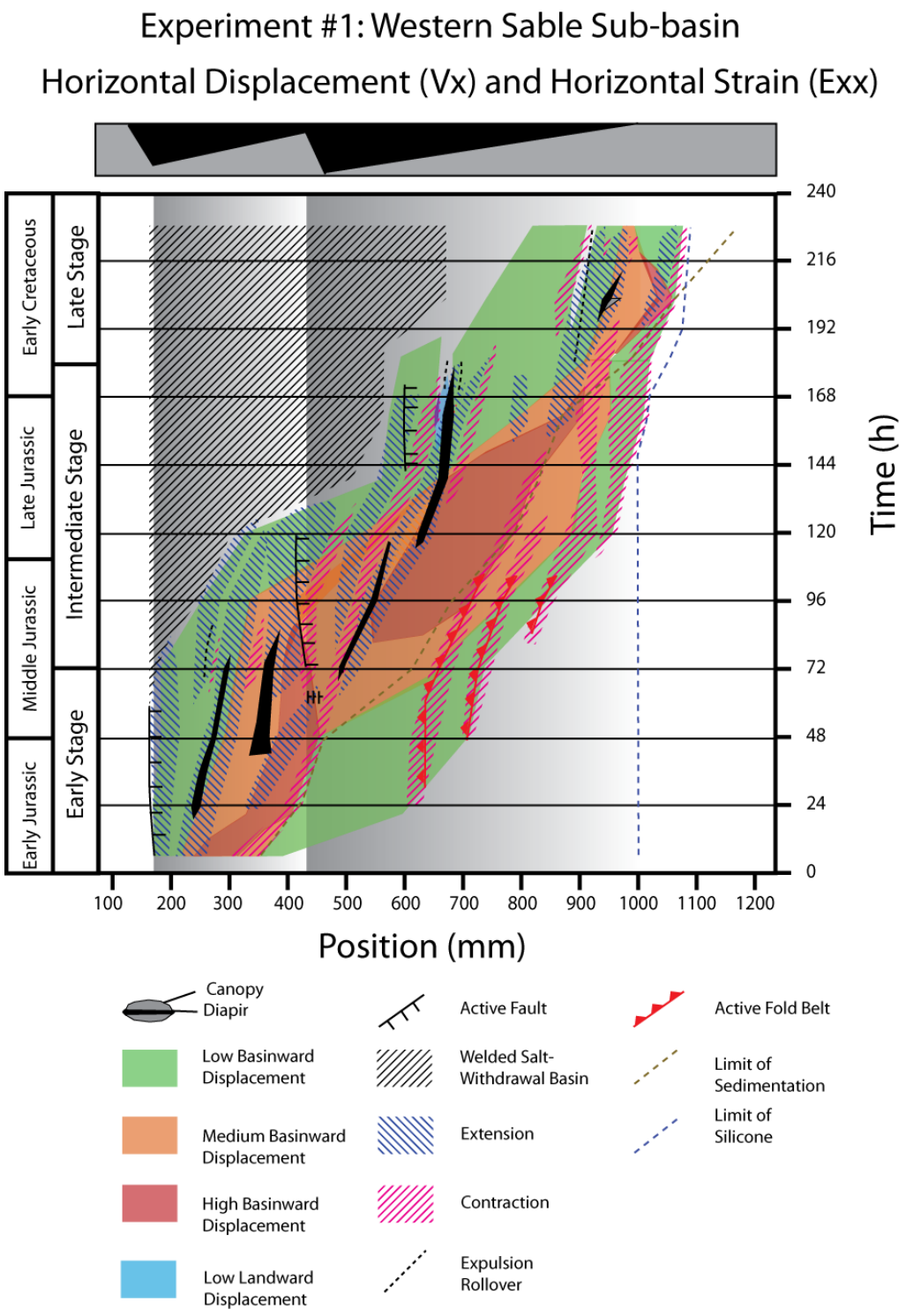

Figure 5-6: Time-space diagram of horizontal displacement and horizontal strain, with respect to structures as they developed throughout the evolution of section 35 cm of experiment 1. Geologic time and salt tectonic stages are presented on the left border of the diagram, the downdip position in mm is on the bottom, and model time is on the right. A schematic illustration of the model basin setup is presented above, which correlates to dark (thick silicone) and light (thin silicone) shades of grey in the diagram.

of the proximal wedge that allowed for the development of reactive diapir (D1: Fig. 5-7 A, B & C) as sediments prograded beyond the region. As the diapir pierced the thin overlying sediments, it became a topographic ridge that segmented the topography in the half-graben area into two separate silicone withdrawal basins, (SW1a and SW1b; Fig. 5-7 C - Vz). Maximum subsidence throughout the early stage was located on the landward side of the diapir D1 (Fig. 5-7 A & B - Vz). As a result of this asymmetric downbuilding, D1 experienced minor seaward translation (Fig. 5-6 and 5-7 A & B -Vx). However, by the end of the early stage, the subsidence on the landward flank of D1 ceased as the overburden welded to the basin floor. During asymmetric downbuilding into the landward flank of D1, the sedimentary package rotated asymmetrically seaward, forming a monoclinal expulsion rollover structure with keystone grabens (ER/KG1: Fig. 5-7 C - Exx). Horizontal translation of sediments on the seaward flank of the diapir was significant and even higher on the seaward-dipping portion of the small-inflated silicone complex at the distal edge of the proximal wedge. This horizontal translation of overlying sand resulted in the formation of an early rafted package of strata.

Landward extension of the sedimentary wedge was balanced by contraction and silicone inflation in the distal silicone basin, where silicone originally tapered to ~0.5 cm (Fig. 5-5: 24 & 48 hours, and 5-7 A & B - Exx). Initially (0 – 24 hours; Fig. 5-7 A - Exx) all contraction in the system was balanced within this region; however, as the sedimentary wedge prograded further seaward (after 24 hours), broad silicone inflation occurred throughout the landward half of the second and larger half-graben. At the transition between the small and large basins, there was strong contraction located at the landward perimeter of the second body of inflated silicone (Fig. 5-5 - 24 to 72 hours; Fig. 5-7 A &

B - Exx). This region of contraction correlates with two notable observations: 1) it was situated between a diapir ($D_{(temp)}$: Fig. 5-7 B – Exx) and a topographic ridge of inflated silicone (inflated silicone massif: Fig. 5-7 B - Vz), but focused at the landward flank of the massif, and 2) it was positioned at the boundary of the leading edge of strong horizontal translation that advances into the large, distal basin (Fig. 5-6 24 & 48 hours; Fig. 5-7 B – Vx). This style of downdip contraction was related to gravity gliding and translation from the seaward flank of the first inflated silicone massif, which became halted by the landward flank of the second, weak inflated silicone massif. At the seaward limit of the second, broad, inflated silicone complex, fold belts formed within the inflated silicone (Fig. 5-5; Fig. 5-7 B - Exx & Vz). These fold belts appear to have accommodated so much contraction that the advancement of seaward inflation was halted until the intermediate stage.

Intermediate Stage (72 – 180 hours)

Depocenters migrated seaward into the second, larger, half-graben wedge during the intermediate stage as regional welds formed beneath SW1a and SW1b (Fig. 5-5 72 - 172 hours). Early in this stage (72 – 120 hours), SW1b became the focus of strong subsidence (Fig. 5-7 C –Vz; Fig. 5-8 A – Vz) and halts the seaward translation of D1, which became shut down as both flanking basins were welded and the diapir was cut off from any silicone source. At this time, a new growth fault (BGF2: Fig. 5-5 72 hours and 5-8 A - Exx) developed at the landward border of the second, larger half-graben due to passive downbuilding of sand into the thick silicone layer (Fig. 5-8 A – Vz). Coeval with this growth fault was the development of diapir D2 (Fig. 5-5 and 5-8 A & B - Exx), which

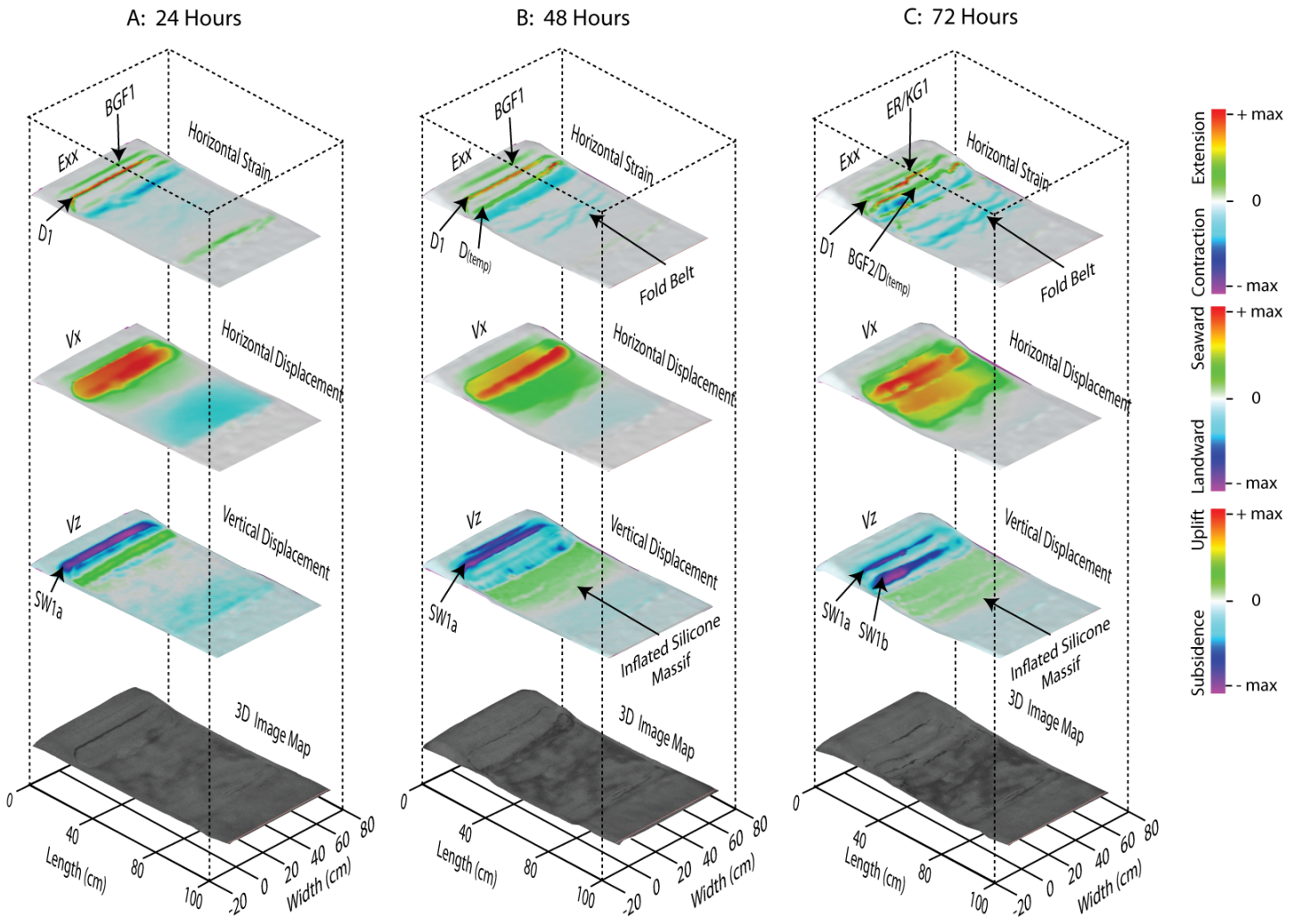

Figure 5-7: 24-hour, 3D surface renders of the model surface image, horizontal displacement, and horizontal strain data. Each of these renders represents the total deformation between each 24-hour interval, and provides detailed insight into salt tectonic processes in experiment 1. Between 0 – 72 hours, most extension occurs at landward regions of the model and translation makes its way into the mid-basin. Contraction is also localized at approximately mid-basin, as sets of fold belts and broad silicone inflation.

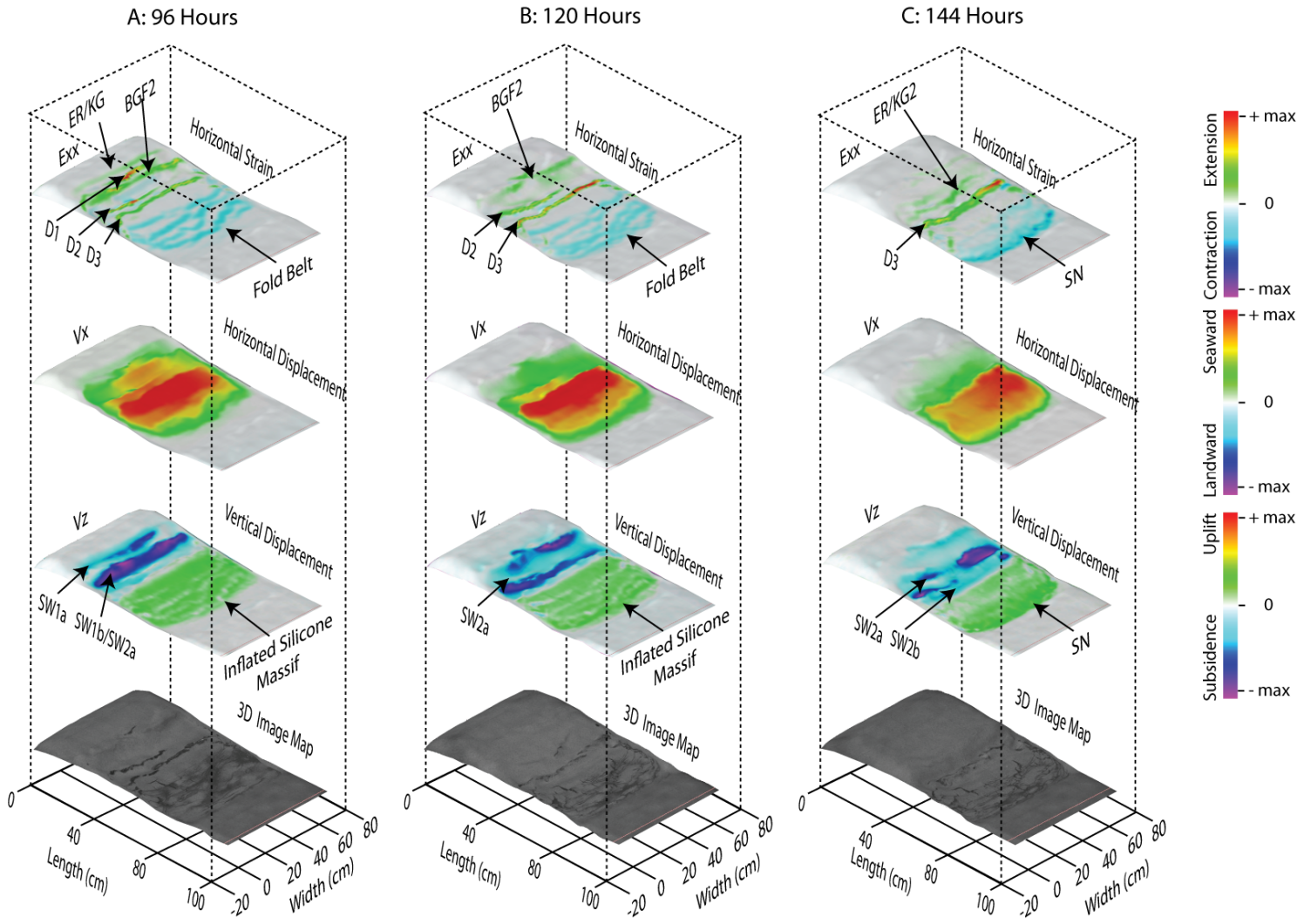

Figure 5-8: 24-hour, 3D surface renders of the model surface image, horizontal displacement, and horizontal strain data. Between 72 – 144 hours, the extensional regime and downbuilding migrate into the second, larger half-graben wedge, to approximately mid-basin. The earlier signs of contraction (fold belts and inflation) migrate further seaward, but are largely halted at the terminus of the basin. At this point (144 hours), the prograding wedge advances over the once contractional regime, creating further downbuilding and extensional overprinting.

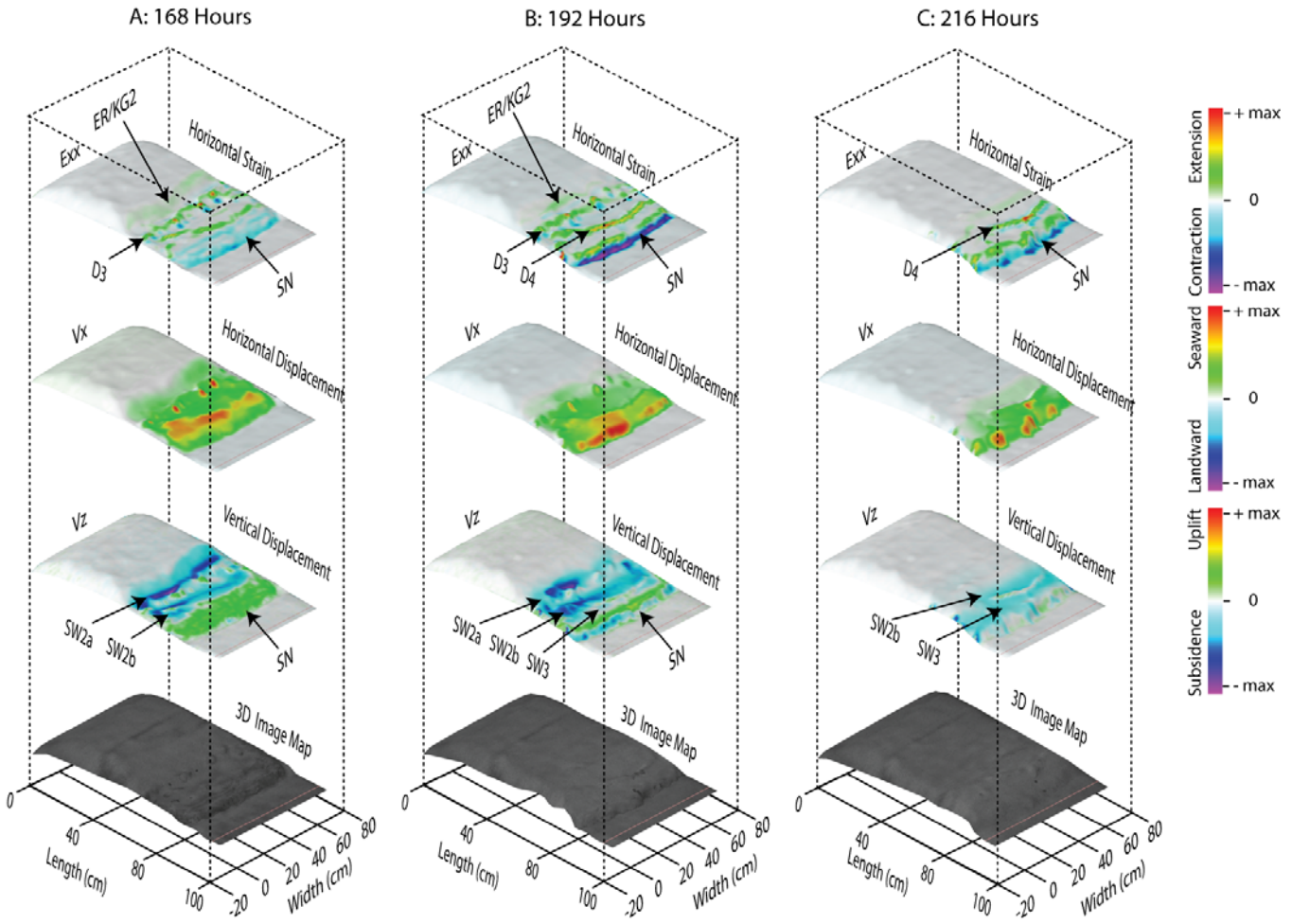

Figure 5-9: 24-hour, 3D surface renders of the model surface image, horizontal displacement, and horizontal strain data. From 144 hours to the end of the experiment, the remainder of silicone is forced out of the original basin, creating a silicone nappe. This expulsion of the silicone nappe was the final stage of contraction, after which the seaward advancement of the sedimentary wedge caused the region to become overprinted by extension.

evolved out of the contractional region that once marked the landward extent of the topographic high of the second inflated silicone massif. However, this diapir was overtaken by sediment progradation within 24 hours and was subsequently buried. Diapir D3 (Fig. 5-5, 5-8 A, B, & C - Exx, and 5-9 A & B - Exx) formed ~10 cm seaward of D2, and persisted throughout the remainder of the intermediate stage. Throughout its evolution, D3 was translated ~10 cm seaward (Fig. 5-5), resulting in asymmetric downbuilding and rotation of landward flanking strata. This resulted in a long-lived expulsion rollover with extensive keystone grabens (Fig. 5-8 C - Exx). Although D2 appears to have formed out of an inflated complex at the transition between the early extensional and contractional regimes, D3 formed out of a purely extensional regime, as shown by both surface extension and translation (Fig. 5-5, & 5-8 A, B, and C - Exx). Unlike D2, it developed in a typical scenario, where early extensional faults and grabens created space for the diapir to rise to the surface. The entire sediment package between BGF2 and D3 is considered as being one major depocenter (SW2a), which began to develop after D2 was formed.

The contractional domain during the intermediate stage is characterized by seaward advancement of the inflated silicone complex (Fig. 5-8 A, B, & C – Vz). However, very little of the silicone was expelled from the autochthonous basin. Rather, silicone inflated to ~2.7 cm at the seaward limit of the basin. The extent (30 cm downdip) of the contractional domain became continuously reduced during this transition (~1/2 of its original width) and it became a seaward topographic high with little overlying sediment.

Late Stage (180 – 244 hours)

During the late stage of experiment 1, the prograding sedimentary wedge advanced beyond the seaward limit of the autochthonous silicone basin. Since the narrow and inflated silicone massif was weaker than the overriding sand, it accommodated most of the strain induced by loading. However, some silicone was extruded past the autochthonous basin, with the exception of a small silicone nappe (Fig. 5-6 and 5-11). Diapir D4 (Fig. 5-5; Fig. 5-9 B & C - E_{xx}) evolved from the silicone massif, as sedimentation was not great enough to override the system. Although D4 was not translated much further seaward, moderate horizontal migration allowed for the development of another expulsion rollover (ER3: Fig. 5-4 – sections 30 cm & 50 cm) on its landward flank, which is also the position of SW2b (Fig. 5-4; Fig. 5-9 A, B, & C – Vz). Sand that flanked the seaward portion of D4 and overlay the silicone nappe also down-built to a significant thickness of ~6.5 cm and marks the most distal salt withdrawal basin (SW3).

Extensional processes dominated the deformation of the distally inflated silicone massif, which later became D4/C2 during the late stage of the experiment; however, there is major contraction at the toe of the advancing silicone nappe at the early stage of its emplacement.

5.7.1.3 Structural and Kinematic Evolution – Sequential Section Restoration

Figure 5-10 shows a representative shelf-slope cross-section (section 35 cm), which was sequentially restored at 24- and 48-hour intervals with the aid of time-series 3D surface elevation and strain data.

24 hours – Onset of Post-Salt Sedimentation and Early Basin Development

A seaward-dipping listric growth fault at the landward limit of the silicone basin was the first structure to develop due to passive downbuilding of early sediments in the small, proximal, half-graben wedge (BGF1: Fig. 5-4, BGF1: Fig. 5-10 – 24 hours). Early sedimentation was mainly confined to the landward half-graben, but a small amount was deposited in the landward area of the deeper, seaward rift graben as well, initiating an early salt-withdrawal basin. The main depocenter (SW1a: Fig. 5-4; Fig. 5-7 A & B – Vz, and Fig. 5-10 – 24 hours) at this time (in the first HGW) initiated early basinward silicone mobilization and up-dip extension in the overburden. This extension resulted in graben formation in the thin sedimentary wedge and reactive diapirism D1 (Fig. 5-7 A & B – Exx; Fig. 5-10 – 24 hours). Within the first 24 hours this reactive diapir pierced the graben center and developed into a passive diapir that separated the main depocenter into silicone withdrawal basins: SW1a and SW1b (Fig. 5-7 C - Vz). Down-dip contraction was chiefly localized over the distal half of the first HGW, which resulted in significant inflation. However, contraction was also broadly (~25 cm) accommodated throughout the landward half of the larger HGW, as seen by slight inflation.

48 hours - Continued Aggradation and Development of Early Diapirs and Expulsion Rollovers

Silicone was evacuated almost completely from beneath SW1a by 48 hours into the experiment, and the basin was welded to the basin floor and activity of the basin-bounding fault (BGF1) ceased. Diapir D1 has translated slightly (~5 cm) seaward and is roughly over the center of the first half-graben. It was still considerably wide at depth at this stage, and is more characteristic of a restricted inflated silicone massif. However, the

silicone body narrows and forms a ridge at the model sea floor so it may be classified as a passive diapir. Some sediments accumulated seaward of the silicone ridge in the landward part of the deep, second half-graben, adding material to the salt-withdrawal basin that began forming in the last time step (furthest subsidence in Fig. 5-7 B – Vz).

96 hours - Onset of Deformation in the Distal Half-Graben

96 hours into model 1, diapir D1 had advanced slightly (~2.5 cm) seaward (D1: Fig. 5-8 A – Exx, and Fig. 5-10 - 96 hours). Massive downbuilding of new sand deposits into the flanks of the broad passive diapir D1 together with seaward translation transformed the adjacent basins in an expulsion rollover with keystone grabens (ER/KG1: Fig. 5-8 A – Exx and Fig. 5-10 – 96 hours). A small silicone remnant was trapped underneath the crest of this expulsion rollover, and displayed resistance of the seaward migration of D1. By this time the sedimentary wedge had overrun D1 and developed a counter-regional expulsion rollover, flanking its seaward side (ER: Fig. 5-10 – 96 hours). Strata that were deposited seaward of D1 appear to have been translated significantly seaward and have been strongly deformed due to later downbuilding and the development of BGF2. From both the restoration and PIV data (Fig. 5-8 A – Vx & Vz; Fig. 5-10 – 96 hours), it is evident that much of the translation occurred over a very thin, and almost welded silicone layer. The landward portion of the second half-graben that became the depocenter forming SW2a, was the source for significant sand accumulation by this time, and pushed the inflated silicone front further seaward (~15 cm).

144 hours - Progradation of the Sedimentary Wedge and Expulsion Rollover/Keystone Graben Formation in the Distal Half-Graben

The sedimentary wedge prograded further into the distal half-graben, (25 cm to 45 cm) and all deformation had ceased in the proximal sub-basin by the end of this time step. Further downbuilding has occurred in SW2a and older strata were translated and rotated seaward along BGF2. A small silicone remnant (where D2 is located along-strike in other sections) remained in the footwall of a basinward dipping normal fault located seaward of BGF2, which displaced earlier stratigraphy. Significant downbuilding occurred within the inflated distal silicone massif, resulting in the development of a regional asymmetric expulsion rollover (ER/KG2: Fig. 5-8 C – Exx, and Fig. 5-10 – 144 hours). D3, which separates silicone withdrawal basins SW2a and SW2b (Fig. 5-8 C – Vz), developed from an expulsion rollover at the margin of the inflated silicone massif, into a passive diapir/symmetric expulsion rollover due to sediment bypass (D3: Fig. 5-8 C – Exx, and Fig. 5-10 – 144 hours). Although extension in the overburden allowed D3 to develop, it appears that the original thinning of silicone due to basin morphology strongly controlled the position of early-inflated silicone that eventually evolved into the diapir.

192 hours – Development of the Allochthonous Silicone Nappe

At 192 hours into experiment 1, the landward expulsion rollover had down-built into the flank of D3. Rotation and bending of rollover sediments resulted in formation of a set of extensive keystone grabens (ER/KG2: Fig. 5-9 B – Exx3). D3 had also been translated slightly (~5 cm) further seaward, and has experienced some diapiric collapse. Consequently, the diapir had widened, but was reduced in its vertical extent. As a result of this extension, strata that were located in SW2b (Fig. 5-9 B – Vx & Vz; Fig. 5-10 –

192 hours) were translated slightly further seaward. The inflated silicone complex became focused at the seaward terminus of the autochthonous silicone basin and the early allochthonous silicone nappe had extended beyond the autochthonous basin. The most significant depocenter at this time was in the mid-portion of the second half-graben (SW2b: Fig. 5-9 B – Vz).

224 hours – Advancement of the Silicone Nappe and Cessation of Deformation

Regional welding below SW2b occurred by 224 hours of the experiment, leaving minor remnants of silicone trapped in situ. Older strata from intervals 140 to 180 hours now dip uniformly seaward and terminate into a small silicone remnant landward of the newly developed diapir D4 (Fig. 5-4). This diapir has formed directly out of the inflated silicone complex as a result of sediment bypass beyond the basin and over the silicone nappe. A small landward overhang of D4 documents a time (~200 hours) of very high silicone extrusion related to rapid withdrawal on its landward flank. Near the end of its evolution, as sand downbuilt into its seaward flank (SW3), a small seaward overhang spread at the model surface at ~212 hours. Downbuilding over the most distal portion of the inflated complex has also provided the loading required to finally expel silicone over early deposited strata beyond the autochthonous silicone basin. Loading of this silicone nappe created accommodation space for the last depocenter (SW3: Fig. 5-4 and 5-9 C – Vz).

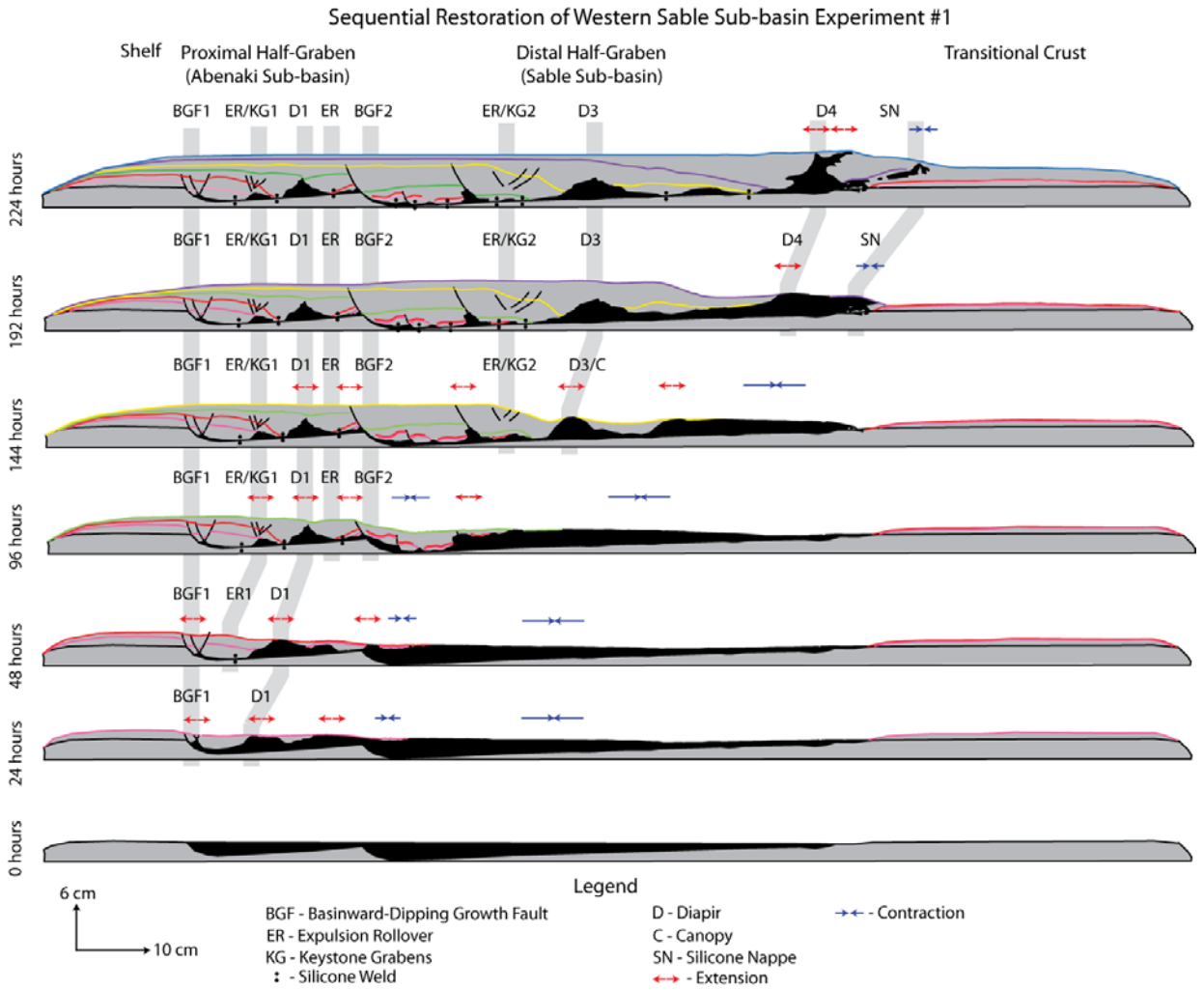

Figure 5-10: Structural restoration of section 35 cm of experiment 1 using time-series surface data, horizontal strain (Exx) and translation (Vx).

5.7.2 Experiment 2 – Proximal Graben and Ramp-Flat Basin with Deltaic and Pro-Deltaic Deposition

Experiment 2 was conducted over 16 days, for a total of 356 hours, and simulated approximately 106.8 Ma of post-rift evolution in the early Jurassic (Sinemurian) to Late Cretaceous (Turonian) at the western Sable sub-basin (Table 5-3).

5.7.2.1 Structural Overview

Structural cross-sections were prepared in the same manner as described for experiment 1 (Appendix C-2). Similarly, structures followed a general trend along-strike, as there was a lack of major strike-parallel variation in sedimentation or basin geometry. However, structures display considerable variability throughout the experiment, resulting from local variations in coupled silicone mobilization and sand input.

Figure 5-11 displays three representative cross-sections (20 cm, 30 cm, and 45 cm) through the final experiment. The landward margin of the small graben is bounded by a seaward-dipping listric growth fault (BGF) that was active during the early stage (0 – 124 hours) of the experiment. Most autochthonous silicone was expelled from the small graben and it was the site of an early silicone withdrawal basin (SW1) that experienced growth from 0 – 144 hours. Over the horst, there is a small silicone remnant, which was once part of a larger diapiric trend that was developing from 0 - ~192 hours. An expulsion rollover (ER/KG) dips into a large diapir (D1: ~5 cm wide, extending to ~192 hours of stratigraphy) within the larger portion of the Sable sub-basin that in some sections (i.e. sections 30 cm and 45 cm) has seaward-spreading overhang. Keystone grabens are present in the crest of the expulsion rollover, and are antithetic to a major seaward-dipping normal fault that soles onto the seaward flank of the aforementioned

silicone roller. The expulsion rollover related to D1 is considered a silicone withdrawal basin (SW2a) because it has experienced considerable growth from ~152–268 hours. There is another silicone withdrawal basin (SW2b) seaward of D1 that has generally uniform growth patterns from ~152–268 hours. However, in most sections, this package contains a silicone sheet that spread landward at ~152 hours sourced by diapir D2 during early stages of its evolution. Overlying this silicone sheet is a seaward-dipping normal fault that soles into its landward border. In sections that accommodated slightly more extension (i.e. section 45 cm) a conjugate fault to the dominant seaward dipping normal fault has developed. Diapir D2, which varies in size and stratigraphic extent, is positioned at the intersections between the horizontal section and ramp of the basin floor. The diapir fed a mid-strata canopy that began to spread just before (~212 hours) the starvation event at ~268 hours. This canopy system has spread in both the landward and seaward directions and is ~10 cm wide. Most commonly, this canopy is the uppermost limit of the diapir, but in certain positions, its main wall climbs through the entire experiment stratigraphy (e.g. section 45 cm). Another package of relatively undeformed sand is positioned between D2 and D3 and has been denoted as silicone withdrawal basin (SW2c), which developed from ~172 hours to the end of the experiment. Diapir D3 is positioned at the last transition in basin-floor geometry, where the ramp in the basin-floor becomes horizontal. Along strike of this diapir is a landward overhang that has developed at approximately the same time and almost connects with the landward canopy C1. The late evolution of the diapir is variable, and may either terminate at this level (i.e. section 30 cm), or continue to climb seaward through the remainder of the stratigraphy as isolated diapir stocks rather than a diapir wall (i.e. section 45 cm). Seaward of diapir D3 is the final silicone withdrawal basin (SW3) which generally encompasses the extent of

the horizontal portion of the silicone basin after the ramp, and developed from ~192 hours to the end of the experiment. Usually this region is efficiently evacuated, but in some sections (e.g. section 30) there is a considerable amount of remnant silicone. At the seaward terminus of the autochthonous silicone basin is the final diapir D4 (~2 cm thick to vertically welded and climbing the entire stratigraphy) that in many sections feeds a late-stage allochthonous silicone sheet. This silicone sheet (~5–10 cm in length) spread in both the landward and seaward directions at ~284 hours to 356 hours and commonly climbs stratigraphy toward its terminus at either end. A small silicone nappe also climbed out of the autochthonous silicone basin at ~216 hours; however, it was shut down relatively quickly due to subsequent loading and welding to the basin floor.

5.7.2.2 Experiment Evolution

The complex evolution of experiment 2 is presented in two time-space diagrams (Fig. 5-12 and 5-13) and 3D experiment data (Fig. 5-14 to 5-18). A representative section (45 cm) of the experiment has been sequentially restored in 24 and 48 hour time steps in a similar procedure as outlined for model 1.

The time-space diagrams (Fig. 5-12 and 5-13) portray the spatial and temporal evolution of salt tectonic structures and related depositional system as deduced from time-series images and PIV strain analysis. The graph is presented in the same format as used for model 1, and uses the section at 50 cm as the basis for structural elements. Figures 5-14 to 5-18 present the experiment evolution in 24-hour intervals with a set of artificially illuminated 3D surface renders. The panels are set up in the same manner as model 1,

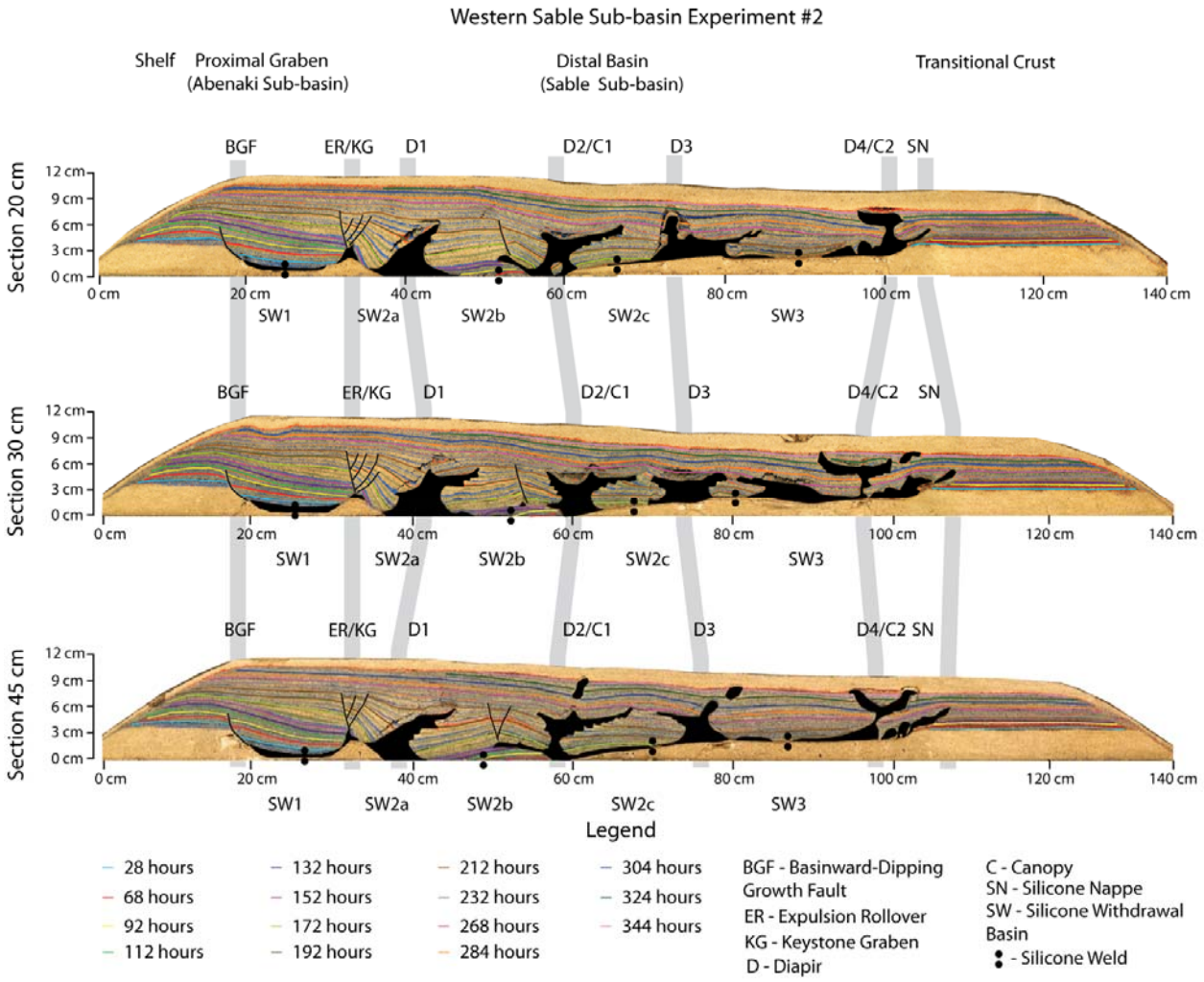

Figure 5-11: Three representative downdip final sections (20 cm, 30 cm, and 45 cm) of experiment 2.

and show the original model surface, horizontal strain, margin normal translation, and vertical displacement.

Although there are no abrupt transitions in model evolution, three kinematic stages, early, intermediate, and late could be differentiated.

- The *early stage (0 - 144 hours)* is characterized by silicone evacuation in the small, proximal, graben, indicated by the development of a seaward-dipping listric growth fault, and the development of a passive diapir over the narrow horst. In the distal basin, three separate fold-belts developed in response to up-dip extension, and are spatially related to underlying basin floor structures.

- The *intermediate stage (144 - 230 hours)* is characterized by the migration of depocenters into the deep seaward Sable sub-basin, the formation of passive diapirs D2, D3, and D4, the emplacement of the allochthonous silicone nappe, and the spreading of allochthonous canopies sourced by D2 and D4. Notably, the development of diapirs D3 and D4 and the emplacement of the silicone nappe began at approximately the same time (~200 hours), which coincided with depocenter migration into the inflated silicone complex that developed earlier over the ramp in the basin-floor. By the end of the intermediate stage, the sediment wedge had advanced beyond the autochthonous silicone basin.

- The *late stage (230 – 356 hours)* is characterized by the overprinting of earlier contractional features with a late extensional domain, the dominance of silicone withdrawal basin SW3, passive diapirism, spreading of allochthonous silicone canopies, and finally cessation of deformation.

Early Stage (0 – 144 hours)

The early stage (earliest post-rift) is characterized by seaward silicone evacuation from the small, proximal graben and the formation of a passive diapir over the narrow horst. Extension began with downbuilding into the small graben, initiating the development of silicone withdrawal basin SW1 (Fig. 5-14 A - Vz). Related to this downbuilding was the onset of growth faulting at the landward limit of the autochthonous silicone basin (BGF: Fig. 5-11, 5-14 A, B, & C - Exx, and 5-15 A & B - Exx). Updip extension resulting from gravitational loading was accommodated by downdip contraction over the horst. This downdip contraction was localized as a topographic ridge in the original silicone layer. However, the prograding sedimentary wedge very quickly restricted this ridge, and it consequently evolved into an extensional passive diapir (D1: Fig. 5-11, 5-14 A, B, & C - Exx, and 5-15 A, B, & C - Exx). By the end of the early stage, the major depocenter had already migrated ahead of D1, and early strata began to be deposited into the position of silicone withdrawal basin SW2a (Fig. 5-15 B & C – Exx). However, a significant amount of translation associated with the development of D2 (Fig. 4-15) soon rafted these sediments into the position of SW2b (Fig. 5-16 A – Vx and Vz).

Early downdip contraction in experiment 2 (Fig. 5-12 and 5-13) was complicated, and revealed significant interaction between early downdip contraction/silicone inflation and basin morphology. Broad inflation in the distal basin occurred with the onset of downbuilding in the proximal graben. At this time, the areal extent of silicone inflation covered the entire Sable sub-basin (Fig. 5-14 A & B – Vz), with exception to the distal region overlying the originally uniform and thin layer of silicone (1 cm). All fold belts in

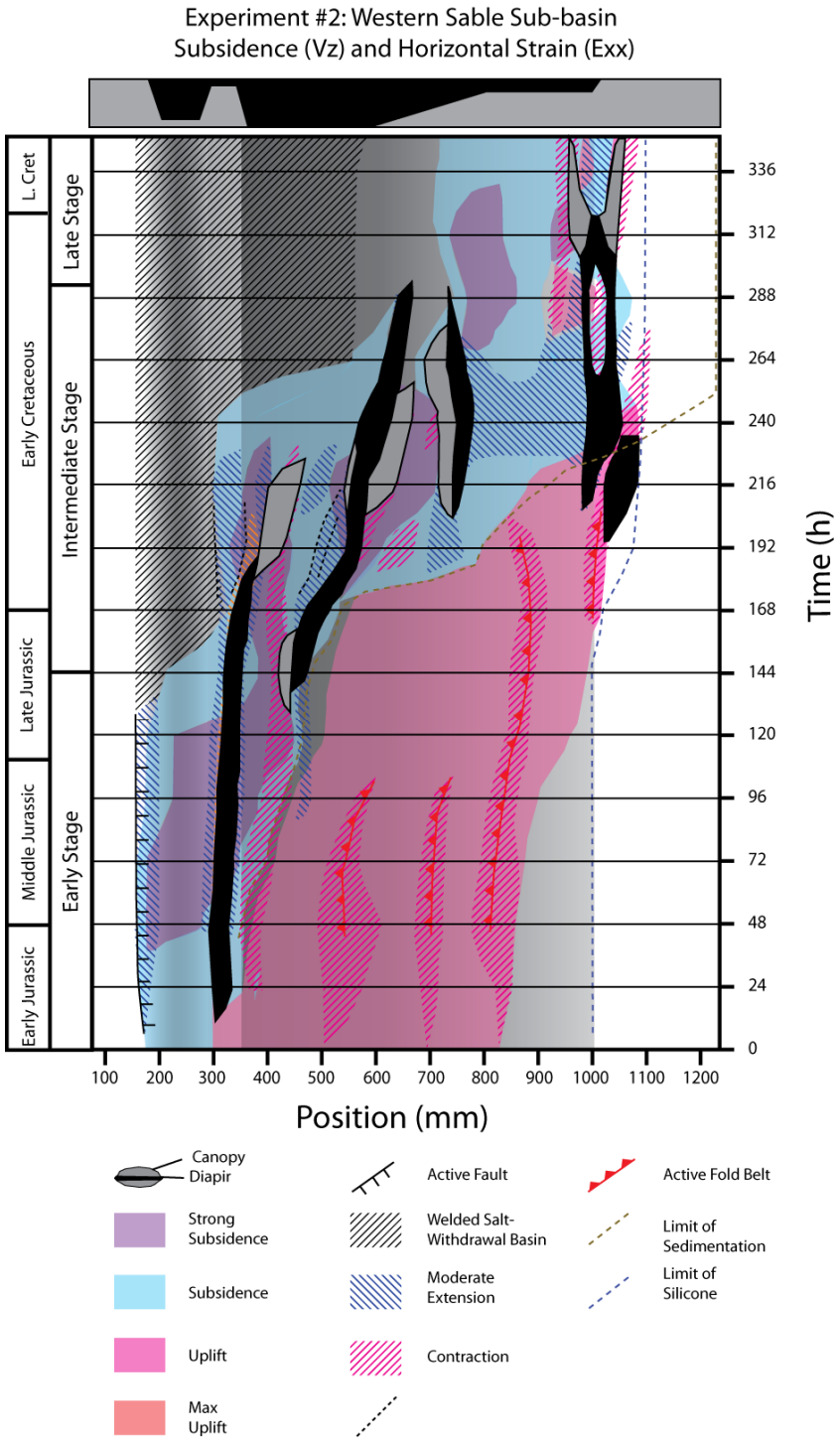

Figure 5-12: Time-space diagram of vertical displacement and horizontal strain, with respect to structures as they developed throughout the evolution of section 45 cm of experiment 2. Geologic time and salt tectonic stages are presented on the left border of the diagram, the downdip position in mm is on the bottom, and model time is on the right. A schematic illustration of the model basin setup is presented above, which correlates to dark (thick silicone) and light (thin silicone) shades of grey in the diagram.

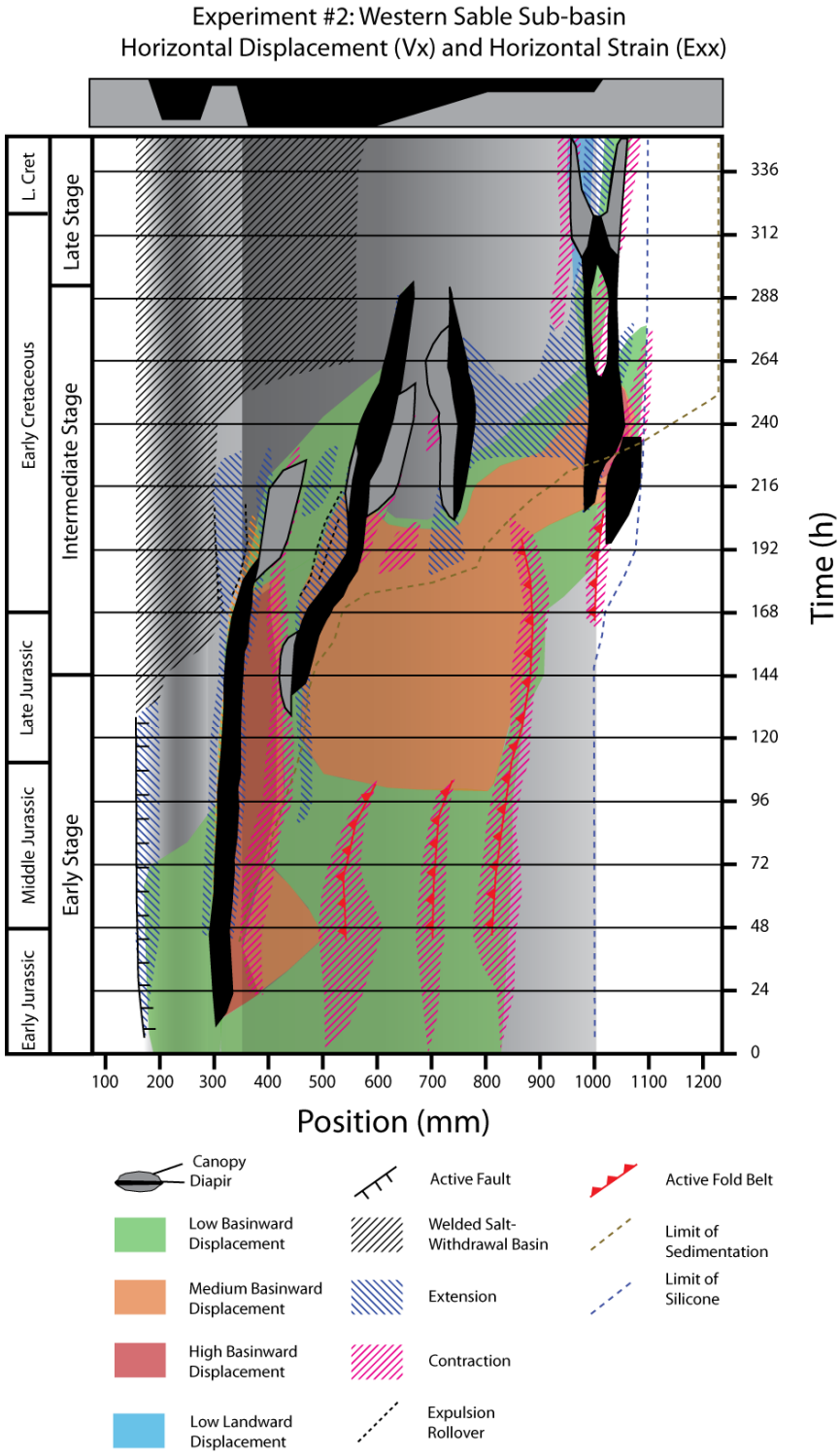

Figure 5-13: Time-space diagram of horizontal displacement and horizontal strain, with respect to structures as they developed throughout the evolution of section 45 cm of experiment 2. Geologic time and salt tectonic stages are presented on the left border of the diagram, the downdip position in mm is on the bottom, and model time is on the right. A schematic illustration of the model basin setup is presented above, which correlates to dark (thick silicone) and light (thin silicone) shades of grey in the diagram.

the inflated silicone complex began to develop at the same time, and their positions were closely linked to variations of original silicone thickness. The first fold belt was located just landward of the basin-floor ramp, the second was located in the middle portion of the ramp, and the last fold belt was located where the basin floor became horizontal with a constant silicone thickness of 1 cm (Fig. 5-3, Fig. 5-14 A, B, &C – Exx). Early contraction was also localized at the landward limit of the broad inflated silicone complex in the deeper basin. Similar to model 1, this contraction was related to gravity driven seaward translation (Fig. 5-14 A, B, & C – Exx and Vx) from the seaward flank of D1 that was buttressed by the inflated silicone complex in the deep basin. By the end of the early stage, this contractional regime became the site of early sedimentation in mini-basin SW2b (Fig. 5-15 C – Vz), which at this time was situated at the position of SW2a. Minor subsidence in this early depocenter allowed for the counter-regional spreading of an allochthonous silicone sheet (Fig. 5-15 C – Vx) before the initiation of diapir, D2.

Intermediate Stage (144 – 290 hours)

Main depocenters migrated into the deeper portion of the Sable sub-basin (Fig. 5-12, 5-16 and 5-17) during the intermediate stage with near-complete evacuation of silicone from the proximal graben. As the wedge prograded over diapir D1 and the horst, it was translated seaward to its final position at the landward limit of the deep Sable sub-basin (D1: Fig. 5-16 A – Exx). To approximately the mid-intermediate stage, D1 continued to climb the model stratigraphy as an allochthonous silicone sheet (~192 to 220 hours: Fig. 5-12; Fig. 5-13; Fig. 5-16 B & C – Exx). Early depocenter SW2b was also translated further seaward, and its initial position became the site of later sand accumulation, denoted as SW2a (Fig. 5-16 A & B – Vz). SW2b became the major

depocenter for much of the intermediate stage and downbuilt into the thick, landward portion of the silicone basin (Fig. 5-6 B – Vz). Diapir D2 (5-16 A, B, & C - Exx) bounds SW2b and developed from the early contractional trend that fed the counter-regional spreading silicone sheet (Fig. 5-15 C – Vx). During its evolution, D2 was translated significantly (40 cm to 60 cm) and was finally arrested where the basin-floor began to climb as a ramp. At the ~mid-intermediate stage (~200 hours), when diapir D2 becomes stationary, diapir D3 (Fig. 5-16 C - Exx) began to develop at the seaward extremity of the basin-floor ramp. Silicone withdrawal basin SW2c also became the major depocenter for the late portion of the intermediate stage, and supplied pressure for silicone extrusion in diapirs D2 and D3 (Fig. 5-16 C – Vz). With increased subsidence and loading in this region, landward and seaward canopies spread from D2 at a low angle (C1: Fig. 5-16 C – Vx, and Fig. 5-17 A – Vx). The evacuation of silicone canopies from diapir D2 resulted in diapir collapse, and it diminished in size. At this time, a counter-regional overhang also developed from D3, as there was high subsidence in SW2c and mild uplift and silicone inflation seaward (Fig. 5-15 C – Vz). Although D3 did not significantly migrate seaward, sediments that are overlying inflated silicone over the basin-floor flat at the distal portion of the basin were translated seaward (Fig. 5-15 C – Vx).

During the intermediate stage, contractional systems became focused at the distal portion of the silicone basin, as the region became strongly inflated (Fig. 5-15 A & B – Vz). The most distal fold belt was persistent through the early intermediate stage, and migrated ~10 cm from its original position. This fold belt was active until the region became the site of salt-withdrawal-basin initiation (SW2c: Fig. 5-16 C – Vz) with the advancement of the sedimentary wedge. When SW2c became strongly developed

between diapirs D2 and D3, there was enough loading of the silicone layer to force a short-lived silicone nappe SN (Fig. 5-16 C – Vz) out of the basin. Shortly after silicone nappe extrusion began, diapir D4 developed out of the contractional inflated silicone massif (Fig. 5-17 B & C – Exx). What appears to have stopped most of the silicone from exiting the basin through SN is a minor amount of sand that was broadly deposited over the distal portion of the inflated silicone complex. This package of sand is slightly translated and rafted over the silicone nappe, but also experienced minor downbuilding, creating a buttress for the inflated ridge of the early form of D4. Unlike other diapirs, D4 continued to grow in the intermediate stage and throughout the late stage of the experiment.

Late Stage (290 – 356 hours)

By the late stage of the experiment (Fig. 5-12 and Fig. 5-13), the main depocenter has migrated to SW3 (Fig. 5-18 A & B – Vz), which is situated over the broad and originally thin portion of the model basin. Complex strain patterns are evident in shut-down regions of the experiment via the PIV data (Fig. 5-12, 5-13, 5-17 C - Exx, and 5-18 A & B - Exx); however, they are on a small order of magnitude (e.g. 0.05) and are likely artefacts induced by minor rail movement. Relatively little happened during the late stage of this model, with the exception of the spreading of allochthonous silicone sheets from D4 (Fig. 5-18 A & B – Exx). These silicone sheets and canopies can be sub-horizontal sections 20 cm and 30 cm; Fig. 5-11) or may have climbed stratigraphy throughout their evolution (section 50 cm; Fig. 5-11). Since the gradient at the model sea floor was not pronounced, canopies spread in both landward and seaward directions.

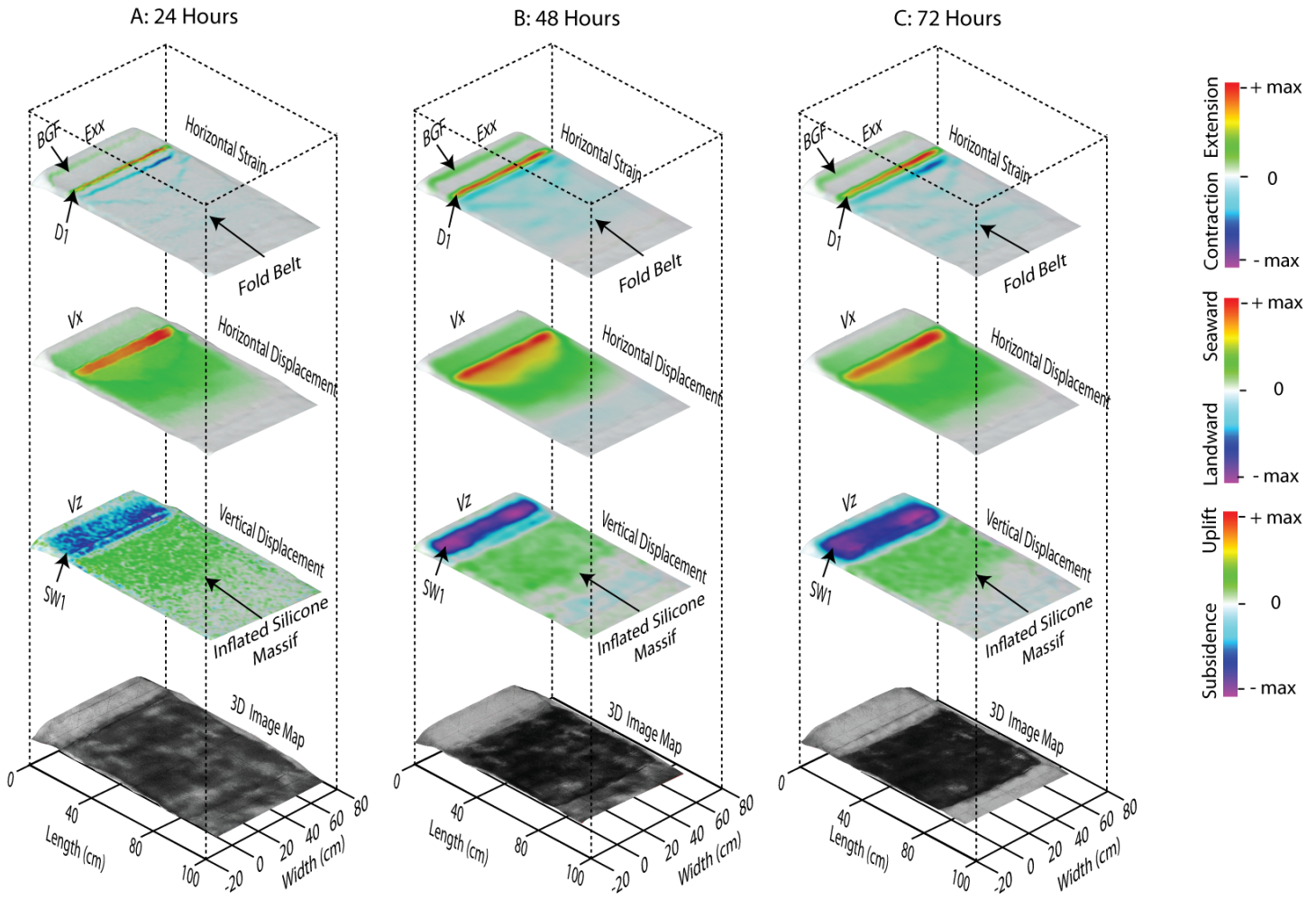

Figure 5-14: 24-hour, 3D surface renders of the model surface image, horizontal displacement, and horizontal strain data. During the first 72 hours of experiment 2, there is modest downbuilding in the proximal graben. Downdip contraction is localized over the horst in the form of a diapir. There is also contraction at the landward limit of the broadly inflated silicone complex as it acts as a buttress to sand that is translating seaward as a result of a seaward gradient, created from the topographic high of the early diapir and a small mini-basin.

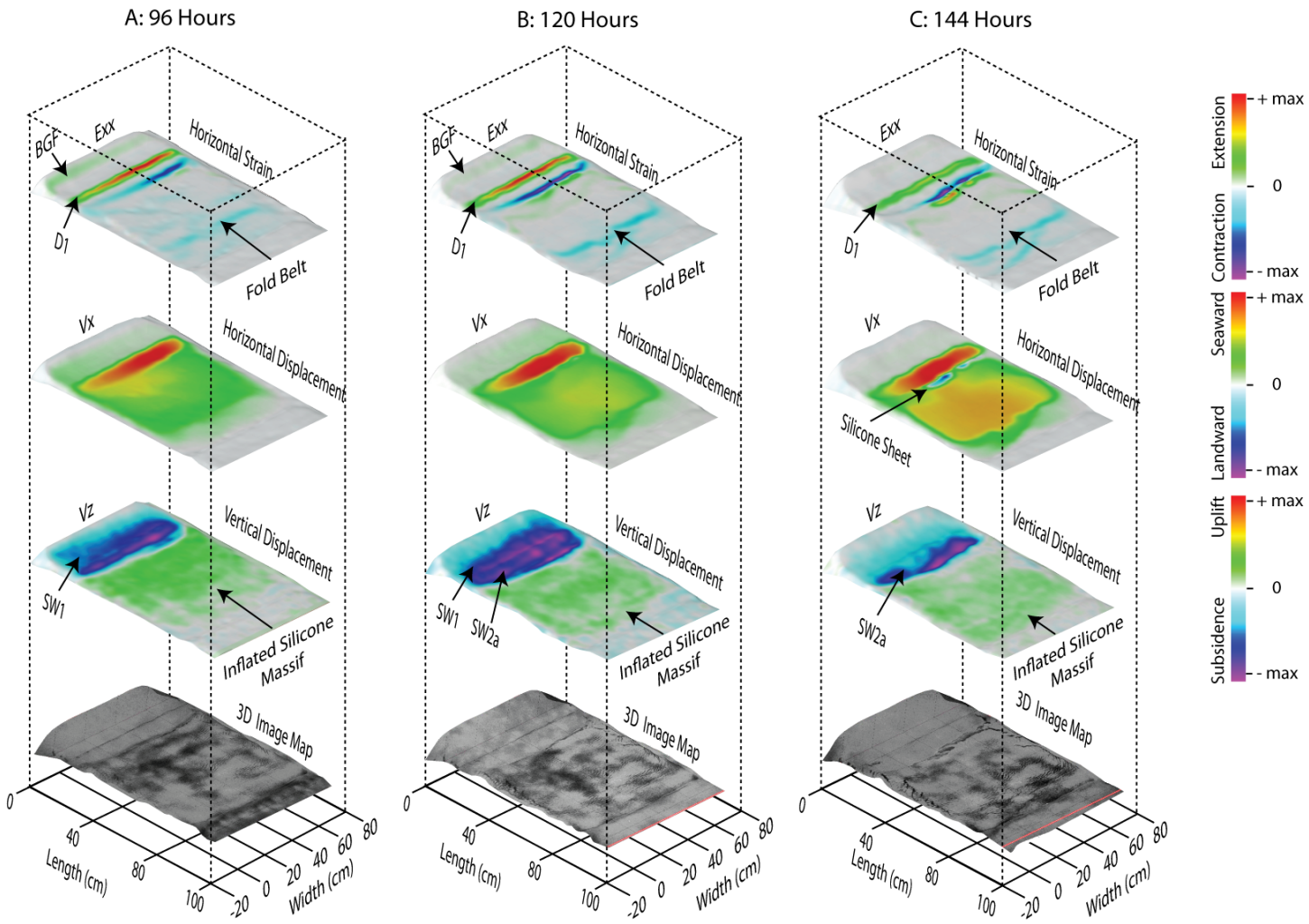

Figure 5-15: 24-hour, 3D surface renders of the model surface image, horizontal displacement, and horizontal strain data. From 72 – 144 hours, broad but modest deposition occurs slightly further seaward as a result of silicone evacuation in the proximal graben and the advancement of the prograding sedimentary wedge. Initially, translation is focused on the seaward flank of an early diapir. However, as deposition becomes more focused in the deep Sable sub-basin, translation becomes more significant throughout the slope and distal regions.

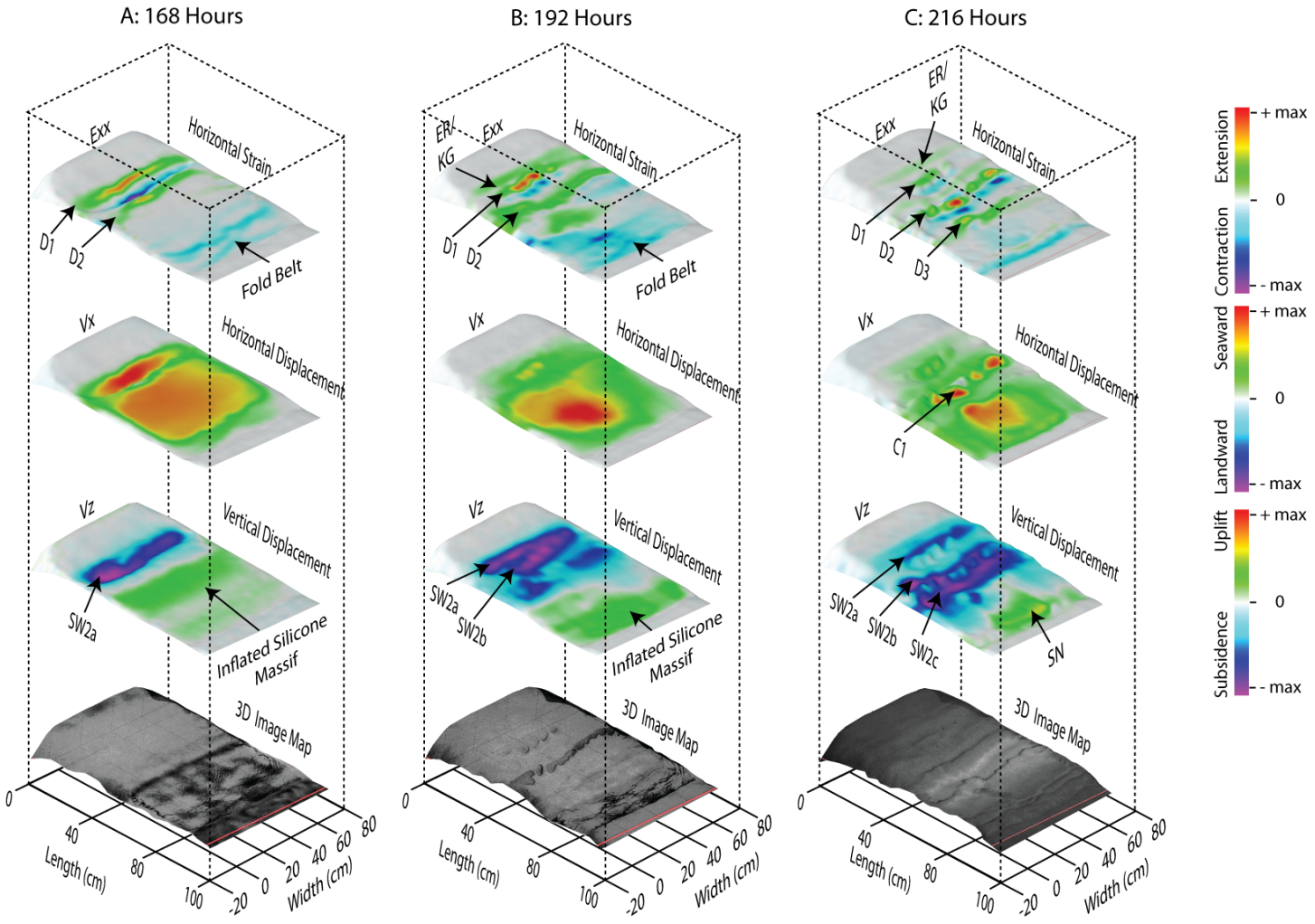

Figure 5-16: 24-hour, 3D surface renders of the model surface image, horizontal displacement, and horizontal strain data. 144 – 216 hours is the most crucial interval of time for the salt tectonic evolution of experiment 2. With increased sediment input during the modeled Missisauga formation, the broadly inflated Sable sub-basin became the focus of long-lived downbuilding, and silicone evacuation. During this time, diapirs become localized at both the landward and seaward extents of the basin-floor ramp, where there were original inflections in silicone thickness. Significant loading between these diapirs provided enough pressure within the silicone to also force a small silicone nappe out of the basin, as seen at 192 – 216 hours.

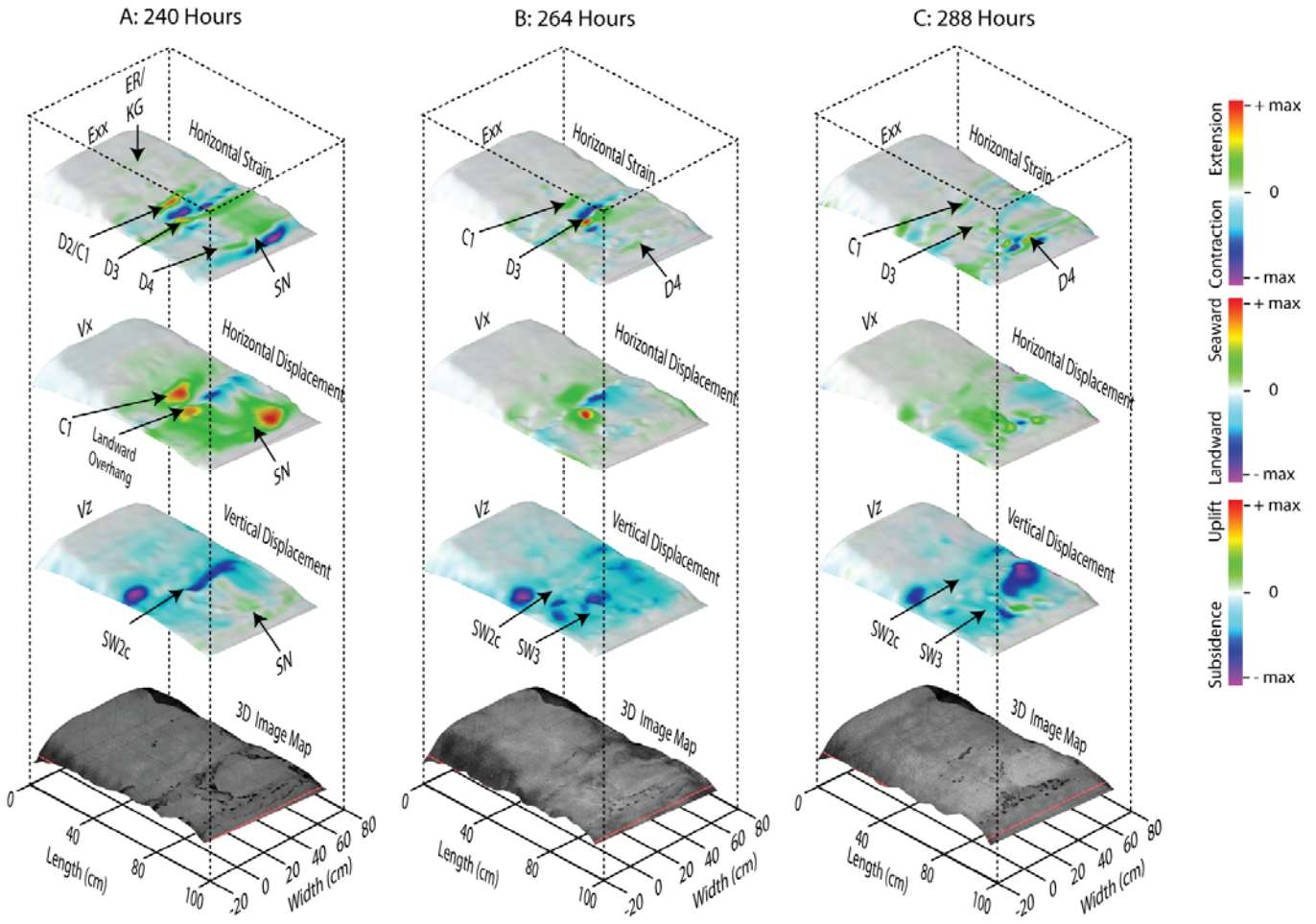

Figure 5-17: 24-hour, 3D surface renders of the model surface image, horizontal displacement, and horizontal strain data. From 216 – 240 hours, canopies have spread from both diapir trends in the slope. Throughout the latter portion of this interval, the main depocenter has shifted to the distal region of the autochthonous basin, which provided enough loading to produce the final diapir trend at the seaward limit of the basin.

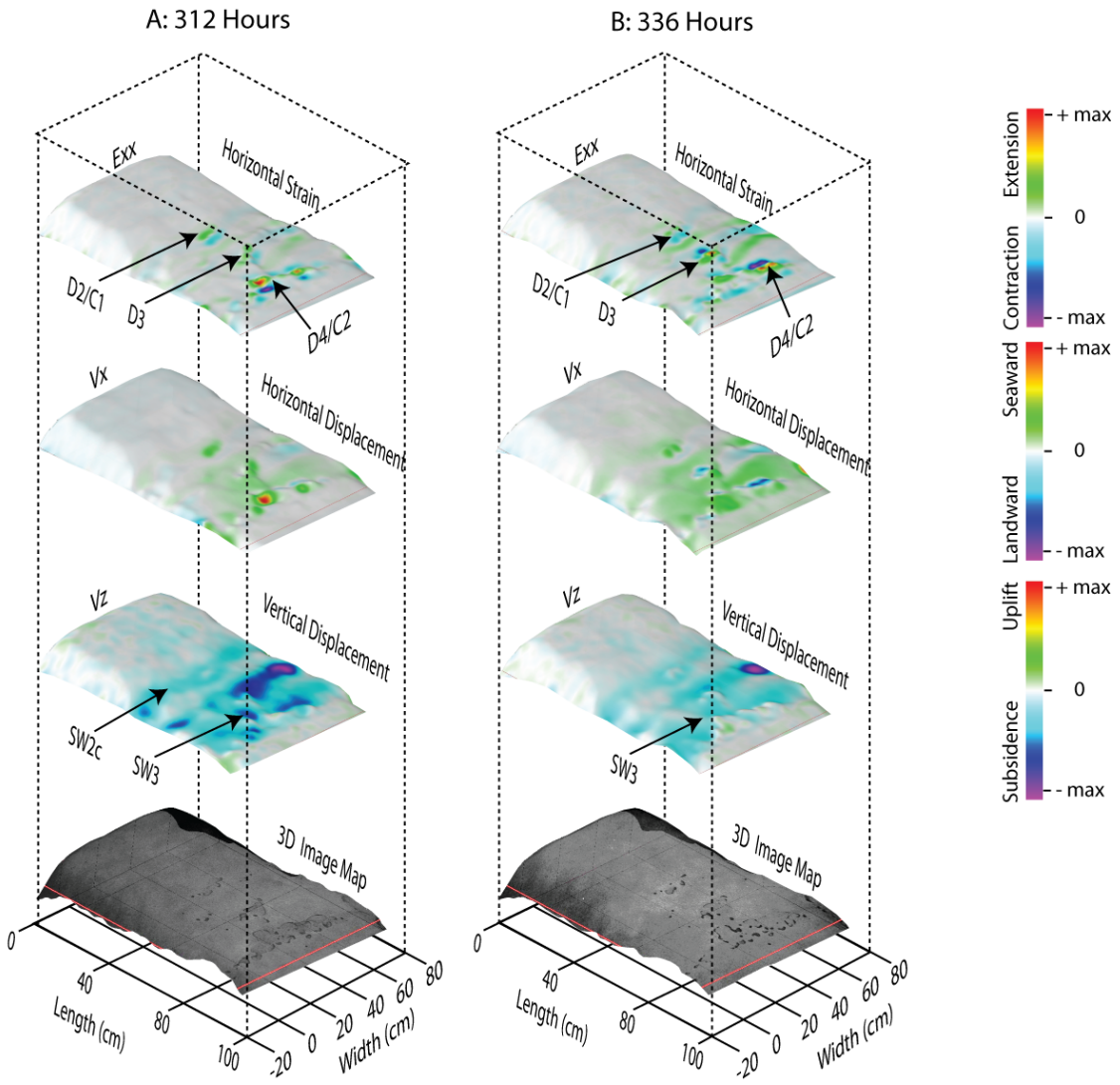

Figure 5-18: 24-hour, 3D surface renders of the model surface image, horizontal displacement, and horizontal strain data. From 288 hours to the end of model 2, subsidence is dominantly focused at the distal limit of the autochthonous silicone basin, and the distal diapir trend passively keeps up with sedimentation, forming canopies that are generally covered by a thin layer of sand as the spread.

5.7.2.3 Structural & Kinematic Evolution – Sequential Section Restoration

Figure 5-19 depicts a representative shelf-slope profile (section 50 cm), which was sequentially restored by 24- and 48-hour intervals with the aid of time-series 3D surface elevation and strain data (e.g. vertical displacement and horizontal strain).

24 hours – Onset of Post-Rift Sedimentation and Early Basin Development

Very little was deposited within the small proximal graben within the first 24 hours. In response to sedimentary loading, a seaward-dipping growth fault developed at the landward limit of the silicone basin (BGF: Fig. 5-14 A – Exx). At this time, silicone began to inflate on the landward flank of the basement horst. Broad inflation also occurred throughout the main portion of the Sable sub-basin (Fig. 5-14 A – Vz); however, it is relatively insignificant and barely resolvable from the surface profiles and restoration.

48 hours – Continued Downbuilding in the Proximal Graben and Broad Distal Inflation

More sand had accumulated in the graben by 48 hours, and as a result more inflation occurred at both the horst and broadly throughout the basin. The topographic ridge positioned over the horst began to evolve into a passive diapir (Fig. 5-14 B – Exx). Fold belts developed by this time (Fig. 5-14 B – Exx); however, they are difficult to resolve with surface profile data. The BGF continueed to develop with increased loading, but growth patterns in the graben were minor (SW1: Fig. 5-14 B – Vz).

96 hours – Increased Downbuilding in the Distal Basin and Development of Diapir (D1)

By 96 hours, diapir D1 (Fig. 5-15 A – Exx) became more prominent in response to the seaward progradation of the sediment wedge, and increased downbuilding beyond the horst (Fig. 5-15 A – Vz). Seaward transport of sand beyond this diapir and the horst was buttressed by the broadly inflated silicone complex in the model deep basin (Fig. 5-15 A – Vx and Vz). BGF (Fig. 5-15 A – Exx) continued to develop with ongoing downbuilding and silicone withdrawal in the proximal graben.

144 hours – Continued Downbuilding in the Distal Basin (SW2a) and Counter-Regional Spreading of an Allochthonous Silicone Sheet

There was continued downbuilding of sand in the proximal graben, but more significantly, a new silicone withdrawal basin formed within the deeper portion of the Sable sub-basin (SW2a: Fig. 5-15 C – Vz). This package of sand translated slightly seaward, but was being buttressed by the inflated silicone in the distal deep basin (Fig. 5-15 C - Vx and Vx). At the same time, this package was subsiding into the underlying silicone and the site consequently became a topographic low that allowed for the landward spreading of an allochthonous silicone sheet (Fig. 5-15 C – Vx). The inflated silicone massif translated further seaward and gently tapered over the ramp in the basin-floor and the originally thin portion of the basin at its seaward terminus.

192 hours – Progradation of the Sedimentary Wedge and Development of Diapirs (D2 & D3)

Significant deformation occurred between 144 and 192 hours. Diapir D1 (Fig. 5-16 B – Exx) had translated from the horst to the deep basin. Over the horst, only remnant silicone remained that was once part of the main body of D1. Earlier strata down-built

into the landward flank of D1, resulting in the formation of an expulsion rollover with keystone grabens (ER/KG: Fig. 5-16 B – Exx). The major fault related to this set of keystone grabens soled into remnant silicone that was trapped over the basement horst. Since there was increased subsidence seaward of D1 (SW2b: Fig. 5-16 B- Vz), the diapir climbed gradually seaward over the basin surface. Significant downbuilding occurred at SW2b, and the underlying silicone was almost completely evacuated. A new diapir (D2: Fig. 5-16 B – Exx) formed out of the inflated silicone complex where the landward allochthonous silicone sheet had previously formed (Fig. 5-15 C – Vx). This diapir is positioned slightly landward of the ramp in the basin-floor and formed a new topographic ridge. The sediment wedge prograded to approximately mid-way through the dip-perpendicular extent of the distal basin, initiating the formation of both SW2c (Fig. 5-16 B – Vz) and diapir D3 (Fig. 5-16 B – Exx). D3 was originally broadly inflated and is situated at the seaward limit of the basin-floor ramp, where the silicone originally thinned.

240 hours – Continued Progradation of the Sedimentary Wedge and Development of Diapir (D4) and a Silicone Nappe

Diapir D1 finally shut down by 240 hours, and only experienced minor seaward translation from the last time step (Fig. 5-17 A – Exx). SW2b was now welded completely and a minor keystone graben formed over the landward allochthonous silicone sheet. Diapir D2 (Fig. 5-17 A – Exx) translated slightly seaward and was arrested at the landward limit of the basin-floor ramp. Over this 48-hour interval, an extensive canopy spread from D2 and climbed the stratigraphy in both landward and seaward directions (Fig. 5-17 A – Vx).

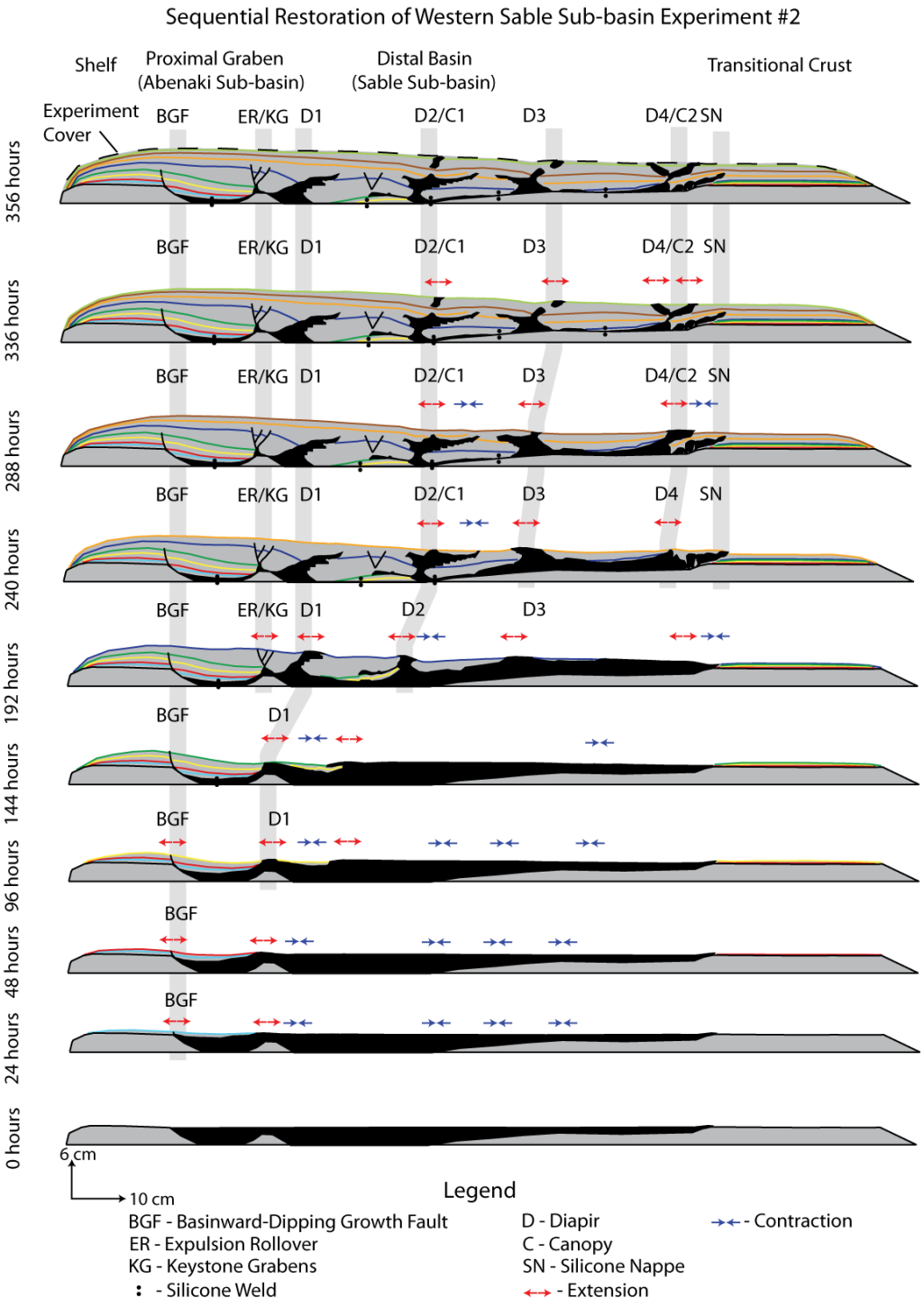

Figure 5-19: Structural restoration of section 45 cm of experiment 2. Like experiment 1, the regional (datum) of each time step was constrained by PIV surface data. Other PIV data, such as horizontal strain (Exx) and translation (Vx) constrained the position of diapirs, as well as how much translation had occurred for packages of sediments contained in mini-basins. The restoration is a simple graphical depiction of the complex evolution of model 2, which displays the interplay between basin geometry, original viscous layer thickness, and diapir localization.

Silicone withdrawal basin SW2c (Fig. 5-17 A – Vz) was nearly welded over the ramp, however, some silicone remains at its seaward region. With increased subsidence in SW2c, a counter-regional overhang has formed from D3 (Fig. 5-17 A – Vx). It is likely that this overhang spread preferentially landward because there was more subsidence in SW2c than further seaward, at SW3 (Fig. 5-17 A – Vz). At this time, the most distal diapir D4 (Fig. 5-17 A – Exx) had begun forming at the seaward terminus of the silicone basin. As well, some silicone made it out of the original basin, and began to climb the stratigraphy as a silicone nappe (SN: Fig. 5-17 A – Exx, Vx, and Vz).

288 hours – Continued Downbuilding in the Distal Basin at SW3

Deposition from 240 to 288 hours was much more widespread than in previous times, as there was considerably less overall subsidence (Fig. 5-17 C – Vz). Although SW3 was actively subsiding, it was less significant compared to the previous depocenters. Therefore, it is apparent that there were no considerable depocenters beyond 240 hours. The sedimentary wedge had overridden the landward overhang of diapir D3 (Fig. 5-17 A – Vx) and uniformly down-built into SW3 (Fig. 5-17 C – Vz). D3 (Fig. 5-17 C – Exx) continued to remain passive through this stage, although it became narrower, particularly at shallow stratigraphic levels. SW2c, which bounds D3 was completely evacuated of underlying silicone, and had become welded at depth. The continued downbuilding in SW3 supplied enough silicone to D4 (Fig. 5-17 C – Exx) that it grew substantially and a silicone sheet/canopy began to spread preferentially seaward.

336 hours – Passive Diapirism of D3 and D4, and Regional Welding in the Autochthonous Silicone Basin

By 336 hours the salt tectonics system was essentially shut down. All earlier depocenters were sites of primary welds between the overburden and the basin-floor. Diapir D2/C1 (Fig. 5-18 A & B – Exx and Vx) persisted to the model surface, but is not directly connected in section 50 cm. Minor downbuilding occurred into the landward flank and landward overhang of diapir D3, and strata slightly rolled over. This diapir (D3: Fig. 5-18 A & B – Exx) climbed preferentially seaward throughout the rest of its evolution and became vertically welded at shallow levels. Relatively uniform deposition occurred within SW3 (Fig. 5-18 B – Vz), as it was nearly welded by the time of deposition. However, both the landward and seaward limits of this sand package preferentially down-built into the flanks of diapirs D3 and D4, resulting is a broad turtle anticline. Diapir D4 and its canopy (Fig. 5-18 B – Exx) were broad and not topographically prominent; as a consequence, this diapir became the site of late subsidence and a minor depocenter. Loading of this structure caused it to climb the stratigraphy in both landward and seaward directions, resulting in divergent allochthonous silicone sheets. The silicone nappe has thinned slightly, but has not extended further seaward, suggesting complex along-strike flow to areas where it may exist as an open-toe system. The experiment was shut down at 356 hours, as the system experienced cessation.

5.8 Comparison of Experiments 1 and 2

Salt-tectonic evolution differed significantly between experiments 1 and 2. The primary control factors for these differences were:

1. Sedimentation rates and mode of deposition (geometry of the prograding sedimentary wedge); and

2. Basin morphology (including initial silicone thickness).

5.8.1 Sedimentation Rates and Modes of Deposition

In experiment 1, the focus on early proximal deposition in the proximal graben drove silicone mobilization seaward much faster than a more widespread distribution (i.e. over both proximal graben and deep basins) of early deposits, as seen in experiment 2. The more localized sediment input of experiment 1 resulted in progrssive, seaward migration of depocenters, and silicone was mobilized and significantly inflated at the seaward border of the silicone basin. When the prograding sediment wedge finally overrode the distal portion of the Sable sub-basin, the inflated complex became the site of significant downbuilding, which resulted in rapid expulsion of silicone from the autochthonous basin and the formation of an extensive silicone nappe. In general, the proximal deposition, coupled with high early sedimentation rates, resulted in early shutdown of salt tectonics in the experiment, which ended during the simulated Early Cretaceous Missisauga formation.

Experiment 2 differed from experiment 1 such that early sedimentation was simulated with widespread deposition, similar to deltaic and pro-deltaic depositional setting. The early aggradation rate was low, and as a result little deformation occurred in the first ~100 hours. Depocenter evolution and migration was different from experiment 1. Instead of a progressive seaward migration of depocenters, the evolution was more complex. Generally, depocenters migrated seaward throughout the experiment; however,

some (i.e. SW2a and SW2b) developed nearly coevally. This style of salt-withdrawal basin evolution has two consequences to the salt-tectonic development: 1) structures experience less horizontal translation, as seaward salt-withdrawal basins buttress more landward diapirs, and 2) salt withdrawal basins are generally broader and often penecontemporaneous. This would be shown, in natural examples, by the lack of variable growth patterns and the absence of structural closures.

5.8.2 Basin Morphology and Initial Silicone Thickness

Despite experiment 1 having high early sedimentation rates, the half-graben wedge geometries hindered seaward silicone translation, and as a result, a significant amount of remnant silicone was trapped in wide diapirs. These diapirs evolved from very broad, inflated complexes that were a direct result of the resistance to seaward silicone mobilization due to thinning of the silicone layer. Two diapirs evolved out of broad inflated complexes over the proximal and narrow half-graben wedge. One of these diapirs (D1: Fig. 5-4) formed slightly landward of its final position, and was arrested at the center of the wedge. The other diapir (D_{temp}: Fig. 5-5, 5-6, and 5-7 B & C – Exx) also developed from a broadly inflated silicone ridge, but was positioned at the seaward limit of the proximal wedge. This diapir was only evident in the early stage of experiment 1 (~48–92 hours), as it was translated into the thick, landward portion of the larger half-graben, and was then deflated during later phases of salt tectonic deformation. Three diapirs (D2, D3, and D4: Fig. 5-4) originated and were trapped in the outboard half-graben wedge. These diapirs all formed slightly landward of their final positions, out of broadly inflated silicone. The diapirs did not become static until silicone withdrawal basins (SW2a, SW2b, and SW3) welded to the basin-floor on their seaward flanks.

Experiment 2 effectively depicted the effects of basin morphology and original silicone thickness. In every instance where there was a decrease in original silicone thickness, there was localization of silicone inflation. These inflated complexes were able to accommodate strain associated with sedimentary loading and evolved into long-lived passive diapirs. In regions where the basin-floor was horizontal, the silicone was more efficiently translated seaward, and diapirs tended to be narrow. Where the basin-floor was forming a ramp, seaward translation of silicone was less efficient and diapirs tended to be wider. In general, the timing of structural evolution, and duration of the salt-tectonics related deformation was similar in experiment 2 and on the GXT 1600 transect. Although early sedimentation rates were probably lower than the natural prototype, the primary control on timing appears to have been the mode of deposition. A broad, gently tapering sedimentary wedge appears to be a more realistic early sedimentation pattern, and was critical in appropriate timing of structures.

5.9 Comparison of Experiment 2 to Nature

Since the result of experiment 2 was very similar to nature, it will be the focus of discussion and comparison to the NovaSPAN line 1600 in the western Sable sub-basin. Although this experiment resulted in a final configuration that is more similar to the natural prototype (Fig. 5-20), there are also some key differences that must be discussed. Both similarities and differences based on model section 50 cm will be addressed and presented in list format from shelf to slope.

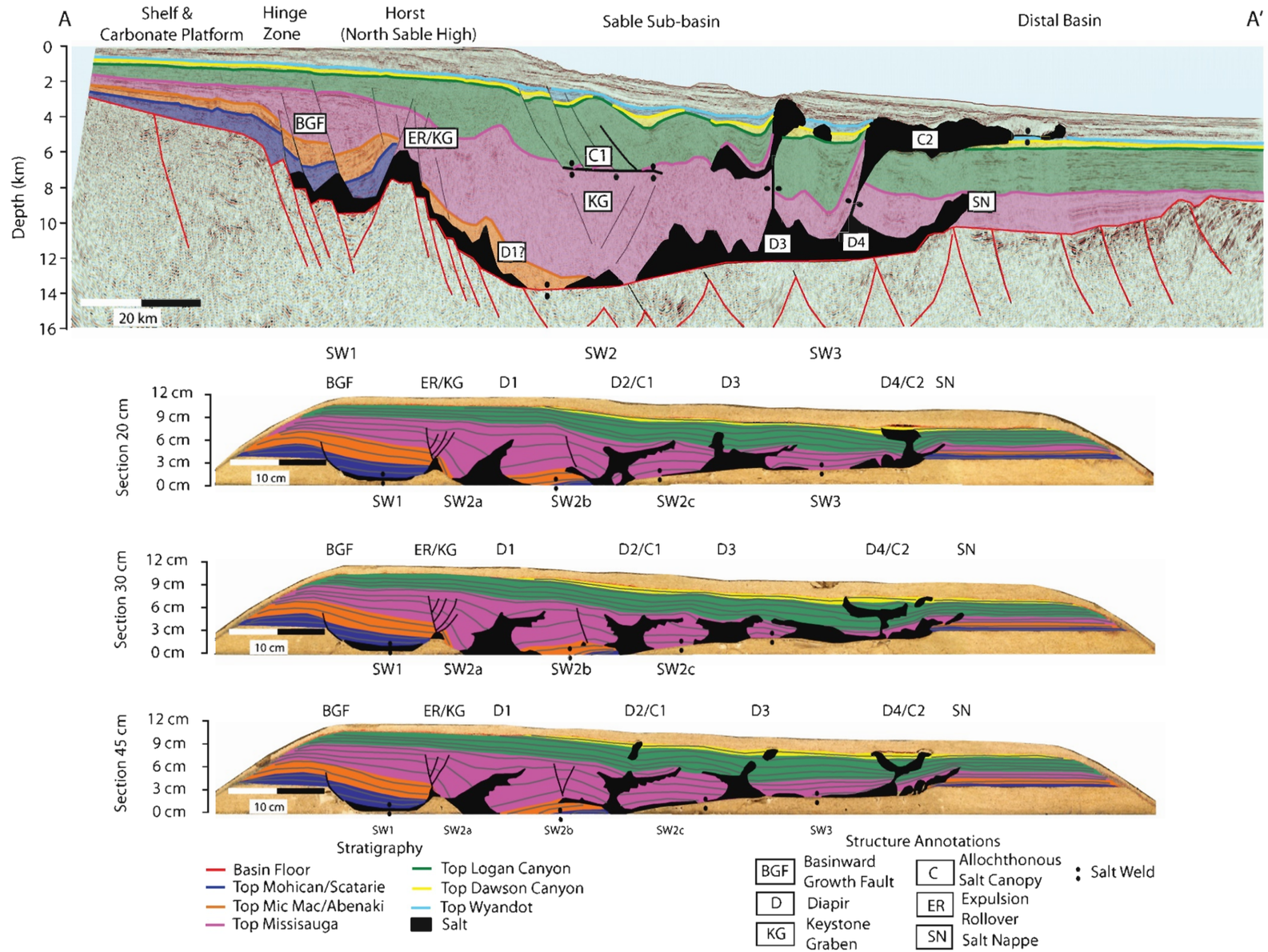

Figure 5-20: Comparison of NovaSPAN line 1600 Interpretation 2 and its corresponding scaled physical experiment. Stratigraphic packages of formations are filled in for ease of comparison.

5.9.1 Similarities

Seaward-dipping Growth Fault System (BGF)

Both experiment 2 and NovaSPAN line 1600 have a seaward-dipping growth fault (BGF) marking the landward margin of the autochthonous salt basin. This fault results from downbuilding within the salt basin, which has dominantly vertical displacement. Rotation occurred along this fault system in both the model and in nature. Underneath the footwall of BGF there is remnant salt/silicone, which filled in space created by minor extension. The BGF borders the hinge zone, which also marks the landward limit of the salt basin in both the experiment and prototype.

Silicone Withdrawal Basin 1 (SW1)

Silicone withdrawal basin 1 is in the same position in the autochthonous salt basin as the prototype and has similar growth patterns associated with downbuilding and rotation along the BGF. In both the experiment and nature, growth appears to have ceased by the end of the Early Cretaceous (Missisauga formation). The thicknesses of both growth packages suggest long-lived silicone (salt) withdrawal from the small, proximal graben.

Expulsion Rollover/Keystone Graben

A feature that is remarkably similar between the experiment and prototype is the expulsion rollover/keystone graben with a small silicone/salt pillow that is trapped over the basement horst. In both cases, the dominant fault associated with the keystone grabens soles into the seaward flank of the remnant pillow. Antithetic faults developed in

the hanging wall of this dominant fault and accommodate further extension created by subsidence and seaward rotation of the overburden. In both the experiment and prototype, these faults appear to extend to the top of the Early Cretaceous Missisauga formation and equivalent deepwater sediments.

Silicone Withdrawal Basin 2a (SW2a)

In the experiment and nature, preferential downbuilding into the deep, Sable sub-basin from the horst structure resulted in formation of an expulsion rollover/keystone graben (ER/KG) and a significant withdrawal basin related to silicone/salt mobilization. There are also synformal geometries within the withdrawal basin (192–212 hours), while there are slight antiformal geometries (~204-220 hours) over the crest of either a diapir or salt pillow.

Balvenie Roho System (BRS)/Canopy (C1)

The development of an allochthonous canopy system in the same position (geographically and stratigraphically) as the Balvenie Roho System is a particularly important result for this study. In both the experiment and Sable basin, this feature was extruded on the seafloor at a rapid rate, and formed a secondary source layer allowing later downbuilding and gravity driven deformation.

Silicone Withdrawal Basin (SW2c)

Experiment strata that comprise silicone withdrawal basin (SW2c) roll seaward into the landward flank of diapir D3, because the basin floor climbs to shallower levels at this position. Similar to the natural case, there is also remnant silicone trapped under the

package of overburden. The amount of remnant silicone is more significant at the landward portion of the basin-floor ramp, and the overburden becomes welded next to the diapir.

Diapir D3

Diapir D3 is another remarkably similar feature between the experiment and prototype. In both the experiment and seismic interpretation, the diapir is situated where the basin-floor ramp levels out. There is a landward leaning overhang that is also present in both the experiment and interpretation, that has spread at approximately the top Missisauga formation time-equivalents. This overhang has a similar thickness (1-2 km) and horizontal extent in the model as nature, and both have accommodated later downbuilding.

Silicone Withdrawal Basin 3 (SW3)

Silicone withdrawal basin 3 (SW3) is positioned between diapirs D3 and D4. Like the interpretation of NovaSPAN line 1600, only minor growth had occurred until the distal basin became the site of late-stage downbuilding at the time of deposition of the Logan Canyon formation equivalents.

Diapir D4

In both scenarios, diapir D4 is seaward leaning, vertically welded, and feeds a late stage allochthonous canopy system is active to the Late Cretaceous.

Silicone Nappe (SN)

The development of the small, short-lived silicone nappe was important for the understanding of regional basin dynamics and allochthonous salt emplacement in the study area. The silicone nappe in the experiment required significant downbuilding within the inflated silicone complex that was once situated over the ramp in the basin-floor. This rapid downbuilding provided enough loading on distal autochthonous silicone to force it out of the basin, even though it was partially counteracted by high amounts of contraction at the seaward terminus of the basin. In both the experiment and the seismic profile, the nappe was shut down within Early Cretaceous times (Missisauga formation), and steeply climbs earlier-deposited stratigraphy.

5.9.2 Differences

Seaward-Dipping Growth Fault System (BGF)

Though generally similar, the BGF is observed as being active for a longer period in the Sable basin than in the experiment and extends as high as the top Early Cretaceous Missisauga formation. Also, the natural system comprises two major listric faults, rather than one, although this appears to be controlled by minor basement offset. More landward rotation of growth packages occurs along both of these faults than is observed in the experiment.

Silicone Withdrawal Basin (SW1)

As noted in discussion of the BGF, sedimentary packages have rotated landward more significantly in nature. Also, these sediments appear to have been thrust over the horst and salt pillow in nature, although the 3D geometry of this feature is unconstrained.

Diapir D1

Diapir D1 has fully developed and has persisted through most of the Early Cretaceous Missisauga formation. Although it is in a similar position as a salt remnant in the seismic profile, the salt remnant is much smaller in size and extent in the experiment. However, as discussed in Chapter 4, antiformal geometries of overlying sediments may suggest that this salt remnant is actually part of a more extensive diapir that grows out of strike. Unfortunately, there are no available data to support this concept.

Salt Withdrawal Basin 2 (SW2 a, b, and c)

Unlike the experiment, the salt-withdrawal basin within the Sable sub-basin in line 1600 is amalgamated and is not segmented by diapirs. However, although the withdrawal basin is segmented in the experiment, strata dip broadly and gently dip seaward into diapir D3.

Diapir D2

Diapir 2, which feeds an allochthonous canopy system in the experiment, is absent in the seismic profile. However, NovaSPAN line 5300 appears to have a diapir only 20 km away from line 1600. If so, this could suggest that diapirs, or at least a diapir, have developed in this portion of the basin, and could have fed the portion of the BRS seen in

line 1600. Furthermore, Deptuck et al. (2009) mapped salt tongue feeders (diapirs) within the western extremity of this region. Unfortunately, their mapping does not extend to line 1600, or further east.

Balvenie Roho System (BRS)/ Canopy (C1)

The main difference between experiment canopy 1 and the Balvenie Roho System is that notable extension, translation, and rotation has occurred over the allochthonous salt sheet in nature. In the experiment, increased subsidence in SW2c (seaward of D2) allowed C1 to continue climbing extensively seaward. Since the experiment canopy was climbing stratigraphy, its leading toe was not open like the BRS in nature. Having an open-toed system may be an important factor in the formation of roho systems, since there is an open conduit for fluid pressure in the salt to become focused. The rapidly extending and deflating salt layer in nature would likely result in extensional failure of overburden sediments.

Diapir D4

Diapir D4 in the experiment is situated at the seaward termination of the silicone basin; however, it is positioned halfway between diapir D3 and the seaward margin of the basin in seismic line 1600. This may have been a consequence of experiment basin configuration. As learned from experiment 1, half-graben wedges that contain gradually thinning silicone wedges typically form prominent diapirs that become arrested in the center of the half graben. It may be true that the distal basin had a slight incline rather than being sub-horizontal. This incline would not be as prominent as the basin-floor ramp, but would cause the syn-rift salt to gradually thin toward the seaward basin margin.

With this taper in original salt thickness, the diapir may have been arrested halfway from the end of the prominent basin-floor ramp and the seaward basin margin, as seen in the seismic profile. Another difference between the experiment and prototype diapir is that in seismic section, the diapir feeds a much more extensive tongue-canopy system that has spread only seaward. In the experiment, this canopy system generally spreads in both landward and seaward directions. Mapped salt distribution by Shimeld (2004) demonstrates a generally broad distribution of shallow salt in this region, but it is unknown from the data available for this project if these canopies do extend landward from feeding diapirs or not.

5.10 Insights into the Evolution of the Western Sable Sub-basin from Experiment Results

Despite having minor differences, the evolution of model 2 resulted in final structures sufficiently similar to that observed in NovaSPAN line 1600 from the western Sable sub-basin to allow for comparison. Therefore, the time-series DIC data for model 2 have been summarized to show the significant changes in evolution for the scaled time intervals that correspond to natural stratigraphic formations of the Sable area (Fig. 5-21 and 5-22). All of the following discussion comes from the model evolution only, but provides insight into natural processes.

5.10.1 Early – Mid Jurassic (Mohican Formation)

The early to mid Jurassic post-rift stage (Mohican formation) (Fig. 5-21) is characterized by subsidence in the small proximal graben/Abenaki sub-basin (SW1: Fig. 5-21 A - Vz) and broad, but minor inflation throughout the distal/Sable sub-basin. Initiation of diapir D1 occurs over the horst, as seen in the surface image as well as in

localized extension shown in the horizontal strain map (D1: Fig. 5-21 A – Exx). Horizontal displacement (Fig. 5-21 A – Vx) indicates gravity driven translation of sediments seaward of D1 into the deeper portion of the Sable sub-basin. However, this translation is halted by broadly inflated silicone in the sub-basin, resulting in contraction (Fig. 5-21 A – Exx). Folding (Fig. 5-21 A – Exx) in the distal basin is positioned in proximity to inflections in original silicone thickness, i.e. just in front of, mid-positioned, and at the end of the basin-floor ramp.

5.10.2 Mid – Late Jurassic (Mic Mac Formation)

During the mid-late Jurassic (Mic Mac formation) highest subsidence is positioned at the seaward portion of the proximal graben/Abenaki sub-basin (SW1: Fig. 5-21 B - Vz) and just beyond the horst in the deeperp portion of the Sable sub-basin (SW2b). Maximum seaward translation of overburden (Fig. 5-21 B – Vx) occurs from a topographic gradient between the ridge of D1 (Fig. 5-21 B – Exx) and the low of the mini-basin (SW2 a & SW2b: Fig. 5-21 B – Vz) that is developing into the Sable sub-basin. However, this moving package of sediments is slowed down by the broadly inflated silicone seaward of the mini-basin (Fig. 5-21 B – Vz). The buttressing effect of the seaward translating overburden results in slight contraction of the package, as well as the landward wall of the silicone juxtaposed to the mini-basin. The stress exerted on the wall of the inflated silicone, combined with downbuilding and subsidence, resulted in landward spreading of an allochthonous silicone sheet (Fig. 5-21 B – Vx) into the mini-basin, which was a relative topographic low.

5.10.3 Missisauga Formation (Early Cretaceous)

The deposition of the Early Cretaceous Missisauga formation had driven the most active salt deformation in experiment 2, and presumably in nature. By the end of deposition of this formation, silicone was almost completely evacuated from the small graben/Abenaki sub-basin, and subsidence and growth in landward regions ceased (Fig. 5-21 C – Vz). Deposition throughout the Sable sub-basin became widespread, resulting in dominantly passive downbuilding (SW2a, SW2b, and SW2c: Fig. 5-21 C – Vz). However, as a result of seaward flow in the silicone, the overburden was also translated significantly throughout the evolution of the system (Fig. 5-21 C – Vx). Diapirs D2 and D3 (Fig. 5-21 C – Exx) developed during the deposition of this formation, and were arrested at both landward and seaward extents of the basin-floor ramp. A canopy system fed from D2 developed by the top Missisauga formation, and continued to spread seaward during the starvation event (D2/C1: Fig. 5-21 C – Exx). A landward overhang has also formed from D3 (section 50 cm; Fig. 5-11) slightly after C1 began to spread and shut down at approximately the same time. Considerable downbuilding into an originally inflated silicone complex over the basin-floor ramp (SW2c: Fig. 5-21 C – Vz) provided enough pressure in the silicone to force the silicone nappe to climb out of the autochthonous basin (SN: Fig. 5-21 C – Exx & Vz); however, as downbuilding ceased the nappe stopped advancing. Although there was relatively minor downbuilding at the seaward extent of the Sable sub-basin compared to landward regions, horizontal translation (Fig. 5-21 C – Vx) was highest, indicating significant flow through the relatively thicker silicone layer at the seaward extent of the basin. Not only did this flow

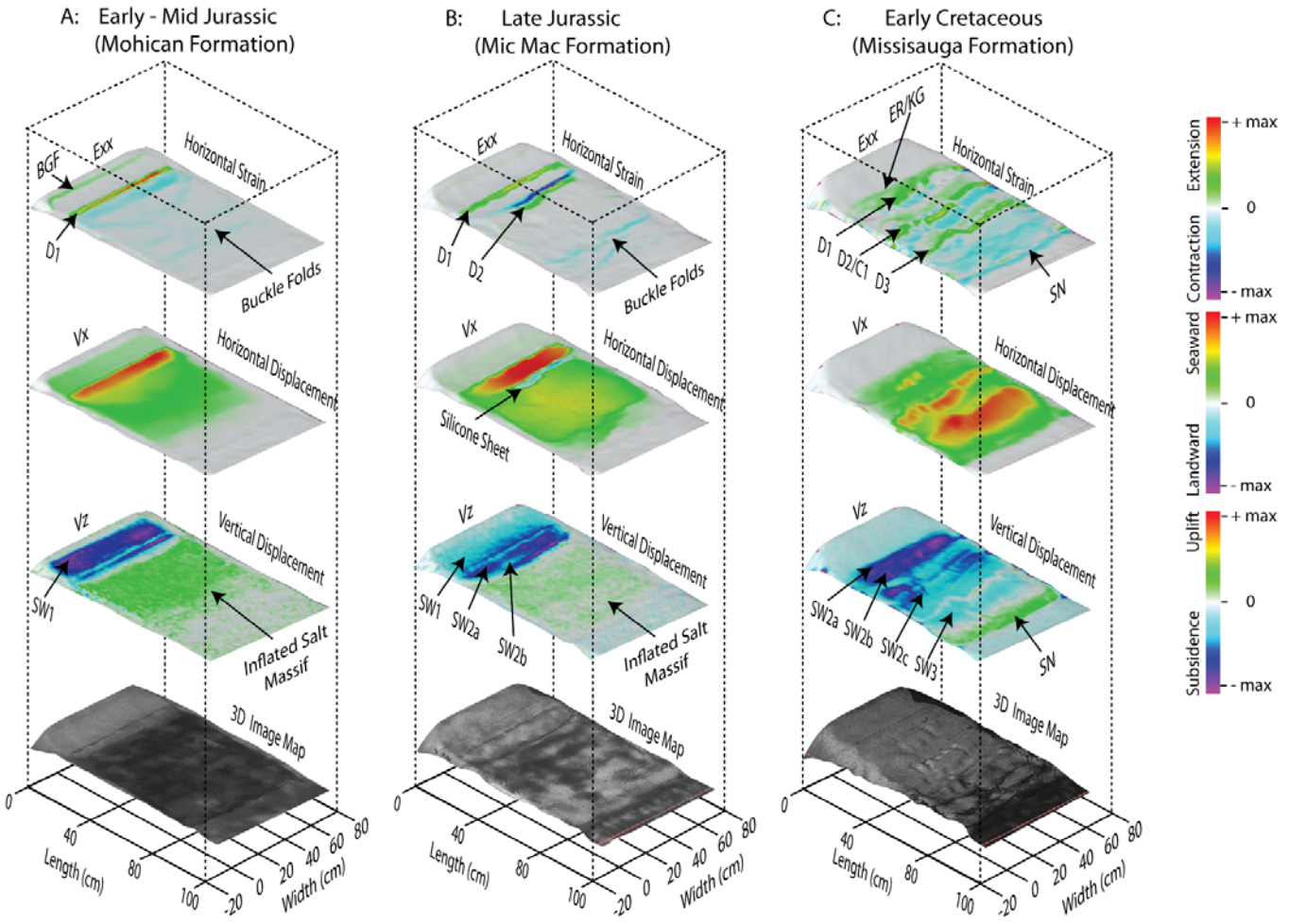

Figure 5-21: Re-processed time-series PIV data of experiment 2 that correspond to experiment formation tops. Each set of surfaces display total deformation between intervals, and is believed to be similar to those times in nature.

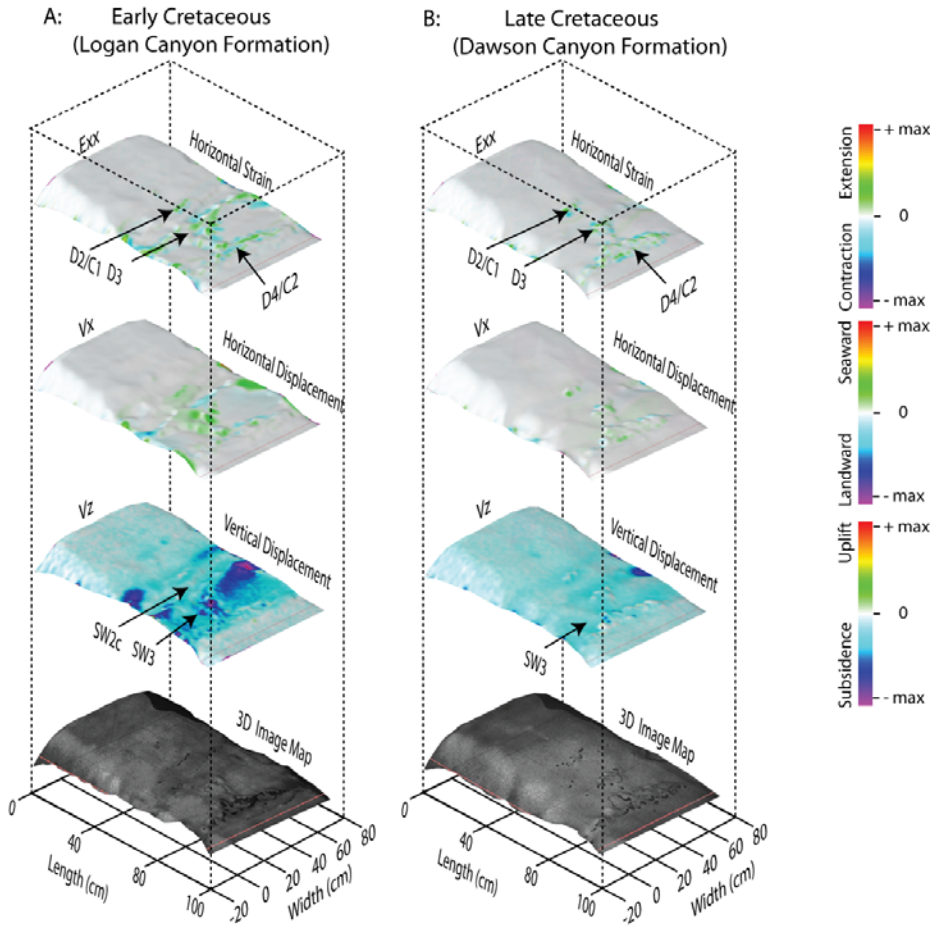

Figure 5-22: Re-processed time-series PIV data of experiment 2 that correspond to experiment formation tops. Each set of surfaces display total deformation between intervals, and is believed to be similar to those times in nature.

result in the emplacement of the silicone nappe, it also translated an overlying mini-basin further seaward (SW3: Fig. 21 A – Vz).

5.10.4 Logan Canyon Formation (Early Cretaceous)

Throughout the deposition of the Logan Canyon formation there was very little silicone mobilization and only minor downbuilding was focused over and beyond the basin-floor ramp (SW3: Fig. 5-22 A – Vz). Sedimentation was more widespread than during previous times since many regions of the experiment have become welded, and subsidence that would allow for growth packages and depocenters had already ceased. Even though the region overlying and seaward of the basin-floor ramp and the basin margin is the site of minor downbuilding, it was only a minor a depocenter compared to earlier ones. Diapir D4 (Fig. 5-22 A - Exx) at the seaward limit of the silicon basin has kept up with sedimentation, but did not develop as rapidly as previously formed diapirs (D2 and D3: Fig. 5-21 C - Exx) due to reduced silicone supply at depth.

5.10.5 Dawson Canyon Formation (Late Cretaceous)

Only a small portion of the Dawson Canyon formation was simulated in the experiment, since the salt-tectonics system was virtually shut down. This portion of the experiment is characterized by cessation of downbuilding (Fig. 5-22 B - Vz) and passive diapirism (D4/C2: Fig. 5-22 B - Exx) at the terminus of the silicone basin.

6.0 Experimental Insights into Salt Tectonics at the Western Sable Sub-basin

The final cross-sections of experiment 2 reveal considerable similarities to salt structures at the western Sable sub-basin (Fig. 6-1). These silicone and salt structures include:

1. Silicone/salt remnant over the North Sable High (NSH) horst
2. Diapir just beyond the NSH horst
3. Early Cretaceous canopy system (Balvenie Roho System; BRS)
4. Two diapirs at the distal portion of the autochthonous silicone/salt basin
5. Early Cretaceous silicone/salt nappe
6. Late Cretaceous silicone/salt canopy system.

There is also a strong correlation between the distribution of key stratigraphic units and the timing of structures between the experiment and nature. Therefore, the evolution of the experiment is useful for making comparisons to the salt tectonics evolution at the Scotian margin, and for understanding how these particular structures may have evolved.

6.1 Salt Tectonic Domains of the Western Sable sub-basin

Both the experiment and seismic section show distinctive salt tectonic domains that characterize the development of both silicone and salt structures. These kinematic domains in both the experiment and seismic section are similar, and include the: (1) *Salt Weld and Reactive Diapir, (2) Expulsion Rollover/Passive Diapir and Early Cretaceous Canopy,* and *(3) Passive Diapir and Late Cretaceous Canopy* domains (Fig. 6-1). In the

following section both silicone and salt will be termed salt in the experiment and seismic section for simplicity.

1. Salt Weld and Reactive Diapir Domain

The extensional *Salt Weld and Reactive Diapir Domain* is situated at the hinge zone and Abenaki sub-basin, and is characterized by growth strata that document extensive salt withdrawal from the Early - Mid Jurassic to the Early Cretaceous (Mid - Missisauga formation). Small salt remnants were previously reactive diapirs that were developing during early stages (Early-Mid to Late Jurassic) of the post-rift basin evolution. In NovaSPAN line 1600, a salt remnant (at the BGF: Fig. 6-1) is positioned at a minor offset in basement, and was probably trapped due to the passive downbuilding of sediments on its seaward flank that eventually welded to the basin-floor. Over the horst, which is part of the larger NSH trend, there is a small salt remnant that an extensive fault system soles into. In both the experiment and nature, this fault system shows both displacements and seaward downbuilding and growth of strata into the larger, Sable sub-basin. Seaward downbuilding and rotation of growth strata into the deep Sable sub-basin has resulted in the formation of keystone grabens that sole into the fault bounding the salt remnant. Unlike the salt rollers in the Abenaki sub-basin, the remnant over the horst was once part of a passive diapir wall (D1), as indicated by experiments (Fig. 5-14 A, B, & C – Exx), although most of this diapir translated into the Sable sub-basin (~10 km), e.g. Fig. 5-19.

2. Expulsion Rollover/Passive Diapir and Early Cretaceous Canopy Domain

The *Expulsion Rollover/Passive Diapir and Early Cretaceous Canopy Domain* is characterized by multiple passive diapirs and an Early Cretaceous Canopy that has recently been mapped as the Balvenie Roho System (BRS) (Deptuck et al., 2009). Unlike other margins where a seaward tilt has created extension in the overburden allowing for passive growth of diapirs (i.e. offshore Angola; Brun and Fort, 2004), these passive diapirs have formed out of originally inflated salt complexes or salt-cored anticlines that were related to basin-floor geometry (see ***6.6.1 Effects of Basin-Floor Morphology*** section), and more importantly, inflections in original silicone/salt thickness. Many of these inflated complexes formed landward of thinning salt; however, they generally migrated (~10 – 15 km) to their final position by the time they became static due to welding of salt-withdrawal basins in their seaward flank. Since the depositional setting for the western Sable sub-basin is generally aggradational throughout the Early to Late Jurassic, these diapirs formed when sediment loading of the inflated salt massifs started at the beginning of the Early Cretaceous, with the onset of progradation.

In seismic profile (NovaSPAN line 1600) there is no direct evidence for a diapir that feeds the BRS; rather there is an underlying expulsion rollover with keystone grabens that dips steeply seaward, documenting extensive downbuilding and rotation. However, along strike, in NovaSPAN line 5300 (Appendix A-3), there is evidence of diapirs in this position that extend even higher into the stratigraphy (Tertiary). Strata in areas that have diapirs at the modern-day slope (and BRS) likely experienced less seaward rotation, as the diapir would take on strain and allow for the translation of rafted salt withdrawal basins (SW2b &SW2c). Both the BRS and landward-directed overhang from diapir D3

have spread at approximately the top of the Early Cretaceous Missisauga formation. This spreading event correlates with two controlling factors; 1) short-lived sediment starvation due to transgression, and 2) high salt extrusion rates due to downbuilding throughout the Early Cretaceous. Diapir D3 was squeezed by late-stage contraction during the Tertiary, which may have occurred during the Paleogene or Early Neogene to Pliocene (Shimeld, 2004). This contraction rejuvenated diapir D3 and resulted in vertical (secondary) welding of its feeder stock.

3. Passive Diapir and Late Cretaceous Canopy Domain

The *Passive Diapir and Late Cretaceous Canopy Domain* is characterized by a final extensional diapir (D4) that feeds an extensive salt tongue canopy that spread during the Late Cretaceous and a small salt nappe that climbs out of the autochthonous salt basin during the Early Cretaceous. The passive diapir, like those in the *Passive Diapir and Early Cretaceous Canopy Domain* developed out of an early-inflated salt complex that was related to contraction in the thinning salt layer at the seaward limit of the autochthonous basin. Since strata strongly drape the diapir in seismic section, it is interpreted that there was either pelagic cover, or a minor mini-basin present before its formation. Since the diapir could not move seaward very efficiently (unlike others present in landward regions), overlying strata were pulled up during its development. Shortening of this salt-withdrawal basin due to the seaward translation of diapir D3 likely aided the sediment sheathing over D4. Tertiary contraction may have contributed to the geometry of the salt withdrawal basin; however, it is likely that the aforementioned process led to most of the deformation. The Late Cretaceous canopy spread during sediment starvation induced by overall transgression of the margin and reduced

sedimentation. Since the Late Cretaceous was a time of sediment starvation, and generally resulted in condensed deposits, the allochthonous salt sheets in nature were able to spread sub-horizontally during a considerable time span (~17 Ma). The salt nappe was extruded from the autochthonous basin as the prograding sediment wedge advanced onto the inflated complex just landward of diapir D3 as recorded by the significant growth (~6 km). Downbuilding into the inflated complex extruded enough silicone/salt to drive the nappe out of the basin and over older sediments during the mid-Early Cretaceous (Fig. 5-16 C – Vz; Fig. 5-17 A – Vz). Experiment results (Fig. 5-12) suggest that the nappe developed at approximately the same time that D4 became passive.

6.2 Improved Understanding of NovaSPAN line 1600

The scaled physical experiments provided insights into the evolution of the salt tectonic system at the western Sable sub-basin (NovaSPAN line 1600: Fig. 6-1).

6.2.1 Basin Morphology

Seismic imaging of the basin-floor is problematic at depth, leaving considerable uncertainties with certain aspects of the interpretation. Although the Abenaki sub-basin is relatively well imaged, revealing a symmetric graben and horst (NSH) structure, the Sable sub-basin is generally acoustically shadowed at depth. The setup for the Sable sub-basin in experiment 2 (Fig. 5-3) consisted of a flat-ramp-flat geometry, and displayed considerably similar evolution to the location of diapirs in seismic section. By testing the effects of a half-graben geometry of basin-floor configuration, it was found that seaward translation of diapirs was inhibited, and that they typically become arrested at ~midway up the wedge (i.e. Fig. 5-10) (***6.6.1 Effects of Basin Morphology*** – this chapter;

MacDonald, 2007). This seems appropriate for the most distal portion of the Sable sub-basin that was simulated as a flat segment in experiment 2.

The basin-floor morphology represented in Fig. 6-1 is similar to the present-day crustal structure along the margin (Zheng and Arkani, 2002, Funck et al., 2004; Wu et al., 2006) (Fig. 3-3 and 3-4). However, it was uncertain if the present day basin-floor morphology reflects its original syn-rift/early post-rift morphology. Experimental results suggest that it does, since original inflections in silicone thickness controlled diapir evolution and locked them in similar positions as observed in the seismic profile. Based on seismic interpretation, it appears that the topography basement blocks by salt did not control variations in original salt thickness, since they are covered by syn-rift sediments. Instead, crustal thinning (Wu et al., 2006; Keen and Beaumont, 1990) appears to be the controlling factor, as they correlate with syn-rift subsidence patterns. This requires a shift from attributing the effects of structure-scale, basement structure controls (i.e. Ge et al., 1997; MacDonald, 2007; Campbell 2007) on variations in salt thickness and their effect on salt tectonics evolution, to a crustal-scale approach.

6.2.2 Tectono-stratigraphic Framework

Stratigraphic picks available from well data are generally confined to the shelf, with exception to recent exploration wells at the modern-day slope (i.e. Annapolis G-24, Crimson F-81, Balvenie B-79). However, these picks have been correlated through the Sable sub-basin with the aid of deepwater stratigraphic horizons (Ebinger and Tucholke, 1979), and the new salt tectonic concepts acquired through the scaled physical experiments. Although it is difficult to confidently make Jurassic picks in the Sable sub-basin, picks used for Early and Late Cretaceous formations agree with recent drilling

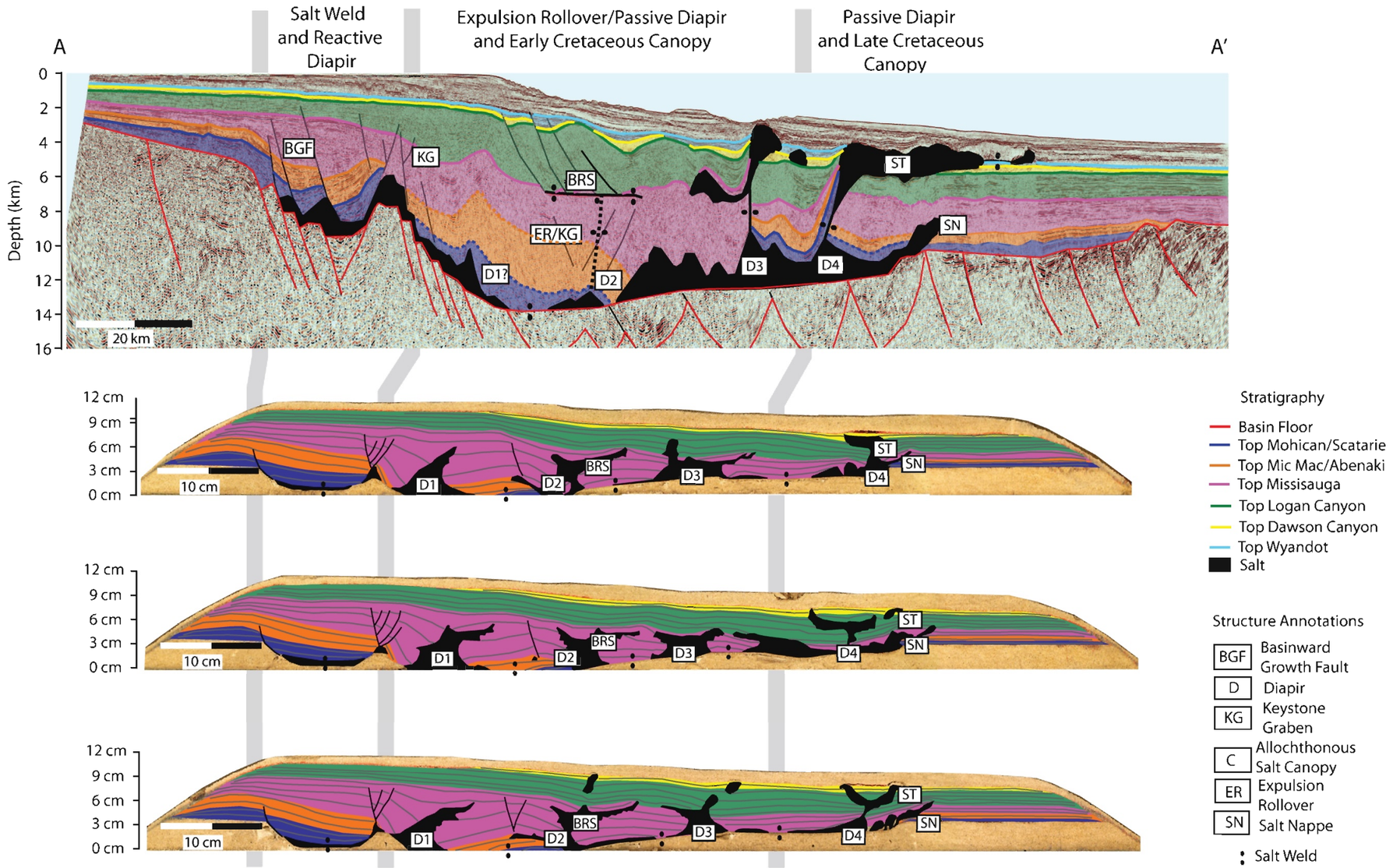

Figure 6-1: Salt Tectonic Domains of NovaSPAN line 1600 compared with those in experiment 2. Experiment 2 has less Mid – Late Jurassic (Mohican Formation and Missisauga Formation) strata, as it was based on a high Early Cretaceous sedimentation end-member interpretation. Although the true stratigraphy is unconstrained at depth, it is believed that there is still a moderate amount of Late Jurassic sediments, as progradation began slightly prior to the Early Cretaceous.

results and seismic interpretations (Kidston et al., 2007). However, even with a lack of well control, it is observed that the stratigraphic packages show significant growth in the Sable sub-basin through the latter portion of the Late Jurassic and the entire Early Cretaceous, controlled by a regional expulsion rollover. The expulsion rollover anticline in the western Sable sub-basin is characterized by significant keystone grabens that directly underlie the BRS. The BRS itself is probably fed by diapirs that are situated under the modern day slope. These diapirs may separate expulsion rollovers and/or regional salt-withdrawal basins along strike. As noted in the discussion of the *Passive Diapir and Late Cretaceous Canopy Domain* section, salt withdrawal basins in the deepwater regions of the western Sable sub-basin dominantly experienced growth during the Early Cretaceous deposition of the Logan Canyon formation, when deposition became broad across the margin.

6.2.3 Salt and Fault Structures

The understanding of numerous strutures related to salt tectonics in the western Sable sub-basin has been significantly improved by this study. Particularly important was are nature of the salt remnant over the NSH horst, the antiformal geometry of strata and possible salt body (D1) in the Sable sub-basin, the occurrence of the BRS and the position from where it was fed, the spreading direction of the landward overhang from diapir D3, and the small salt nappe (SN).

The scaled physical experiments suggest that the salt remnant over the horst was formed by the localization of early downdip contraction in salt caused by slow, aggradational deposition that resulted in extension at the hinge zone. The resulting contractional salt massif then evolved into a passive diapir as bypassing sediments began

to downbuild into its seaward flank. In experiment 2, preferential downbuilding of sediments in the proximal graben overlying the landward portion of the diapir forced the main portion of this diapir into the Sable sub-basin, leaving only a minor salt remnant overlying the horst (Fig. 5-19). If the same process happened in nature, then it is possible that the antiformal strata and underlying salt body in the landward portion of the deep portion of the Sable sub-basin are really the along-strike flank of a diapir. This diapir could have begun developing over the horst and been translated into the Sable sub-basin with further Jurassic and Early Cretaceous loading. In the scaled physical experiment, D1 grew to approximately to the top of the unit time-equivalent to the Early Cretaceous Missisauga formation, when regional welding halted its development. The seismic character tends to mirror this observation, as the development of the antiform diminishes at the top of the Early Cretaceous Missisauga formation, when major growth packages cease at depth. Although this interpretation remains speculative, it is attractive since it does not require any contraction to be induced in the extensional domain.

The BRS is positioned directly beneath the modern-day slope and acts as a major allochthonous detachment surface in the Sable sub-basin. However, it is not known from where this shallow allochthonous salt system was fed. Experimental results suggest that feeder diapirs may exist directly beneath the BRS itself, and that the position of these diapirs can be correlated with changes in the original basin morphology. In experiment 2 (Fig. 5-12 and 5-13), this diapir developed out of an inflated silicone complex ~5 cm seaward of the NSH horst; however, it was translated to the base of the ramp in the basin-floor, where the original silicone layer thinned. Similarly, this is the position of the BRS in the seismic profile (Fig. 6-1), although no diapir is observed in the seismic section. In

the strike line (NovaSPAN 5300; Appendix B-4), there are diapirs to the southwest of this position, and are also localized with respect to shallowing of the basin-floor downdip and along-strike. In experiment 2, at this level the canopy began to develop rapidly before the starvation event, due to strong downbuilding and silicone supply from depth. Extensive downbuilding appears to have happened during the Early Cretaceous in nature, and may have supplied salt to the BRS very rapidly as well. The minor transgressive event that resulted in the Naskapi shale on the shelf likely resulted in the sub-horizontal spreading of this allochthonous system.

Diapir D3 developed a landward-directed overhang in the seismic profile; however, it is not known if it truly spread in the landward direction, or if it reflects a portion of a salt structure that is more complex in 3D. In experiment 2 (Fig. 5-16 C - Exx), diapir D3 evolved over the ramp and was trapped in a position similar to that seen in the seismic profile. Due to prolonged downbuilding and high subsidence rates on its landward flank, the region directly landward of the diapir became a topographic low and allowed an allochthonous silicone sheet to spread in the landward direction. Since there is a very thick (~6 km) growth package at the landward flank of D3 in the seismic profile, it is likely that this process occurred in nature. The landward overhang is positioned at the same stratigraphic level as the BRS; therefore, its formation may have been aided by the same minor transgressive event in the Early Cretaceous. During later loading and extensional failure of sediments that had been prograding over the BRS canopy during the Early Cretaceous (Logan Canyon formation), the landward overhang may have accommodated downdip contraction, resulting in its squeezed (bulbous) appearance (Fig. 6-3 B). However, late-stage Tertiary uplift of mainland Nova Scotia that

squeezed diapir D3 may also owe to the contractional appearance of the landward overhang.

The salt nappe in the seismic profile (Fig. 6-1) is positioned beneath an extensive salt tongue canopy system, at depths where seismic imaging quality degrades significantly. However, irregular geometries of strata underlying the salt tongue, as well as continuous, non-conformable, high-amplitude reflectors that bound a chaotic package suggest its occurrence (Fig. 4-3 and 4-7). Experimental results (Fig. 5-16 C – Vz; Fig. 5-17 A - Vx) indicate that this salt nappe developed at approximately the same time as diapir D4 became passive in the mid-Early Cretaceous. The expulsion of the silicone nappe in the experiment required significant downbuilding over the basin-floor ramp, which is also the position of most significant Early Cretaceous downbuilding in NovaSPAN line 1600.

6.4 Conceptual Model for the Development of Salt Tectonics at the Western Sable Sub-basin

From the work done by the Salt Dynamics Group, it is interpreted that the western portion of the Sable sub-basin had the youngest evolution at the north central Scotian margin due to southwest migration of the Laurentian fan and Sable delta depocenters and related early salt withdrawal and regional welding in SP IV. Thus, the Early Cretaceous period was the most crucial time for the development of salt structures and depocenters. Figures 6-2 and 6-3 are schematic reconstructions of the salt-tectonic system based on the results of the scaled analogue experiments that were presented in chapter 5. Both thermal and loading subsidence have been qualitatively applied to the schematic representations, but are not based on the experiments. Thermal subsidence is simulated by adjusting distal

regions of the schematic basin to a level that would allow for the prograding sedimentary wedge to deliver an appropriate amount of sediment beyond the salt basin. ~70 - 80 Ma after breakup, thermal subsidence is not accounted for, as significant Early Cretaceous deposits are transported over the transitional crust. Loading subsidence is simulated by lowering the continental crust appropriately with respect to the sedimentary load coming into the system at each time step. Since the crust thins dramatically beyond the hinge zone and towards the transitional crust, loading subsidence is more significant at the distal regions of the section due to less buoyant compensation. Although only qualitative, both of these mechanisms must be factored into the conceptual model to result in a section that is similar to the seismic section.

6.4.1 Scatarie/Mohican Formation (Mid Jurassic)

Since the main depocenter during the Early-Mid Jurassic was in SP IV and V, the western portion of the margin received relatively less sediment via aggradation, which was confined to the proximal graben and the landward regions of the Sable sub-basin (Fig. 6-2 B; Fig. 6-4; Fig. 6-6). Downbuilding and extension of these deposits resulted in contraction in front of and above the horst of the North Sable High, due to significant thinning of the original salt layer. This contraction was accommodated by narrow inflation of salt that immediately evolved into a passive diapir. Once the diapir was emplaced, it became a site of weakness, and accommodated strain created by downbuilding and salt withdrawal in the proximal graben. Sediments that were downbuilding into the Sable sub-basin were strongly translated seaward, but were buttressed by a broadly inflated salt in distal regions. The leading part of the sedimentary

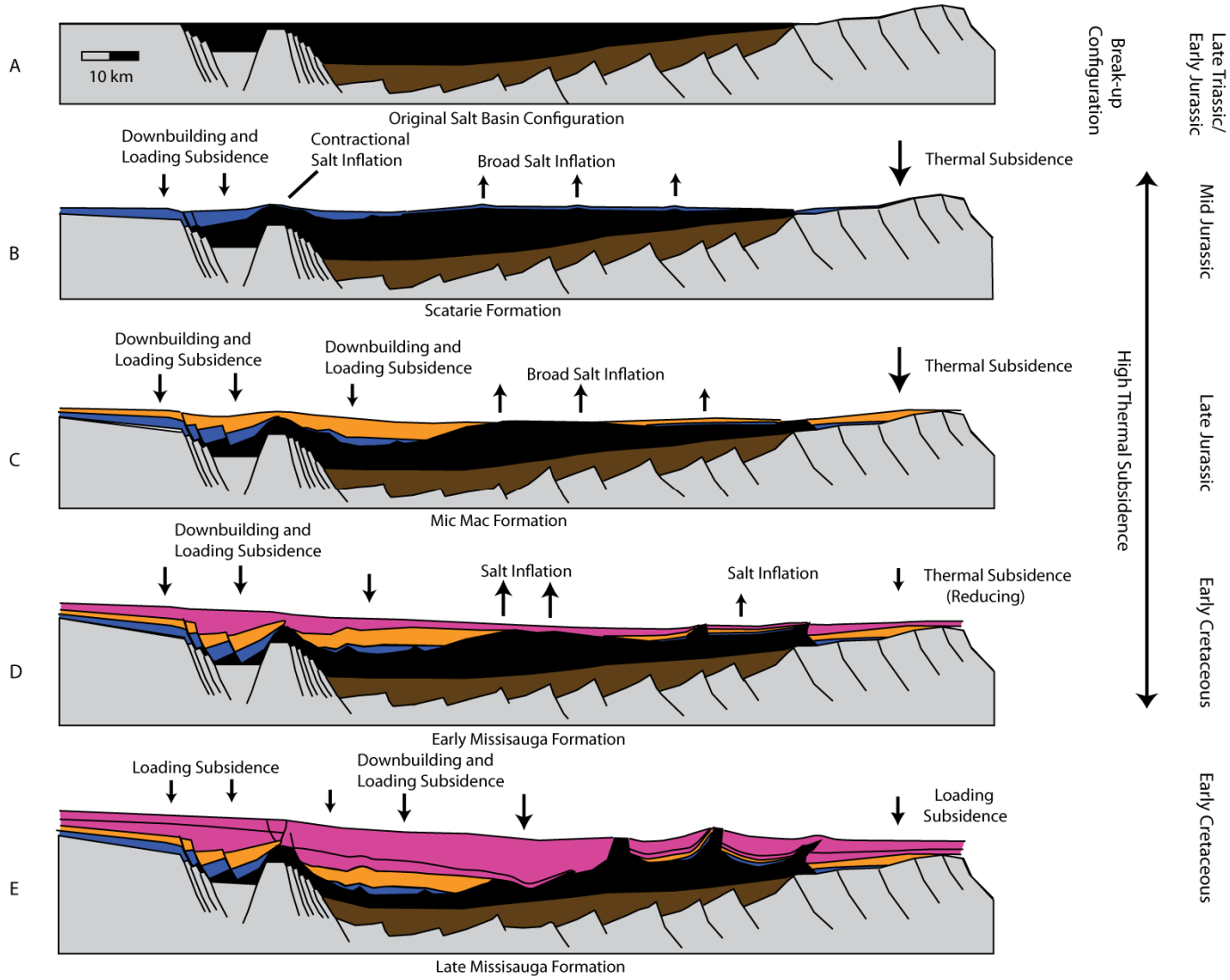

Figure 6-2: Conceptual model for the evolution of the western Sable sub-basin at key stratigraphic intervals (Mid Jurassic Mohican formation to Early Cretaceous Missisauga formation).

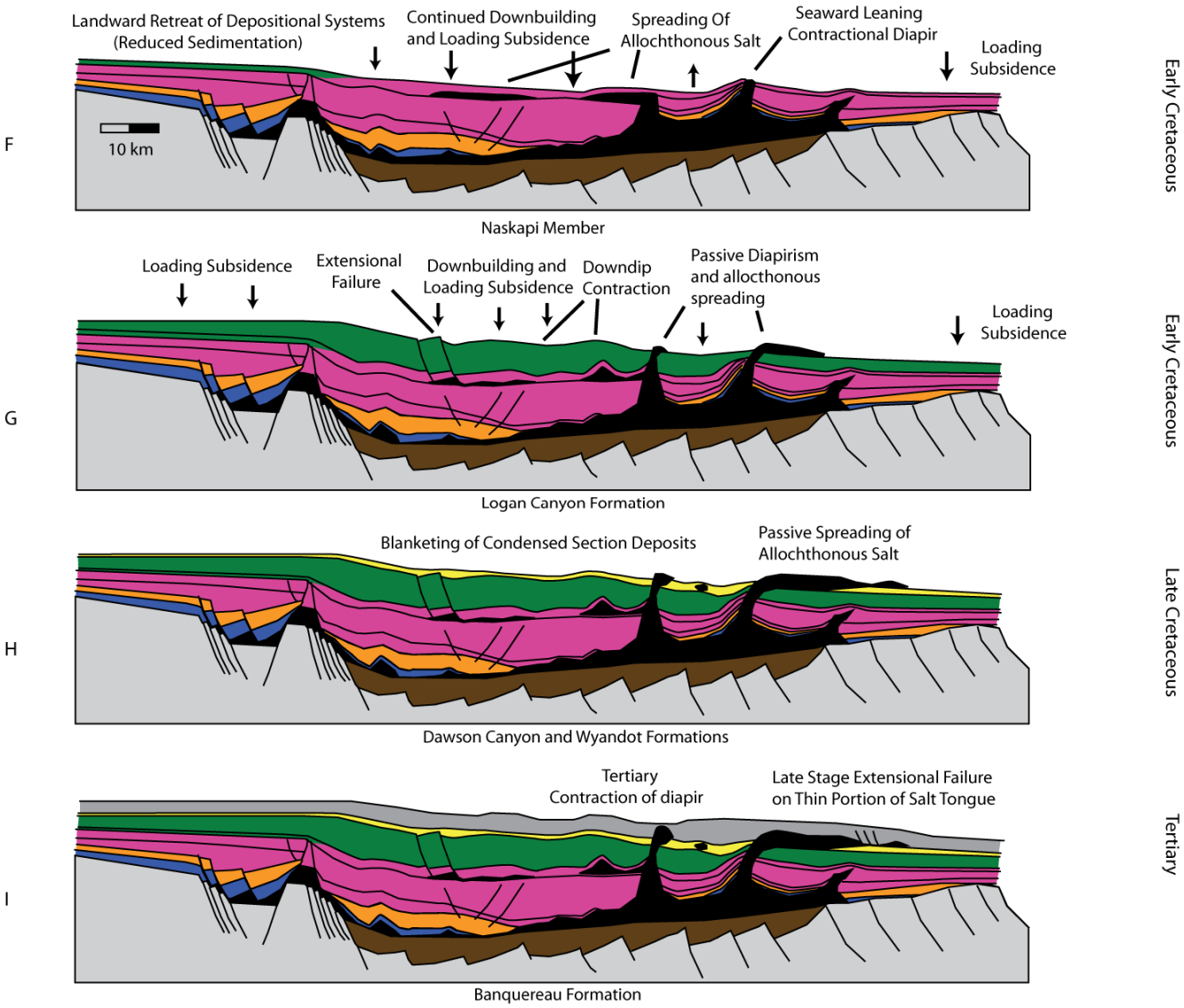

Figure 6-3: Conceptual model for the evolution of the western Sable sub-basin at key stratigraphic intervals (Early Cretaceous Naskapi Member to the Tertiary Banquereau formation).

package and the landward flank of the inflated salt complex probably experienced contraction as a result of this buttress effect; however, no significant deformation of the sediment package is evident. The position of the inflated salt appears to be related to the shape of the original salt basin, and more importantly the original thickness of the salt layer. Salt began to inflate early where the basin-floor began to ramp up towards the transitional crust and salt broadly thinned. As well, early, narrow fold belts in the inflated salt massif and thin overburden likely existed at this time, and were positioned at inflections of salt thickness (i.e. Fig. 5-14 B & C – Exx). In the experiments, the fold belts were later overprinted by extensional deformation with the advancement of the sedimentary wedge. This process may have occurred in nature, erasing any evidence of earlier folding. The localization of fold belts was probably controlled by the thickness of the salt layer, since it had a strong control on Poiseuille flow (for further discussion see ***6.6.1 Effects of Basin Morphology*** later in this chapter).

The distal portion of the basin was likely subsiding rapidly due to thermal subsidence during the early post-rift period. This early thermal subsidence was probably more significant than the effects of landward sedimentary loading, as the prograding sedimentary wedge did yet not deposit a thick package in the distal basin. Strong thermal subsidence at the distal portion of the basin likely played an important role in allowing early sediments to reach the transitional crust and Sohm abyssal plain.

6.4.2 Mic Mac Formation (Late Jurassic)

Similarly to the Early - Mid Jurassic, the main depocenter for Late Jurassic sediments was in the northern regions of the margin (Fig. 6-2 C). However, early subsidence and downbuilding from loading of Mohican formation sediments created

accommodation space that allowed further deposition in both the proximal graben and deep portion of the Sable sub-basin. Increased downbuilding in the Abenaki sub-basin resulted in further salt withdrawal, mobilizing it over the horst and under the salt withdrawal basin forming in the Sable sub-basin. This downbuilding also resulted in extension of the overburden that allowed for a minor reactive diapir to be trapped in the hanging wall of a basinward-dipping growth fault. The diapir over the NSH horst was no longer passive and was experiencing some collapse, as salt was being evacuated into the Sable sub-basin. With this diapir collapse and seaward advancement of prograding sediments, the bathymetry of the sea floor became broader and more sediment reached the distal regions of the margin.

Thermal subsidence was likely ongoing and relatively rapid at this time, and may have aided distal sediment transport by increasing the gradient of the sea floor. Although landward loading subsidence most likely increased during this time with Late Jurassic deposition, it was probably balanced by distal thermal subsidence.

6.4.3 Missisauga Formation (Early Cretaceous)

Since the early portion of the Early Cretaceous is interpreted to be the most important time of salt-tectonic deformation, the Missisauga formation is described in three stages: the *early, late, and transitional stage.*

Early Stage

The early stage of deposition of the Early Cretaceous Missisauga formation (Fig. 6-2 D) is similar to that of the Mic Mac formation in the Late Jurassic. However, an increased amount of sediment began advancing into the western portion of the Sable sub-

basin, because of the southwest migration of depocenters from the Sable Delta due to shutting down of salt tectonics in the north. By the end of this stage, the overburden in the proximal graben was welded to the basin-floor indicating the near complete evacuation of salt. Continued downbuilding and translation of sediments in the deeper Sable sub-basin resulted in increased seaward salt mobilization. In response to this, the inflated salt complex narrowed and became localized further seaward. If broadly inflated salt was not exposed at its crest, it was likely close to the surface. A prominent diapir ridge was probably present at the landward region of the complex. At the same time, the distal portion of the salt basin inflated slightly more, and both a diapir and salt nappe started to develop.

Although thermal subsidence was likely ceasing, an already significant portion of sediments had made spread beyond the broadly inflated salt basin, allowing for increased distal loading subsidence. Regardless of the effects of both loading and thermal subsidence, the basin appears to have retained a very similar geometry to its starting configuration.

Late Stage

During deposition of the late stage of the Early Cretaceous Missisauga formation (Fig. 6-2 E), deposition became focused in the Sable sub-basin. Earlier deposited strata subsided; however, unlike basins found in previous times, this salt-withdrawal basin did not experience much seaward translation as the bathymetric gradient was reduced by the collapse of the diapir over the horst. The major depocenter migrated seaward as most salt was evacuated from the landward region of the Sable sub-basin, resulting in a thick,

growth package of sediments and an asymmetric expulsion rollover (Fig. 6-1). This thick package of sediments evacuated salt from the previously inflated complex, which then became localized as a passive diapir at an inflection in the basin floor, where salt previously thinned. Rafted sediments trapped between the two diapirs were being asymmetrically pulled up by the landward flank of the most distal diapir, as it was buttressed and could not move seaward during its evolution. As well, these sediments were experiencing shortening induced by the seaward translation of the aforementioned diapir, D3. This shortening was likely the major control on the sheath-like geometry of sediments on the most distal diapir, D4. Sediments had also spread beyond the two distal diapirs, resulting in minor downbuilding that aided the rapid emplacement of a small salt nappe that was shut down by the end of this time.

Thermal subsidence is not likely to have been a major component of basin evolution at this point in time due to exponential cooling of the crust after break-up. However, increased loading of the considerably thinned transitional crust resulted in continued subsidence in distal regions.

Transitional Stage (Naskapi Member)

The transitional stage marks the end of Early Cretaceous Missisauga formation (Fig. 6-3 F), which is characterized by transgression and starvation in the basin and landward retreat of depositional systems that led to the deposition of the Naskapi shale tongue at the shelf. As sea level was rising, the modern-day slope and deepwater basin were becoming progressively sediment starved. During this time, salt fed from passive diapirs was able to spread passively at the sea floor. It is interpreted that fine, pro-delta

and pelagic sediments were being deposited during the spreading of the Balvenie Roho System and other allochthonous salt sheets at this level, and because of this there is a thin cover of Missisauga formation time-equivalents. Since the allochthonous salt sheets at this stratigraphic level are sub-horizontal and the minor transgressive event was relatively short-lived, the salt supply must have been very high, indicating a significant loading of the salt layer. This was likely the case at the Sable sub-basin, as the progradation of the Early Cretaceous Missisauga formation had significantly loaded the autochthonous salt. Since a significant package of overburden was still downbuilding with high subsidence rates into autochthonous salt landward of D3, salt was able to spread landward in the topographic low. The Naskapi shale tongue was deposited on the shelf by the end of this transgression, which conformably transitions into the top, condensed portion of the Missisauga formation in the basin.

6.4.4 Logan Canyon Formation (Early Cretaceous)

The Early Cretaceous Logan Canyon formation (Fig. 6-3 G) is characterized by relatively broad deposition throughout the Sable sub-basin and tapers towards the transitional crust. Loading of the BRS has resulted in extensional failure and seaward translation of the overburden. Downdip contraction associated with this extensional failure appears to be localized at the seaward limit of the BRS and the landward-directed overhang from the first distal passive diapir, as strata comprise a considerable antiform. However, it is difficult to determine how much contraction was responsible for this feature, as considerable downbuilding had occurred into the landward flank of the overhang, and contributed to the antiformal geometry. Furthermore, Tertiary uplift of Nova Scotia may have contributed to the geometry of the antiform via late-stage

contraction. Considerable downbuilding occurred between the distal diapirs, causing salt to be pumped rapidly through the furthest seaward diapir, resulting in the early stage of the quickly spreading allochthonous salt tongue canopy. Both diapirs appear to climb at a seaward incline in the seismic profiles, and in NovaSPAN line 5300 (Appendix B-4), salt from diapirs is seen to also climb the stratigraphy in a similar fashion along strike, suggesting that this is not unique to only downdip orientation. The steep, progressive climbing of stratigraphy indicates either an increase of sediment influx, salt supply, or both. In fact, it is likely that both factors played an important role in this structural style, since there was considerable loading of inflated underlying salt, and sea level was gradually rising during this time.

Since the deposition of the Logan Canyon formation is relatively widespread, loading subsidence is interpreted as being generally uniform.

6.4.5 Dawson Canyon and Wyandot Formations (Late Cretaceous)

By the Late Cretaceous (Fig. 6-3 H), the salt-tectonic system was nearly shut down and sea level was relatively high. Although this was a period of depositional cessation, the load already provided by Early Cretaceous sedimentation continued to downbuild into underlying salt, pumping it through the distal diapir. This continuous supply of salt with only minor sedimentation allowed for continued sub-horizontal spreading of the salt tongue canopy. Overall, Late Cretaceous deposits consist of only a relatively thin package of sediments that represent a significantly long period of time (~17 Ma).

6.4.6 Banquereau Formation (Tertiary)

Very little salt-related deformation occurred in the Tertiary, although late stage contraction is seen in diapirs and possibly the landward overhang, suggesting landward uplift occurred. Through extensive mapping, Shimeld (2004) noted that this contraction spanned the late Paleogene/early Neogene to the Pliocene. The contraction effectively rejuvenated the diapirs, pulling up overlying strata such that they are continuous in thickness and are folded over the bulb of the diapir. Throughout the Tertiary, a roho system also developed over the salt tongue canopy where it was originally thin, and is now welded. Little to no contraction associated with this extensional failure was accommodated in the overburden because the salt tongue was an open-toe system during the time of deformation.

6.5 Regional Implications for the Scotian Margin including Co-Studies

6.5.1 Configuration of the Original Salt Basin

6.5.1.1 Consequences of Rifting to Salt Basin Geometry

The morphology of the syn-rift salt basin appears to be strongly dependent on crustal structure, which can vary considerably along strike of the passive margin. As discussed in chapter 3, the crustal structure of the Scotian margin developed during syn-rift extension (Wu et al., 2006, Funck et al., 2004, Keen and Beaumont, 1990), and has been subsequently altered by post-rift loading subsidence and crustal flexure. However, the present-day structure observed in deep seismic profiles reflects the original syn- and post-rift salt basin geometry, and sediment loading has exaggerated its morphology.

The most notable along-strike characteristic is the drastic shallowing from the deep Sable sub-basin to the southwestern part of the salt basin outboard of the LaHave Platform. This shallowing of the basin is directly correlated to the crustal thickness, as it is thicker than beneath the Sable sub-basin (SMART Lines; Fig. 3-3 and Fig. 3-4). Linear seaward thinning of the crust has affected the geometry and structural style of the hinge zone along the LaHave Platform such that it developed as a set of broadly spaced faults gradually offsetting the basement towards the basin center. This broad zone of faults may impact salt tectonics outboard of the LaHave Platform such that there may be more syn-depositional extension via gravity gliding over a regional slope of the basin-floor. This style of salt-tectonic deformation is characterized by strong updip extension due to gravity gliding, and is similar to what is observed at the Angolan margin (Brun and Fort, 2004). At the Abenaki sub-basin, the hinge zone is most commonly observed as set of faults that abruptly offset the basement, downbuilding into the basin, by ~4 km.

Complex strain partitioning and variable crustal thinning during rifting have led to basement highs, one of which in NovaSPAN Line 1600 separates the proximal graben form the main portion of the Sable sub-basin (Fig. 6-4). This high is not present as a horst like structure in its entirety (as seen in NovaSPAN line 1600), but also as a set of rotated asymmetric fault blocks that have not experienced as much vertical offset as those underlying the Abenaki and Sable sub-basins. The asymmetric half grabens created by these rotated fault blocks appear to be nearly or completely in-filled by syn-rift lacustrine and fluvial red-bed deposits. The occurrence of highs can be observed in measurements of crustal thickness completed by Wu et al. (2006) and Funck et al. (2004), as well as nominal gravity models by Zheng and Arkani-Hamed (2002).

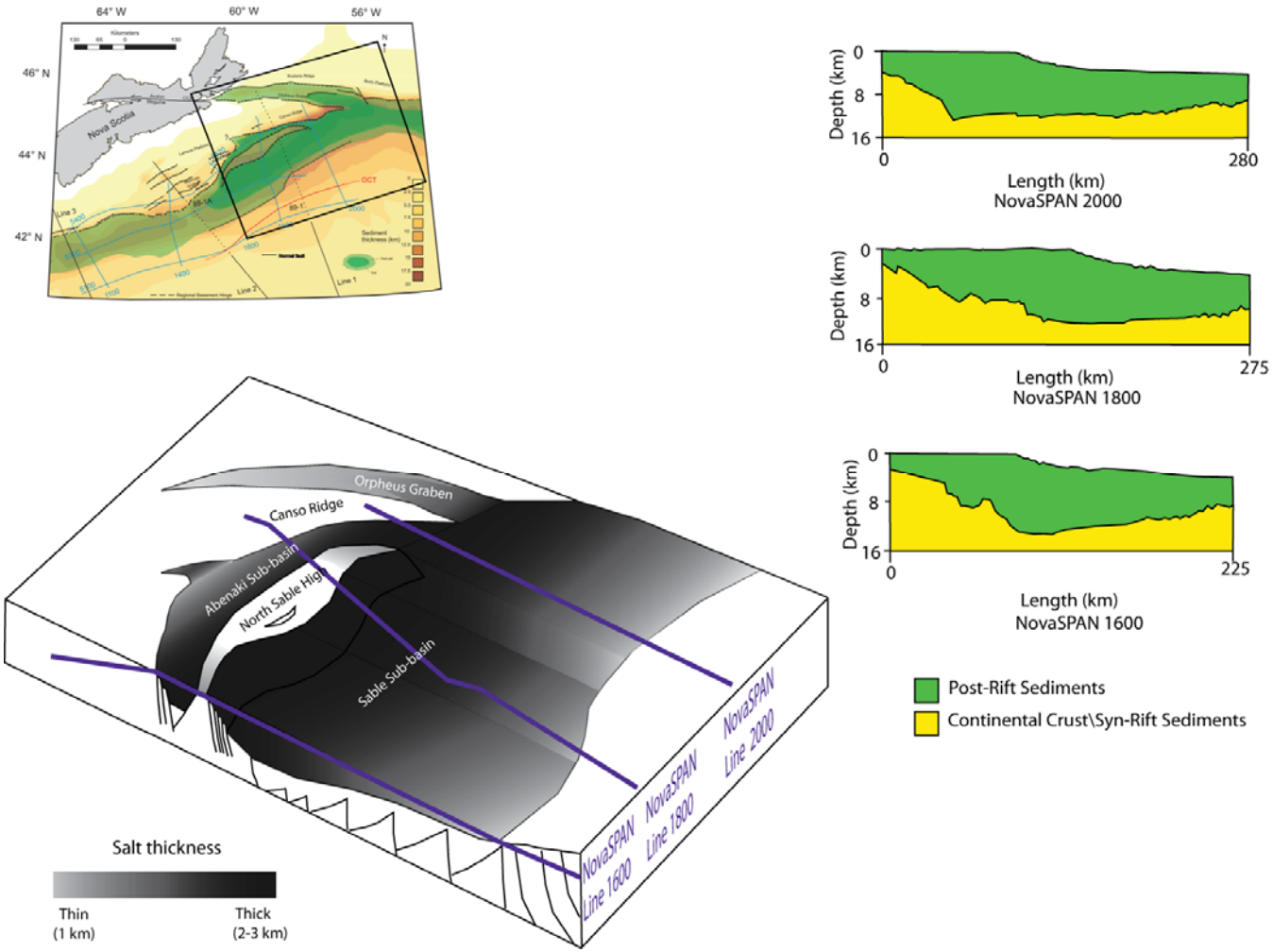

Figure 6-4: Schematic diagram illustrating the interpreted original salt basin geometry with general salt thickness and present-day basin-floor geometry from NovaSPAN lines 1600, 1800, and 2000.

The NSH has an arcuate geometry in map view, and follows the trend of the hinge zone. The width of the NSH is widest at its center (intersecting NovaSPAN line 1800 and underlying Sable Island) and tapers at both ends. The NSH narrows so dramatically at NovaSPAN line 1600 that is seen as an individual horst block, with a series of basinward-dipping faults that step into the deep Sable sub-basin. The high is particularly important to the salt-tectonic evolution at the Scotian margin, as it partially decouples the salt structures and related depositional systems between the Abenaki and Sable sub-basins.

6.5.1.2 Variations of Original Salt Thickness at the North Central Scotian Margin

Syn-rift crustal thinning, extension, and subsidence patterns appear to have significantly controlled the thickness and extent of the late syn-rift Argo formation salt (Fig. 6-4; Fig. 6-5). In general, salt is thickest where there are major fault systems, such as the hinge zone or the seaward shoulder of the North Sable High. The thickest regions of syn-rift Argo formation salt were found to occur at the landward extremity of the Sable sub-basin, where the basement steps down (~4.5 km) from the NSH.

The mapping of the NSH is preliminary, but is interpreted as being a paleo-high during salt deposition and separated the interconnected salt-basins. The proximal graben was a deep, but restricted salt basin since it was separated from the main trend of the Sable sub-basin. When salt was mobilized from the proximal graben, it was dominantly buttressed seaward at the NSH, resulting in the formation of extensive diapirs. The NSH also correlates with the position of the Sable Delta during the Early Cretaceous (Fig. 6-6 and Fig. 6-7). It may have contributed to the position of the Sable Delta since it remained as a relative high throughout the Mid Jurassic to mid Early Cretaceous while salt

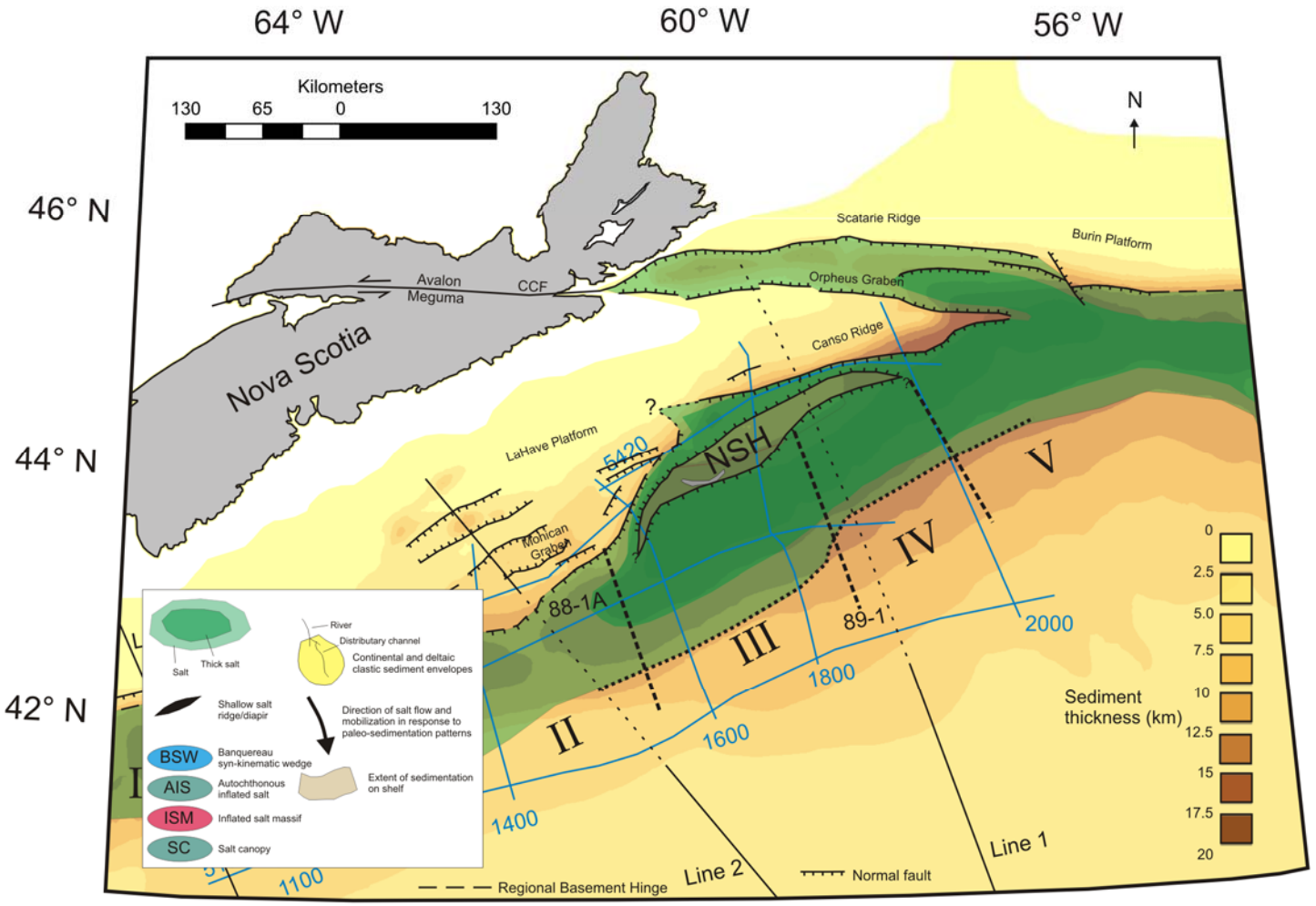

Figure 6-5: Map of the original salt basin with structural elements, sediment thickness, and salt sub-provinces that were defined by Shimeld, 2005.

withdrawal was causing subsidence in the Abenaki and Sable sub-basins (Fig. 6-7 and Fig. 6-8).

Contrary to the extent of the autochthonous salt basin mapped by Shimeld (2004), the basinward limit of the salt basin generally follows the trend of the hinge zone (Fig. 6-5). It extends furthest seaward at SP III, as evidenced by NovaSPAN lines 1600 and 1800, but narrows at SMART 1 and NovaSPAN line 2000. How it thinned toward the OCT varied significantly between northern and southern regions (Fig. 6-4). In SP IV and V, the salt probably tapered as a thinning wedge. In contrast, the basin-floor at the western portion of SP III is complicated by an almost ramp-flat geometry that resulted in relatively defined inflections in salt thickness.

6.5.2 Basin-Scale Sedimentation Patterns

Prominent depocenters have not only migrated from shelf to slope through the evolution of the Scotian margin, but also along the rift basin axes from northeast to southwest. The opening of the Atlantic Ocean occurred from north to south (Chapter 3-2), likely setting up early offshore depositional systems in northernmost regions. Rapid deposition at the northern region of the margin was probably aided by the break-up of Iberia and Newfoundland during the Late Jurassic. The Sable and Laurentian deltas (SP IV and V) were the dominant sediment sources throughout the early post-rift stage. Although the Sable sub-basin was also providing sediments into SP III, higher sediment influx and salt-withdrawal in salt SP IV and V resulted in increased accommodation space in northern regions of the margin. Along with this salt withdrawal was inflation of salt in the southwest (SP III), which became a topographic high, further funneling sediments into SP IV and V.

6.5.2.1 Mohican Formation (Early – Mid Jurassic)

The major depocenter of the Mid-Jurassic Mohican formation (Fig. 6-6) was situated in the northeast portion of the margin (SP IV and V). Since the salt basin in SP IV was narrower than in SP V due to the prominent North Sable High, sediments were bypassed into more distal regions of the margin, initiating early salt inflation and evacuation at the seaward termination of the basin. Salt to the northeast and southwest of this region became broadly inflated, and the dynamically controlled topographic highs may have focused sediments further into distal regions of SP IV. The deposition of the Mohican formation had mobilized much of the autochthonous salt in landward regions of SP IV. Minor deltaic sedimentation was focused in the Abenaki sub-basin at SP III, and subsidence due to salt withdrawal channeled sediments to the southwest.

6.5.2.2 Mic Mac Formation (Late Jurassic)

Most salt was evacuated from the Abenaki Sub-basin by the end of the Late Jurassic (Fig. 6-7). High sedimentation rates in northern regions of the Sable sub-basin resulted in expulsion of a salt nappe, which was overrun by prograding sediments, forming the Banquereau Syn-Kinematic Wedge (BSW) in SP IV. In SP V, a large inflated complex was also extruding outboard of the salt basin climbing the deepwater stratigraphy, but was not experiencing as much loading as the BSW.

Most autochthonous salt in SP III was withdrawn from the Abenaki sub-basin by the Late Jurassic, reducing accommodation space for Early Cretaceous sediments. Since active subsidence in the Abenaki was slowing down, the Sable Delta was able to prograde into the landward regions of the Sable sub-basin, resulting in minor salt withdrawal.

6.5.2.3 Missisauga Formation (Early Cretaceous)

SP III became the main depocenter for the Early Cretaceous Missisauga formation causing the near-complete evacuation of salt from SP IV and V, and major salt withdrawal in the Sable sub-basin (Fig. 6-8). Throughout this stage, main depocenters sequentially migrated seaward because of continuous salt withdrawal and seaward salt inflation. Since inflated salt complexes that evolved into passive diapirs were translated considerably seaward, rafted packages of sediments in distal mini-basins have been pushed closer to the limit of the autochthonous basin. Passive diapirs that evolved from inflated salt complexes became localized at portions of the basin where the basin-floor ramped to shallower levels. The landward flank of the first major passive diapir wall just seaward of NovaSPAN line 5300 is the site of the thickest growth package, and was the most prominent depocenter throughout the evolution of the Scotian margin.

6.5.2.4 Logan Canyon Formation (Early Cretaceous)

There was a minor transgressive event that starved the deep portions of the basin during the transition from the Early Cretaceous Missisauga formation to the Late Cretaceous Logan Canyon formation and also resulted in the deposition of the Naskapi shale on the shelf. This transgression resulted in mainly pelagic sedimentation at the modern-day slope, allowing salt sheets, such as the Balvenie Roho System spread at the sea floor. However, once sea level fell, the prograding sediments were broadly deposited over the entire salt basin and the transitional crust. The remainder of the Logan Canyon formation is transgressional and allowed further spreading of extensive canopies as the basin became increasingly starved. Schematic channel systems mapped by Wade and MacLean (1990) appear to be consistent with breaks in these shallow canopy systems,

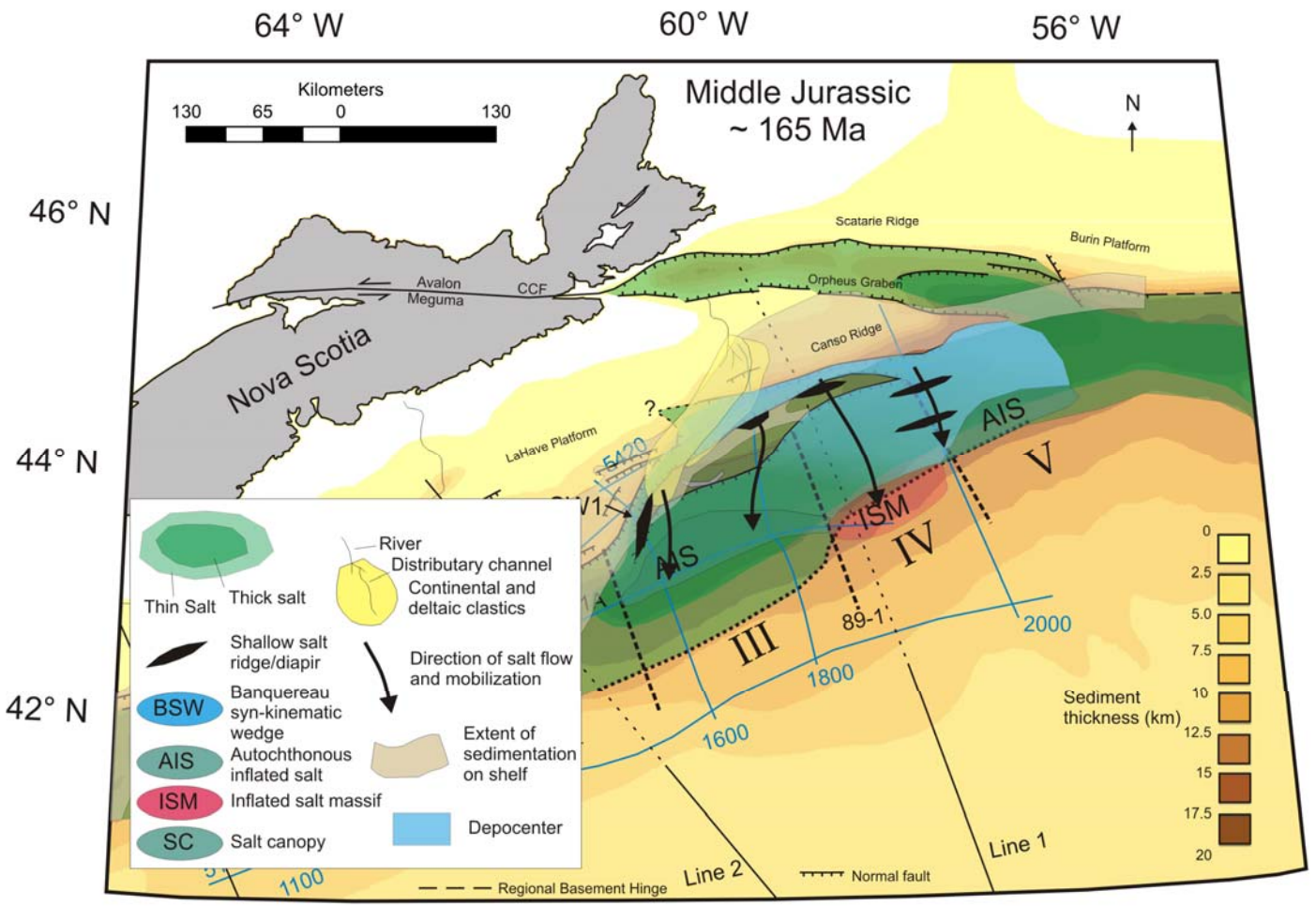

Figure 6-6: Depositional systems, major depocenters (of the western Sable sub-basin), salt withdrawal basins, and salt withdrawal directions during the Middle Jurassic (top Mohican formation). Depositional systems modified from Wade and MacLean, 1990.

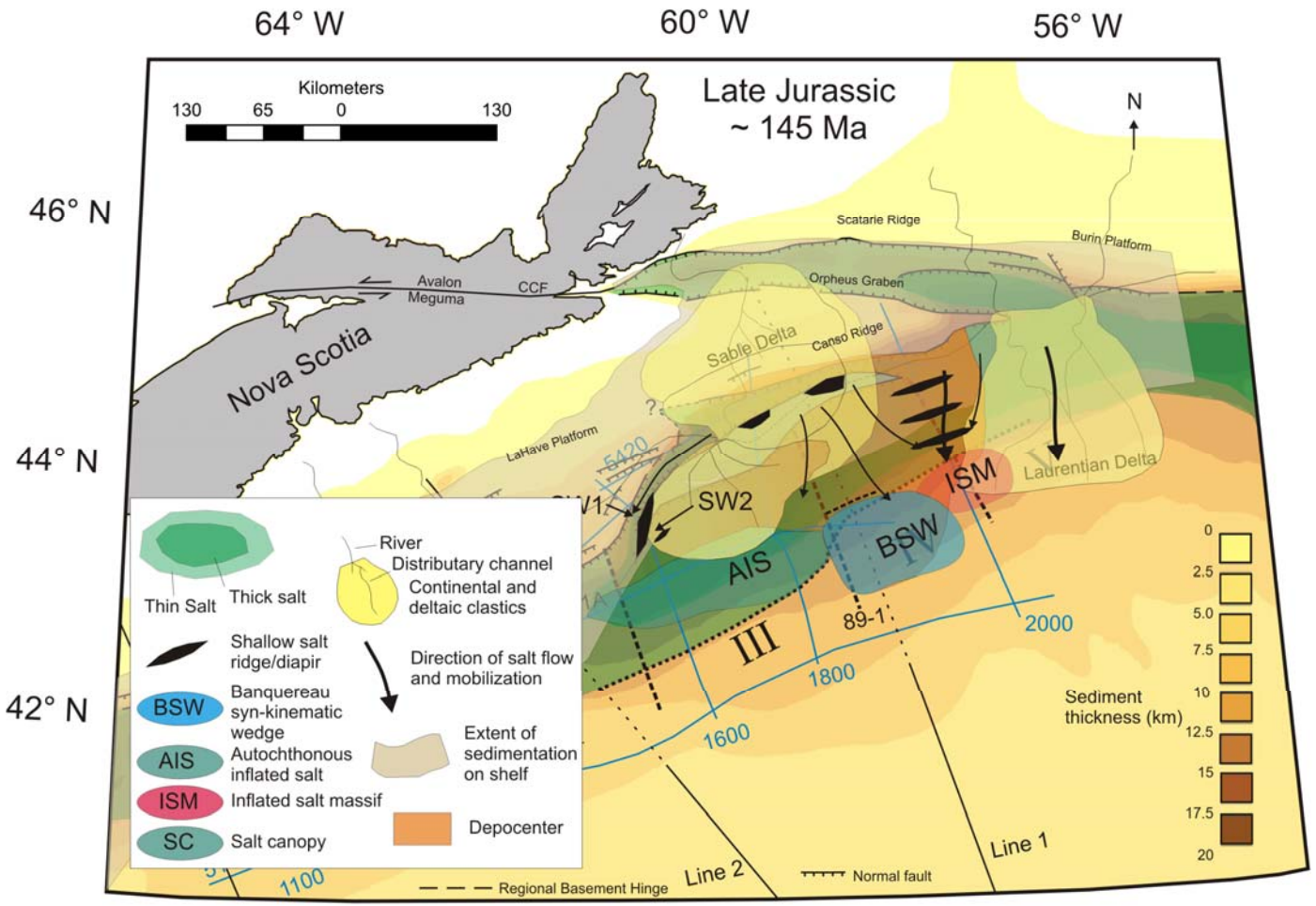

Figure 6-7: Depositional systems, major depocenters (of the western Sable sub-basin), salt withdrawal basins, and salt withdrawal directions during the Late Jurassic (top Mic Mac formation). Depositional systems modified from Wade and MacLean, 1990.

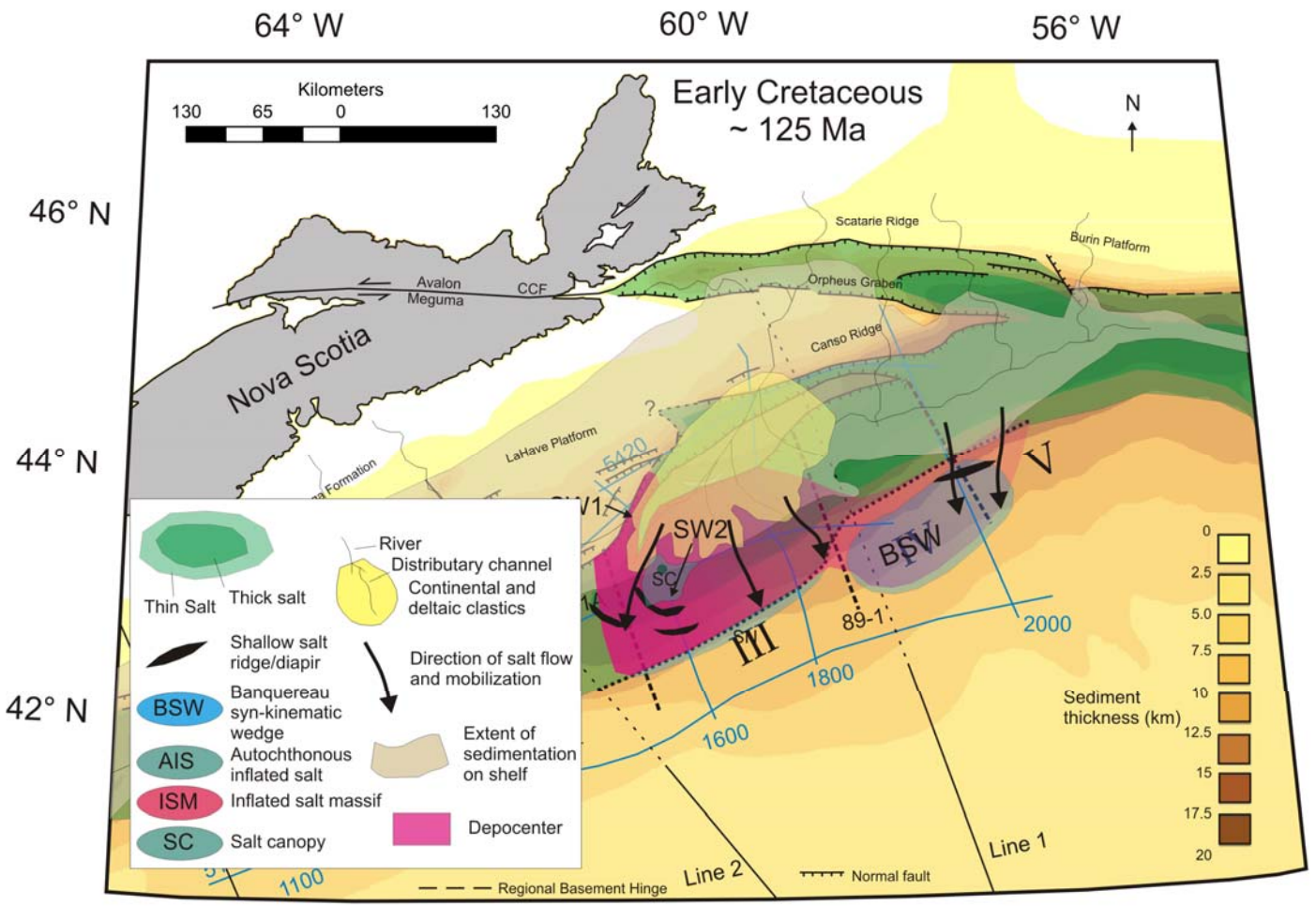

Figure 6-8: Depositional systems, major depocenters (of the western Sable sub-basin), salt withdrawal basins, and salt withdrawal directions during the Early Cretaceous (top Missisauga formation). Depositional systems modified from Wade and MacLean, 1990.

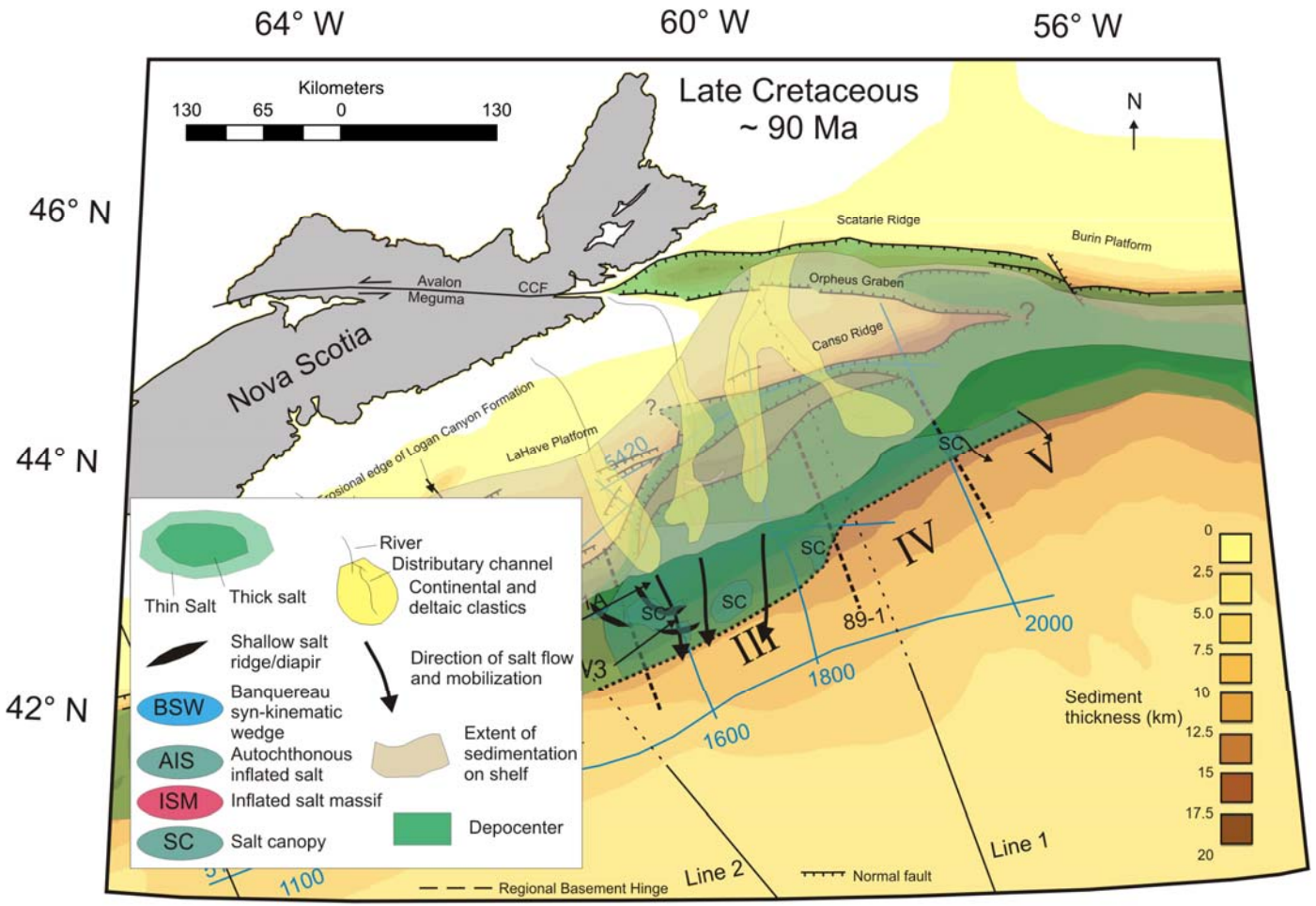

Figure 6-9: Depositional systems, major depocenters (of the western Sable sub-basin), salt withdrawal basins, and salt withdrawal directions during the Late Cretaceous (top Logan Canyon formation). Depositional systems modified from Wade and MacLean, 1990.

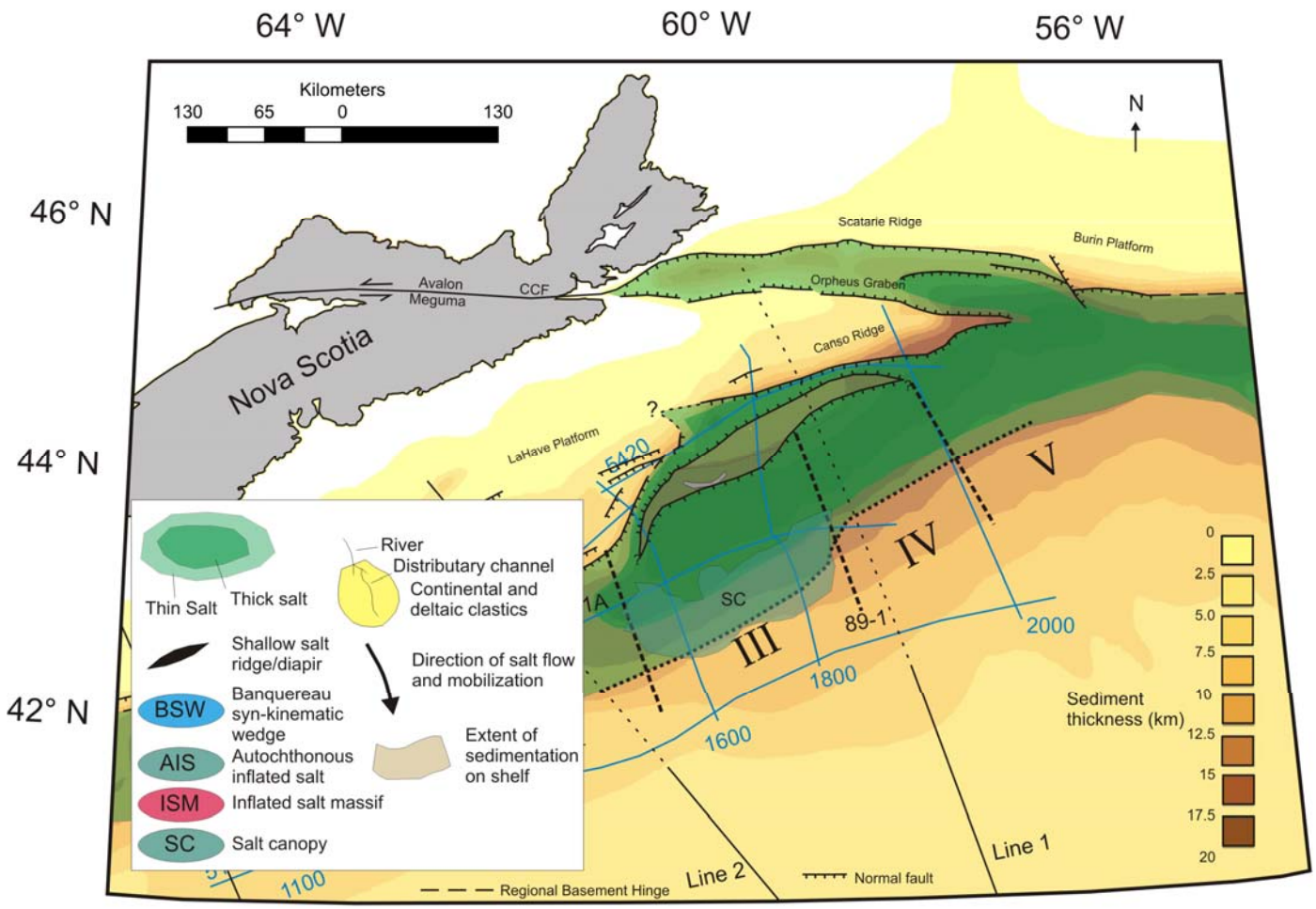

Figure 6-10: General trend of Salt Canopies during the Tertiary (top Wyandot formation).

and may document areas of increased sediment input, as the they were not able to spread in these regions (Fig. 6-9).

6.5.2.5 Dawson Canyon and Wyandot Formations (Late Cretaceous)

Salt tectonics had generally shut down by the Late Cretaceous Dawson Canyon formation, with the exception of deep-water passive diapirs that extended into the Tertiary section (Fig. 6-10). Low sedimentation rates during deposition of the Late Cretaceous Dawson Canyon formation allowed for the spreading of extensive salt tongue canopies that persisted until the Tertiary. Because little to no subsidence was associated with salt withdrawal, regional depocenters are likely absent. Deep-water channel systems were likely controlled by canyon formation in shelf and modern day slope regions, but may have been affected by the extensive and passively spreading canopy systems in distal portions of the margin.

6.6 Lessons Learned From Physical Experiments and the Reconstruction of Salt Tectonics at the Western Sable Sub-basin

6.6.1 Effects of Basin Morphology

Experimental results from physical experiments suggest that inflections in salt thickness strongly affect the seaward mobilization of salt and determine the localization of inflated salt complexes that later evolve into diapirs. A layer of constant thickness will result in efficient seaward salt mobilization; however, if this tabular layer meets an abrupt change in thickness (e.g. over the NSH horst), the mobilized salt will be buttressed, resulting in an inflated complex that later evolves into a passive diapir.

A basin-floor ramp that has tapering salt will inflate more broadly and significantly than if there was an abrupt transition, such as a fault scarp (Ge et al., 1997; MacDonald, 2007; Campbell, 2007). If the wedge is narrow, there will commonly be a diapir that becomes arrested at approximately the mid-point of the ramp. However, if the ramp is sufficiently wide there will be repeated sets of diapir formation, which are regularly spaced along the width of the wedge. The only time a diapir will not evolve from an inflated complex over a basin-floor ramp is if the sedimentation rate is very high, and there is some sort of near-flat basin-floor geometry beyond the ramp. In this case, the high sedimentation rate will mobilize the salt seaward, where it will evolve into a passive diapir at a transition in basin-floor geometry and salt thickness. The location of the previously inflated salt over the ramp can then be recognized from an extensive expulsion rollover in the sedimentary overburden.

Lastly, diapirs may also form where the salt layer drastically thickens (e.g. seaward of the NSH, at the edge of the Sable sub-basin). This happens when an inflated complex forms over the high due to early downdip contraction, and is then translated into the deep basin. At this stage, the inflated complex evolves into a diapir that persists until regional welding occurs at its flanks.

6.6.2 Sedimentation Rates, Geometry of the Prograding Wedge, and 3D Depositional Patterns

A number of important lessons have been learned concerning the interplay between sedimentation and salt mobilization in the North-Central Scotian Basin. These findings have been sub-divided into: *sedimentation rates, the geometry of the prograding wedge, and the effects of 3D depositional patterns*

6.6.2.1 Sedimentation Rates

Sedimentation rates chiefly control the rate at which salt is mobilized seaward. However, the relative time that the sedimentation rate increases or decreases complicates this effect. If inflated salt complexes become localized at distal regions of the basin before the sedimentation rate increases, the already thickened salt will take on the high amount of strain associated with rapid progradation, resulting in high amounts of subsidence with very little extensional faulting in the overburden. This rapid downbuilding and subsidence then creates accommodation space in the proximal basin that inhibits the seaward advancement of sediments. This mechanism is likely the best explanation of why there may be a considerably thicker package of Early Cretaceous Missisauga formation sediments beneath the modern-day slope than over the transitional crust in NovaSPAN line 1600 (Fig. 6-1 and Fig. 6-2 D & E). If the sedimentation rate is high from early post-rift stage, then the salt will rapidly be expelled to and beyond the autochthonous limit of the basin. This style of deformation has apparently occurred in northern portion of the margin, where a salt nappe that evolved into the BSW was rapidly extruded from the salt basin (Fig. 6-6; Fig. 6-7).

6.6.2.2 Geometry of the Prograding Wedge

The geometry of the prograding wedge is closely linked to sediment input and related salt weld formation, but is also probably controlled by the proximity of the sediments to their source (i.e. a system dominated by proximal, continentally derived deposits, versus a pro-delta dominated system). As discussed in chapter 5, experiment 1, which had a consistently steeper and narrower wedge than experiment 2, mobilized silicone seaward much more efficiently due to significantly higher differential loading.

This more efficient mechanism of silicone withdrawal resulted in a sequential migration of depocenters and strongly affected the timing of structural evolution and duration of experiment 1 compared to experiment 2. If sediments are broadly deposited including more distal areas (such as in experiment 2), they will reduce the differential load across the system, effectively slowing down salt deformation in the system.

At the southwestern portion of the margin (NovaSPAN line 1600), the prograding wedge was likely broad, even during the southwest migration of the Sable Delta during the Early Cretaceous. This is likely related to the position of the region with respect to the delta, such that pro-delta sediments chiefly drove salt tectonics in the deeper Sable Sub-basin, even though the delta migrated seaward and deposition shifted to the southwest from the Late Jurassic to the Early Cretaceous. Sand concentrations mapped by Wade (1991) (Fig. 6-11) suggest that pro-delta deposition was occurring in the Sable sub-basin. This region is considerably different from the Laurentian Sub-basin to the northeast, as it was closer to two sources (Laurentian and Sable Deltas) during salt mobilization.

6.6.2.3 3D Depositional Patterns

The geometry of the prograding sedimentary wedge is not only important in dip direction, but also in 3D. The focus of this study was to examine the structural evolution of the western Sable sub-basin based on regional dip-lines; however, valuable insight comes from comparing these observations to those seen in published maps (Wade and MacLean 1990; Shimeld, 2004), dip-parallel lines (i.e. SMART profile 2), and margin-parallel lines (i.e. NovaSPAN line 5300). At a regional scale, the simplification of dip-oriented interpretation appears to be suitable for NovaSPAN line 1600. However, there

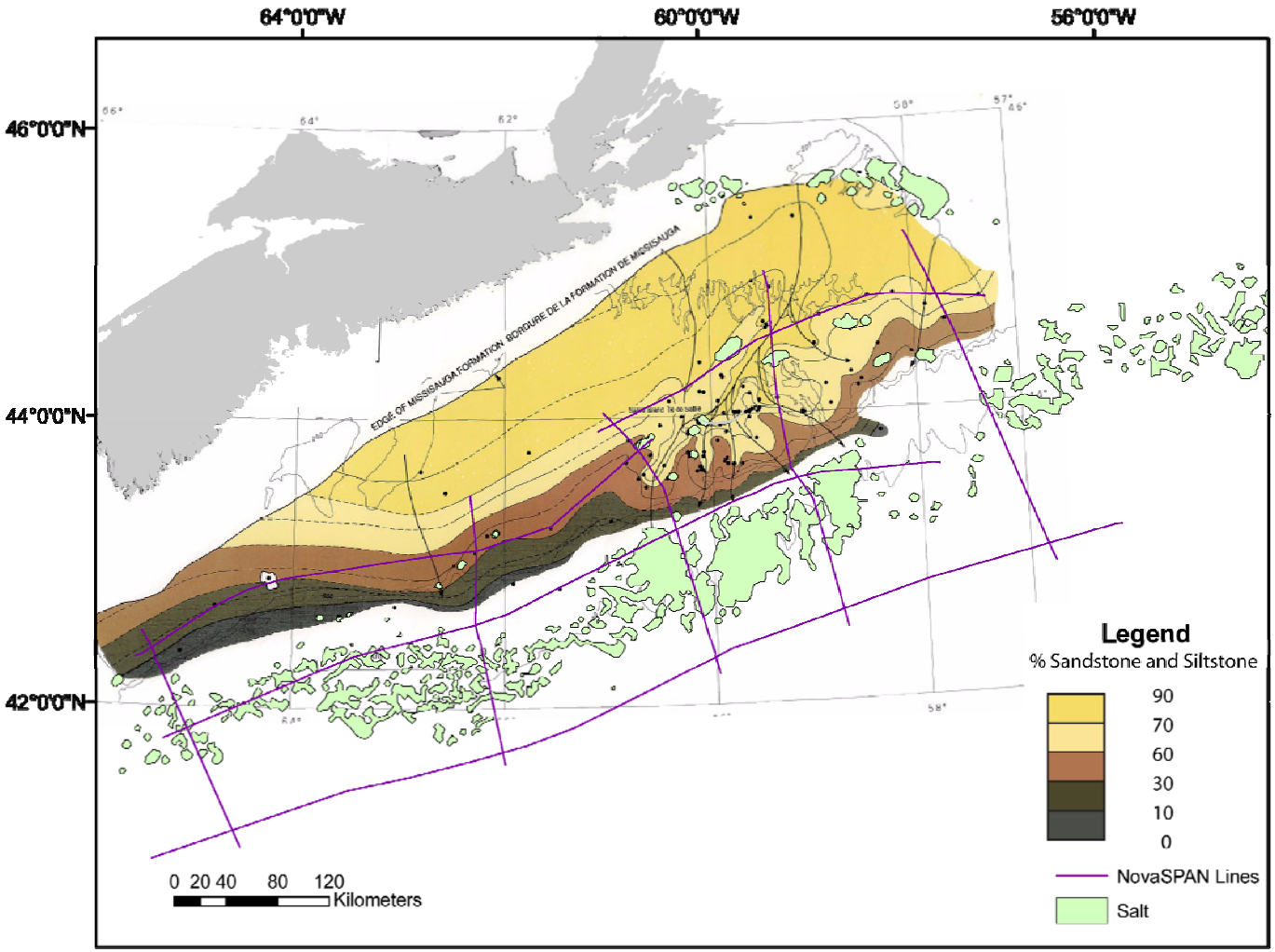

Figure 6-11: Mapped rivers, channels, and sand and siltstone concentrations by Wade (1991) geo-referenced to the Salt Dynamics Group GIS database to illustrate the pro-deltaic nature of sediments entering the Sable sub-basin during the Early Cretaceous.

are a few notable features in the western Sable sub-basin during the Early Cretaceous, when the Sable Delta was feeding the system. During the deposition of the Missisauga formation (Fig. 6-8), the delta lobe appears to have had an oblique transport direction, suggesting that salt mobilization followed a similar trend. When correlating diapirs and allochthonous salt sheets (i.e. BRS), this appears to be at least partially true. However, it is more accurate to describe the salt tectonics as developing in a radial fashion, such that the structures developed under similar mechanisms in down-dip, margin oblique, and margin parallel directions to the southwest. If any true diapiric walls, or aligned diapir trends exist, it is likely that they follow the trend of the shallowing basin-floor towards the LaHave Platform.

By the latter portion of the Early Cretaceous (Logan Canyon formation: Fig. 6-9), it appears that the largest depocenter became focused beneath the modern-day slope between NovaSPAN lines 1600 and 1800, and that sediments have had a more linear and downdip transport direction. The reason for this switch in transport direction was probably related to regional salt withdrawal and welding at the modern-day slope, and the position of the Sable Delta. This stage of Scotian basin development illustrates that once diapirs become localized and bounding basins welded to the basin-floor, the depositional pattern ceases to influence the mobilization of autochthonous salt. Instead, the weak diapir ridges and inflated salt complexes dictate the transport direction of sub-aqueous channels.

6.6.3 Thermal and Loading Subsidence

Thermal and loading subsidence greatly affects the architecture of a sedimentary basin by asymmetrically tilting the margin and flexing the crust respectively.

Thermal subsidence occurs as the upwelling lithospheric mantle cools over time. Therefore, the amount of thermal subsidence that the crust experiences is related to the thickness of the underlying mantle lithosphere (Huismans and Beaumont, 2008). Thermodynamic models by Keen and Beaumont, 1990, suggest that the mantle lithosphere may be completely absent due to necking at approximately the limit of the autochthonous salt basin (e.g. SMART 1: Fig. 3-7). Therefore, distal portions of the margin are expected to have experienced significantly more thermal subsidence than proximal regions, such as the shelf.

Sedimentary loading is one of the dominant driving forces involving salt tectonics at passive margins. However, loading also flexes the crust via isostasy, in which the continental crust, with a constant density of ~2.7 g/cm^3, subsides into the mantle (~3.3 g/m^3) due to increasing accumulations of sediments (~2.3 g/cm^3). Since the crust thins dramatically toward the continent-ocean boundary (Fig. 3-4), there should be more subsidence of the distal continental crust when loaded by the prograding sedimentary wedge.

For this study, thermal and loading subsidence can only be addressed from the development of the conceptual model for the western Sable Sub-basin, since neither process was tested by scaled physical experiments. Thermal subsidence was necessary for attaining a realistic geometry of the prograding wedge from the Early Jurassic to the beginning of the Early Cretaceous in the conceptual model, and to allow for an appropriate volume of sediments to be transported over the transitional crust. Although it was depicted as being nearly, or completely balanced by loading subsidence at major landward depocenters (Fig. 6-2 B – D), this interpretation will remain speculative unless

tested by geodynamic models. If thermal subsidence in nature was more prominent than shown in the conceptual model, it may have produced a seaward gradient of the margin that could cause gravity-driven mobilization of salt. If this occurred, it is likely that original inflections in salt thickness would still result in early inflation, similar to what was demonstrated in models driven only by passive downbuilding. Interpretation of seismic profiles suggests that passive downbuilding appears to have been the dominant mechanism of salt mobilization versus salt flow due to seaward tilt of the margin, as there are few extensional structures excluding diapirs that were originally formed out of contractional inflated salt complexes. However, since sedimentation rates during the early post-rift period were relatively low, and the style of deposition was aggradational, it is difficult to determine if any salt movement was generated by a seaward tilt of the margin, rather than being driven chiefly by sedimentary loading. Also, if the flow of salt driven by distal thermal subsidence and margin tilt was slow enough, there may not have been enough basal traction at the salt-sediment interface to result in extensional failure of the overburden, making differentiation of the processes difficult to impossible via observation of seismic data.

Significant accumulations of sediments were being transported beyond the salt basin and onto the transitional crust by the time of the Early Cretaceous Missisauga formation, when thermal subsidence was likely diminishing due prolongued cooling of the upwelled lithospheric mantle. These sediments, combined with the thin nature of the continental crust, probably allowed for loading subsidence in distal regions to become more prominent, as there was less buoyant compensation than in landward regions with thick crust. Throughout the post-rift evolution of the conceptual model, it is apparent that

the regional basin morphology remains consistent due to the interplay between early distal thermal subsidence and long-lived loading subsidence.

7.0 Conclusions

The conclusions of this study are presented in four sections: 1) Seismic Interpretation, 2) Experiment results, 3) Regional application, and 4) Relevance to Petroleum Exploration.

7.1 Seismic Interpretation

7.1.1 Salt Basin Morphology

The morphology of the salt basin at NovaSPAN line 1600 is controlled by the crustal structure, and consists of: a ~16 km wide proximal graben beyond the hinge zone, followed by a ~7 km horst block that separates the interconnected salt basins of the Sable sub-basin. The main extent of the Sable sub-basin has a salt basin geometry that is relatively wide (~30 km), but the basin floor ramps up via segments with different ramp angles (4° and 2°) for ~60 km to the seaward termination of the salt basin. Gravity models (Zheng and Arkani-Hamed, 2002) have been used to provide better confidence in the interpretation of the salt basin morphology and generally agree with the interpretation at NovaSPAN line 1600. Geodynamic models of Scotian basin formation (Keen and Beaumont, 1990) coupled with crustal thinning estimations by Wu et al. (2006) have provided a better understanding of how the basin evolved during rifting. In the western Sable sub-basin, areas of increased crustal extension led to variable syn-rift subsidence at extensive fault systems. These fault systems (the hinge zone and seaward shoulder of the horst) are also areas of thickest original syn-rift salt accumulations.

7.1.2 Salt Structures

Salt diapirs at the western Sable sub-basin appear to have formed via a different mechanism than explained at other margins where they have formed out of reactive-passive stages in the up-dip extensional domain (Jackson and Vendeville, 1994). In the deep Sable basin, the diapirs are situated at changes in salt basin floor morphology, suggesting that they formed successively out of earlier inflated salt massifs in the downdip contractional domain, rather than originally in the updip extensional domain. The observed characteristic salt structures in NovaSPAN line 1600 can be subdivided in 3 kinematic domains:

- The *Salt Weld and Reactive Diapir Domain* is characterized by a thick package (~6-7 km) of growth strata in the proximal graben, and remnant salt that was left over the horst complex during seaward translation of a major passive diapir.

- The *Extensional Diapir and Early Cretaceous Canopy Domain* is characterized by three major extensional diapirs in the Sable sub-basin, one of which feeds the Early Cretaceous Balvenie Roho System (BRS). The two most landward diapir systems are assumed to exist within the region of NovaSPAN line 1600 (see discussion in chapters 4, 5, & 6) although they are not obviously present in section, and seem to be individual stocks rather than diapir walls. The most distal diapir appears to be a part of a diapir wall, as evidenced by interpretation of public seismic lines (Appendix B).

- The Passive *Diapir and Late Cretaceous Canopy Domain* is situated at the seaward limit of the autochthonous salt basin, and is characterized by a prominent

diapir that feeds an extensive allochthonous salt-tongue canopy system, and a small salt nappe outboard of the salt basin. The salt-tongue canopy began to climb the stratigraphy at the end of the Early Cretaceous (Logan Canyon formation) during transgression. During starved deposition of the Dawson Canyon and Wyandot formations, salt from passive diapirs was able to spread freely at the sea floor. The salt tongue canopy is sub-horizontal and has spread approximately 30 – 40 km from the diapir crest. The salt nappe was expelled from the salt basin during extensive Early Cretaceous loading of the salt massif during the deposition of the Missisauga formation. However, sediment loading on top of the small nappe quickly resulted in welding, cutting it off from further salt supply.

7.1.3 Depositional Systems

- Early to Late Jurassic sedimentation at the western Sable sub-basin appears to have been more widespread and aggradational in contrast to the major focused depocenters of salt province IV at this time. Minor deltaic deposition drove salt withdrawal in the proximal graben, while pro-delta deposits were loading the Sable sub-basin.

- The onset of sediment progradation of the Sable delta likely occurred late in the Late Jurassic, as sedimentation began to migrate into the western Sable sub-basin.

- The North Sable High appears to have contributed to the position of the main delta lobe and tributaries during the Middle – Late Jurassic, as mapped by Wade (1991). This may indicate that it was a high during the Late Jurassic that allowed

the delta to propagate seaward, while the proximal graben was an active salt withdrawal basin and was accommodating sands from the delta.

- The Early Cretaceous was the most important time for salt tectonics in the western Sable sub-basin, because of high rates of progradation. Maximum sedimentation rates (~110 m/My) occurred during deposition of the Missisauga formation. During the late Early Cretaceous, moderate sea level rise starved the modern-day slope of clastic sediment input and led to the regional deposition of a shale tongue in the shelf (Naskapi Member). This period of starvation aided the spreading of the Balvenie Roho System. Sedimentation rates were high during deposition of the Logan Canyon formation (~120 m/My), although they steadily declined with overall transgression.

- In the Sable sub-basin, Early Cretaceous sedimentation was widespread and dominantly pro-deltaic. Instead of sequential seaward propagation of depocenters, the sub-basin displayed salt-withdrawal basins were separated by passive diapir walls. These salt-withdrawal basins are different than those to the northeast (SPIV) as they are nearly penecontemporaneous; the onset of formation and regional welding young only slightly seaward.

7.2 Experimental Results

7.2.1 Salt Thickness

- Physical experiments suggest that thick (2 – 3 km) salt is conducive to the development of thick salt-withdrawal basins that were significantly translated seaward through their development.

- Thick salt results in a low mechanical coupling between it and overlying sediments. Consequently, little to no brittle failure occurs in systems driven by passive downbuilding, as Poiseuille (channel) flow in the salt layer dominates and there is only minor Couette (shear) flow at the salt-sediment interface.

- Variations in the thickness of the original salt layer result in the localization of downdip contraction in inflated salt massifs and salt-cored anticlines due to reduced internal flow velocities. These areas of inflated salt later take on much of the strain induced by loading and often evolve into passive diapirs triggered by the seaward-prograding sedimentary wedge.

- Changes in salt thickness, in relation to the basin-floor geometry, controls evolution of positions of the kinematic domains as described in ***7.1.2 Salt Structures***.

7.2.2 Salt Basin Geometry

Experimental results confirm the important role of the geometry of the salt basin in controlling the development of diapirs and other structures, such as salt nappes and canopies.

- During seaward salt mobilization from the updip extensional regime, broad ramps in the salt basin floor tended to induce contraction in the salt layer and broad fold systems in the overburden that later evolved into inflated salt complexes. These inflated complexes formed at the toe of the prograding sedimentary wedge and tapered to the seaward termination of the salt basin. Repeated sets of diapirs

formed regularly with shallowing of the basin floor that correlate with progradation stages of sedimentary wedge.

- Basement highs, such as the NSH horst in NovaSPAN line 1600, resulted in the formation of diapirs from localized inflated salt complexes. However, as the prograding sedimentary wedge advanced, the diapirs migrated seaward, leaving only salt remnants on top of the horst.

7.2.3 Sedimentation Rates and Geometry of the Prograding Sedimentary Wedge

Both sedimentation rates and the geometry of the prograding wedge had a significant impact on the timing of silicone mobilization in physical experiments.

- Widespread, regional pro-delta sedimentation with relatively low sedimentation rates during the Jurassic controlled the timing, location and development of the initial salt structures in the western Sable sub-basin. The pro-delta sedimentation caused the development of early distal salt-withdrawal basins that persisted throughout the salt-tectonic evolution. These salt-withdrawal basins were important for localizing the later diapirs in the Sable basin, as they acted as buttresses and, when welded to the basin floor, lock the diapirs in place.

- Increased sedimentation in the Early Cretaceous, correlating with the southwest shift of the Sable Delta lobe, governed most of the salt-tectonic evolution at the western Sable sub-basin. Other areas were experiencing dominantly aggradational deposition.

- Periods of sediment starvation aided the spreading of allochthonous salt sheets from passive diapirs. Extensive salt-withdrawal at depth provided a high salt supply through passive diapirs, resulting in broad allochthonous salt sheets and canopies.

7.3 Regional Implications

- Thin-skinned, gravity driven salt tectonics began in the northeast portion of the Scotian margin (SP IV-V) during the Middle Jurassic, and salt was evacuated from the autochthonous salt basin of the Sable area by the Early Cretaceous.

- Depocenters in northern regions of the Scotian Basin sequentially propagated seaward as consequence of the high clastic sediment input (100 m/My and 200 m/My) during the Middle and Late Jurassic respectively, driving salt out of the basin very efficiently. In SP IV allochthonous salt was extruded gradually over Middle - Late Jurassic deepwater sediments forming an extensive salt nappe. Late Jurassic and Early Cretaceous sediment progradation onto the salt nappe resulted in high amounts of roho-style extension in the sedimentary overburden, resulting in the BSW.

- Due to southwest migration and the onset of progradation of the Sable Delta, the central and western regions of the Sable sub-basin experienced increased salt-tectonic deformation at the north central Scotian margin during the Early Cretaceous.

- In the Sable basin, deltaic and pro-deltaic deposition was bypassing the Abenaki sub-basin and North Sable High during the Early Cretaceous and formed a large

expulsion rollover, as sediments mobilized salt seaward. Seaward of the expulsion rollover is a major passive diapir zone that formed during deposition of the Early Cretaceous Missisauga formation.

- The western Sable sub-basin had the youngest salt-tectonic evolution of the north central Scotian margin, and was driven by the Sable Delta during the Early Cretaceous.

- Most of the prominent salt structures at the western Sable sub-basin (i.e. salt diapirs, expulsion rollovers, and salt withdrawal basins) formed during the deposition of the Early Cretaceous Missisauga formation.

- Salt-withdrawal basins that formed during the Early Cretaceous at the western Sable sub-basin (SP III) had a more complex evolution than those in SP IV, and were greatly affected by early downdip contraction and inflation of allochthonous salt and widespread deposition of pro-deltaic deposition. Rather than sequentially younging seaward, salt withdrawal basins began to form at approximately the same time and were separated by passive diapir trends.

- At both the central and western Sable sub-basin, the salt-withdrawal basins became regionally welded to the basin floor by the deposition of the Early Cretaceous Logan Canyon formation. In response to regional welding, depocenters became much more widespread and individual salt-withdrawal basins became less significant for major accumulations of sediments.

- At the LaHave Platform, the effects of the Sable Delta were not as prominent, since it was situated updip of the Sable sub-basin. Although the stratigraphy in

this region was not yet investigated, it is believed that the depositional history and timing of salt tectonics is much different. Since there were no major delta systems delivering sediments outboard of the LaHave Platform, it is likely that the timing and evolution of salt structures was much more gradual.

- The basin morphology at the LaHave Platform is much different than that of the north-central Scotian margin. Instead of having an abrupt offset of the basement at the hinge zone, the margin displays broadly spaced faults, that provide a gradual slope into the deeper portion of the basin. Since the basin floor has a slope, there is likely a higher degree of gravity driven extension in the overburden, similar to the Angolan margin (Brun and Fort, 2004).

7.4 Relevance to Petroleum Exploration

- Major Early Cretaceous salt-withdrawal basins are situated at depths that are uneconomical for drilling and production (~8 to ~12 km). Petroleum exploration should be focused on Early Cretaceous (Logan Canyon formation) channel systems and growth structures along landward diapir flanks.

- Channel systems and turbidite deposits were likely affected by extensional faults that sole into allochthonous salt sheets (i.e. the BRS). Since the hanging walls of the faults were continuously subsiding, most sands are likely focused at the plane of the fault hanging wall, similarly to what is observed at the Angola margin (Anderson et al., 2000).

- Although seaward overhangs of salt diapirs provide attractive trap and seal mechanisms, each diapir likely acted earlier as a topographic high throughout its

passive stage. Sand immediately seaward of these structures is not as likely as on their landward flanks (e.g. the Weymouth A-45 well; Kidston et al., 2007), although some minor accumulations may have migrated around the 3D diapir stocks. However, more significant accumulations may have been buttressed on their landward flanks as mass transport complexes and turbidites were translated seaward due to extensional failure updip.

- Experimental results suggest that syn-depositional, growing, antiformal structures are not conducive to accumulation of reservoir sands as they were generally topographic highs during margin evolution. Sands likely bypassed these areas and accumulated seaward, at actively subsiding regions at the landward flanks of deepwater passive diapir zones that eventually became expulsion rollovers. Unfortunately, most of these accumulations are at depths that are uneconomical for drilling (~8 km or deeper).

References

Adam, J. Urai, J.L., Wieneke, B,. Oncken, O., Pfeiffer, K., Kukowski, N., Lohrmann, J., Hoth, S., van der Zee, W., and Schmatz, J., 2005. Shear localization and strain distribution during tectonic faulting--new insights from granular-flow experiments and high-resolution optical image correlation techniques. Journal of Structural Geology **27**: 283–301).

Anderson, J.E., Cartwright, J., Drysdall, S.J., and Vivian, N., 2000. Controls on turbidite sand deposition during gravity-driven extension of a passive margin: examples from Miocene sediments in Block 4, Angola. Marine and Petroleum Geology, **17**: 1165-1203.

Ascoli, P., 1976. Formaniferal and ostracod biostratigraphy of the Mesozoic-Cenozoic, Scotian Shelf, Atlantic Canada. Maritime Sediments, Special Publication No. 1: 653-771.

Barss, M.S., Bujak, J.P., and Williams, G.L., 1979. Palynological zonation and correlation of sixty-seven wells, eastern Canada. Geological Survey of Canada, Paper **78-24**: 118.

BASIN database. Available from http://basin.gsca.nrcan.gc.ca/index_e.php [cited 8 September 2009].

Bates, R.L., and Jackson, J.A., 1987, Glossary of geology, 3rd ed.: Alexandria, Virginia, American Geological Institute: 788

Brace and Kohlshedt, 1980. Limits on lithospheric stress imposed by laboratory experiments. Journal of Geophysical Research, **85**: 6248-6252.

Brun, J.P., and Fort, X., 2004. Compressional salt tectonics (Angolan margin). Tectonophysics, **328**: 129-150.

Brun, J.P., and Mauduit, T.P-O., 2008. Rollovers in salt tectonics: The inadequacy of the listric fault model. Tectonophysics, **457**: 1-11.

Brun, J.P., and Mauduit, T. P.-O., 2009. Salt rollers: Structures and kinematics from analogue modelling. Marine and Petroleum Geology, **26**: 249-258.

Byerlee, J.D., 1968. Brittle-ductile transition in rocks. Journal of Geophysical Research, **73**: 4741-4750.

Byerlee, J.D., 1975. The fracture strength and frictional strength of Webster sandstone. International Journal of Rock Mechanics and Mining Sciences, **12**: 1-4.

Byerlee, J.D., 1978. Friction of rocks. Pure and Applied Geophysics, **116**: 615-626.

Calassou, S., and I. Moretti, I., 2003. Sedimentary flattening and multi-extensional deformation along the West African margin. Marine and Petroleum Geology, **20**: 71-82.

Campbell, C., 2007. Physical Modeling of the Salt Tectonics of Allochthonous Canopy and Nappe Systems at Deepwater Continental Margins: Applications to the Abenaki and Sable Sub-Basins, Scotian Margin. B.Sc. Thesis, Dalhousie University, Halifax, N.S.

Costa, E. and B.C., Vendeville, 2002. Experimental insights on the geometry and kinematics of fold-and thrust belts above weak, viscous evaporitic decollement. Journal of Structural Geology **24**: 1729-1739.

Cummings, D.I., and Arnott, R.W.C., and Hart, B.S., 2006. Tidal signatures in a shelf-margin delta. Geology, **34**(4): 249-252

Davies, E.H. 1986. The correlation and geohistory of the Hibernia Field. *I*n, Programand abstracts for the Canadian Society of Petroleum Geologists 1986 Convention, Calgary

Deptuck, M.E., K. Kendell, and B. Smith. Complex deepwater fold-belts in the SW Sable Subbasin, offshore Nova Scotia. *In* Frontiers + Innovation – 2009 CSPG CSEG CWLS Convention.

Doeven, P.H., 1983. Cretaceous nannofossil stratigraphy and paleoecology of the Canadian Atlantic Margin. Geological Survey of Canada, Bulletin **356**: 70.

Ebinger, C.J., and B.E. Tucholke 1988. Marine Geology of Sohm Basin, Canadian Atlantic Margin. The American Association of Petroleum Geologists Bulletin, **72** (12): 1450-1468.

Eliuk, L.S., 1978. The Abenaki Formation, Nova Scotia Shelf, Canada – a depostional and diagenetic model for the Mesozoic carbonate platform. Bulletin of Canadian Petroleum Geology, **26**: 424-514.

Fort, X., Brun, J.P., and Chauvel, F., 2004. Salt tectonics on the Angolan margin, synsedimentary deformation processes. American Association of Petroleum Geologsists Buletin, **88**: 1523-1544.

Funck, T., H. R. Jackson, K.E. Louden, S.A. Herler, and Y. Wu., 2004. Crustal structure of the northern Nova Scotia rifted continental margin (eastern Canada). Geophysical Journal International, **166**(2): 878-906

Ge, H., Jackson, M.P.A., and Vendeville, B.C., 1997. Kinematics and dynamics of salt tectonics driven by progradation. The American Association of Petroleum Geologists Bulletin, **81**(3), 398-423.

Gemmer, L., Ings, S.J., Medvedev S., and Beaumont, C., 2005. Salt tectonic driven by differential sediment loading: stability analysis and finite-element experiments. Basin Research, **17**: 382-402

Gradmann, S., Beaumont, C., and Albertz, M., 2009. Factors controlling the evolution of the Perdido Fold Belt, northwestern Gulf of Mexico, determined from numerical models. Tectonics, **28**, TC2002, doi:10.1029/2008TC002326

Huismans, R.S., and Beaumont, C., 2008. Complex rifted continental margins explained by dynamical models of depth-dependent lithospheric extension. Geology, **36**(2): 163-166.

Ings, S.J., and Shimeld, J.W., 2006. A new conceptual model for the structural evolution of a regional salt detachment on the northeast Scotian margin, offshore eastern Canada. American Association of Petroleum Geologists Bulletin, **90**(9): 1407-1423.

Jackson, M.P.A., and Talbot, C.J., 1986. External shapes, strain rates, and dynamics of salt structures. Geological Society of America Bulletin, **97**: 305-328

Jackson, M.P.A., and Vendeville, B.C., 1994. Regional extension as a geologic trigger for diapirism. Geological Society of America Bulletin, **106**: 57-73

Jansa, L.F., Bujak, J.P., and Williams, 1980. Upper Triassic salt deposits of the western North Atlantic. Canadian Journal of Earth Sciences, **17**: 547-559.

Jansa, L.F., and Wade, J.A., 1975. Geology of the continental margin off Nova Scotia and Newfoundland. *In* Offshore geology of Eastern Canada, **2**, Regional geology. *Edited by* W.J.M. van der Linden, J.A. Wade. Geological Survey of Canada: 74-30, 51-106.

Keen, C.E., and C. Beaumont, 1990. Geodynamics of rifted continental margins. *In* Volume I-1 of Decade of North America Geology. *Edited by* M.J. Keen and G.L. Williams. Publication of Geological Survey of Canada and Geological Society of America: 393-472.

Kidston, A.G., Smith, B.M., Brown, D.E., Makrides, C., and Altheim, B., 2007. Hydrocarbon Potential of the Deep-water Scotian Slope, Canada-Nova Scotia Offshore Petroleum Board, Open Report: 111

Krezsek, C., Adam, J., and Grujic, D., 2007. Mechanics of fault and expulsion rollover systems developed on passive margins detached on salt: insights from analogue modeling and optical strain monitoring. Structurally Complex Reservoirs, Geological Society, London, Special Publications **292**:103-121.

Lehner, F.K., 2000. Approximate theory of substratum creep and associated overburden deformation in salt basins and del- tas. In: Aspects of Tectonic Faulting. *Edited by* y F.K. Lehner & J.L. Urai. Springer-Verlag, Berlin: 21- 47.

Lohrmann. J., N. Kukowsky, J. Adam, and O. Oncken, 2003. The impact of analogue material properties on the geometry, kinematics, and dynamics of convergent sand wedges. Journal of Structural Geology, **25**: 1691-1711.

Louden, K.E, Tucholke, B.E., and Oakey, G.N., 2004. Regional anomalies of sediment thickness, basement depth and isostatic crustal thickness in the North Atlantic Ocean. Earth and Planetary Science Letters, **224**: 193 – 211.

MacDonald, C. 2007. Analogue modeling of the salt tectonics system, offshore Nova Scotia: insights into initial salt mobilization and autochthonous salt structures, B.Sc. Thesis, Dalhousie University, Halifax, N.S.

Mauduit, T. P-O., Gaullier, V., Brun, J.P., and Lecanu, H., 1997. Raft tectonics: The effects of basal slope value and sedimentation rate on progressive extension. Journal of Structural Geology, **19**: 1219-1230

Mauduit T. P-O., and Brun, J.P., 1998. Growth-fault/rollover systems: birth, growth, and decay. Journal of Geophysical Research, **103/B8**: 18119-18136.

McIver, N.L., 1972. Mesozoic and Cenozoic stratigraphy of the Nova Scotia Shelf. Canadian Journal of Earth Sciences, **9**: 54-70.

MIRAGE – Map Image Rendering database forGEoscience. Available from http://apps1.gdr.nrcan.gc.ca/mirage/db_search_e.php [cited 8 September 2009].

Nelson, T.H., 1991. Salt tectonics and listric-normal faulting, *in* Salvador, ed., The Gulf of Mexico Basin. Geological Society of America, The Geology of North America, **J**: 73-89.

Oakey, G.N., and Stark, A., 1995. A digital compilation of depth to basement and sediment thickness for the North Atlantic and adjacent coastal land mass, Geological Survey of Canada, open file # 3039, 1995.

Piper, D.J.W., Pe-Piper, G., and Ingram, S.I., 2004. Early Cretaceous sediment failure in the southwestern Sable Subbasin, offshore Nova Scotia. American Association of Petroleum Geologists Bulletin, **88**(7): 991-1006

Ramberg, H., 1981, Gravity, Deformation and the Earth's Crust: Academic Press, London, 2nd ed., 452.

Rowan, M.G., 2008. Practical Salt Tectonics: A 2-day Short Course Emphasizing the Geometry and Evolution of Salt Structures. *In* Proceedings of the Central Atlantic Conjugate Margins Conference, Halifax, N.S., Canada.

Sandwell, D.T., and Smith, W.H.F., 1997. Marine gravity anomaly from Geosat and ERS 1 satellite altimetry. Journal of Geophysical Research, **102**: 10039-10054.

Shimeld, J.W., 2004. A comparison of salt tectonic sub-provinces beneath the Scotian Slope and Laurentian Fan, :24th Annual GCSSEPM Foundation Bob F. Perkins Research Conference, Exended Abstract CD: 502-515.

Sibson, R.H., 1974. Frictional constraints on thrust, wrench and normal faults. Nature, **249**: 542-544.

Spiers, C.J., Urai, J.L., Lister, G.S., Boland, J.N., and Zwart, H.J., 1986. The influence of fluid-rock interaction on the rheology of salt rock. Commission of the European Communities, Nuclear Science and Technology, Final Report, EUR 10399 EN: 131.

Ter Heege, J.H., De Bresser, J.H.P. and Spiers, C.J., 2005. Rheological behaviour of synthetic rocksalt: The interplay between water, dynamic recrystallization and deformation mechanisms. Journal of Structural Geology, **27:** 948-963.

Truscheim, F., 1960. Mechanism of salt mobilization in northern Germany. American Association of Petroleum Geologists Bulletin, **44**: 1519-1540.

Urai, J.L., Spiers, C.J., Zwart, H.J., and Lister, G.S., 1986. Weakening of rock salt by water during long-term creep. Nature, **324**: 554-557.

van Keken, P. E., Spiers, C.J., van den Berg, A.P., and Muyzert, E.J., 1993. The effective viscosity of rocksalt: Implementation of steady-state creep laws in numerical models of salt diapirism, Tectonophysics, **225**(4): 457–476.

Vendeville, B.C., 2005. Salt tectonics driven by sediment progradation: Part I — Mechanics and kinematics. American Association of Petroleum Geologists, **89**: 1071–1079.

Vendeville, B.C., Jackson, M.P.A., 1992. The fall of diapirs during thin-skinned extension. Marine and Petroleum Geology, **9**(4): 354-371.

Wade, J.A., 1991. Frontier Geoscience Program – East Coast Basin Atlas Series: Scotian Shelf. Available from Geological Survey of Canada (Atlantic), Halifax, N.S. Cat. No. M40-48/2-1991. ISBN: 0-660-56531-5.

Wade, J.A and MacLean, B.C., 1990. The geology of the southeastern margin: aspects of the geology of the Scotian Basin from recent seismic and well data. *In* Geology of the Continental Margin Eastern Canada. *Edited by* M.J Keen and G.L. Williams. Geological Survey of Canada, Geology of Canada, **2**: 167–238

Wade, J.A., MacLean, B.C., and Williams, G.L., 1995. Mesozoic and Cenozoic stratigraphy, eastern Scotian Shelf: new interpretations. Canadian Journal of Earth Sciences, **32(**9): 1462-1473.

Weijermars, R., 1986. Flow behavior and physical chemistry of bouncing putties and related polymers in view of tectonic laboratory applications. Tectonophysics, **124**: 325-358.

Weijermars, R., M.P.A., Jackson, & B.C., Vendeville, 1993. Rheological and tectonic modeling of salt provinces. Tectonophysics **217**, (1-2): 143-174.

Weijermars, R., and Schmeling, H., 1986. Scaling of Newtonian and non-Newtonian fluid dynamics without inertia for quantitative modelling of rock flow due to gravity (including concept of rheological similarity). Physics of the Earth and Planetary Interiors, **986**: 316-330.

Williams, G.L., Ascoli, P., Barss, M.S., Bujak, J.P., Davies, E.H., Fensome, R.A., and Williamson, M.A., 1990. Biostratigraphy and related studies. *In* Geology of the continental margin off eastern Canada. *Edited by* M.J. Keen and G.L. Williams. Geological Survey of Canada, Geology of Canada, **2**: 87-137.

Wu, Y., K.E. Louden, T. Funck, H.R. Jackson, and S.A. Dehler, 2006. Crustal structure of the central Nova Scotia margin off Eastern Canada. Geophysical Journal International, **166**: 878-906.

Appendix A: Salt Tectonics Structures and Terminology

Salt Tectonics Structures and Terms

Overburden – The upper part of a sedimentary deposit that compacts and consolidates material below (Bates and Jackson, 1987).

Substratum – Substratum refers to a ductile salt layer, which is positioned below the brittle overburden and above subsalt strata or basement (Jackson and Talbot, 1991).

Feeder – A conduit, typically in the form of a diapir that supplies salt from a source layer (Jackson and Talbot, 1991).

Weld – Welds form after the complete, or nearly complete, withdrawal of salt the original source layer (Appendix A-1). Primary welds are defined by the contact between overburden sediments and subsalt strata or basement. Primary welds are often identified by discontinuous, high amplitude reflectors, with angular discordance between strata on either side (Rowan, 2005). Secondary welds are defined by lateral discontinuity of overburden sediments along a squeezed or depleted diapir. Tertiary welds develop in a similar fashion to primary welds, but are located in allochthonous positions over salt nappes or canopies.

Growth Strata – Growth strata (Appendix A-1) are the result of syn-kinematic sedimentation. Apparent thickening of stratigraphic packages occurs in areas where accommodation space had increased due to salt withdrawal or displacement along faults.

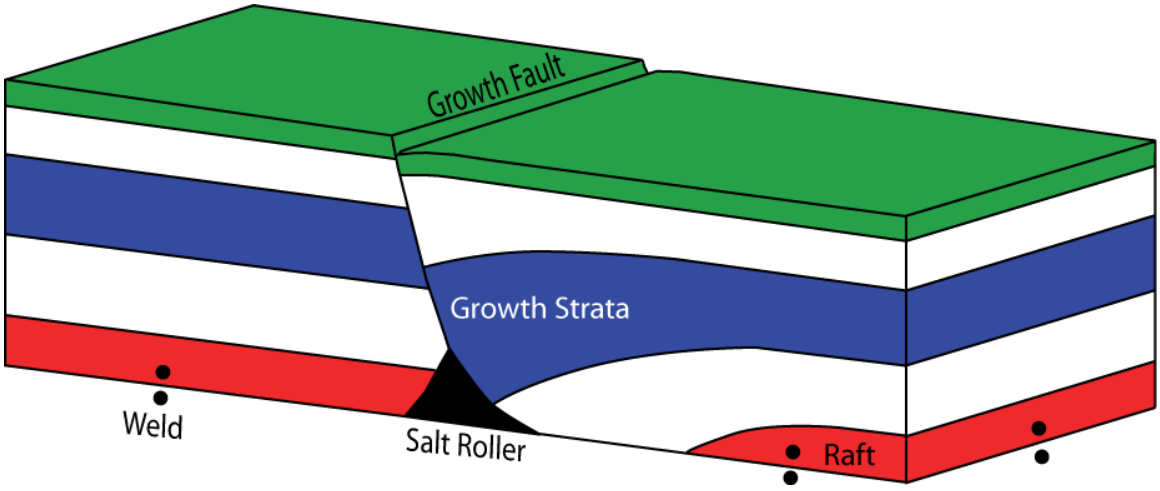

Appendix A-1: Various salt structures associated with passive downbuilding of sediments into an underlying salt layer. Structures include: a growth fault, salt roller, growth strata, a raft, and welds.

Growth Fault Rollover – Thickening and displacement of strata toward the hanging wall of a fault (Appendix A-1). Strata appear to dip towards, but roll away from the fault, and are displaced vertically and laterally by rotation along the fault surface.

Expulsion Rollover – Monoclines that form due to asymmetric downbuilding and rotation into and along salt diapirs or inflated salt massifs (Appendix A-2). Expulsion rollovers document a progressive basinward shift of depocenters during times of regional progradation. The rollover takes on rletively little strain (which reulst in keystone grabens); instead, the adjacent salt body takes on most of the strain induced by downbuilding, and it is displaced seaward.

Keystone Grabens – Small-scale extensional structures that form in the crest of a rollover due to flexure of the brittle overburden during asymmetric downbuilding and rotation (Appendix A-2). Keystone grabens often extend to the base of salt, as it is an effective detachment surface, and are typically associated with low mechanical coupling due to low sedimentation rate or thick salt.

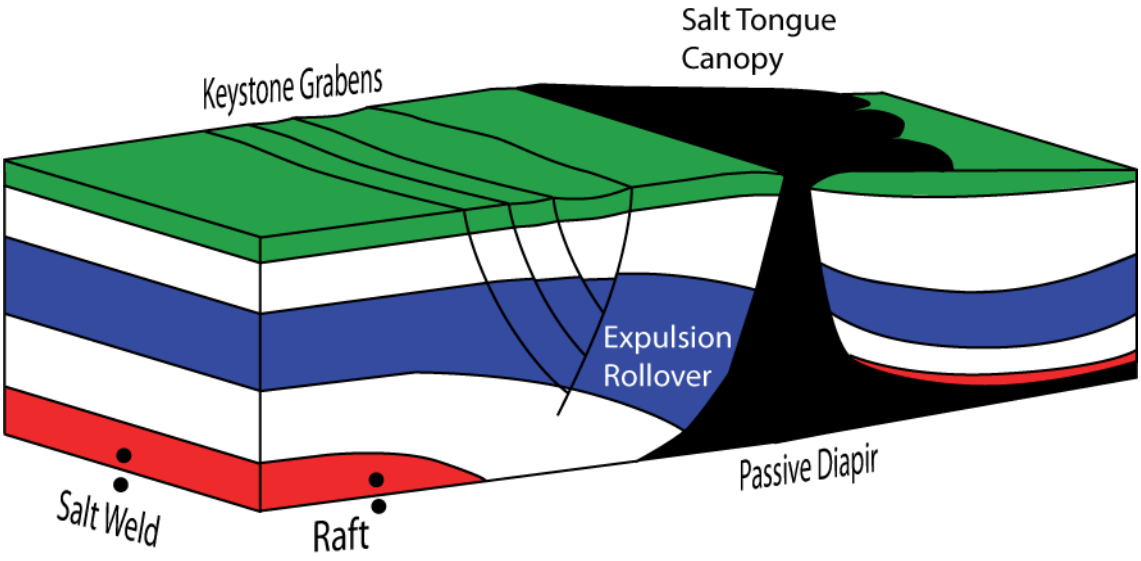

Appendix A-2: Various salt structures associated with passive downbuilding of sediments into an underlying salt layer. Structures include: an expulsion rollover with associated keystone grabens, a raft, salt welds, a passive diapir, and a salt tongue canopy.

Salt Withdrawal Basin (Mini-Basin) – Salt-withdrawal and mini-basins form in response to displacement of salt from an area under differential load during extension. As salt is displaced, areas flanking the overburden become inflated and form bathymetric highs. Continuous downbuilding in the proto-basin allows for the accumulation of more sediments and further salt withdrawal, resulting in a positive feedback system. The differentiation between a salt withdrawal basin and a mini-basin is based on the position of the salt layer and extent of growth. Salt withdrawal basins are typically regional features that formed directly out of the autochthonous salt layer. Mini-basins are smaller, local features that develop over allochthonous salt nappes or canopies.

Turtle Structures – Turtle structures are sometimes found in mini-basins and result from continued downbuilding and salt withdrawal. The early stage of turtle structure evolution is characterized by downbuilding of a mini-basin into an allochthonous salt sheet. After the center of the mini-basin welds to sub-salt strata, downbuilding and salt withdrawal

continues at its flanks. This process causes inversion in the geometry of the mini-basin, making it into an antiformal structure.

Salt Diapir – Diapirs are the most commonly documented and studied salt structures from observations in both seismic reflection data and in the field. They are defined by a dome or anticlinal fold, which is cored by salt and may or may not be presently covered by overburden. Diapir evolution (Appendix A-3) is been broken into three stages (Jackson and Vendeville, 1994): reactive, active, and passive. Reactive diapirism is always the first stage of diapir initiation and rise, and is dependent on regional extension that results in growth fault and graben formation. Extensional faulting creates differential unloading of overburden from the roof of salt by fracturing and thinning it (Jackson and Vendeville, 1994). When fault blocks shift laterally, pressurized salt can rise into the space created from extension. Therefore, the process is independent of overburden lithology, thickness, and density. Although differential loading drives regional salt mobilization, it is extension in the overburden that allows diapirs to rise to the surface. When the overburden becomes sufficiently thinned and weakened, the pressure in the salt diapir may be great enough to cause it to pierce through to the surface. This phase of diapir evolution, termed the active stage, only occurs over geologically brief intervals of time. The passive stage of diapir evolution begins immediately after salt breaches the overburden and flows at the sea floor. Once a diapir reaches the passive stage, its crest will remain at or near the sea floor as long as there is fluid pressure to drive salt flow. The diapir will shut down and become covered by the prograding sedimentary wedge upon the formation of primary or secondary weld, which cuts off further salt supply. If it experiences later extension, the diapir will collapse in response to a loss of fluid pressure.

After collapse, the diapir will become the location of a topographic low for incoming sediments.

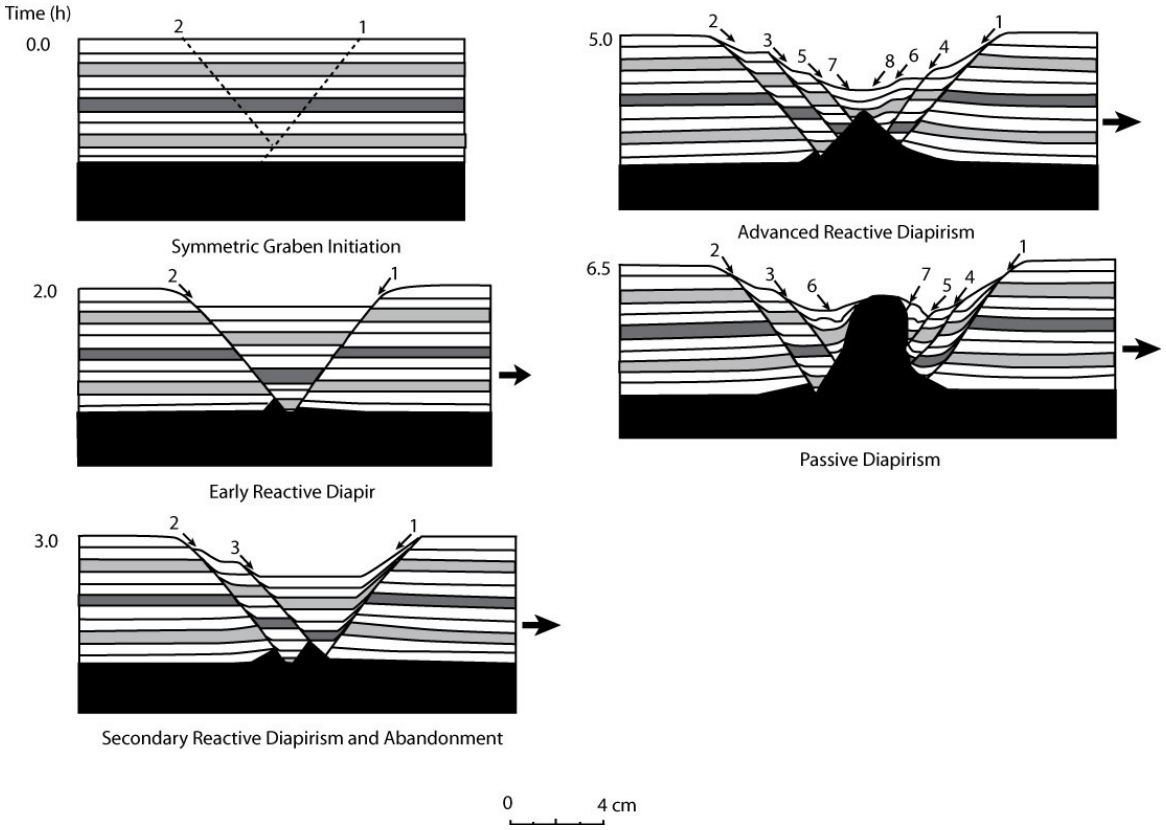

Appendix A-3: Stages of diapir initiation and rise under extension and overburden translation. Time in hours is model time, and numbers with arrows indicate order of faults. After Jackson and Vendeville, 1994.

Salt Canopy – Salt canopies form when multiple allochthonous salt sheets coalesce at the sea floor, and are identified via sutures between individual sheets. There are three forms of salt canopies: salt stock canopies, salt wall canopies, and salt tongue canopies (Jackson and Talbot, 1991). Salt stocks are plug-like diapirs that are sub-circular in planform (Truscheim, 1960). Salt walls are laterally continuous diapirs that form in linear, or arcuate trends. Although these diapirs may bhave a bulbous roof, they are not sub-circular in planform because of their lateral extent. Salt tongues (Appendix A-2) are

characterized as lengthy, basinward-trending, and sub-horizontal salt sheets. The location where any of these allochthonous salt sheets merge is called a suture (Rowan, 2005).

Salt Nappe – Salt nappes are another form of allochthonous salt sheet, but instead of being sub-horizontal they climb distal stratigraphy with a ramp-flat geometry. Unlike other styles of allochthonous sheets that are fed from passive diapirs and spread during times of low sedimentation, nappes are fed from inflated salt massifs and are forced out of the basinward limit of autochthonous salt basin during high sedimentation rates. Salt nappes are often laterally extensive, and may be associated with high amounts of overburden extension (e.g, Ings and Shimeld, 2006).

Roho: Rohos are packages of highly extended (faulted) overburden that have failed and detached over an allochthonous salt-tongue canopy. Extension is either accommodated by distal shortening structures, and/or the seaward and lateral propogation of salt at the sea floor (Rowan, 2008).

Appendix B: Public Seismic Reflection Profiles – Shell 8624-S006-032E

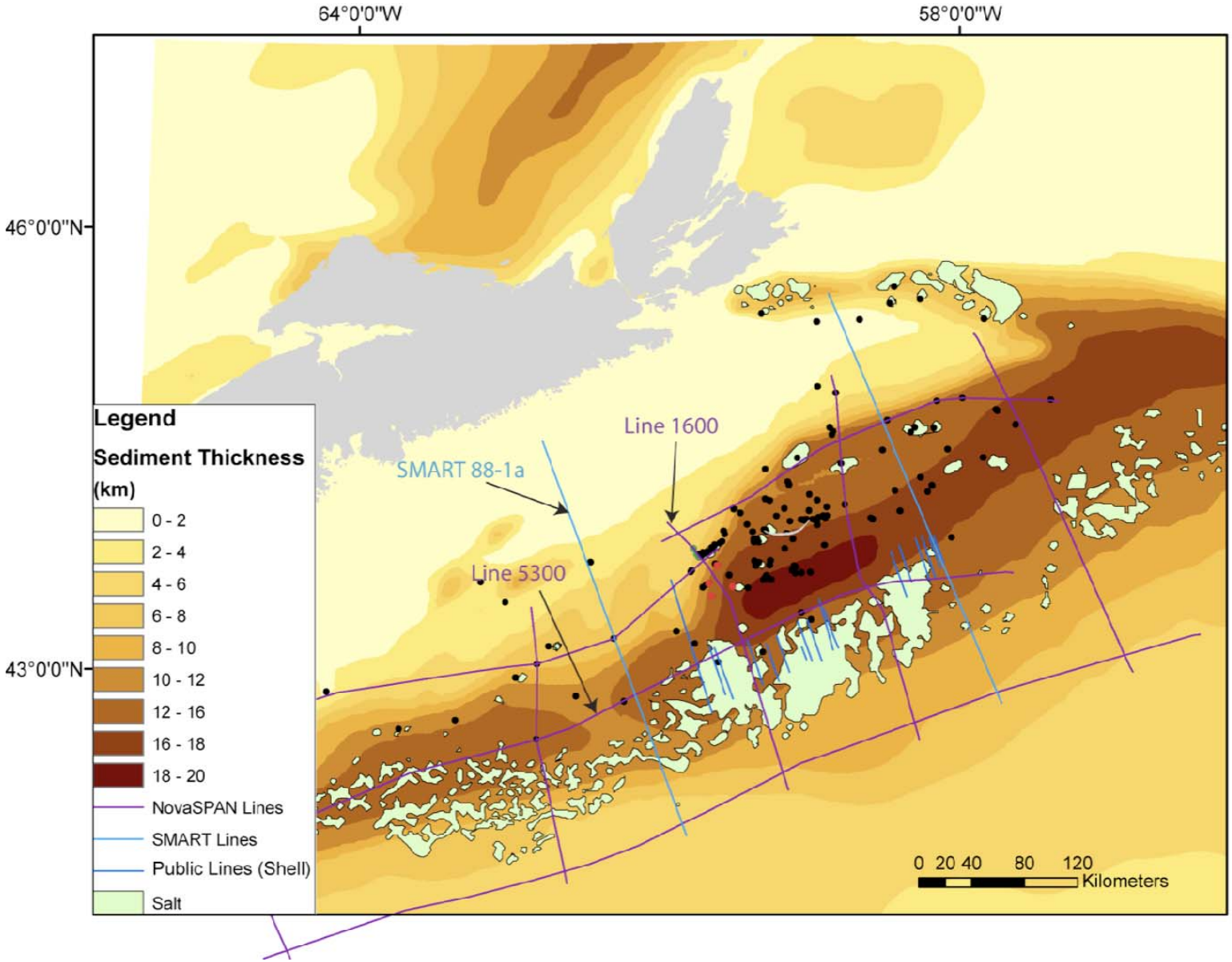

Appendix B-1: Map showing sediment thickness, present-day shallow salt bodies, NovaSPAN lines 1600 and 5300, and SMART transect 88-1a.

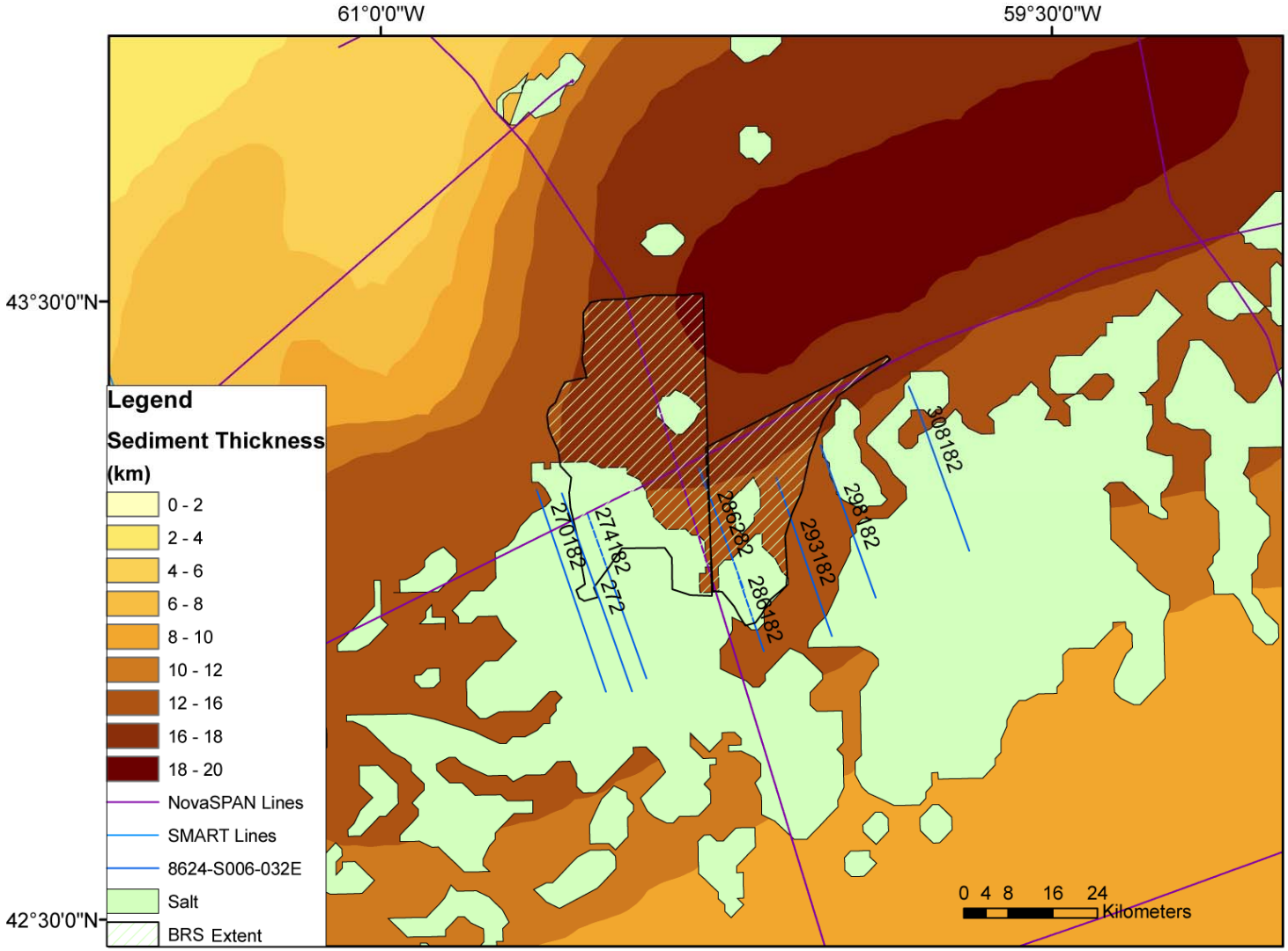

Appendix B-2: Map of sediment thickness, present-day shallow salt bodies, public seismic transects by Shell Canada, and the known extent of the Balvenie Roho System from mapping within this study, as well as Deptuck, 2009.

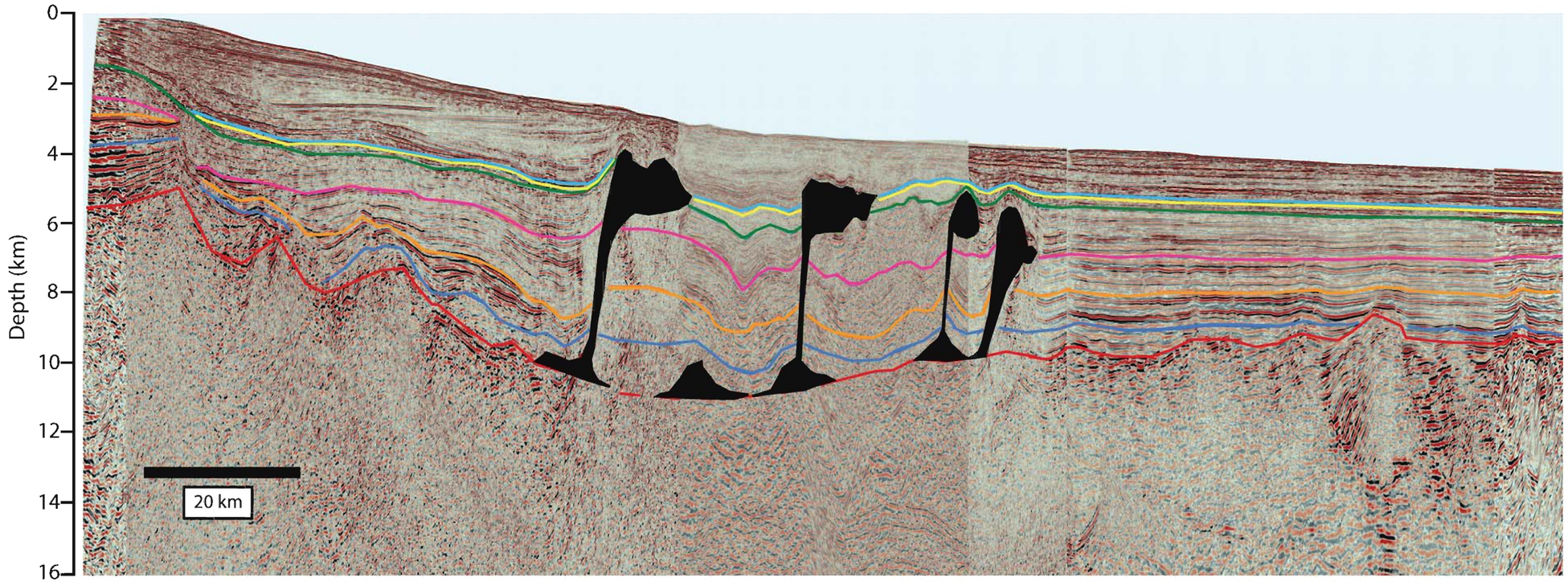

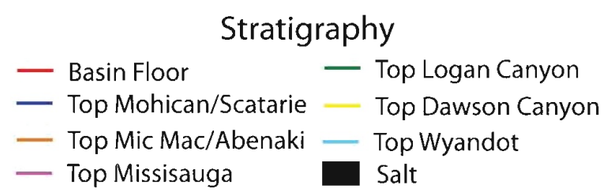

Appendix B-3: Dip section of SMART transect: 88-1a displaying salt tectonics of Salt Province II beyond the LaHave Platform. The basin in this region is much more shallow than in the Sable sub-basin, and has less salt related deformation. The main salt structures are passive diapirs that have overhangs that have begun to spread during the Dawson Canyon and Wyandot Formations. However, there is also a small over hang on the furthest basinward diapir at the top Missisauga spreading event.

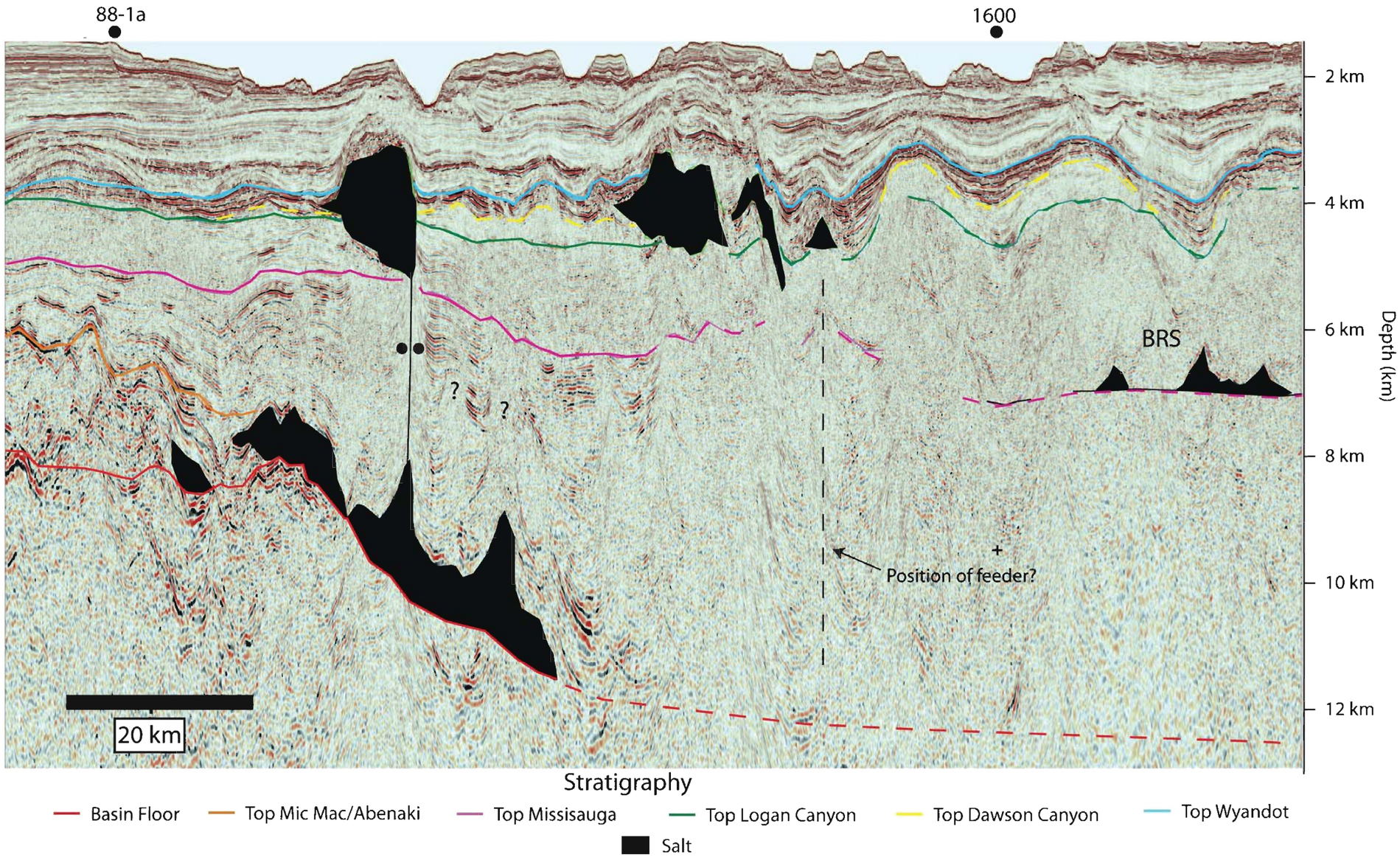

Appendix B-4: Along strike profile of NovaSPAN Line 5300 showing occurrence of extensive diapirs and the Balvenie Roho System. The downdip profiles: NovaSPAN line 1600 and SMART transect 88-1a are positioned over the section. Imaging at depth is too poor for interpretation.

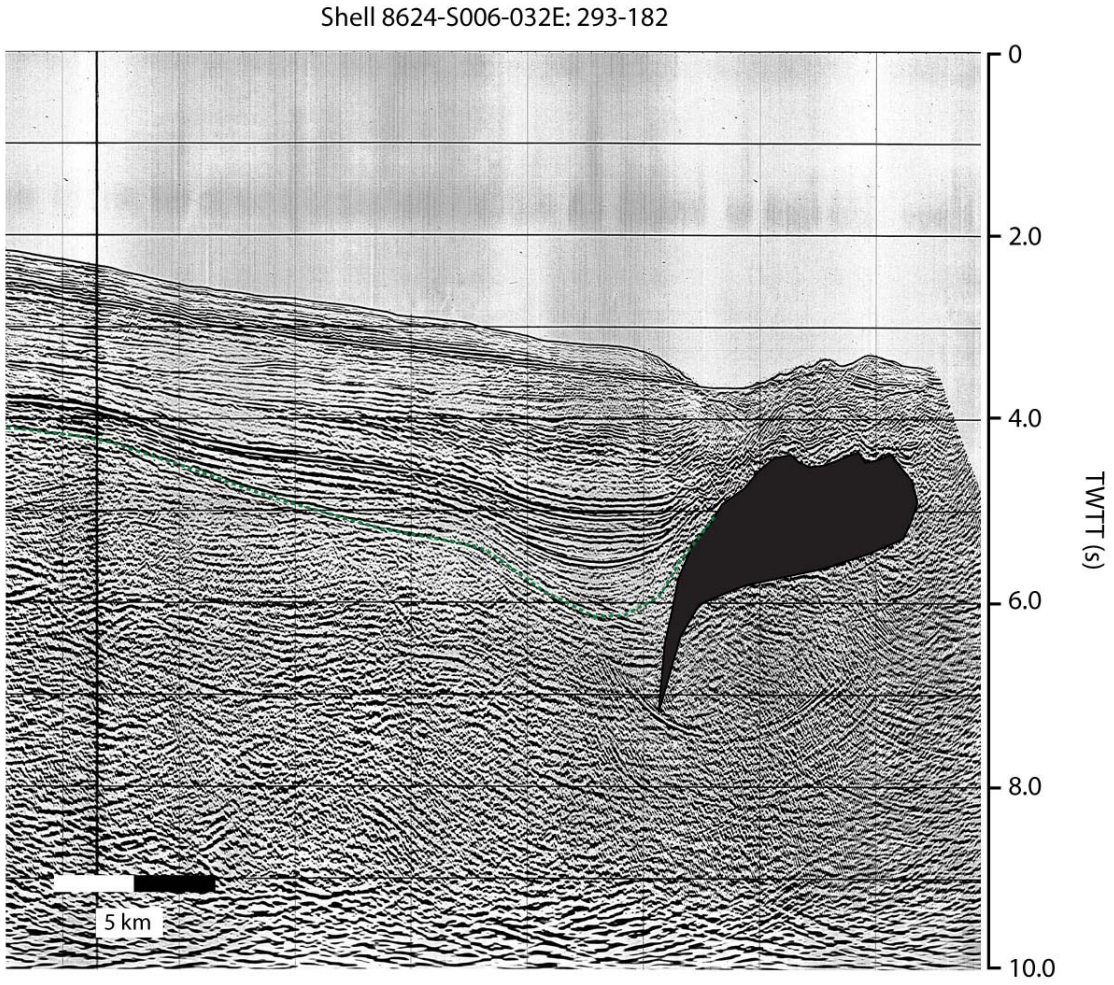

Appendix B-5: Publicly available time-domain seismic reflection profile Shell 8624-S006-032E: 293-182. The approximate top pick for the Early Cretaceous Logan Canyon formation is shown by a dashed green line, and is based on a major unconformity that is also seen in NovaSPAN line 1600.

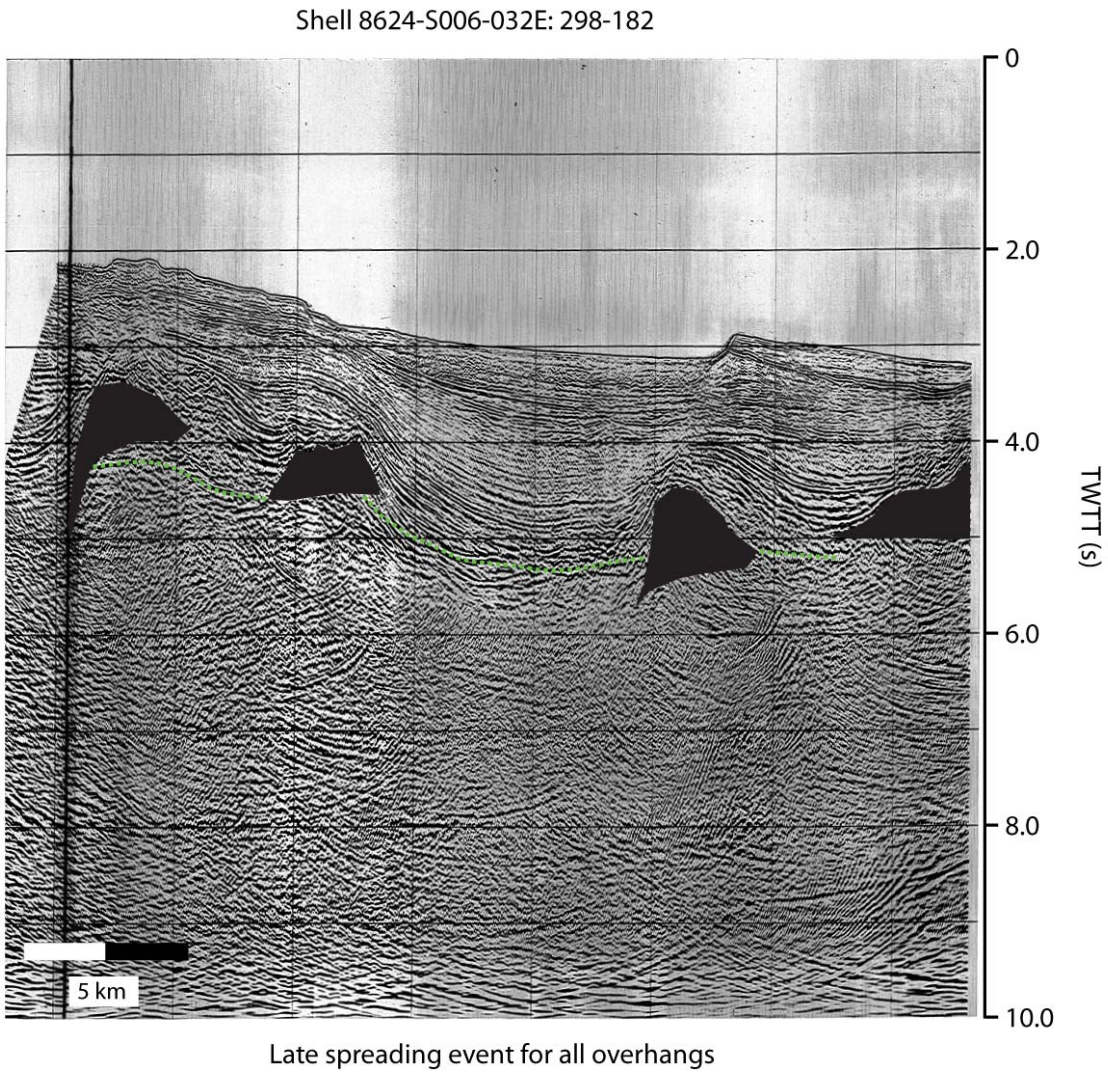

Appendix B-6: Publicly available time-domain seismic reflection profile Shell 8624-S006-032E: 298-182. The approximate top pick for the Early Cretaceous Logan Canyon formation is shown by a dashed green line, and is based on changes in seismic character.

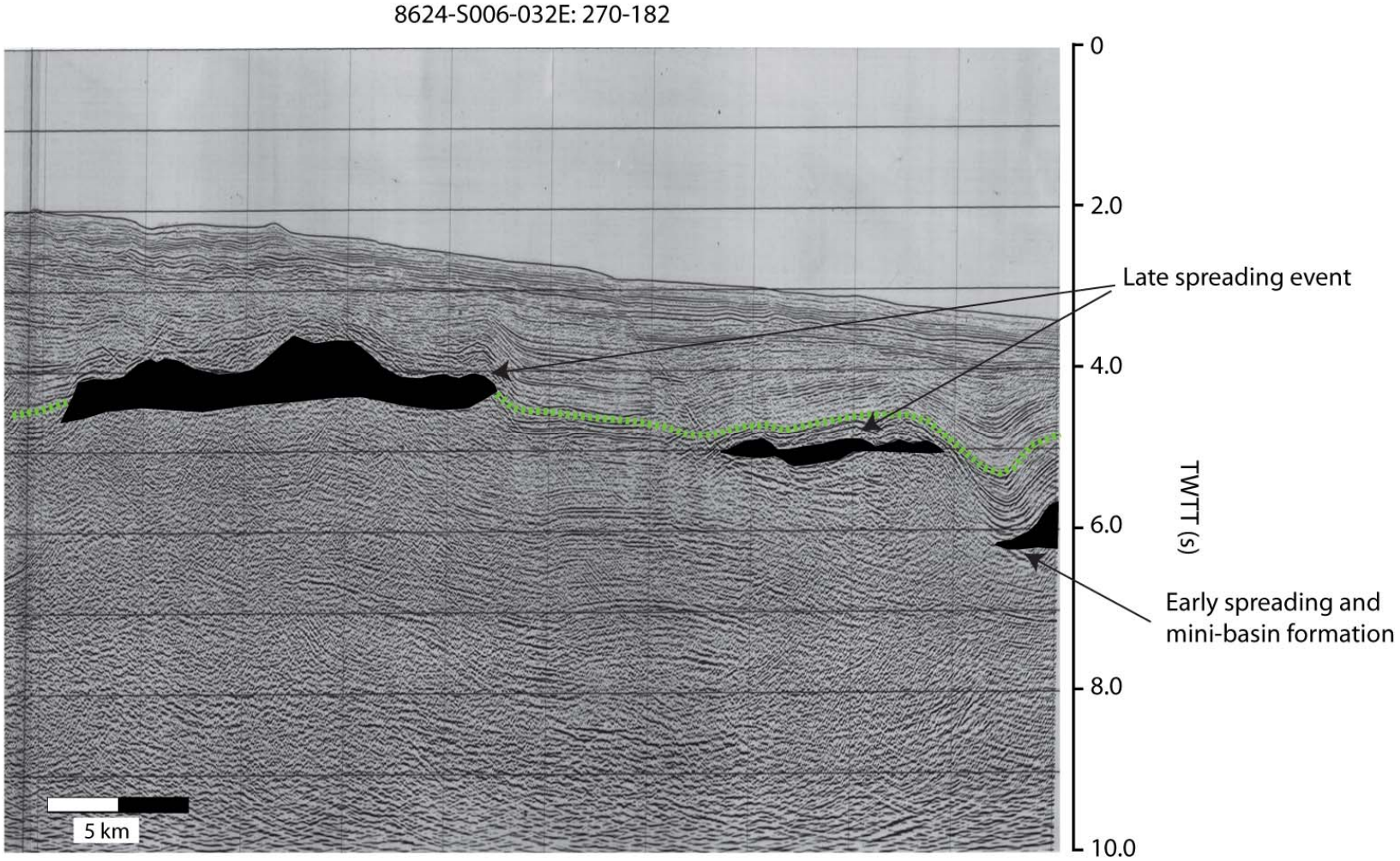

Appendix B-7: Publicly available time-domain seismic reflection profile Shell 8624-S006-032E: 270-182. The approximate top pick for the Early Cretaceous Logan Canyon formation is shown by a dashed green line, and is based on changes in seismic character.

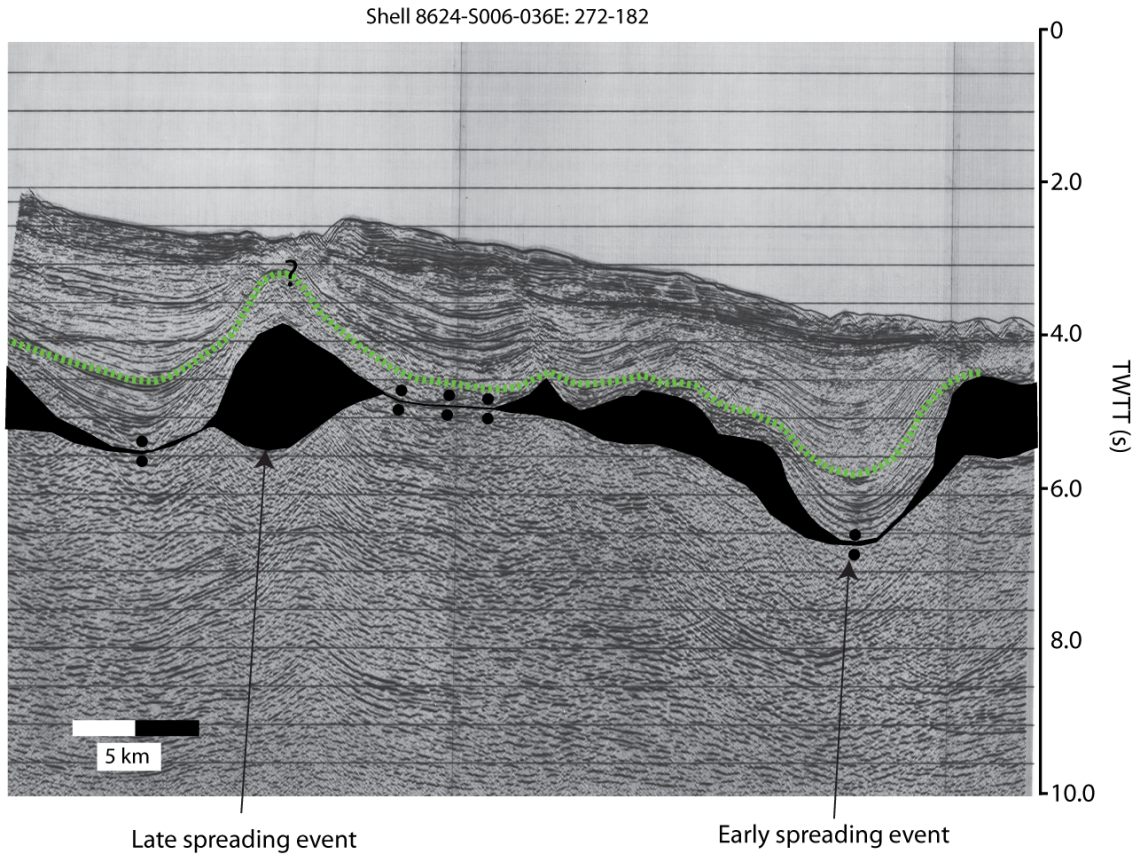

Appendix B-8: Publicly available time-domain seismic reflection profile Shell 8624-S006-032E: 272-182. The approximate top pick for the Early Cretaceous Logan Canyon formation is shown by a dashed green line, and is based on changes in seismic character.

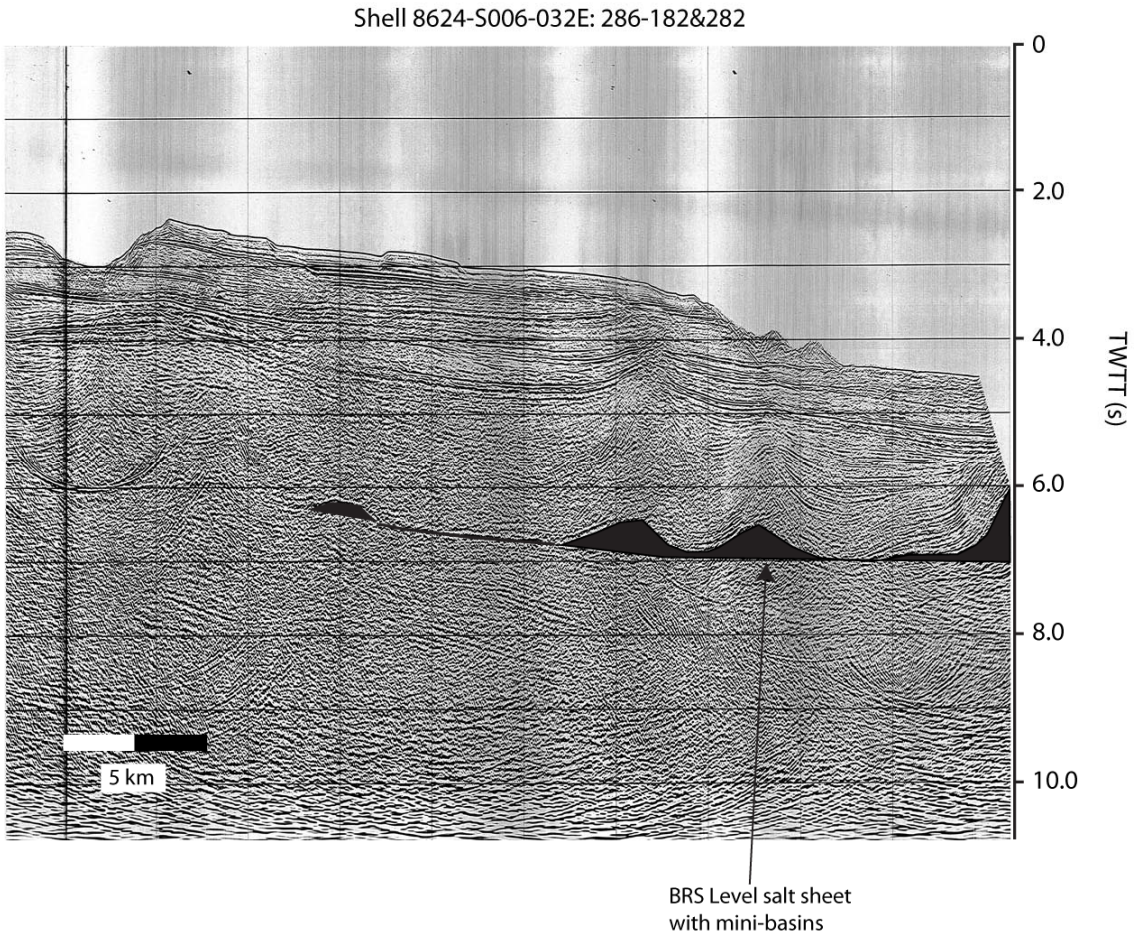

Appendix B-9: Publicly available time-domain seismic reflection profile Shell 8624-S006-032E: 286-182.

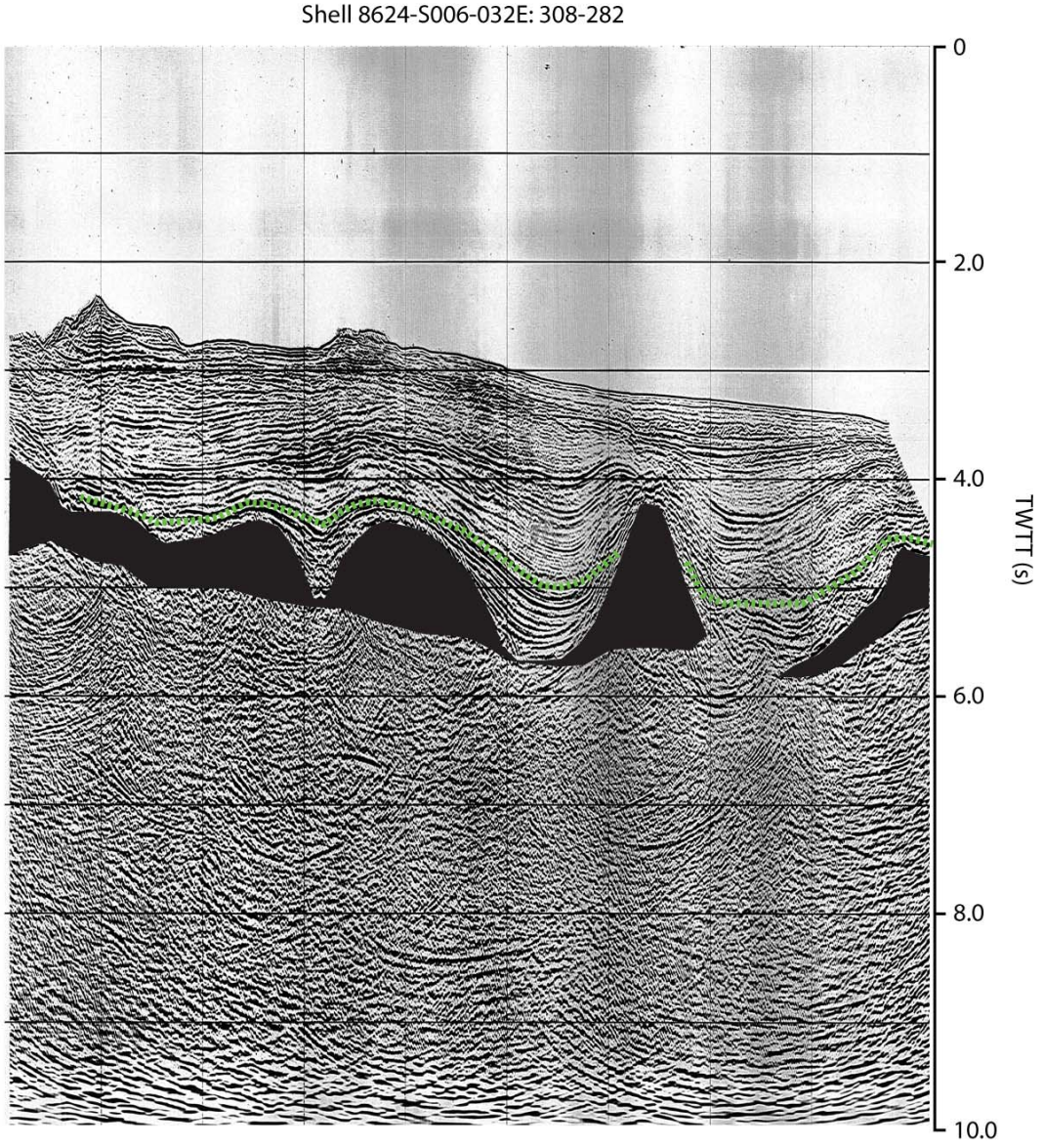

Appendix B-10: Publicly available time-domain seismic reflection profile Shell 8624-S006-032E: 308-282. The approximate top pick for the Early Cretaceous Logan Canyon formation is shown by a dashed green line, and is based on changes in seismic character.

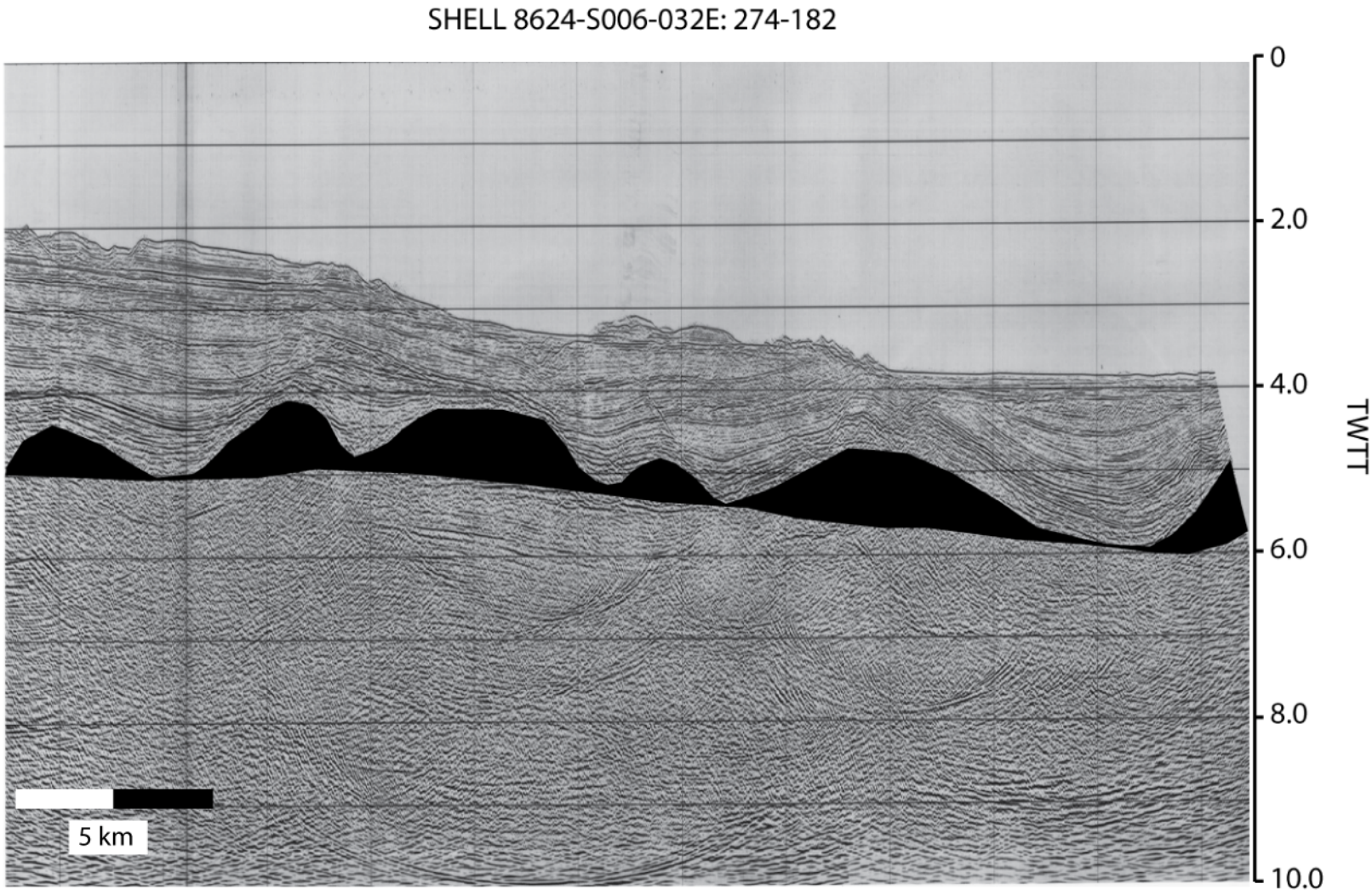

Appendix B-11: Publicly available time-domain seismic reflection profile Shell 8624-S006-032E: 274-182.

Appendix C:

Appendix C-1

Experiment 1: Two Asymetric Half-Grabens with Early Proximal Depocenters

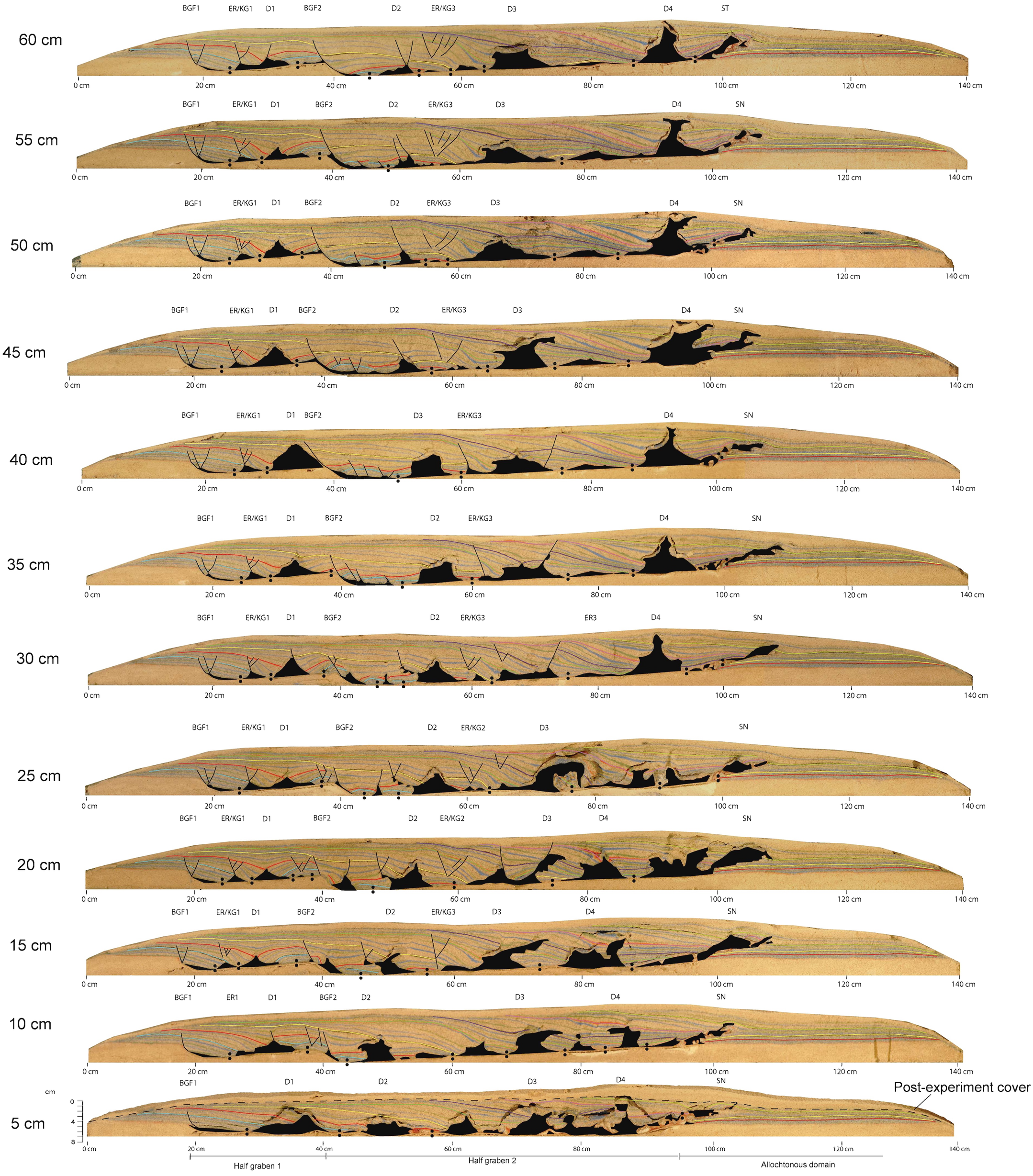

Experiment parameters

Setup

Experiment base: horizontal, 75 cm (width) x140 cm (length)
Initial early post-rift salt ("silicone") basins:
- Half-graben 1: 65 cm (width) x 20 cm (length) x 3 to 0.5 cm (thickness)
- Half-graben 2: 65 cm (width) x 60 cm (length) x 3 to 0 cm (thickness)

Sedimentation

- Mid Jurassic: 1.6 mm/8h [70 m/My]
- Late Jurassic: 2.0 mm/8h [85 m/My]
- Early Cretaceous1: 0.9 mm/4h [110 m/My]
- Early Cretaceous2: 0.8 mm/4 h [90 m/My]

Duration of experiment = 244 hours

Annotations

BGF - Basinward-Dipping Growth Fault
D - Diapirs
ER - Expulsion Rollover
KG - Keystone Graben
SN - Silicone Nappe
⁝ - Salt Weld

Appendix C-2

Experiment 2: Proximal Graben and Ramp-Flat Basin with Widespread Deposition

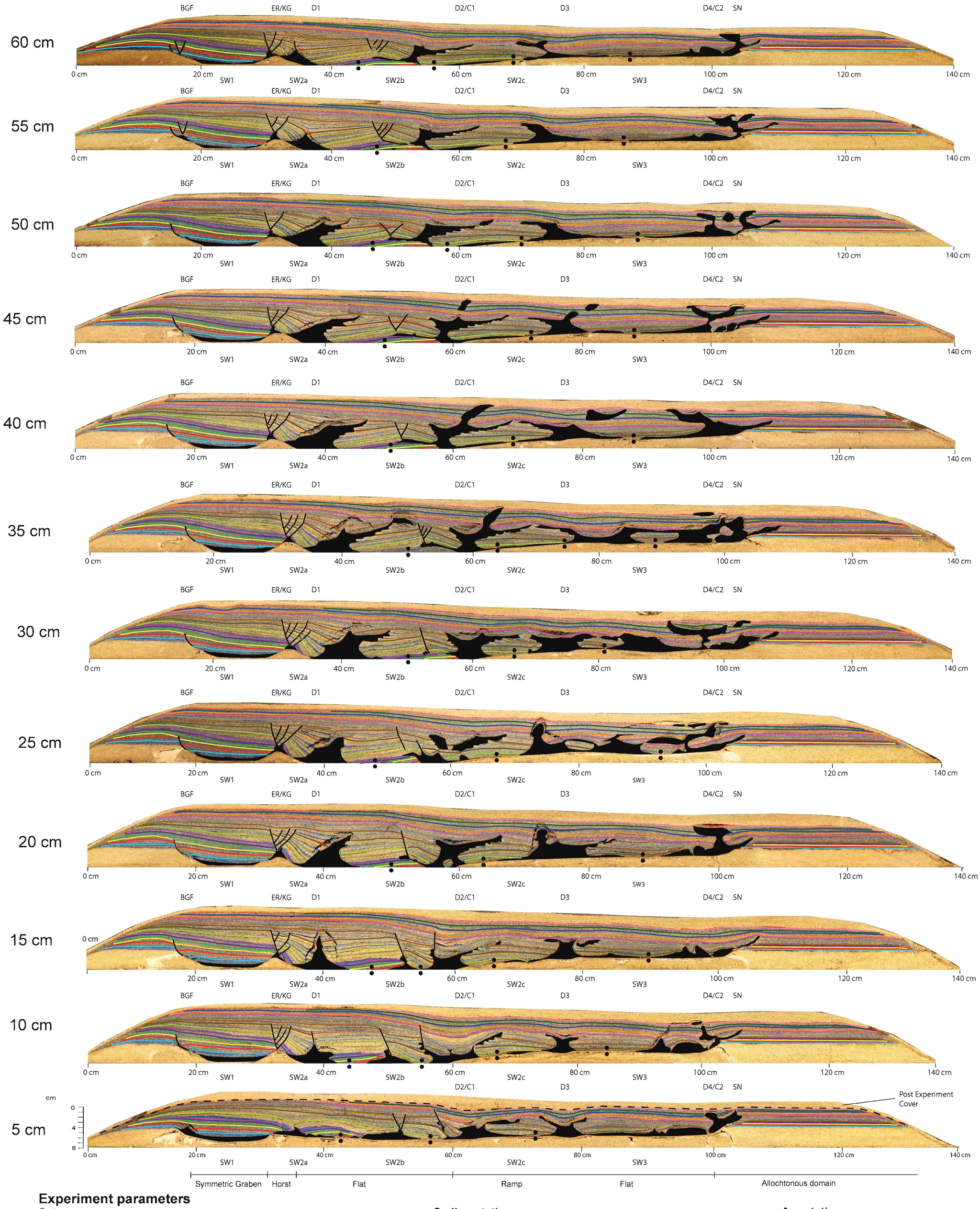

Experiment parameters

Setup

Experiment base: horizontal, 75 cm (width) x140 cm (length)
Initial early post-rift salt ("silicone") basins:
Symmetric Grabe: 75 cm (width) x 10 cm (length) x 3 cm (thickness)
Horst: 75 cm (width) x 5 cm (length) x 0.5 to 0 cm (thickness)
Flat: 75 cm (width) x 25 cm (length) x 3 cm (thickness)
Ramp: 75 cm (width) x 20 cm (length) x 3 to 1 cm (thickness)
Flat: 75 cm (width) x 20 cm (length) x 1 cm (thickness)

Sedimentation

Mid Jurassic: 0.7 mm/8h [40 m/My]
Late Jurassic: 0.4 mm/8h [50 m/My]
Early Cretaceous1: 1.0 mm/4h [160 m/My]
Early Cretaceous2: 0.8 mm/4 h [120 m/My]
Early Cretaceous2: 0.5 mm/4 h [30 m/My]

Duration of experiment = 356 hours

Annotations

BGF - Basinward-Dipping Growth Fault
D - Diapirs
ER - Expulsion Rollover
KG - Keystone Graben
C - Canopy
SN - Silicone Nappe
⋮ - Salt Weld

Appendix C1

Experiment 1: Two Asymetric Half-Grabens with Early Proximal Depocenters

Experiment parameters

Setup

Experiment base: horizontal, 75 cm (width) x140 cm (length)
Initial early post-rift salt ("silicone") basins:
- Half-graben 1: 65 cm (width) x 20 cm (length) x 3 to 0.5 cm (thickness)
- Half-graben 2: 65 cm (width) x 60 cm (length) x 3 to 0 cm (thickness)

Sedimentation

- Mid Jurassic: 1.6 mm/8h [70 m/My]
- Late Jurassic: 2.0 mm/8h [85 m/My]
- Early Cretaceous1: 0.9 mm/4h [110 m/My]
- Early Cretaceous2: 0.8 mm/4 h [90 m/My]

Duration of experiment = 244 hours

Annotations

BGF - Basinward-Dipping Growth Fault
D - Diapirs
ER - Expulsion Rollover
KG - Keystone Graben
SN - Silicone Nappe
⋮ - Salt Weld

Appendix C2

Experiment 2: Proximal Graben and Ramp-Flat Basin with Widespread Deposition

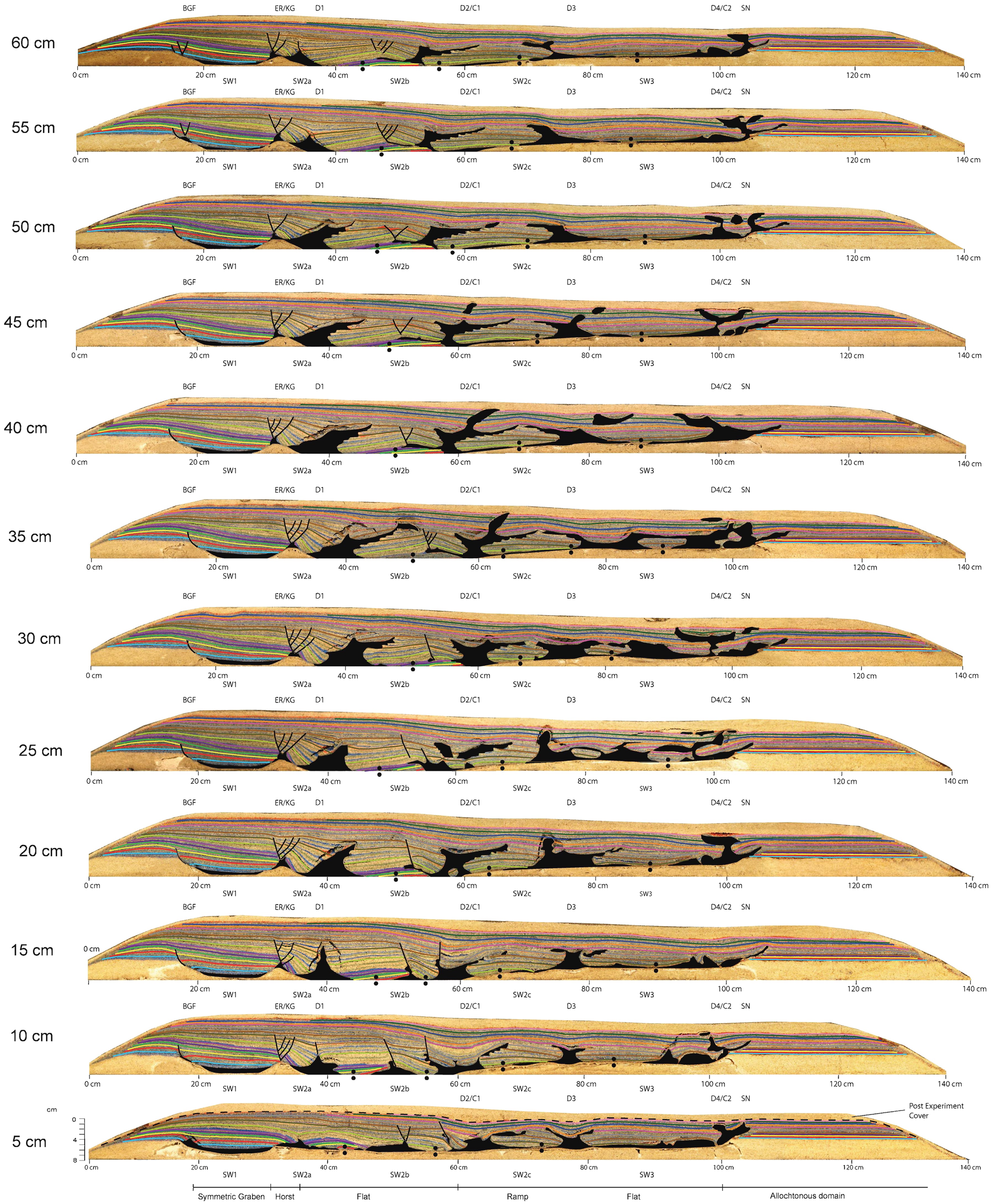

Experiment parameters

Setup

Experiment base: horizontal, 75 cm (width) x140 cm (length)
Initial early post-rift salt ("silicone") basins:
Symmetric Grabe: 75 cm (width) x 10 cm (length) x 3 cm (thickness)
Horst: 75 cm (width) x 5 cm (length) x 0.5 to 0 cm (thickness)
Flat: 75 cm (width) x 25 cm (length) x 3 cm (thickness)
Ramp: 75 cm (width) x 20 cm (length) x 3 to 1 cm (thickness)
Flat: 75 cm (width) x 20 cm (length) x 1 cm (thickness)

Sedimentation

Mid Jurassic: 0.7 mm/8h [40 m/My]
Late Jurassic: 0.4 mm/8h [50 m/My]
Early Cretaceous1: 1.0 mm/4h [160 m/My]
Early Cretaceous2: 0.8 mm/4 h [120 m/My]
Early Cretaceous2: 0.5 mm/4 h [30 m/My]

Duration of experiment = 356 hours

Annotations

BGF - Basinward-Dipping Growth Fault
D - Diapirs
ER - Expulsion Rollover
KG - Keystone Graben
C - Canopy
SN - Silicone Nappe
⋮ - Salt Weld

Appendix D:

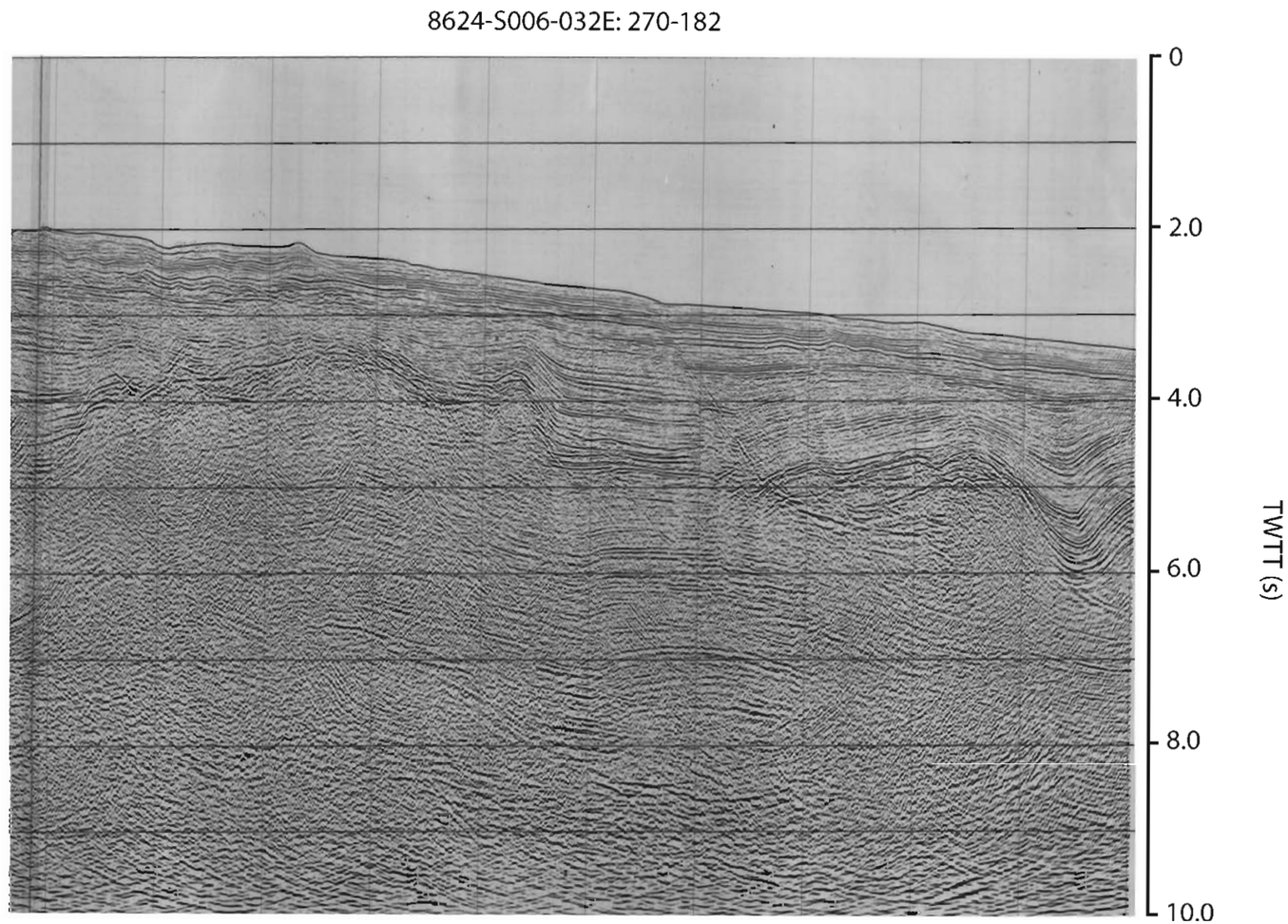
8624-S006-032E: 270-182
0
2.0
4.0
6.0
8.0
10.0
TWTT (s)

SHELL 8624-S006-032E: 274-182

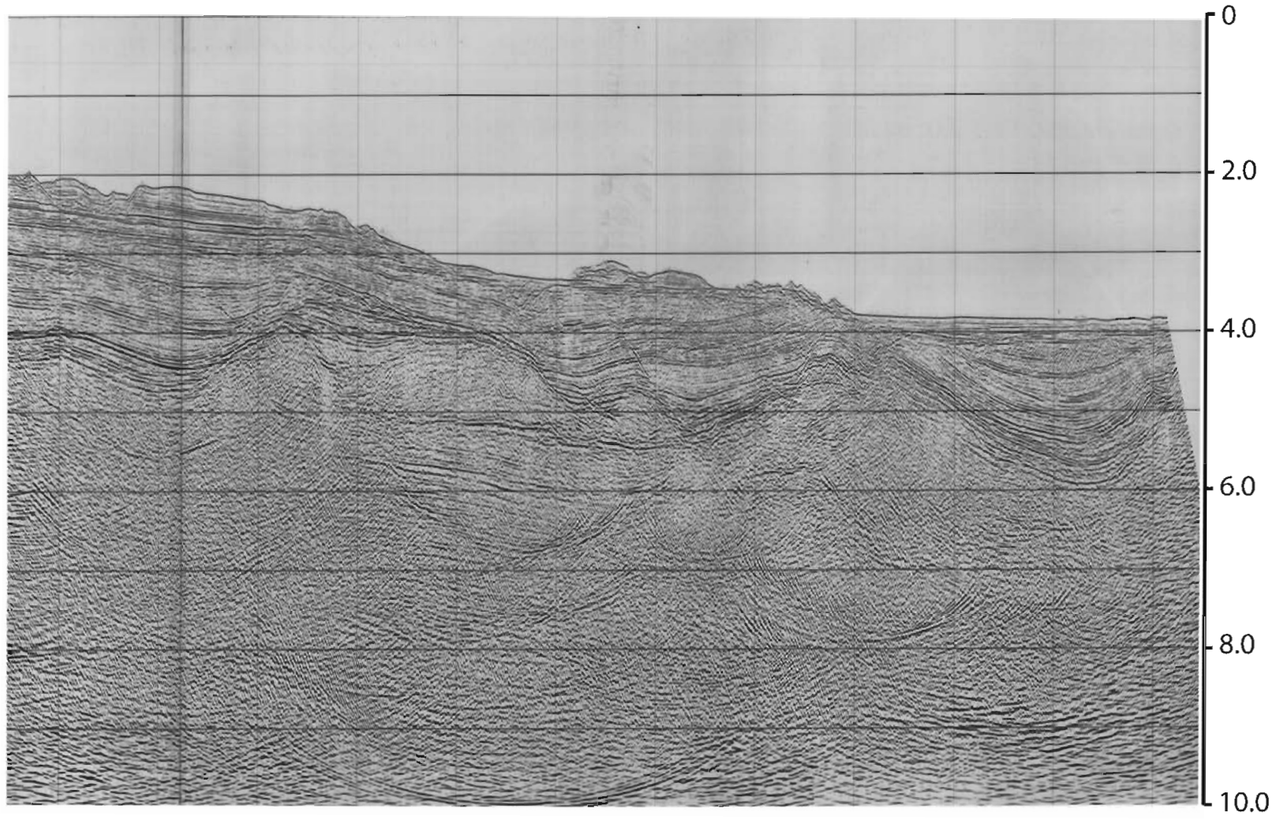

8624-S006-032E: 272-182

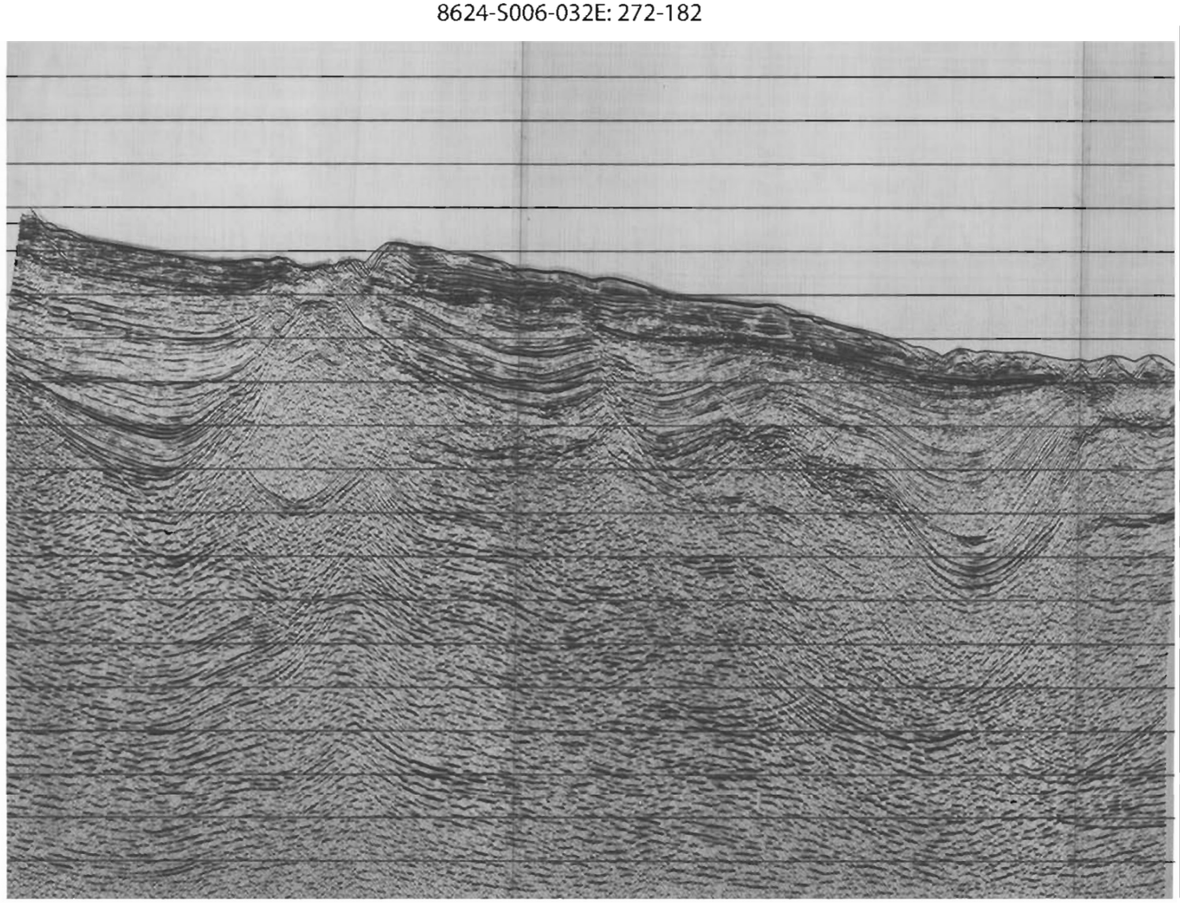

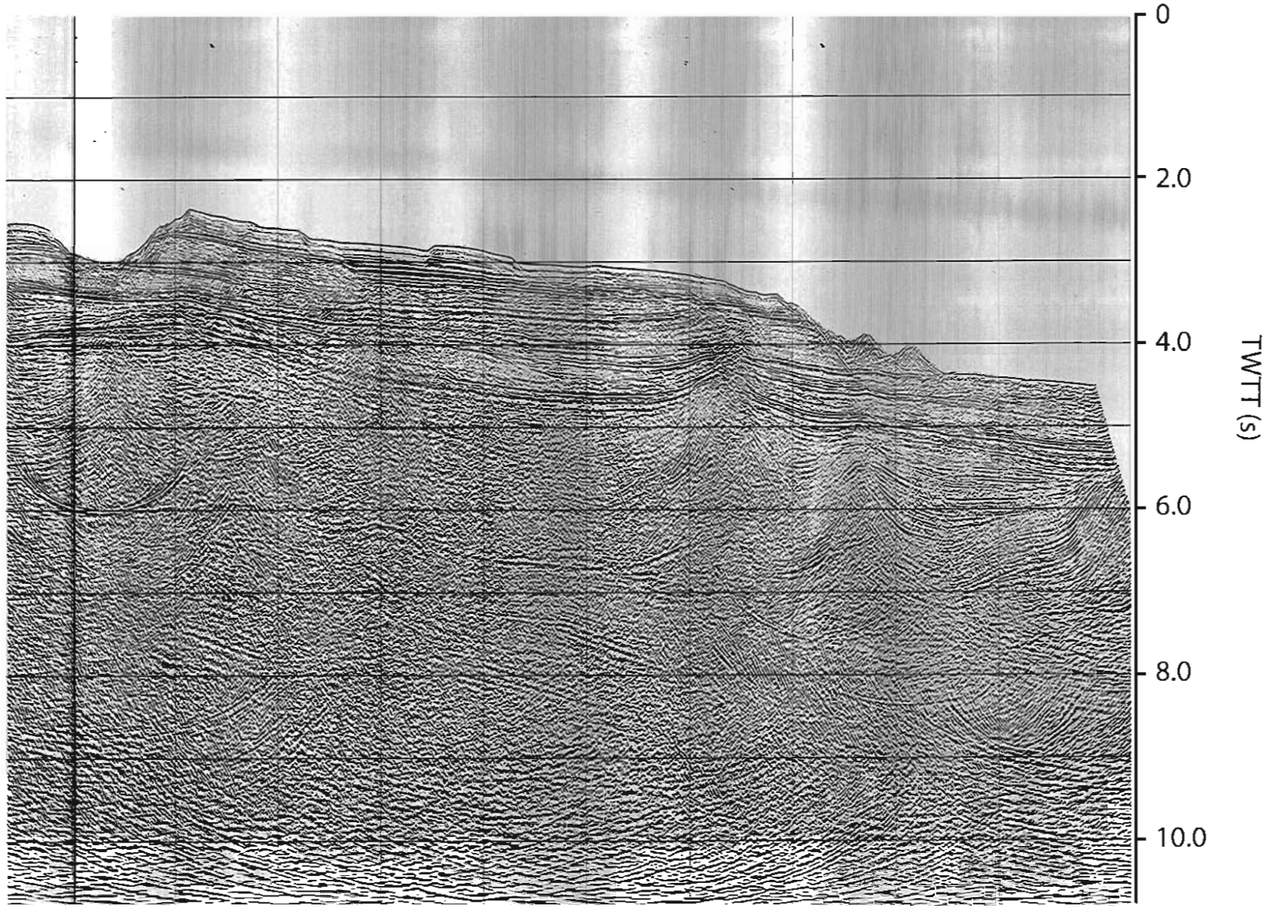
Shell 8624-S006-032E: 286-182&282
0
2.0
4.0
6.0
8.0
10.0
TWTT (s)

Shell 8624-S006-032E: 293-182

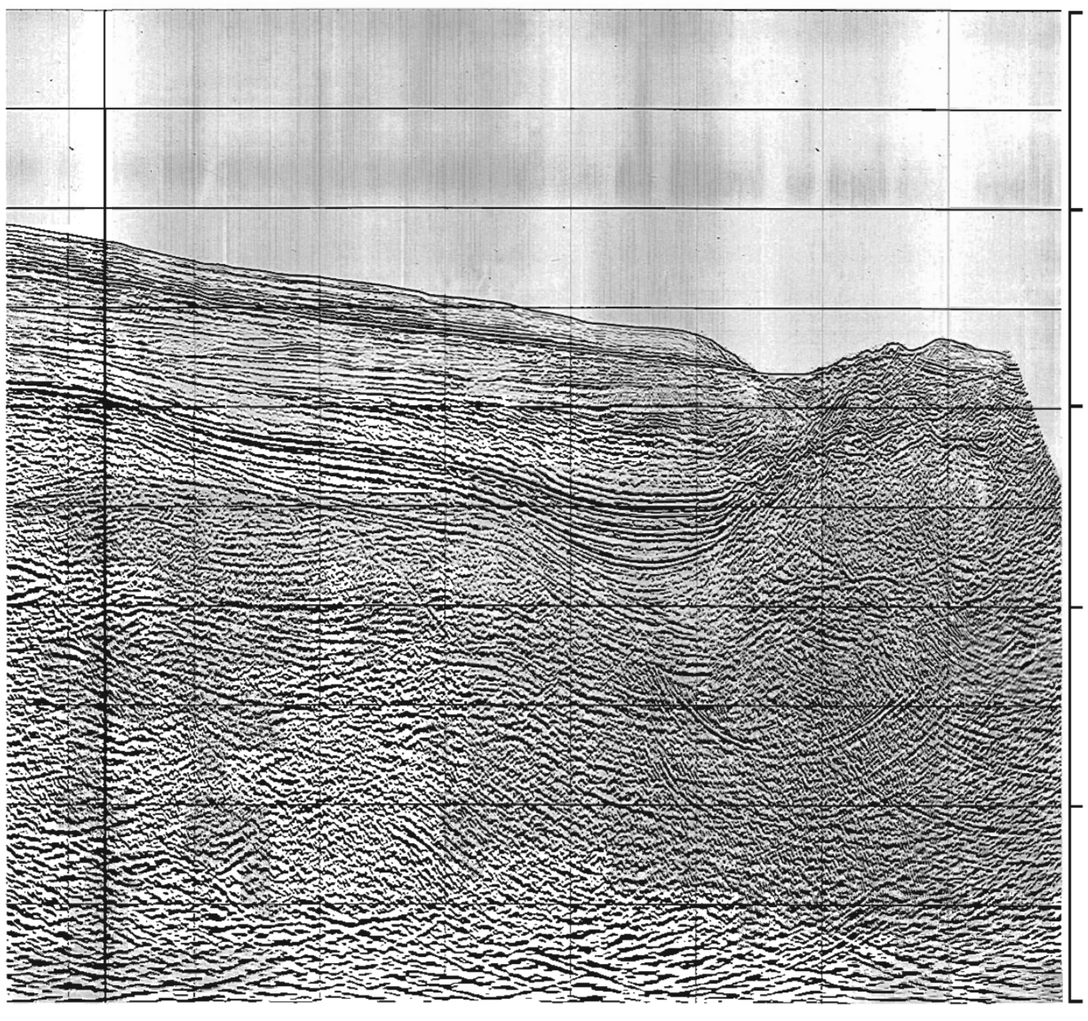

Shell 8624-S006-032E: 298-182

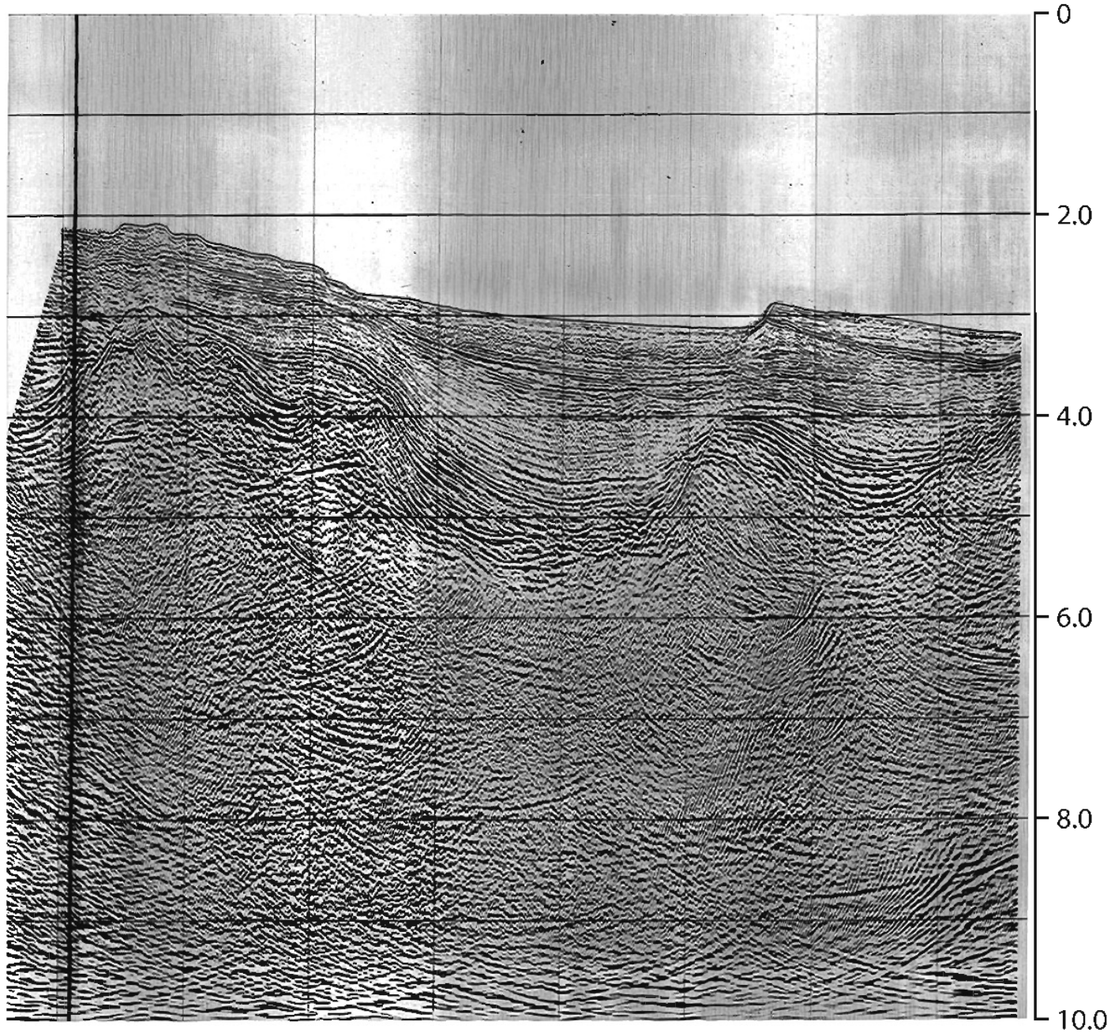

Shell 8624-S006-032E: 308-282